



<https://theses.gla.ac.uk/>

Theses Digitisation:

<https://www.gla.ac.uk/myglasgow/research/enlighten/theses/digitisation/>

This is a digitised version of the original print thesis.

Copyright and moral rights for this work are retained by the author

A copy can be downloaded for personal non-commercial research or study, without prior permission or charge

This work cannot be reproduced or quoted extensively from without first obtaining permission in writing from the author

The content must not be changed in any way or sold commercially in any format or medium without the formal permission of the author

When referring to this work, full bibliographic details including the author, title, awarding institution and date of the thesis must be given

Enlighten: Theses

<https://theses.gla.ac.uk/>
research-enlighten@glasgow.ac.uk

Biocompatibility of Orthopaedic Metal Implants: The Influence of Surface Chemistry and Topography

David Osian Meredith

Submitted for the degree of PhD to the University of Glasgow, UK

October, 2005



AO Research Institute,
Clavadelerstrasse,
CH 7270 Davos,
Switzerland.

***The Centre for Cell Engineering
at Glasgow***



Centre for Cell Engineering,
Division of Infection and Immunity,
University of Glasgow, G12 8QQ,
United Kingdom.

ProQuest Number: 10390734

All rights reserved

INFORMATION TO ALL USERS

The quality of this reproduction is dependent upon the quality of the copy submitted.

In the unlikely event that the author did not send a complete manuscript and there are missing pages, these will be noted. Also, if material had to be removed, a note will indicate the deletion.



ProQuest 10390734

Published by ProQuest LLC (2017). Copyright of the Dissertation is held by the Author.

All rights reserved.

This work is protected against unauthorized copying under Title 17, United States Code
Microform Edition © ProQuest LLC.

ProQuest LLC.
789 East Eisenhower Parkway
P.O. Box 1346
Ann Arbor, MI 48106 – 1346

GLASGOW
UNIVERSITY
LIBRARY:

Thesis Abstract

The initial aim of this work was to investigate *in vitro* fibroblastic response to the orthopaedic grade materials stainless steel (SS), titanium and Ti-6Al-7Nb (TAN), with the primary aim of assessing and comparing the soft tissue response towards TAN. The industrial 'standard' surface finish of orthopaedic implant materials varies considerably between smooth and rough, despite their use in similar applications. For this investigation, electropolished variants of titanium and TAN were specially produced to help distinguish between the effects of the material and those of the topography, no roughened SS was included due to being an industrially non-viable surface. Thermanox was included as a control substrate.

All materials were characterised using atomic force microscopy (AFM), profilometry, scanning electron microscopy (SEM) and contact angle measurements. Profilometry and AFM provided strictly topographical assessments while the SEM's various modes helped establish not only topography, but elucidate the elemental distribution on the surface. SS had a very smooth topography and its alloyed composition was visible with the SEM. Both electropolished titanium (TE) and TAN (NE) were not as smooth as (standard) electropolished SS. Both 'standard' preparations of titanium (TS) and TAN (NS) were rough and had similar roughness measurements, however, their topographies varied considerably. TS had characteristic 'basket weave' topography, while NS had an undulating topography punctuated with protruding particles – these particles are the β -phase of TAN and an element of its microstructure.

The *in vitro* investigation of cell growth, morphology and adhesion provided a basis upon which to establish a material or topography's cytocompatibility. The smooth metal topographies of SS, TE and NE, in addition to control Th, were demonstrated to both qualitatively and quantitatively allow for favourable cell growth. For TS, the roughened topography was not inhibitory to cell growth on the surface, however, NS demonstrated considerable growth impairment. Cell morphology was observed to be spread on all the smooth metal topographies. The roughened microtopography of NS visibly and quantitatively changed the morphology, with adherent cells being less spread and more elongated. Surface roughness also reduced the number and length of focal adhesions, which were lower in both number and size on TS and lowest on NS. Four features of NS were identified to possibly influence cells; surface chemistry, surface topography, β -phase particle endocytosis and ion leeching.

Endocytosis of β -phase particles was investigated by cell recovery from the surface of NS – these were demonstrated to have internalised β -phase particles. Clathrin staining of cells on NS failed to demonstrate any visible signs of endocytosis. Cells cultured in the presence of NS displayed endocytosed particles but their growth was not significantly inhibited, suggesting that particle endocytosis was not a contributory factor. This also ruled out ion leeching affecting the cells, and reduced NS cell influence to topography and/or chemistry.

Gene expression analysis was conducted to further elucidate cell reactivity on the surfaces. All sample types were compared to cells cultured on Thermanox. Of the smooth samples,

only SS demonstrated some low expression changes while TE and NE demonstrated no significant differences compared to Th. These results confirmed that the surface chemistry and minimal topography did not affect cell behaviour. Gene expression on TS resulted in 274 regulation changes - observed changes related to extracellular matrix production, increased cell replication and proliferation, and cell signalling, and were probably due to the rougher surface topography. The lack of cell growth on NS reduced extracted RNA amounts, and the introduction of amplification steps resulted in indicative rather than quantitative changes - however, indications of apoptosis were observed. Extracellular matrix remodelling was examined by means of labelling cellular fibronectin. Changes pertaining to surface roughness were observed, however, with the exception of NS, a confluent monolayer of cells resulted in a surface-wide fibrillar network. Fn production on NS was only considered to be less due to the lower cell numbers on the surface. Cell viability was also examined at 24hr, 5 and 10 days for all the surfaces but no evidence of apoptosis was found on NS.

The influence of surface chemistry, in the cellular reactions observed on NS, was investigated using two separate surface chemistry models. The surfaces were created by masking NS (also Th, SS, TS) with either gold or titanium, while retaining the surface topography. Cell growth, measured by means of cell counts, demonstrated no significant differences between the cells on uncoated or coated versions of each surface - cells could be cultured to confluency on coated versions of Th, SS and TS, while cell numbers were consistently low on coated NS. This established that the surface topography was the probable sole cause of the cell reactions observed on NS. An interesting observation, on nearly all the coated surfaces, was that cells aligned to the border between the coated and original surface - a property not clearly attributed to either surface chemistry or topography.

The surface topography of NS is dominated by protruding β -phase microspikes and it was this aspect that was hypothesised to be the cause of the poor cell growth and survival on NS. To test this hypothesis, the dimensions and spatial frequency of the microspikes was created based on an artificial, representative microtopography. Cell behaviour on this microtopography compared with that found on NS - culminating in low cell growth. This suggests that the microspike surface feature of NS, represented in the form of a fabricated topography, contributed significantly if not completely to the observed cell growth suppression.

The initial aim of assessing the *in vitro* soft tissue compatibility of TAN demonstrated that while the material was suitable, the standard topography in its current form was not, and for implanting TAN in sites near soft tissues a different surface topography or roughening treatment would be recommended. In general, the behavioural cues for fibroblasts on implant metal surfaces were generally confined to the influence of surface topography over that of surface chemistry. The microfabrication of specific surface characteristics, identified from implant metals, is a novel approach elucidating important factors of implant surface topographies and might aid in future developments of metal implants for optimisation of both soft and hard tissue integration to the metal implant.

Contents

	<i>Contents</i>		i
	<i>Acknowledgments</i>		iii
	<i>Abstracts and Papers</i>		iv
	<i>Figure Index</i>		v
	<i>Table, Chart & Equation</i>		vii
	<i>Index</i>		
	<i>Graph Index</i>		viii
	<i>Sample Name</i>	Quick Reference	ix
	<i>Abbreviations</i>		
	<i>Abbreviations and Symbols</i>		x
	<i>Index</i>		
Chapter 1 –	<i>General Introduction</i>	Orthopaedic Fracture Fixation and Implants	1
		The Orthopaedic Implant Environment	8
		Experimental Approach	18
Chapter 2 –	<i>Metals & Surfaces</i>	Abstract.....	19
		Introduction	20
		Materials & Methods	26
		Results	29
		Discussion	37
Chapter 3 –	<i>Cell Growth, Morphology... & Adhesion</i>	Abstract.....	42
		Introduction	43
		Materials & Methods	47
		Results	56
		Results Summary Table	85
		Discussion	86
Chapter 4 -	<i>β-Phase Particles</i>	Abstract.....	93
		Introduction	94
		Materials & Methods	96
		Results	98
		Discussion	106
Chapter 5 -	<i>Gene Expression Analysis</i> ...	Abstract.....	108
		Introduction	109
		Materials & Methods	111
		Results	118
		Discussion	129

Chapter 6 -	<i>Surface Chemistry</i>	Abstract	137
		Introduction	138
		Materials & Methods	140
		Results	142
		Discussion	160
Chapter 7 -	<i>Surface Topography</i>	Abstract	166
		Introduction	167
		Materials & Methods	169
		Results	175
		Discussion	202
Chapter 8 -	<i>General Discussion</i>	Materials and Surfaces	207
		Cell Growth, Morphology and Adhesion	212
		Microfabrication	218
		Summary	220
Chapter 9 -	<i>References</i>	222

CD-ROM	<i>Appendix I</i>	Additional Chemicals.....
	<i>Additional Images</i>	Chapter 5.....
		Chapter 6
		Chapter 7

Conference Abstracts

Papers

Acknowledgments

This work is dedicated to Heddwen and David Meredith. Thanks for all your support and taking an interest in what I've been up to all these years. Diolch yn fawr.

To Iestyn, Dyfed, Helen and Sion for taking less of an interest and reminding me that there is a world outside the thesis.

A very special thank you to Mairead for her unwavering support, scientific advice and motivational speeches (.....are you not done yet!!!) during the writing of this thesis. Thanks so much.

In Davos, I'd like to thank and am indebted to Geoff for taking me on all those years ago and his continued support and guidance during the course of this work and other studies. I look forward to further collaboration in years to come. I'd also like to thank Erich Schnieder and AO Research for employing me for all those years, Llinos Harris and Gethin Owen along with members past and present at Interface Biology, Robbie Peter, Christoph Sprecher, Keita Ito and Mauro Alini. I'd also like to thank Tom, Laszlo and Nora, and many others, for making my time at the AO and Davos very enjoyable.

In Glasgow, I am indebted to both Adam Curtis and Mathis Riehle for the support and guidance I have received over the years, and Mathis especially for giving me time off to finish the thesis! I would also like to thank Nikolaj Gadegaard for his assistance in microfabrication and all things thesis and otherwise, Matt and Cath Dalby for both their scientific advice and ready source of accommodation, Alison and Derek Beattie and everyone at the CCE. Also, I could not have finished this study without the help of Mary Robertson, Sara McFarlane and Chris Wilkinson at the Department of Electrical Engineering, and Georgia Riboldi-Tunncliffe and Pawel Herzyk at Sir Wellcome Functional Genomics Facility.

Abstracts

List of abstracts accepted for oral or poster presentation related to this PhD study.

Identifying and mimicking features of unfavourable topography and investigating cellular reactions. Invited Oral Presentation, **Biosurf VI**, Lausanne, CH, 2005

Utilisation of microscopy techniques to investigate cell-biomaterial interactions. Oral presentation, **European Microscopy Congress**, Davos, CH, 2005

Effect of orthopaedic metal implant surface on fibroblast behaviour. Poster Presentation, **Swiss Society for Biomaterials Meeting**, CH, 2005.

Effect of standard orthopaedic metal implant surfaces on cell behaviour. Oral Presentation, **European Cells & Materials Conference**, Davos, CH, 2004

Human fibroblast proliferation and cytoskeleton reactivity to characterised metal implant surfaces. Poster Presentation, **European Cells & Materials Conference**, Davos, CH, 2004

Cell proliferation and structure is defined by specific metal microtopography. Oral Presentation, **Tissue and Cell Engineering Society**, Keele University, Great Britain, 2004.

Cell Structure and Genetic Reactivity to Orthopaedic Materials. Oral Presentation, **7th World Biomaterials Congress**, Sydney, Australia, 2004.

Characterisation of Sheep Paratenon Cells and Human Fibroblasts on Standard Orthopaedic Materials. Poster Presentation, **European Society of Biomaterials**, Stuttgart, Germany, 2003.

Papers

Papers written or co-authored by the candidate on work related to this PhD study.

Meredith, D.O., Eschbach, L., Riehle, M.O., Curtis A.S.G., Richards, R.G. (2005) Human Fibroblast Reactions to Standard and Electropolished Titanium and Ti-6Al-7Nb, and Electropolished Stainless Steel. *J Bio Mat Res. A.* **75**, 3, 541-555.

Owen, G.R., Meredith D.O., ap Gwynn, I., Richards, R.G. (2005) Focal adhesion quantification – A new assay of material biocompatibility?:Review. *Eur Cell Mat.* **9**, 85-96.

Wood, M.A., Meredith, D.O., Owen G.Rh., Richards, R.G, Riehle, M.O. (2005) "Utilising Atomic Number Contrast for FESEM Imaging of Colloidal Nanotopography Underlying Biological Cells", *Nanotechnology.* **16**, 1433-1439.

Wood, M.A., Meredith, D.O., Owen G.Rh. (2002) "Steps Towards a Model Nanotopography", *IEEE Transaction on Nanobioscience.* **1**, 4, 133-140.

Figures Index

Chapter 1 – <i>General Introduction</i>	Fig 1.1.....	2
	Fig 1.2	9
	Fig 1.3	11
Chapter 2 – <i>Metals & Surfaces</i>	Fig 2.1.....	23
	Fig 2.2	24
	Fig 2.3	25
	Fig 2.4	29
	Fig 2.5	31
	Fig 2.6	32
	Fig 2.7	33
	Fig 2.8	34
	Fig 2.9	35
	Fig 2.10	35
	Fig 2.11	36
Chapter 3 – <i>Cell Growth, Morphology... & Adhesion</i>	Fig 3.1.....	44
	Fig 3.2	49
	Fig 3.3	54
	Fig 3.4	55
	Fig 3.5	57
	Fig 3.6	58
	Fig 3.7	61
	Fig 3.8	62
	Fig 3.9	63
	Fig 3.10	65
	Fig 3.11	66
	Fig 3.12	68
	Fig 3.13	73
	Fig 3.14	74
	Fig 3.15	76
	Fig 3.16	78
	Fig 3.17	79
	Fig 3.18	81
	Fig 3.19	89
Chapter 4 - <i>β-Phase Particles</i>	Fig 4.1.....	99
	Fig 4.2	100
	Fig 4.3	101
	Fig 4.4	102
	Fig 4.5	103
	Fig 4.6	104

Chapter 5 -	<i>Gene Expression Analysis...</i>	Fig 5.1.....	124
		Fig 5.2	125
		Fig 5.3	126
		Fig 5.4	126
		Fig 5.5	127
		Fig 5.6	127
		Fig 5.7	127
		Fig 5.8	128
Chapter 6 -	<i>Surface Chemistry.....</i>	Fig 6.1.....	143
		Fig 6.2	144
		Fig 6.3	145
		Fig 6.4	146
		Fig 6.5	147
		Fig 6.6	149
		Fig 6.7	153
		Fig 6.8	154
		Fig 6.9	156
		Fig 6.10	158
		Fig 6.11	159
Chapter 7 -	<i>Surface Topography.....</i>	Fig 7.1.....	170
		Fig 7.2	171
		Fig 7.3	172
		Fig 7.4	172
		Fig 7.5	175
		Fig 7.6	176
		Fig 7.7	177
		Fig 7.8	178
		Fig 7.9	178
		Fig 7.10	179
		Fig 7.11	180
		Fig 7.12	182
		Fig 7.13	183
		Fig 7.14	184
		Fig 7.15	189
		Fig 7.16	190
		Fig 7.17	191
		Fig 7.18	192
		Fig 7.19	194
		Fig 7.20	195
		Fig 7.21	197
		Fig 7.22	198
		Fig 7.23	199

Table Index

Chapter 2 – <i>Metals & Surfaces</i>	Table 2.1.....	26
	Table 2.2	30
	Table 2.3	36
Chapter 3 – <i>Cell Growth, Morphology... & Adhesion</i>	Table 3.1.....	60
	Table 3.2	60
	Table 3.3	69
	Table 3.4	70
	Table 3.5	71
	Table 3.6	71
	Table 3.7	83
	Table 3.8	84
	Table 3.9	85
Chapter 4 - <i>β-Phase Particles</i>	Table 4.1.....	105
Chapter 5 – <i>Gene Expression Analysis</i> ...	Table 5.1.....	113
	Table 5.2	119
	Table 5.3	120
	Table 5.4	121
	Table 5.5	122
Chapter 6 - <i>Surface Chemistry</i>	Table 6.1.....	140
	Table 6.2	152
	Table 6.3	157

Chart Index

Chapter 5 - <i>Gene Expression Analysis</i> ...	Chart 5.1.....	111
--	----------------	------------

Equation Index

Chapter 2 – <i>Metals & Surfaces</i>	Equation 2.1.....	27
---	-------------------	-----------

Graph Index

Chapter 3 – <i>Cell Growth, Morphology... & Adhesion</i>	Graph 3.1.....	59
	Graph 3.2	70
	Graph 3.3	72
	Graph 3.4	82
	Graph 3.5	83
	Graph 3.6	84
Chapter 4 – <i>β-Phase Particles.....</i>	Graph 4.1.....	105
Chapter 6 – <i>Surface Chemistry.....</i>	Graph 6.1.....	150
	Graph 6.2	155
Chapter 7 – <i>Surface Topography.....</i>	Graph 7.1.....	185
	Graph 7.2	187
	Graph 7.3	200
	Graph 7.4	201

Sample Name Abbreviations

Summary of material/surface denoting symbols used through the following chapters.

<i>Symbol</i>	<i>Full Name</i>	<i>Description</i>
Standard Samples		
<i>Th</i>	Thermanox	Polyethylene terephthalate, Cell culture plastic
<i>SS</i>	'Standard' Stainless Steel	Orthopaedic implant quality (IQ) material with the standard finish of electropolishing
<i>TE</i>	Electropolished commercially pure (cp) Titanium	IQ material with a custom finish of electropolishing
<i>TS</i>	'Standard' cp Titanium	IQ material with the standard finish of a roughened surface
<i>NE</i>	Electropolished Ti-6Al-7Ni	IQ material with a custom finish of electropolishing
<i>NS</i>	'Standard' Ti-6Al-7Ni	IQ material with the standard finish of a roughened surface
Coated Samples		
<i>ThG</i>	Thermanox coated with Gold	Thermanox plastic coated with 50 nm of gold
<i>ThT</i>	Thermanox coated with Titanium	Thermanox plastic coated with 50 nm of titanium
<i>SG</i>	SS coated with Gold	'Standard' Stainless Steel coated with 50 nm of gold
<i>ST</i>	SS coated with Titanium	'Standard' Stainless Steel coated with 50 nm of titanium
<i>TG</i>	TS coated with Gold	'Standard' cp Titanium coated with 50 nm of gold
<i>TT</i>	TS coated with Titanium	'Standard' cp Titanium coated with 50 nm of titanium
<i>NG</i>	NS coated with Gold	'Standard' cp Ti-6Al-7Ni coated with 50 nm of gold
<i>NT</i>	NS coated with Titanium	'Standard' cp Ti-6Al-7Ni coated with 50 nm of titanium
Microfabricated Samples		
<i>Pyr</i>	Pyramid	Polycaprolactone (PCL) sample with pyramid microtopography
<i>AuPyr</i>	Gold Pyramid	PCL sample with the pyramid microtopography coated with 50nm of gold
<i>TiPyr</i>	Titanium Pyramid	PCL sample with the pyramid microtopography coated with 50 nm of titanium
<i>Plan</i>	Planar	Polycaprolactone (PCL) sample with minimal features
<i>AuPlan</i>	Gold Planar	Polycaprolactone (PCL) sample with minimal features coated with 50 nm of gold
<i>TiPlan</i>	Titanium Planar	Polycaprolactone (PCL) sample with minimal features coated with 50 nm of titanium

Abbreviations and Symbols Index

β-ME.....	β-Mercaptoethanol
199	Media 199
AFM	Atomic Force Microscopy
ANOVA	Analysis of Variance
BSA	Bovine Serum Albumin
BSE	Backscattered Secondary Electrons
cDNA	Complementary DNA
CO ₂	Carbon Dioxide
cpTi	Commercially Pure Titanium
DAPI.....	4',6-diamidino-2-phenylindole
ddH ₂ O	Double Distilled Water
DMEM	Dulbecco's Modified Eagles Medium
DNA	Deoxyribonucleic acid
ECM	Extracellular Matrix
EDTA	Ethylenediaminetetraacetic Acid
EDX	Energy Dispersive X-Ray
FAK	Focal Adhesion Kinase
FCS	Foetal Calf Serum
FESEM.....	Field Emission Scanning Electron Microscope
Fn	Fibronectin
HTERT	Human Telomerase Reverse Transcriptase
hTERT BJ-1	Infinity TM Telomerase-Immortalized Fibroblasts
IL-β	Interleukin-β
IL-6	Interleukin-6
IQ	Implant Quality
LISS	Less Invasive Stabilisation System
MMP7	Matrix Metalloproteinase 7
mRNA.....	messenger RNA
RNA	Ribonucleic acid
MTOC	Microtubule-organising Centre
NaOH	Sodium Hydroxide
PBS	Phosphate Buffered Solution
PET	Polylethylene terephthalate
PCL	Polycaprylactone
PCR	Polymerase Chain Reaction
PDGF	Platelet-derived growth factor
PIPES.....	Piperazine-NN'-bis-2-ethane Sulphonic Acid
Ra	Roughness average
rpm	Revolutions per minute
SDS	Sodium Dodecyl Sulfate
SE	Secondary Electrons
SEM	Scanning Electron Microscopy
SS	Stainless Steel
SSC	Saline Sodium Citrate

TAN.....	Ti-6Al-7Ni
TBSS	Tyrode's Balanced Salt Solution
TGF- β	Transforming Growth Factor- β
TNF- α	Tumour Necrosis Factor- α

Chapter 1 - General Introduction

Implantable devices have a wide and continually expanding range of applications in medicine that include; medical emergencies (intubation), essential corrective measures (coronary stents, heart valves, pacemakers), orthopaedic augmentation and replacement (plates, intramedullary nails, hip and knee prostheses), dental implants and cosmetic enhancement (breast implants). There is also significant interest in the engineering of replacement degenerative connective tissues (bone, cartilage, ligaments) and even entire organs (liver) (Laurencin *et al.*, 1999). The demand for such developments goes hand in hand with the extended life expectancy found in westernised countries, driven by medical necessity, a financial rationale or simply to preserve an accustomed lifestyle. These devices can be removable in the short or long term or even become permanent fixtures in the body, and the range of possible applications is only limited in number by the range of 'biomaterials' developed and utilised in their realisation.

Biomaterials are classed by their ability to elicit a biocompatible response, generally defined as the "*ability of a material to perform with an appropriate host response in a specific application*" (Williams, 1999). This infers that biocompatibility is not a specific response, but one dependent on the location and the role of the implant. As will be mentioned in a later section, the goal or 'appropriate host response' for soft tissue integration with orthopaedic implants would be to minimise infection and prolonged inflammation while encouraging tissue colonisation and adherence.

In the following section I will introduce and focus on the use of implants in orthopaedic fracture fixation. Covered within this section are the basic concepts of internal fixation, the materials commonly utilised and issues surrounding their use.

1. Orthopaedic Fracture Fixation and Implants

In the context of implantable biomaterials, bone fracture fixation was addressed early on in the development of the field with treatment reportedly using iron wires in 1775 (Laing, 1979), and the first documented use of plates and screws (nickel-plated screws and sheet

steel) in 1886 (Ratner, 2004). Current day orthopaedic devices can be separated into two general categories, the fixation of fractured bones and the replacement of worn out articulating joints. In this instance bone fixation will be focused upon.

1.1 - Internal Fixation

The concept of internal fixation has developed from initial observations that external immobilisation of a fracture site by a cast is not always beneficial for the patient, and can be insufficient to stabilise the site. The accompanying muscles, tendons and ligaments located at the immobilised zone can degenerate if not exercised frequently, requiring further rehabilitation of the area after healing of the initial fracture site (Schatzker, 2000). The compressive alignment and stabilisation of the fracture site allows healing with minimal callus formation (a mass of healing bone tissue) while allowing for the limb area to be exercised and thus full use can be returned in a comparatively brief time interval (Schatzker, 2000; Schlich, 2002). In addition, when fractures occur at an articulating edge, proper alignment is essential as the misalignment of these surfaces can cause premature joint wear, pain and arthritis (Jupiter and Ring, 2005). A common method of internal fixation is the screw and plate concept; the plate is utilised as a splint for alignment of the bone fragments, while the screws secure the fragments to the plate and allow for compression of the fragment ends (Fig 1.1a). Another concept utilised is intramedullary nailing, in which rods usually of metal are inserted into the bone marrow medullary cavity of long bones, such as the femur, to provide stability and allow early loading of the bone (Fig 1.1b) (Krettek, 2000; Perren, 1991).

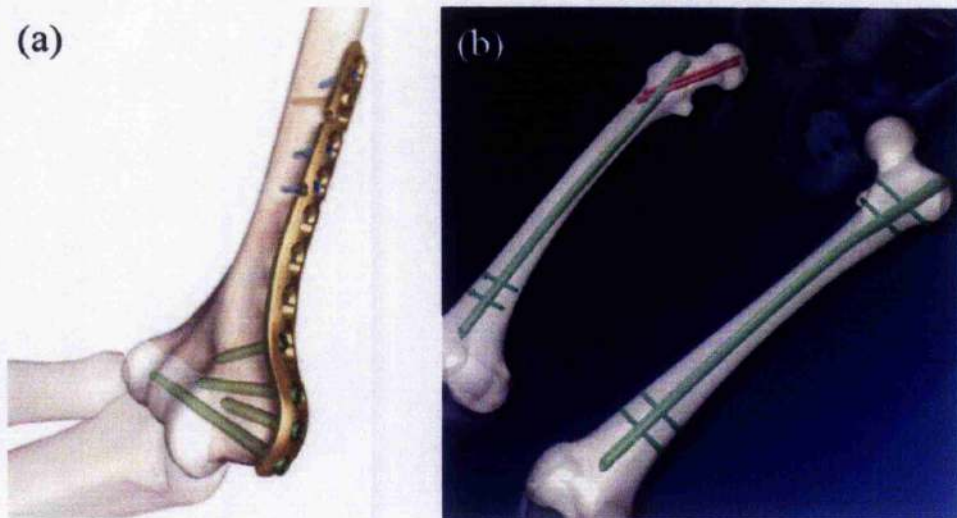


Fig 1.1 – Internal fixation methods (a) The screw/plate methodology used to align and secure bone fragments. (b) Intramedullary nailing system; a long shaft is inserted into the medullary canal and secured by strategically placed screws. Images with kind permission of AO Research.

1.2 - Metals in Orthopaedics

The discovery and development of biologically ‘inert’ or biocompatible metals has progressed in parallel with the development of orthopaedic implants and also the field of dentistry, with landmark discoveries advancing both fields. 1924 saw the first experiments into implanting various metals in dogs, and introduced the notion of biological tolerance of some metals (Laing, 1979). It also became apparent that the primary problem of numerous metal types tested was the lack of resistance to the corrosive wound healing environment (specifically a low pH) of the mammalian body (Disegi and Eschbach, 2000; Laing, 1979). For dental purposes, Vitallium (cobalt-chromium-molybdenum alloy) was settled upon in the late 30’s meeting the requisites of mechanical stability, corrosion resistance and biological tolerance. The same material was also introduced into artificial hip manufacture (Laing, 1979; Ratner, 2004). In orthopaedic plates and screws, numerous stainless steel alloy compositions were investigated through the 40’s and 50’s before eventually settling upon Type 316 (18% chromium- 14% nickel- 2.5% molybdenum) as meeting the mechanical, materials and biological requirements.

1.3 - Stainless Steel

To the present day type 316 and its low carbon counterpart, type 316L, are still the standard composition for stainless steel implants. It is primarily composed of iron, constituting up to 60% of its bulk with major alloying elements of chromium (18%), nickel (14%) and molybdenum (2.5%). Chromium and molybdenum aid in the steel's corrosion resistance by forming a strongly adherent surface oxide layer (Cr_2O_3), however, it also weakens its microstructure. Nickel is currently used to counteract this by stabilising steel thus producing a stronger microstructure (Brunski, 2004; Disegi, 1998b; Disegi and Eschbach, 2000).

Stainless steel (SS) of type 316 is still the most frequently used biomaterial for internal fixation devices due to its 'tried and tested' clinical track-record, favourable mechanical properties and corrosion resistance coupled with low production costs (Disegi and Eschbach, 2000; Kramer, 2000). Its widespread utilisation over the course of the last 50 years has allowed for the identification of its many advantages and disadvantages. While resistant to environmental corrosion, SS cannot counteract plate/screw fretting where mechanical disruption of the two components coming into contact removes the resistant passive layer (Layens and Peters, 2003). Once corrosion, defined as the visible destruction of metal (Steinemann, 1998), has been initiated it is near to impossible to prevent its progress in the body, and this also results in the dissolution of ions from the material (Disegi, 1998a). A cytotoxic component of SS is nickel (Steinemann, 1996), and various sources claim from 1-10% nickel hypersensitivity in patients (Voggenreiter et al., 2003). There is also a mismatch in the elastic properties of SS compared to bone, SS being seven times stiffer and can lead to stress shielding of the healing bone (Dee *et al.*, 2002a). In stress shielding, the loading subjected to the healing bone is transferred to the implant thus decreasing the bone's 'workload' and as a result can cause bone resorption rather than production (Anderson, 1999; Dee *et al.*, 2002a).

1.4 - Titanium

Titanium is the ninth most abundant element in the earth's crust, however it is only relatively recently been available in bulk, due to the development of new industrially viable

extraction methods in 1946 (Disegi, 1998a; Pohler, 2000). It had been considered since the late 40s for both orthopaedic and dental use, however Branemark's discovery of osseointegration elevated its status. Here was a material that, rather than being simply biologically inert (it is already saturated in the tissues (Steinemann, 1996)), actually encouraged a tight integration with bone (Ratner, 2004). Theories for this include protein absorption (Ratner, 2001) and its elemental proximity to calcium (Morehead and Holt, 1994) amongst others. It also has other advantages as an implant material, such as an accelerated spontaneous oxide formation under a low pH which passivates the surface and thus works against screw/plate fretting thus reducing the chance of corrosion (Disegi, 1997; Disegi, 1998a; Layens and Peters, 2003; Perren and Pohler, 1987). It is classed as a light metal (Layens and Peters, 2003) and the resulting lower elasticity modulus figure (denoting an increased elasticity) is half that of SS, thus closer to that of bone and therefore reducing the level of stress shielding that can be expected (Dee *et al.*, 2002a).

'Commercially pure' titanium's (cpTi) biocompatible properties have allowed it to become the 'next-generation' metallic biomaterial and acts as a benchmark with which to compare new materials (Steinemann, 1998). However, titanium is not without its own drawbacks, one being a higher cost (Disegi and Eschbach, 2000; Kramer, 2000). An further notable disadvantage is its reduced tensile strength, which makes it too brittle for numerous orthopaedic situations that require the fixation of areas exposed to high cyclic loading (e.g walking) (Dee *et al.*, 2002a; Disegi and Eschbach, 2000; Kramer, 2000; Oliveira *et al.*, 1998).

1.5 - Titanium Alloys

Titanium alloys are a class of materials that retain many of the advantages of pure titanium but are equipped with enhanced mechanical properties. To describe briefly, the microstructure of titanium can be separated into α or β phase. At room temperature pure titanium is in its α -phase, where the titanium atoms are packed into a hexagonal lattice structure (Layens and Peters, 2003). At 882°C the β -phase transition is crossed and the microstructure transforms to the β -phase of titanium, where the titanium atoms are rearranged to cubic packing (Dee *et al.*, 2002a; Kramer, 2000; Layens and Peters, 2003;

Pohler, 2000). This change in microstructure impedes the dislocation properties of the structure reducing its plasticity – thus increasing its rigidity (Layens and Peters, 2003). By alloying titanium with certain elements known as β stabilisers, the β -phase of titanium can be stabilised at decreased temperatures (Freese *et al.*, 2001). The simultaneous alloying of α and β stabilising elements leads to the formation of a two phase $\alpha+\beta$ microstructure at room temperature, thus increasing material tensile strength. The resulting alloys are utilised in numerous orthopaedic applications where mechanical loads are borne (Dohle *et al.*, 2002; Gasser, 2001; Layens and Peters, 2003).

The first commonly utilised titanium alloy for orthopaedics was Ti-6Al-4V and it is still a popular choice today (Gasser, 2001). However, the alloying elements of vanadium, and to a lesser extent aluminium, have both been noted to demonstrate some toxic effects when their ions are released from the implant (Black, 1988; Gerber and Perren, 1980; Wapner, 1991), and it is believed that this leads to the impaired bone ultrastructure seen around the said implants (Albbrektsson, 1990; Johansson *et al.*, 1989). This has driven the development and investigation of numerous other titanium alloys that offer similar mechanical properties and corrosion resistance, with less toxic alloying components such as Ti-6Al-7Nb, Ti-13Nb-13Zr, Ti-5Al-2.5Fe and Ti-15Mo to name but a few (Disegi and Wyss, 1989; Disegi, 2000; Khan *et al.*, 1999). Many current biomaterial publications list countless alloy compositions that could be beneficial to the field in search of the ‘perfect recipe’ (Eisenbarth *et al.*, 2004; Okazaki *et al.*, 1998).

1.6 - Ti-6Al-7Nb (TAN)

Ti-6Al-7Nb (TAN) is an example of an $\alpha+\beta$ phase alloy that is utilised in intramedullary nailing systems due to its similar corrosion and sliding wear resistance in comparison to Ti-6Al-4V (Disegi, 1993; Disegi, 2000; Kramer, 2000; Semlitsch, 1987; Semlitsch *et al.*, 1985). SS and titanium are generally favoured for plate/screw applications (Kramer, 2000), although TAN has had limited exposure in recently developed fracture fixation techniques such as the ‘Less Invasive Stabilisation System’ (LISS) (Frigg *et al.*, 2001). These plate/screw applications bring the material into contact with a more complex environment of hard and soft tissues. TAN’s osseointegration performance has been documented

(Disegi, 1993; Lavos-Valereto *et al.*, 2001a; Lavos-Valereto *et al.*, 2001b), however TAN's soft tissue reactivity can only be indirectly assessed from preliminary clinical LISS studies where no severe difficulties have been reported so far (Cole *et al.*, 2003; Syed *et al.*, 2004).

1.7 – Surface Finish

The metallurgy is not the only difference between these material types. The industrially produced standard surface finish of the materials varies considerably in view of their use in similar applications. 'Standard' SS has a smooth mirror-like electropolished surface primarily consisting of corrosion resistant Cr_2O_3 (Brunski, 2004; Disegi, 1998b; Disegi and Eschbach, 2000). Titanium (cpTi) and titanium alloys such as TAN are deliberately roughened by sandblasting to help promote osseointegration, and electrochemically anodized to enhance the corrosion resisting natural oxide layer, increasing its thickness from 2-5nm to 50nm (Disegi, 1997).

1.8 – Further Development

While the number of implant metals utilised in orthopaedics is growing rapidly, an encouraging trend has emerged. Initially titanium and alloys, such as Ti-6Al-4V, were developed for other industries such as aerospace, and were only utilised as biomaterials by default (Layens and Peters, 2003). Ti-6Al-7Nb heralded a new concept where the implantable material was selected or developed for use as an orthopaedic implant with consideration given to the requirement of including biocompatible elements (Disegi, 1993). This trend has even seen its way into the development of steel compositions with low or negligible levels of nickel (Fini *et al.*, 2003). However, the fact that the individual material elements composing a material are biocompatible does not automatically make the material itself biocompatible, and thorough *in vitro* and *in vivo* testing is still required.

2. The Orthopaedic Implant Environment

The biological environment surrounding the plate/screw orthopaedic implant is a complex site that is generally divided into two separate fields, the hard and soft tissue environments. *In vitro* and *in vivo* biomaterials studies of metallic materials are often undertaken with a view to investigate how hard tissues such as bone will react, and more specifically to assess osseointegration. How soft tissue reacts to such implants is an aspect that is commonly overlooked or at least investigated less thoroughly. The argument for orthopaedics, that if osseointegration is not achieved then the use of the material may be limited, can be countered by the fact that the absence of soft tissue integration at the implant interface also has a major influence in assessing biomaterial performance (Richards *et al.*, 1999; Ungersbock *et al.*, 1994; Ungersbock *et al.*, 1996; von Recum, 1986). In the following section I will focus on soft tissue wound healing and foreign body reactions and their significance ultimately for *in vitro* implant investigations with soft tissues.

2.1 - Wound Healing

An obvious aspect of a fracture site, and therefore the point of a plate insertion, is that it is a wound environment, and thus the wound healing cellular cascade is evident and crucial in the integration of the material. The three phases of soft tissue wound healing are termed, an exudative phase, a granulation phase and finally tissue remodelling (Fig 1.2) (Koopmann, 1995). The exudative phase starts with the wounding and lasts 3 to 4 days (Dee *et al.*, 2002b). The first step in this phase is an influx of blood to the wound site, with components such as activated platelets triggering coagulation and producing chemotactic signals such as platelet-derived growth factor (PDGF) and transforming growth factor- β (TGF- β) to promote cell migration towards the site (Fig 1.3a) (Anderson, 1999; Anderson *et al.*, 2004; Dee *et al.*, 2002b). An acute inflammatory response ensues after 5 hr with the arrival of neutrophils, and macrophages within 24 hr (Fig 1.3b) (Koopmann, 1995; Tomlinson and Ferguson, 2003). The neutrophils are effectively vacuum cleaners whose role it is to phagocytose pathogens and foreign materials while also releasing chemical signals. Their attraction to the site, as well as their life-span, is short lasting only a few hours, after which point only macrophages remain (Anderson, 1999). Numerous texts discussing wound healing freely interchange between the terms monocytes and macrophages, however this is

inaccurate as monocytes are immature mononuclear phagocytes that can be found in the circulating blood (Edelson and Cohn, 1976), and when they emigrate out to the tissue and wound sites they mature into macrophages (Fedorko and Hirsch, 1970). Macrophages fill various roles in the healing cascade such as; phagocytosing any remaining pathogens, debridement or clearing of the injured and necrotic tissues by releasing enzymes into the extracellular spaces (Dee *et al.*, 2002b; Morehead and Holt, 1994), and the release of additional growth factors such as leukotriene B₄ (LTB₄), fibroblast growth factor (FGF) in addition to PDGF and TGF- β to initiate fibroblast and endothelial cell recruitment and proliferation (Anderson, 1999; Koopmann, 1995; Waldorf and Fawkes, 1995).

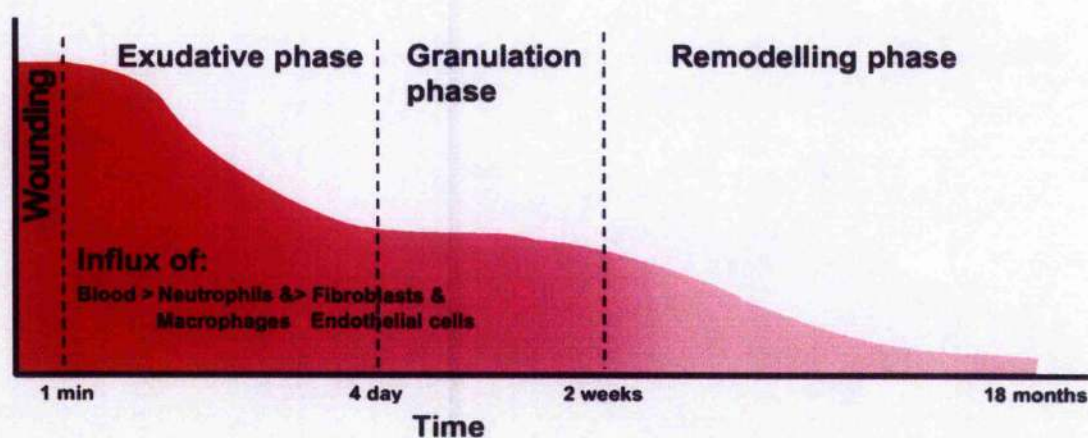


Fig 1.2 – A relative timeline of the wound healing phases and the intensity of the reaction. Immediately after wounding the exudative phase is initiated. This phase encompasses the influx of blood and platelet activation, initiation of an inflammatory reaction and the migration of fibroblasts and endothelial cells to the wound site. This is followed by the granulation phase where new granular tissue is formed sealing the wound site. The final phase is remodelling, consisting of wound site contraction and extensive extracellular matrix remodelling.

After the first day the exudative response has initiated the migration and proliferation of fibroblasts and vascular endothelial cells to the site. After 3 to 4 days this tissue, known as granulation tissue becomes visible and is characterised by its pink, soft granular appearance (Fig 1.2, 1.3c) (Waldorf and Fawkes, 1995). The proliferating fibroblasts are synthesising extracellular components such as collagen, and the endothelial cells have formed new small blood vessels (Anderson, 1999; Dee *et al.*, 2002b). Essentially, the formation of this tissue fills the void caused by the wound and also seals it from external influences. The final phase involves reduction and remodelling of the wound site and occurs over a much longer

time period of up to 6-18 months (Fig 1.2) (Koopmann, 1995; Waldorf and Fawkes, 1995). The cellular and vascular content of the tissue decreases and cells known as myofibroblasts actively contract the wound site (Dee *et al.*, 2002b). The extracellular matrix (ECM) is extensively remodelled, however the new tissue may not retain the functional characteristic of the tissue it has replaced and is known as scar tissue (Dee *et al.*, 2002b). This account of wound healing does not take into consideration the presence of an implant.

2.2 – Foreign Body Response

The insertion of an implant constitutes a foreign object and induces the formation of a fibrous tissue capsule and inflammation, both collectively known as the foreign body response (Anderson *et al.*, 2004; Dee *et al.*, 2002b; Morehead and Holt, 1994). These reactions to a foreign body are initiated during the exudative and granulation phases of wound healing and can persist for the duration of the implants lifetime in the body (Anderson, 1999). When these reactions reach extreme proportions resulting in complications such as delayed wound healing and infection, the removal of the implant becomes a necessity (Dee *et al.*, 2002b). Inflammation, as noted in wound healing, is a natural and unavoidable injury response, however, in some instances the inflammation persists and becomes chronic (Anderson, 1999; Anderson *et al.*, 2004). Contributory causes for this can be the chemical or physical properties of the implant or the presence of an infection at the wound site (Morehead and Holt, 1994). Generally, adherent solitary macrophages and fused macrophages, known as foreign body giant cells (FBGC), persist on the surface continually releasing inflammatory cytokines and degradative oxygen radicals (Zhao *et al.*, 1992) in what is hypothesised to be an unsuccessful attempt to phagocytose the surface (Dee *et al.*, 2002b; Morehead and Holt, 1994).

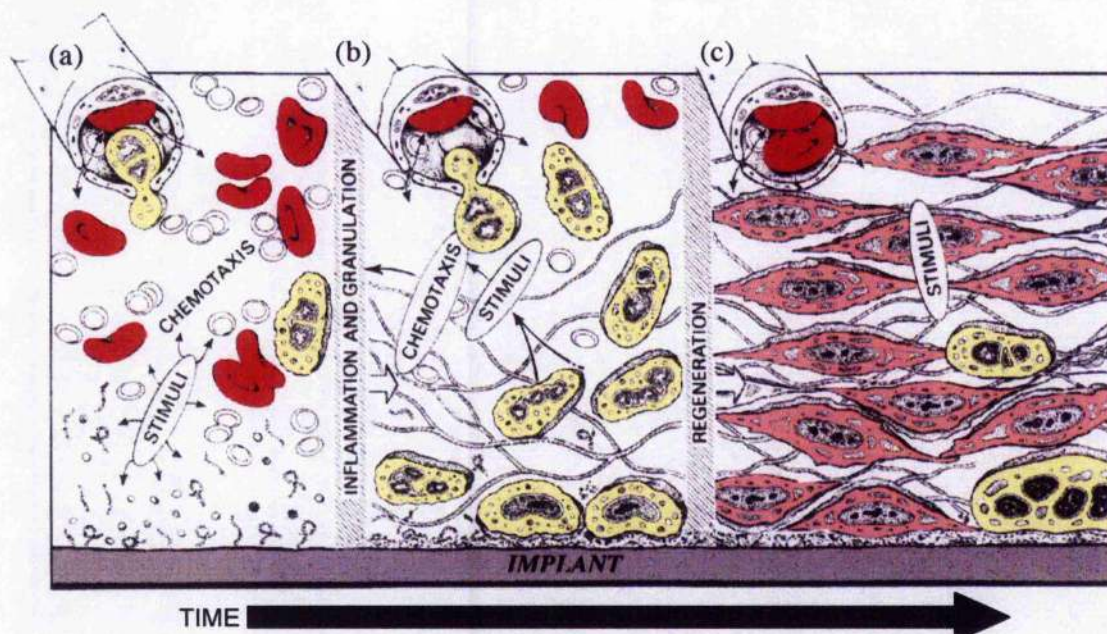


Fig 1.3 – Foreign body response at the implant surface. (a) Insertion of the implant creates a wound site with an influx of blood (red). The activated platelets from the blood produce chemotactic signals drawing neutrophils and macrophages (yellow) to the site. (b) Macrophages dominate the inflammatory reaction adhering to the surface and release growth factors for the recruitment of fibroblasts (pink) and endothelial cells. (c) In the later stages of granulation and eventually remodelling, fibroblasts dominate the area producing a fibrous tissue adherent to the implant surface. Figure reproduced and modified from '16. Titanium in soft tissues' (2001), Holgers, K.-M., Esposito, M., Kalltorp, M. and Thomsen, p517. In *Titanium in medicine*, (eds D. M. Brunette P. Tengvall M. Textor and P. Thomsen). Berlin, Heidelberg, New York: Springer.

Fibrous encapsulation is the body's method of isolating foreign objects that cannot be disposed of (Dee *et al.*, 2002b; Morehead and Holt, 1994) (Fig 1.3). It stems from the granulation phase of wound healing and can produce a tough fibrous tissue mainly consisting of fibroblasts and collagen (Anderson *et al.*, 2004). The fibrous capsule generally adheres to the implant (Fig 1.3c), but in the absence of this adherence the mechanical irritation of the implant/tissue interaction can lead to the formation of thicker fibrous layers and a liquid filled space surrounding the implant (von Recum and van Kooten, 1995). The production of a thicker capsule layer diminishes the blood supply to the region, however, there is also evidence for signalling contributing to this lack of vascularisation. With the utilisation of knockout mice, the absence of a matricellular protein called thrombospondin 2 was found to produce a highly vascularised fibrous capsule (Kyriakides *et al.*, 1999). Apart from inadequate nutrition, the lack of vascularisation can present another severe problem

(Anderson, 1999); any surgical intervention results in bacterial contamination (Clivaz *et al.*, 1990), however, in the instance of the foreign body capsule an immuno-incompetent zone is created by the poorly vascularised fibrous tissue (Gristina, 1994) and the liquid film covering the implant becomes an unregulated zone ideally suited for pathogen proliferation (Ungersbock *et al.*, 1994; Ungersbock *et al.*, 1996). The low oxygen tension at the foreign body site promotes anaerobic bacteria proliferation, while macrophages are unable to function normally (Waldorf and Fawkes, 1995). Therefore, there is an essential need for initial and long term adhesion to the implant as this counteracts the production of this immuno-incompetent zone, but also the early colonisation of the surface by the host tissues allows any small in pathogen to be dealt with before major difficulties arise (Gristina, 1994). This early colonisation is predominantly conducted by fibroblasts, and thus illustrates that implant and soft-tissue integration centralises around fibroblast reactivity with the implant surface.

2.4 – Soft Tissues and Orthopaedic Metals – In Vivo

The importance of fibroblastic integration onto the surface is reinforced further when examining *in vivo* soft tissue reactions with orthopaedic metals. Generally it is assumed that the inflammatory reactions for both stainless steel and titanium are similar and not a significant problem (Rosengren *et al.*, 1996; Voggenreiter *et al.*, 2003). On implanted standard titanium (a rough topography), fibroblasts are the main cell type observed adjacent to the implant on the soft tissue side, with only a few macrophages scattered around the surface (Langford and Frame, 2002).

In vivo, a major issue for successful soft tissue integration of orthopaedic metals appears to be surface roughness; as mentioned previously the standard finishes of SS and titanium differ considerably (Section 1.7). In rabbit and sheep models, the standard rough surface of titanium is generally thought to prevent excessive motion between the implant and soft tissue, and results in the observed formation of a comparatively thin fibrous tissue layer tightly adherent to the implant surface (Ungersbock *et al.*, 1994). The smooth electropolished SS implants induce a thicker fibrous layer observed (Ungersbock *et al.*, 1996), and occasionally lead to the formation of a fluid filled space between the implant

and the fibrous capsule (Ungersbock *et al.*, 1995; Ungersbock *et al.*, 1994). The thicker fibrous tissue and occasional fluid filled space are considered to be formed due to the mechanical irritation of the tissue moving with respect to the implant surface (Perren, 1991). It must be noted in these studies that the plates were implanted at locations of considerable motion. However, the question of topography involvement is far from conclusive in all soft tissue areas; in studies of oral implants no differences were observed in connective tissue attachment for rough and smooth titanium (Abrahamsson *et al.*, 2002; Buser *et al.*, 1992), a viewpoint echoed by Holgers in her review of soft tissue reactions towards titanium (Holgers *et al.*, 2001). Indeed, the question of surface chemistry is also inconclusive, Shannon observed that smooth titanium rods implanted in rats elicited thicker fibrous tissue formation than smooth SS rods (Shannon *et al.*, 1997).

As previously mentioned, the orthopaedic applications of TAN are generally limited to the hard tissue environment while soft tissue studies are rare. TAN's introduction in long bone fracture systems (the LISS system) (Cole *et al.*, 2003; Syed *et al.*, 2004) should have aided in elucidating this soft tissue role, however, the 'high energy' long bone fractures that are addressed by LISS commonly cause severe soft tissue damage and complications, therefore any contributory effect of the metal would not necessarily be attributed and documented (Stannard *et al.*, 2003).

2.5 – Fibroblasts and Orthopaedic Metals - In Vitro

It is difficult to locate initial references to the *in vitro* fibroblast response on the standard implant materials of SS and titanium as both are so widely accepted as implantable metals that they are now considered controls for comparison of new metals and surface treatments (Bordji *et al.*, 1996; Diener *et al.*, 2005; Giordano *et al.*, 2004; Groessner-Schreiber *et al.*, 2002). *In vitro* experiments on SS generally utilise an electropolished surface, as this processing step is integral for the corrosion resistance of the surface. When roughened SS has been studied it resulted in decreased cell spreading (Richards, 1996) but more importantly decreased cell numbers (Bataille *et al.*, 1997). Most cell studies report that cells on electropolished SS become well spread and proliferate rapidly (Bordji *et al.*, 1996; Meredith *et al.*, 2005).

For titanium, surface topography is a contentious topic. As mentioned previously, standard titanium for *in vivo* implantation is roughened as part of its preparation, therefore *in vitro* studies should also utilise this material as a control substrate. However, material roughening results in an un-defined and non-reproducible surface that is totally dependent on the methodology of its manufacture and what might be termed implant quality titanium with a standard topography may in fact vary considerably (Brunette, 1988). Harris and co-workers studied two standard titanium surfaces from different manufacturers and found roughness parameters and consequent fibroblast spreading varied between the surface types (Harris *et al.*, 2005). *In vitro* studies have generally utilised implant quality titanium with smooth surfaces or varying degrees of roughness, however, studies using standard topographies supplied by actual implant manufacturers are rare.

For general cell compatibility with titanium, it is commonly acknowledged that the surface topography affects the cell shape (Brunette, 1988; Brunette, 2001). While the accepted optimal *in vitro* morphology for fibroblasts is a well spread cell, as an indication of sufficient adhesion and growth (see Chapter 3, Introduction), roughened titanium does not interfere significantly with spreading, adhesion or growth (Brunette, 1988; Meredith *et al.*, 2005; Richards, 1996), although these findings are not universal (Kononen *et al.*, 1992; Mustafa *et al.*, 1998). Optimum fibroblast and osteoblast behaviour upon surfaces differ, as a lack of spreading in osteoblasts (a cuboidal morphology) is associated with differentiation into secretory bone-forming cells (Kale *et al.*, 2000). Studies with titanium are therefore focused on encouraging the osteoblast cuboidal morphology by means of surface roughness to promote cell differentiation (Boyan *et al.*, 2003; Martin *et al.*, 1995).

In a similar effort, *in vitro* investigations on TAN have also been more focused on osteoblast activity rather than that of fibroblasts. Studies examining osteoblasts cultured on roughened TAN found them to be less spread than those observed on smooth SS, and also slightly depressed in their proliferation, again in comparison to SS (Schmidt *et al.*, 2001; Schmidt *et al.*, 2002). As mentioned in the previous paragraph, the unspread morphology and low cell proliferation of osteoblasts could be indicative of differentiation on the surfaces (Boyan *et al.*, 2003; Lincks *et al.*, 1998). However, Schmidt also notes a

significantly lower expression of Alkaline Phosphatase, an early osteogenic marker whose activity would be expected to rise early on in the instance of osteoblast differentiation (Lincks *et al.*, 1998; Owen *et al.*, 1990). These findings might indicate that the observed decrease in proliferation was something other than cell differentiation, though this marker alone is insufficient to conclude this.

2.6 – Correlation of *in Vivo* and *in Vitro* Studies

For orthopaedic metals there can be inconsistencies between the soft tissue performance of materials *in vitro* and *in vivo*. For instance, studies have demonstrated *in vitro* that fibroblasts adhere and spread on the smooth SS, however *in vivo* it is perceived in some instances, such as under shear conditions, that the lack of topography can cause the fibrous cell layer to be removed relatively easily. It could be assumed from this *in vivo* observation that the cohesive properties of the fibrous tissue were stronger than the adhesive properties of its constituent cells to the surface. *In vitro*, mechanical interference utilising a 'jet impingement' technique to measure cell adhesion on materials demonstrates that similar forces were required to remove cells from SS compared to a similar roughness of titanium (Bundy *et al.*, 2001). Utilising centrifugation methods, Lotz determined that flat cells with large surface areas were the most adhesive cell morphology (Lotz *et al.*, 1989), a morphology commonly found on smooth SS. To explain the soft tissues apparent preference to rough titanium, Brunette opines that the fibroblast morphology on the rough surface is closer to that found in the three-dimensional matrix found *in vivo* (Brunette, 2001). These inconsistencies between *in vitro* and *in vivo* findings still leave a raft of open questions, and while the mechanical explanation has merit in implant locations experiencing motion and loading, studies into implanted smooth SS and titanium in areas of less motion demonstrated no such spaces and instead noted variation in the ECM structures of the fibrous tissue; thus the influence of material composition cannot be completely discounted (Shannon *et al.*, 1997; von Recum *et al.*, 1993).

While the implications of *in vitro* studies could be criticised by subjective *in vivo* studies, the sheer volume of *in vitro* studies that can be initiated due to their flexibility and low cost far outweigh any drawbacks encountered. *In vivo* studies are limited by ethical and

financial constraints that can influence sample numbers, time intervals chosen and practices employed. *In vitro* studies do not suffer the same constraints as multiple sample types and time intervals amongst other parameters can be utilised, all in a carefully controlled environment (Brunette, 1988; Brunette, 2001). This concept applies for many tissue types and even Davies concludes that *in vitro* methods are invaluable to model tissue mechanisms such as bone formation with regards to implant surfaces (Davies, 1996).

2.7 - The Fibroblast Model for Foreign Body Response

As the main cellular constituent of the foreign body associated fibrous tissue, fibroblasts provide an adequate model for implant/soft tissue integration. Their presence in native loose connective tissues (Campbell, 1996; Kessel and Kardon, 1979) and guided migration into wound healing sites (Waldorf and Fawkes, 1995) ensures that fibroblasts are ubiquitously present close to an implant. Initial fibroblast adhesion *in vitro* is a good representative of how the implant is initially perceived and while *in vivo* the surface would first come in contact with blood, serum protein contained in culture media can serve a similar purpose, however with omitted fibrinogen, and complement factors. The rate of cell growth provides many cues pertaining to the cytotoxicity of the material (Wallin, 1999) and the performance of its surface chemistry (Folkman and Moscona, 1978) and topography (Kononen *et al.*, 1992). Cell growth reaching confluency should be indicative that granulation of the wound site could be achieved, which is a promising sign in material integration.

In relation to metals, macrophage involvement is generally overlooked, especially *in vitro*. Contrary to fibroblasts, macrophage spreading and adherence is encouraged by surface roughness (Rich and Harris, 1981; Wojiak-Stodart *et al.*, 1995), and when investigated on roughened titanium, this trend was also observed (Refai *et al.*, 2005; Takebe *et al.*, 2002). However, the roughened titanium also elicited upregulation of proinflammatory/anti-wound healing cytokines such as interleukins (IL) 6 and tumour necrosis factor- α (TNF- α) (Brodbeck *et al.*, 2002a; Refai *et al.*, 2005), but also IL1 β , a proinflammatory/pro-wound healing cytokine associated with fibroblast proliferation (Brodbeck *et al.*, 2002a). This again illustrates disparity between the *in vivo* and *in vitro* situation. A possible reason for

lack of macrophage studies on orthopaedic metal surfaces is that *in vitro* tissue modelling is generally focused on a single cell type, fibroblasts for soft tissue and osteoblasts for bone. Macrophages are representative of a complex model for inflammation, however they are not the only component of this model (Waldorf and Fawkes, 1995). For implanted metals, the initial inflammatory reaction is unavoidable, however unless an infection develops at the site it eventually subsides (Holgers *et al.*, 2001; Langford and Frame, 2002). Most *in vitro* studies of macrophages relating to metals have been concerned with the hypothesis that their activation by metal debris from periprosthetic hip replacements can initiate bone loss, which poses a serious clinical problem (Haynes *et al.*, 1997; Rogers *et al.*, 1997). Investigations of actual adherence onto biomaterials generally pertain to polymers such as poly(tetrafluoroethylene), a polymer utilised in vascular prostheses, and they concentrate on persistent chronic inflammation as a cause of the material cracking and failure (Brodbeck *et al.*, 2002a; Brodbeck *et al.*, 2002b).

3. Experimental Approach

The initial aim of this work was to investigate *in vitro* fibroblastic response to the orthopaedic grade materials stainless steel, titanium and Ti-6Al-7Nb (TAN), with the primary aim of assessing and comparing the soft tissue response towards TAN. As stated previously, the industrial standard surface finish of the orthopaedic implant materials varies considerably in view of their use in similar applications. For this investigation, electropolished variants of titanium and TAN were specially produced to help distinguish between the effects of the material and those of the topography, further investigated by other means in Chapter 6 and 7. No form of roughened SS was included, as this would decrease its corrosion resistance, deeming it biologically and commercially non-viable as an implant material. All surface finishing techniques were industrially viable and are presently, or in the near future, implemented in the process of surface finishing orthopaedic implant materials. Utilising a fibroblastic cell line, a comprehensive study of cell growth, morphology, adhesion, cytoskeletal aspects and gene regulation was initiated on these materials to attain a broad assessment of cell behaviour of different material types and/or different topographies.

Chapter 2 - Metals and Surfaces

Abstract

This chapter focuses on the surface characterisation of the commonly utilised orthopaedic materials, with standard and experimental finishes, that were studied during the course of this work. Included materials were Stainless Steel in its standard electropolished form, titanium ('commercially pure' Titanium) and TAN (Ti-6Al-7Nb) in standard roughened form and experimental electropolished versions. Also included was a control substrate of Thermanox plastic. All materials were characterised using atomic force microscopy (AFM), profilometry, scanning electron microscopy (SEM) and contact angle measurements to provide a synergistic characterisation methodology. Profilometry and AFM provided strictly topographical assessments while the SEM's various modes help establish not only topography, but elucidate the elemental distribution on the surface. The contact angle method stood alone in examining surface wettability. Thermanox was found to be a hydrophilic polymer with only a nanometric topography. SS had a very smooth topography and its alloyed composition was visible with the SEM. Both electropolished titanium and TAN were not as smooth as the 'Standard' electropolished SS, and both retained unique micro and nanotopographies. For electropolished TAN, the SEM analysis demonstrated that the surface had embedded particles within and on the surface, although their topography was minimised. Both 'standard' preparations of titanium and TAN had similar roughness measurements, however, their topographies varied considerably. Standard titanium had a characteristic 'basket weave' topography, while TAN had an undulating topography punctuated with protruding particles. For standard TAN this microtopography amplified a hydrophobic surface characteristic.

Chapter 2 – Metals and Surfaces

Introduction

The industrial standard surface finish of orthopaedic materials varies considerably in view of their use in similar applications. ‘Standard’ stainless steel has a smooth electropolished finish (Disegi, 1998b) while titanium (‘commercially pure’ titanium) (cpTi) and TAN (Ti-6Al-7Nb) are deliberately roughened to enhance osseointegration (Brunette, 2001). For the purpose of this investigation, specially produced electropolished (smoothed) variants of cpTi and TAN were utilised to help distinguish between the effects of the material and those of the topography in the following chapters. No form of roughened SS was included, as this would decrease its corrosion resistance, deeming it biologically and commercially non-viable. This chapter seeks to evaluate and characterise the sample types included in the study in addition to a control substrate, Thermanox.

Thermanox (polyethylene terephthalate [PET]) is a surface treated (oxidised) plastic that is commonly utilised as a control substrate in biomaterial studies. It has proved a suitable material/surface for studying a number of cell types, which can benefit from highly reproducible results observed utilising the material. The versatility of Thermanox is also extended by the number of specimen preparation methods that are possible using it; however, one drawback is its autofluorescence which can cause excessive background with Rhodamine and FITC labels.

Biomaterial characterisation can be divided into three major fields; bulk characterisation, surface characterisation and biological/toxicology evaluation (von Recum, 1999). For the materials used in this study, the bulk characterisation was very much established from the development of the materials. Surface characterisation is more important due to the varying fabrication methods used by different manufacturers, and is the subject of this chapter. The biological evaluation is covered in the forthcoming chapters. Essentially, this chapter covers a series of surface characterisation methods that complement each other in producing a comprehensive description of the sample types in macro (mm), micro (μm) and nano (nm) dimensions, from a topographical and elemental perspective, numerical characterisation and surface wettability.

White Light Profilometry

Profilometry, also known as Interferometry, is a non-contact technique for gathering height information of a surface topography over relatively large areas. A light source illuminates the surface, and the reflected light is brought into interference with a reference light source. This interference causes a pattern of fringes that can be analysed by the apparatus to allow the determination of height differences (Schmit *et al.*, 2005; von Recum, 1999). The instrument's software can utilise the interference pattern measurements to recreate the vertical axis measurements relative to X,Y axis coordinates, producing a three-dimensional (3D) reconstruction of the surface. A distinct advantage of profilometry is that it is possible to produce accurate height measurements for large areas of the surface. This allows sufficient measurements for the calculation of numerical surface parameter values such as arithmetic mean of the roughness height (R_a) (Brune *et al.*, 1997; Li *et al.*, 2003).

Atomic Force Microscopy

The atomic force microscope (AFM) is a scanning probe instrument with the probe situated in contact with the sample. The probe is a nanometric scale tip attached to a flexible cantilever that is rastered across the specimen surface (Drake *et al.*, 1989; Gadegaard, 2005). As it scans, the tip's height is adjusted in relation to the specimen surface – this height change is controlled by a constantly adjusting piezo electric crystal. The voltage applied to the piezo to adjust the tip height can be converted into height measurements. Advantages of the AFM include nanometric resolution of the specimen with no prior surface preparation (unlike SEM), however, the scanning area is generally reduced by the higher resolution (Grainger and Healy, 1999). The mapping of surface features is limited to those accessible from above, and the lateral resolution is limited by the dimension of the tip.

Scanning Electron Microscopy

Scanning Electron Microscopy (SEM) is a versatile tool used frequently in both material and biological disciplines. It is an electron optical instrument utilising a stream of focused electrons to illuminate the specimen (Bozzola and Russell, 1992; Chapman, 1986). The focused beam of electrons is scanned across the specimen surface; signals generated from

this beam are detected by a scintillator-photomultiplier and translated into an image. The interaction of the impinging electrons produce a variety of signals that can be utilised to build up images of three distinct types: these are secondary electrons (SE), backscattered electrons (BSE) and characteristic X-rays. SE is the most popular detection method, producing a pseudo-3D representation of the specimen topography. BSE provides information about material density and topography, while X-rays provides information about the elemental composition of the specimen (Bozzola and Russell, 1992).

Both SE and X-ray signals are the result of a type of specimen interaction termed inelastic scattering (Everhart *et al.*, 1959; Goldstein *et al.*, 2003). When an electron from the incident beam impinges on an atom from the specimen's uppermost layers, it liberates an electron orbiting this atom (Fig 2.1a). The liberated electron, a secondary electron (SE), possesses a lower energy. It is drawn towards the SE detector kept at a positive potential thus constructing an image of topographic contrast using a scintillator-photomultiplier (Bozzola and Russell, 1992; Chapman, 1986). The incident beam electron loses energy to the specimen. For the impinged atom, the liberation of an electron from a lower energy orbital leaves it temporarily ionised and the vacancy needs to be filled to stabilise the atom. An electron from one of the atoms' higher energy orbitals must drop to fill the vacancy. To enable this, the electron must jettison surplus energy; this energy is released in the form of characteristic X-rays where the energy levels are specific for the atomic number - thus each element emits an unique signature amount of energy (Fig 2.1b) (Morgan, 1985). These can be detected using Energy Dispersive X-Ray (EDX) detectors which are equipped with semi-conductors to measure the characteristic X-Ray emissions from the sample (Bozzola and Russell, 1992; Garratt-Reed and Bell, 2003; Morgan, 1985).

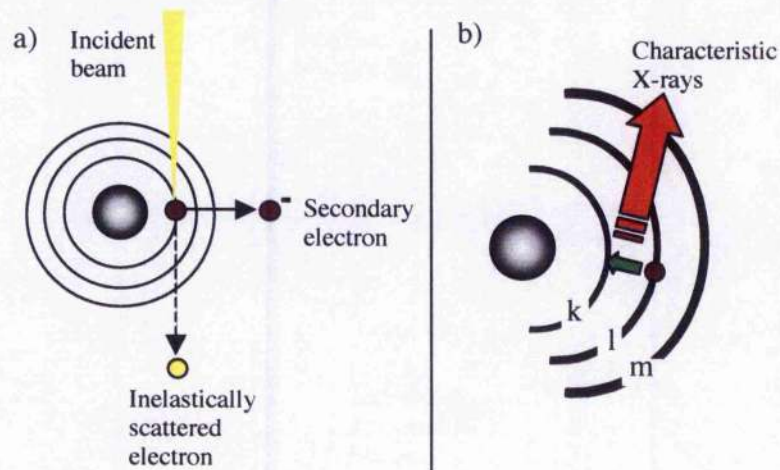


Fig 2.1 – Diagrammatic representation of inelastic scattering. (a) An electron from the incident beam impinges upon an atom from the specimen's uppermost layers liberating an orbiting electron. The liberated electron is a Secondary Electron. The incident beam electron loses energy and transmits into the specimen. (b) The atom is now unstable and therefore an electron from the atoms' higher energy orbital must drop to fill the vacancy. To enable this, energy is released in the form of characteristic X-rays. Modified from Chapman, 1986 and Bozzola and Russell, 1992.

BSE signals result from a type of specimen interaction termed elastic scattering. The incident beam electron collides or passes through at close proximity to the atom's nucleus and changes direction without losing energy (Morgan, 1985). This electron can further transmit through the sample as an elastically scattered electron, interact with other atoms to produce an SE electron, or can be deflected back towards the direction of the incident beam - the latter is known as backscattered electrons (BSE) (Fig 2.2). Their high energy permits them to exit from deeper within the specimen as well as from the surface (Chapman, 1986). The amount of BSE's released is dependent on the atomic number of the element; the denser materials produce a higher number of BSE due to the larger numbered elements having more orbitals for the beam electrons to interact with. When detected by a separate scintillator-photomultiplier, BSE's are displayed in the form of atomic number contrast (Z-contrast), the brighter objects in the specimen are areas of high atomic number with more BSE's (Palluel, 1947; Richards and ap Gwynn, 1995; Richards *et al.*, 1999).

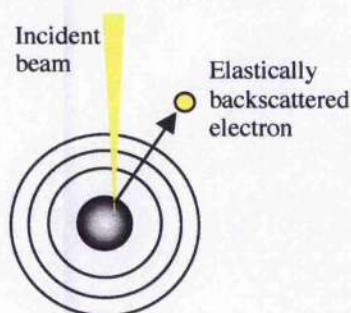


Fig 2.2 - Diagrammatic representation of elastic scattering. The incident beam electron collides or passes through at close proximity to the atom's nucleus and changes direction without losing energy. If the electron is deflected back towards the direction of the incident beam it is known as a backscattered electron (BSE). Adapted from Bozzola and Russell, 1992.

During the course of this work all signal detection methods were used to help answer various questions posed. For the material and surface characterisation SE and BSE were utilised while EDX was not used in this capacity as the sample composition was already well documented (Disegi, 1993; Disegi, 1998a; Disegi, 1998b). EDX also has a disadvantage in that X-rays are produced from up to 1 μ m of sample depth therefore details of the surface chemistry of alloyed samples might be misrepresentative of the immediate surface (Kasemo and Lausmaa, 1988).

Contact Angle Measurement

Solid-liquid-vapour contact angle measurement is a sensitive method for assessing a material's wetting properties. It is used as a qualitative measurement of a solid's chemistry by a liquid, and is defined as the angle formed by a liquid at the three-phase boundary where a liquid, gas and solid intersect (Fig 2.3). Water is chosen as the probe because it is clean and also the simplest biologically relevant environment for measurement, and because of its dipole characteristics which allow for a high surface tension (Andrade, 1985a; Andrade, 1985b). A high water contact angle indicates a specimen's hydrophobic properties; the water droplet cannot spread as its molecules are attracted more to each other than to the specimen surface.

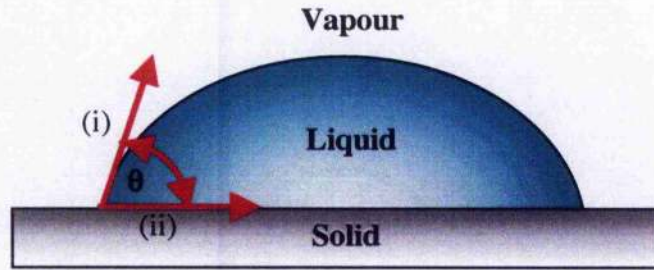


Fig 2.3 – The contact angle (θ) is measured as the angle between the liquid-vapour axis (i) and the solid-liquid line (ii). Modified from Andrade, 1985b.

Materials and Methods

All sample types were produced in 11mm diameter discs and larger 49mm diameter discs. The disc manufacturing methods are included in Table 2.1. Due to manufacturing costs only a limited supply of the larger 49mm discs was produced and these were used only for molecular work described in Chapter 3: Experiment 6 and Chapter 5: Experiment 11. All other work was conducted using the smaller 11mm diameter discs. A control substrate was included in all studies in the form of a tissue culture plastic, Thermanox™ (polyethylene terephthalate, Nalge Nunc International, USA). There were used in the form of 13mm discs (Cat No. 174950) or modified from 22 x 66mm rectangles (Cat No. 174942).

<i>Material</i>	<i>Denoting Symbol</i>	<i>Raw Material</i>	<i>Band Grinding (grit¹)</i>	<i>Vibratory Grinding (ceramic tumbling)</i>	<i>Ball Blasted</i>	<i>Pickled (Acid etching)</i>	<i>Electropolished</i>	<i>Anodised</i>	<i>Gamma sterilised</i>
cp. Titanium	TS ²	Sheet	320	✓	INOX ³	✓	-	Gold colour (55V)	✓
	TE	Sheet	220 & 320	✓	-	✓	✓ (Steiger SA)	Gold (55V)	✓
Ti-6Al-7Ni	NS ²	Bar	220 & 320	✓	INOX	✓	-	Gold (57V)	✓
	NE	Bar	220 & 320	✓	-	✓	✓ (Steiger SA)	Gold (57V)	✓
Stainless Steel	SS ²	Sheet	320	-	-	-	✓ (Mathys AG)	-	✓

Table 2.1 – A summary of sample types used and processes employed in the course of their manufacture. ¹Ceramic grit particle size, ²Material in 'standard form' ³INOX stainless steel balls.

Experiment 1 – White Light Profilometry

Two examples of each sample type were quantitatively measured with a non-contact 'white-light' FRT MicroProf® 200 Profilometer (Fries Research & Technology, Germany). Roughness average (Ra - arithmetic mean of the roughness height) (Equation 2.1) was measured from a 2mm x 2mm analysis area scan at a point density of 500 points/mm. Prior to roughness calculations a linear regression to eliminate surface inclinations was performed on each profile with the L_c (cut-off) set to 0.4mm. Six separate points were scanned split between the two samples of each type. A three dimensional representation of one of these points was produced to provide a visual representation of the scan.

$$Ra = \frac{1}{LxLy} \int_0^{Ly} \int_0^{Lx} |h(x,y)| dx dy$$

Equation 2.1 – Formula used to calculate the Roughness average, defined as the roughness height arithmetic mean. $h(x,y)$ represents the height distribution on the surface. Lx and Ly are the dimensions of the projected plane on the surface. Equation taken from Li et al., 2003.

Experiment 2 – Atomic Force Microscopy

Atomic Force Microscopy (AFM) measurements were performed using either a Digital Instruments Dimension 3100 in ‘tapping mode’ or a Digital Instruments MultiMode IIIa in ‘contact mode’. Measurement data were processed using Nanoscope software (Digital Instruments). A three-dimensional representation of the measurements was created for each surface.

Experiment 3 – Scanning Electron Microscopy

The morphology of the sample type surface was examined using a Hitachi S4100 field emission Scanning Electron Microscope (FESEM) fitted with an Auratya yttrium aluminium garnet (YAG) backscattered electron (BSE) scintillator type detector. The images were taken in both secondary electron mode (SE) and BSE, with an accelerating voltage of 5kV, an emission current of 45 μ A, an aperture of 100mm (apt1), working distance of 12mm and a positive tilt of 15°.

Experiment 4 – Contact Angle Measurements

Contact angle measurements were conducted using a Drop Shape Analysis System (Contact Angle Measuring Instrument G10 and Control Unit DSA 10, KRÜSS GmbH). Samples were placed in a preheated chamber (20°C) with an additional water source to maintain a steady humidity. 20 μ l droplets were dispensed using the computer-controlled apparatus. The resulting water droplet was imaged exactly 1 minute after the drop was dispensed onto the sample surface. The contact angle was extracted from the resulting image using the ‘Tangent-Method 1’ angle measurement method using Drop Shape Analysis 1.50 software (KRÜSS GmbH). In this instance, the angle between the baseline of the H₂O drop, and the tangent line originating from the drop boundary is measured. Two separate measurements

were possible on one 12mm sample. These measurements were repeated on a further 2 examples of each sample type, making a total of 6 measurements (except TE and NE, these measurements were only conducted twice due to sample number limitations).

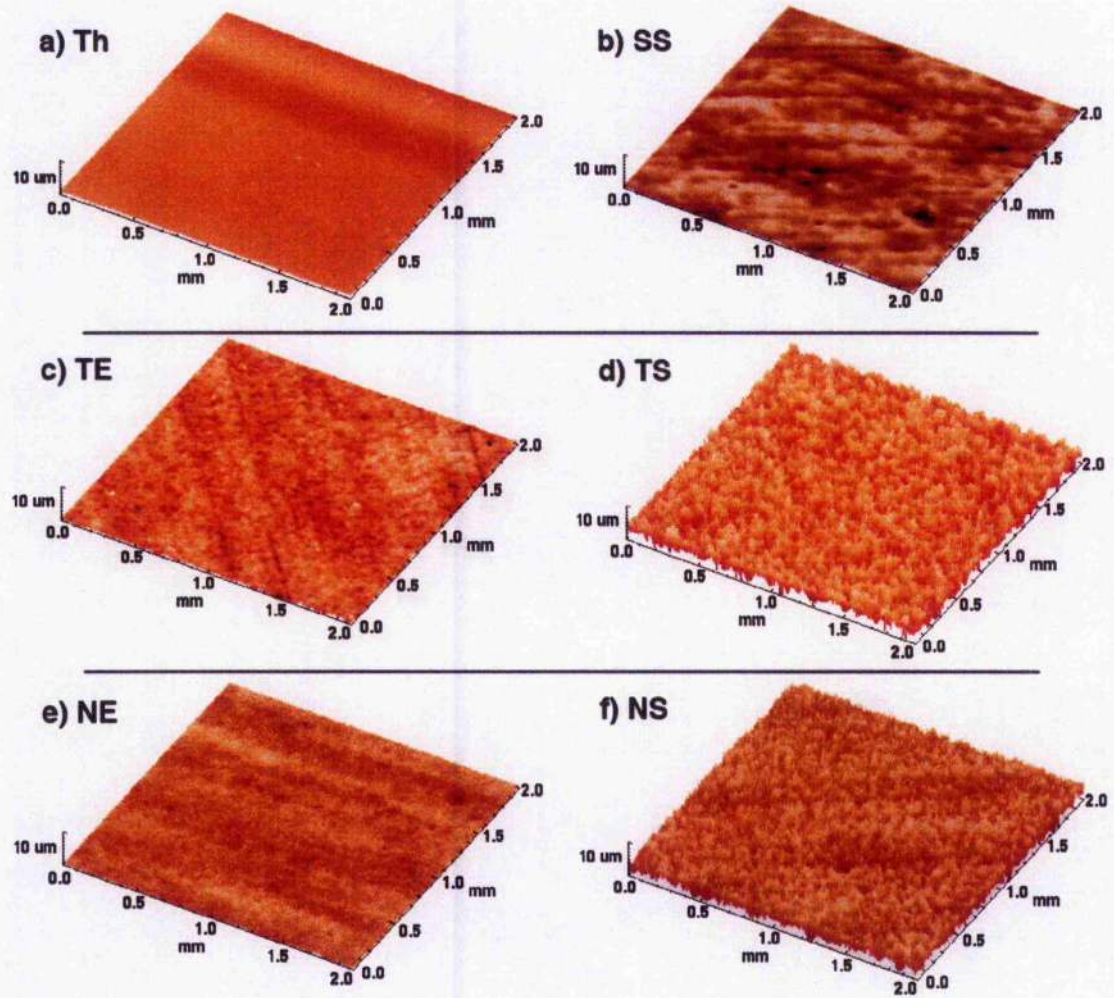
Results*Experiment 1 - White Light Profilometry*

Figure 2.4 – 3D profile of a scanned area for each of the test samples.

<i>Sample</i>	<i>Mean Ra (μm)</i>	<i>Standard Deviation (μm)</i>
Th	0.14	± 0.045
SS	0.19	± 0.022
TE	0.19	± 0.030
TS	0.90	± 0.027
NE	0.18	± 0.037
NS	0.77	± 0.076

Table 2.2 – Mean Roughness Average and Standard Deviation of 6 measurements divided between two examples of each sample type.

Profilometry of large surface areas of the sample demonstrate two distinct sample types; smooth and rough. The smoother surfaces include Thermanox and the three electropolished materials (SS, TE and NE), these all have very similar Ra's all within $0.05\mu\text{m}$ of each other and the 3D profile demonstrates no notable surface features (Fig 2.4 a,b,c,e). The rougher materials, TS and NS, also have similar Ra's and the 3D profile demonstrate quite similar surface features (Fig 2.4 d,f).

Experiment 2 – Atomic Force Microscopy

AFM measurements of the sample surfaces demonstrated that Thermanox was not unblemished, but appeared to be chemically etched with a very fine topographical roughness (Fig 2.5a). SS was demonstrated to be a very smooth material; the diagonal lines on the surface were artefact from the tip scanning the surface (Fig 2.5b). TE was relatively smooth, however some surface detail remains on the surface after electropolishing (Fig 2.5c). TS was again confirmed to be a rough surface, this roughness taking the form of jagged cuts into the surface (Fig 2.5d). NE was shown to have a uniform undulating topography dissimilar to the other two electropolished metal surfaces (Fig 2.5e). NS displayed a rough surface; its main roughness features consisted of numerous 'microspikes' (Fig 2.5e).

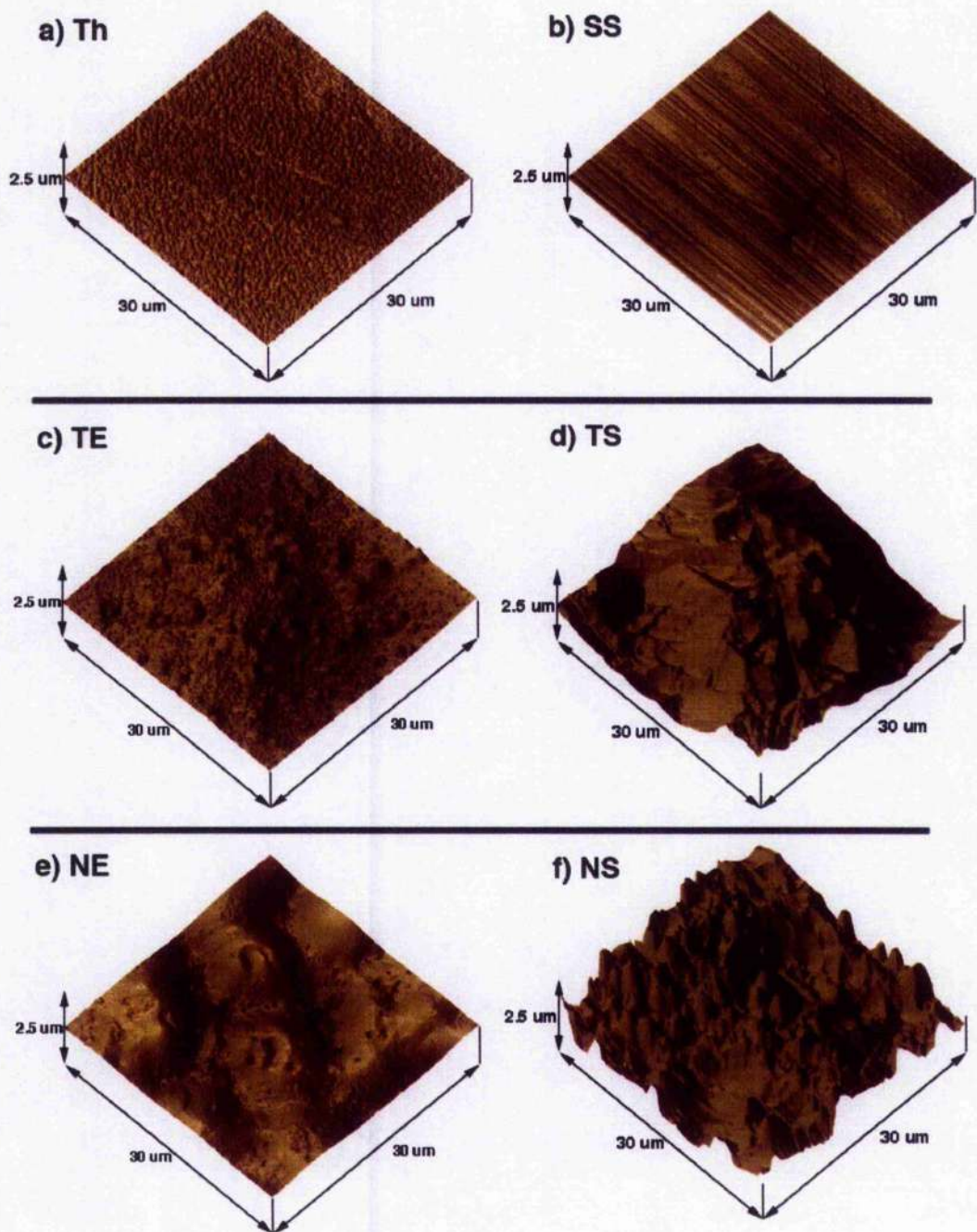


Fig 2.5 – Pseudo-3D representation of AFM measurements of the sample surfaces. (a) Thermanox was a chemically etched surface with a very fine topographical roughness. (b) SS was demonstrated to be a very smooth material - the diagonal lines on the surface were artefact. (c) TE had some surface detail remaining on the surface after electropolishing. (d) TS had a rough surface, this roughness taking the form of jagged cuts into the surface. (e) NE had a uniform undulating topography dissimilar to the other two electropolished metal surfaces. (f) NS displayed a rough surface; its main roughness features consisted of numerous 'micro-spikes'.

Experiment 3 – Scanning Electron Microscopy

Samples were imaged with both the Secondary Electron (SE) detector and Backscattered Electron detector (BSE) modes.

Thermanox

Due to the lack of topography on the surface of Thermanox, it was very difficult to find a point for focusing on the surface. Only small micrometer disturbances on the surface were visible along with handling scratches (Fig 2.6). The surface detail was primarily visible in SE mode; BSE mode did not expand upon the detail revealed in SE.

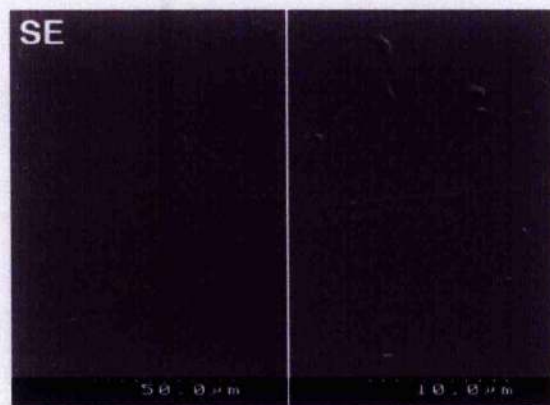


Fig 2.6 – SE mode image of Thermanox. There was very little surface detail visible, only micrometer disturbances and scratches on an otherwise smooth surface.

SS - Stainless Steel

SE image of the surface demonstrated a very smooth topography with only small scratches from handling during and after the manufacturing process. It was also possible to resolve a faint outline 'marble-like' contrast of its alloyed constituent elements (Fig 2.7a). This was more apparent when looking at the BSE image; here the densities of the alloying elements are better contrasted (Fig 2.7b).

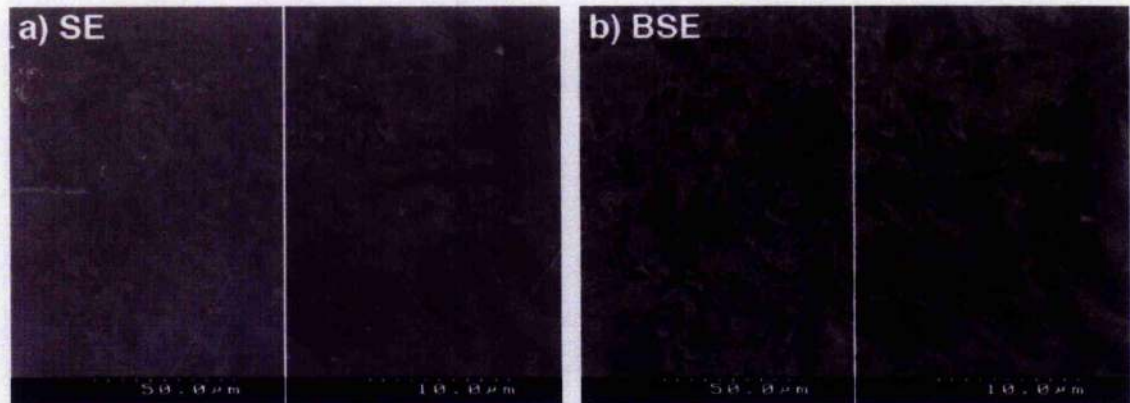


Fig 2.7 – SS – (a) SE imaging of the surface demonstrates a very smooth surface with no visible topographical detail. (b) BSE demonstrates the material's alloyed constituent elements are present in a 'marble-like' pattern.

TE – Electropolished Titanium

In SE mode the surface appeared to be relatively smooth, interspersed with small nodules of nano and micrometric dimensions. (Fig 2.8a). While these nodules were contrasted from the underlying surface in SE mode, in BSE there was no contrast difference suggesting that they were not elementally different from the base surface material. In addition to the nodule topography, a smaller nano-pit topography was visible at the higher magnification BSE mode (Fig 2.8b).

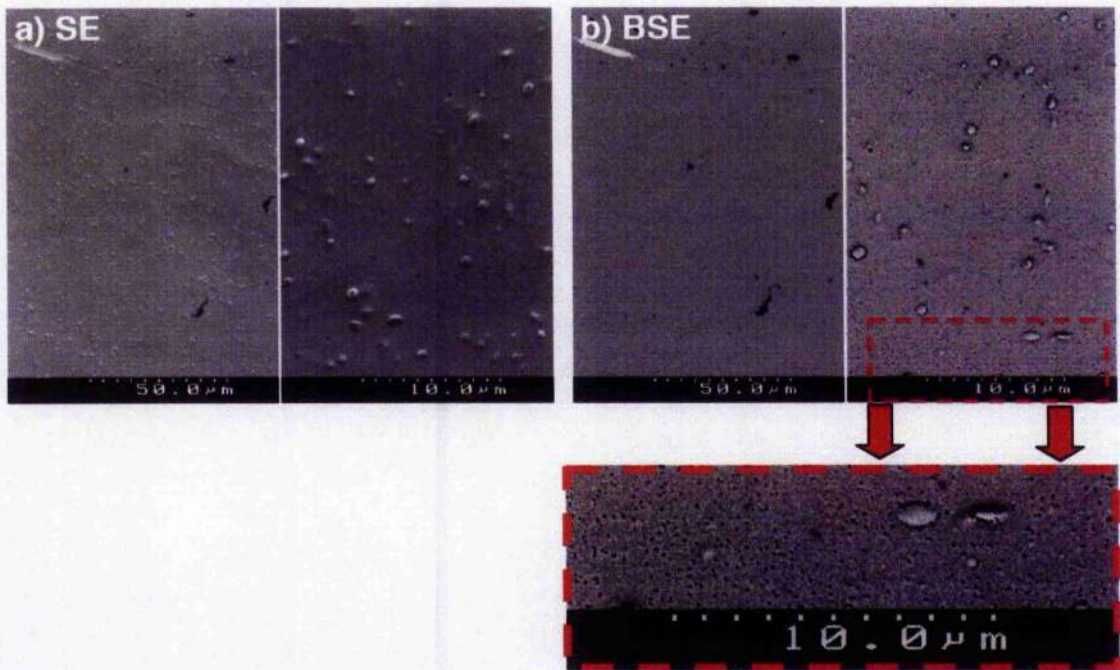


Fig 2.8 – TE (a) In SE the surface was relatively smooth, interspersed with small hills of nano and micrometric dimensions. (b) BSE demonstrates that the nodules were not elementally different from the base surface material (lack of contrast). In addition to the nodule topography, a smaller nano-pit topography was visible at the higher magnification BSE mode.

TS – Standard Titanium

In SE mode the surface of TS was rough, taking the form of jagged ‘right angled’ changes in topography height, similar to a ‘basket-weave’ pattern (Fig 2.9a). The BSE mode demonstrated that the surface was elementally homogenous, with only some contaminants in the form of black specks (of lower density). It was possible at the higher magnification to see the ‘basket-weave’ effect more clearly (Fig 2.9b).

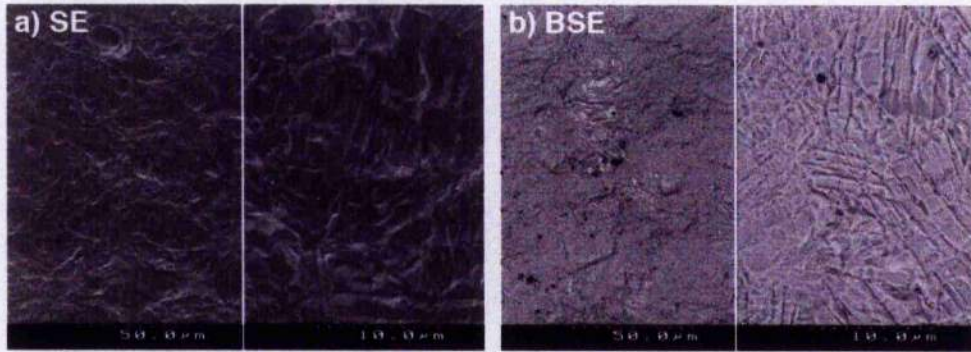


Fig 2.9 – TS (a) In SE mode, the surface has a rough topography; this takes form as jagged ‘right angled’ changes in topography height similar to a ‘basket-weave’ pattern. (b) The BSE mode demonstrated that the surface was elementally homogenous. It was possible at the higher magnification to see the ‘basket-weave’ effect more clearly.

NE - Electropolished TAN

In SE mode, the undulating topography of NE was confirmed. At a higher magnification, an additional topography could be seen in the form of small metal particles embedded in the surface (Fig 2.10a). Compositional contrast with BSE mode imaging showed that these particles were elementally different from the base material of the sample surface (Fig 2.10b).

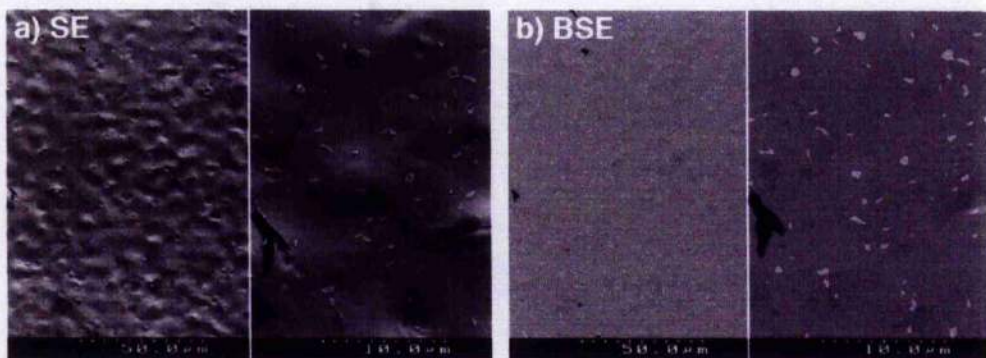


Fig 2.10 – NE (a) Low magnification SE mode imaging demonstrates an undulating surface. High magnification demonstrated an additional topography in the form of embedded small metal particles. (b) BSE mode compositional contrast demonstrates that the particles were elementally different from the base material.

NS – Standard TAN

In SE mode, the overall appearance of the NS topography at a low magnification could be likened to that of opaque patterned glass (Fig 2.11a). There was an undulating topography punctuated by protruding microspikes. At a higher magnification the microspikes were revealed to be metallic particles protruding from the surface of the base material, their shapes being random but had a length averaging between 1-4 μm (Fig 2.11a). In BSE mode, a compositional contrast of the material demonstrated that the particles were elementally different from the base material (Fig 2.11b). There was also a high amount of surface contamination present as black specks (lower density).

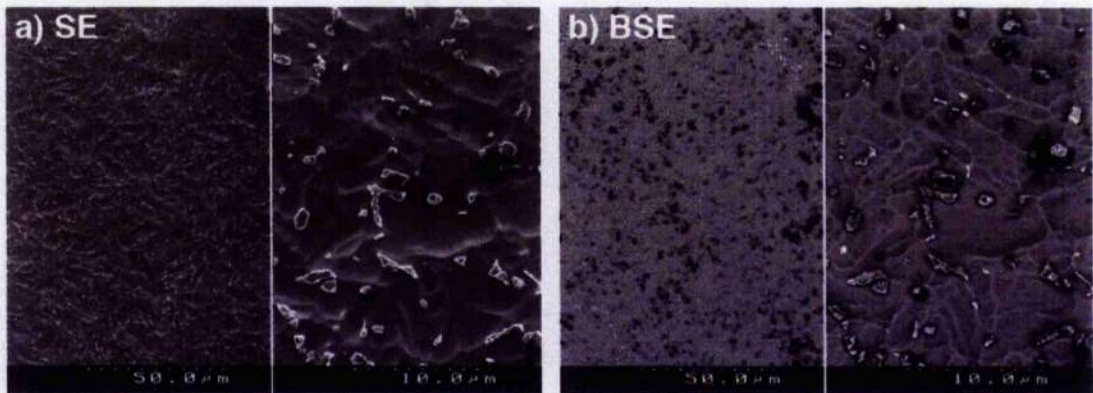


Fig 2.11 – NS (a) In SE mode, the surface was an undulating rough surface punctuated with metallic particles protruding from the surface. (b) In BSE mode, the particles could be seen to be elementally different from the base material. There was also a high amount of surface contamination present as black specks.

Experiment 4 – Contact Angle Measurements

Sample	Contact Angle
Th	67.7° ± 1.9
SS	73.1° ± 9.9
TE*	78.4°
TS	80.2° ± 2.3
NE*	78.6°
NS	85.2° ± 3.3

Table 2.3 – List of mean contact angle measurements for the materials. (6 repeats of 3 samples)

*Due to sample shortages, these samples were averaged over 2 measurements.

The contact angle measurements follow a roughness trend - the electropolished samples having the lowest angle while the rougher standard preparations provide the higher angles increasing in this order - Th<SS<TE<NE<TS<NS.

Discussion

The four characterisation methods provide exclusive information about the sample types, but also combine to provide a synergistic characterisation methodology. While Profilometry and AFM are strictly topographical assessments, the SEM's various modes help establish not only topography, but elucidate the elemental distribution on the surface. The contact angle method stands alone in looking at a separate biologically relevant aspect of surface wettability. Clinically, when the biomaterial is implanted it instantly comes into contact with an aqueous environment (Andrade, 1985) consisting of water, dissolved ions and free biomolecules derived from blood (Kasemo and Lausmaa, 1988). This initial interaction with the surface dictates the long term performance of the implant as cells will only 'see' the absorbed biomolecules on the implant surface, therefore any information pertinent to this initial interaction is welcome.

Profilometry

Both the 3D profiles and the numerical representation (Ra) of the samples point to two surface groups regardless of their raw material composition. The smooth samples were predominantly electropolished, bar Thermanox. Using SS as the 'benchmark' for an orthopaedic grade smooth surface preparation, it is clear that the chosen treatments of electropolishing titanium (TE) and TAN (NE) compare favourably at this scale, with both Ra's and 3D profiles showing a lack of any significant surface detail. The Thermanox control substrate also falls within this 'smooth' surface category. The 'rough' surface category contains the standard preparations of titanium (TS) and TAN (NS). The surface preparation of both these samples demonstrates consistency in producing surfaces of similar Ra's with indistinguishable 3D profiles.

Atomic Force Microscopy

With the assistance of the AFM's nanometric resolution, numerous profilometry-based conclusions were immediately dispelled. Although flat at the 1000nm scale, all the surfaces, even the 'smooth' ones, had nano or micrometric topographical features. While SS was still the smoothest orthopaedic grade surface, it had numerous handling scratches. TE and NE in fact had notable topographies demonstrating that the electropolishing step

produced different results for different materials. Thermanox also appears to have a pitted surface confirming the surface etching treatment employed for finishing. Secondly, the standard surface treatment of titanium (TS) and TAN (NS) produced different surface morphologies. TS had a rugged surface consisting of jagged cuts into the surface, while NS had a distinct ‘microspiked’ topography that appeared to have some uniformity.

Scanning Electron Microscopy

SEM analysis, utilising SE and BSE modes, aided in elucidating additional surface characteristics as well as resolving questions raised from the previous analysis methods. Thermanox was a very smooth surface with minimal surface detail. SS was confirmed to be a very smooth surface and it was also demonstrated that the parallel lines seen in AFM images (Fig 2.5b) were due to an artefact. In BSE mode, the atomic number contrast demonstrates the SS’s inhomogeneous alloyed composition (Disegi, 1998). A faint outline of this contrast was also visible in the SE image; this is due to the fact that a small amount of BSE interacts with the SE detector (Everhart *et al.*, 1959).

For the titanium-derived samples of TE and TS, the SEM analysis confirmed the previous observations. The electropolished sample surface (TE) was covered in nodules, first observed in the AFM. The atomic number contrast demonstrated that the density of these nodules and the base material was homogenous. It also demonstrated that the electropolishing process produces another surface feature – nano-pits which cover the whole surface. For TS it is clear at a higher magnification in BSE mode that the surface topography has a level of organisation to it. The surface appears to have sets of parallel cuts that orientate themselves to appear similarly to a ‘basket-weave’. This topography is known in metallurgy as a lamellar microstructure and appears during the initial processing of the raw titanium when cooling from β to α -phase (Layens and Peters, 2003). Its prominence on the TS surfaces is due to the pickling process employed to clean and roughen the surface of all titanium and TAN samples (Sittig *et al.*, 1999b). Pickling is a form of acid etching, in this case a mix of nitric and hydrofluoric acid, which effectively dissolves the outer layer of the material. It characteristically dissolves more titanium at grain boundaries – in the instance of TS these boundaries are the lamella (Sittig *et al.*,

1999b). The topography is obscured in TE due to the electrochemical etching process being non-selective to boundaries or other structures.

SEM analysis yielded the most significant findings for the TAN derived samples of NE and NS. For NE, the undulating topography observed with the AFM was confirmed in SE mode, a probable cause for this might be that these represent the α -phase grain boundaries. Secondly, visible at high magnification in SE mode are embedded particles about a micron in diameter. BSE analysis demonstrates that the atomic number contrast of these particles differ from the base material. For NS, the surface is relatively rough and is punctuated again by protruding particles, albeit larger and more prominent. This was a surface aspect that was undetected prior to SEM analysis, as all were aspects previously thought to be part of the general roughened topography. The elementally different particles found in both NE and NS were particles of β -phase titanium. As mentioned in the previous chapter (Chapter 1; Section 1.5), TAN is an $\alpha+\beta$ duplex alloy with aluminium enriching the α -phase titanium and niobium stabilising the β -phase titanium. The notable microtopography of NS was due to the pickling process (Disegi, 1993; Sittig *et al.*, 1999b). The harder β -phase particles dissolve at a slower rate than the α -phase, thus creating the protruding β -phase seen here and in other studies (Sittig *et al.*, 1999b; Textor *et al.*, 2001). Their prominence in NE is diminished due to the electrochemical etching process (electropolishing) being non-selective.

Contact Angle

While no distinct grouping of the sample types could be observed with the contact angle measurements, there was a correlation with the scale of roughness - generally the rougher the surface (defined by Ra), the more hydrophobic it was. The relationship of surface roughness and surface wetting properties is a contentious topic, although the general consensus is that the introduction of a rougher topography only enhances an already hydrophobic or hydrophilic surface chemistry (Martines *et al.*, 2005). However, studies have demonstrated that controlling the surface nanostructure can induce more hydrophobic properties (Adbelsalam *et al.*, 2005).

In the instance of Thermanox surfaces, the plastic has a proprietary surface treatment (oxidisation) to enhance cell attachment and growth, however, from the measurements it would appear that this treatment creates a hydrophilic surface (in comparison with the other sample types). If the goal is protein binding, as a precursor to cell attachment, this seems rather odd as hydrophilic surfaces tend to bind less protein (Dee *et al.*, 2002; Vogler, 1998). Kasemo points out that hydrophilic surfaces maintain a layer of water that allows for protein interaction with minimal conformation change, while with hydrophobic surfaces the absorption occurs directly with the surface and can cause conformation changes that are possibly undesirable (Kasemo and Lausmaa, 1988). Contact angle measurements for stainless steel were similarly low, however as its biological interaction has a clinically proven 'track record' it is probably cytocompatible.

Both the electropolished (TE) and standard finish (TS) titanium had similar values. As a final manufacturing step, all titanium and TAN derived surfaces underwent anodisation. Anodisation is an electrochemical process that increases the inert oxide layer on the material surface (Disegi, 1997). For titanium, the oxide layer is primarily composed of TiO_2 with marginal additions of TiO and Ti_2O_3 (Kasemo, 1983; Kasemo and Lausmaa, 1988). As the chemistry is similar for TE and TS, the only difference in surface composition was an increase in the surface area. The larger area surface interaction (Dee *et al.*, 2002) is the likely explanation for the relatively small increase in hydrophobicity between the two measurements. In the literature, contact angle measurements for rough titanium can be found varying between 33° and 89° , however, as the industrial manufacture of titanium varies considerably there appears to be no right or wrong figure in this context (Taborelli *et al.*, 1997; Walivaara *et al.*, 1994).

For TAN derived materials, the difference in measurements between the electropolished and standard finish was greater. A possible reason, as previously stated for titanium, was the larger surface area of the standard finish. Another possibility lies in that the oxide layer of TAN is somewhat more complex (Sittig *et al.*, 1999a; Sittig *et al.*, 1999b; Textor *et al.*, 2001). Work by Sittig examining polished and pickled surfaces demonstrated that while titanium oxides are found throughout the layer, oxides of the aluminium and niobium

stabilising elements were found in topographical relation to the underlying surface composition (Disegi, 1993; Sittig *et al.*, 1999b). Al_2O_3 , found above the α -phase, was considerably increased in the oxide layer on both types. Ni_2O_3 was generally found to be less in volume than the bulk, however an increase in β -phase particle exposure by pickling increases the concentration of Ni_2O_3 in these areas up to six-fold (Sittig *et al.*, 1999a; Textor *et al.*, 2001). These changes in composition alter the surface's isoelectric point (IEP) and could consequently affect the hydrophobic properties of the surface (Sittig *et al.*, 1999a; Sittig *et al.*, 1999b).

Summary

Sample	Comments
Th	A hydrophilic polymer with only a nanometric topography visible through AFM analysis.
SS	The 'benchmark' smooth orthopaedic grade metal. Its alloyed composition was visible only in BSE mode of the SEM.
TE	The experimental surface treatment compared well to SS with only some nanometric details visible on the surface.
TS	The benchmark 'roughened' orthopaedic grade metal. The surface treatments produce a characteristic topography.
NE	The experimental surface treatment smoothed the complex topography to an undulating morphology. BSE mode detection demonstrated that the β -phase particles were maintained on the surface, although their topography was minimised.
NS	The standard surface treatment amplifies the microstructural components with the β -phase particles gaining considerable prominence. This structure also amplifies a hydrophobic surface characteristic.

Chapter 3 – Cell Growth, Morphology & Adhesion

Abstract

The investigation of cell growth, morphology and adhesion provides a comprehensive basis with which to establish a material or topography's cytocompatibility. The smooth metal topographies of SS, TE and NE, in addition to control Th, were demonstrated to both qualitatively and quantitatively allow for favourable cell growth. For TS, the roughened topography was not inhibitory to cell growth on the surface, however NS demonstrated considerable growth impairment. Cell morphology was observed to be well spread on all the smooth metal topographies, however the micro and nano-topography measured on TE and NE did influence cell spreading. TS's roughened topography was observed to influence cell spreading however this was not confirmed quantitatively. The roughened microtopography of NS visibly and quantitatively changed the morphology with adherent cells being less spread and more elongated. Surface roughness also visibly and quantitatively impaired the mean number and length of focal adhesions, which were lower in both number and size on TS and lowest on NS. Based on these measurements and observations I propose that the impairment of focal adhesion maturation and cell spreading to a possibly sufficient threshold blocks cell cycle progress and eventually cell growth on NS. Two features of NS thought to influence the resulting cell growth are the surface chemistry and surface topography, however the influence of β -phase particle endocytosis and ion leeching could not be discounted.

Chapter 3 – Cell Growth, Morphology & Adhesion

Introduction

For *in vitro* characterisation of cell behaviour and compatibility, cell morphology and growth encompass many essential biological processes. With many *in vitro* biomaterial studies, there is a tendency to examine these aspects without realising that apparently simple processes such as adhesion and growth are in fact very complex and still not fully understood, and knowledge of these processes can enhance the conclusions drawn concerning the biomaterials in question. Non-transformed cell growth depends on two phenomena - anchorage and cell-shape – which are generally combined in stating the cells' requirement of substrate attachment and modulation of cell morphology to permit cell growth (Folkman and Moscona, 1978; Iwig and Glaesser, 1991).

Cell Adhesion

In vitro, cells utilise several mechanisms for attaching to substrates which are mediated through absorbed extracellular matrix (ECM), including focal adhesions, focal complexes and fibrillar adhesions (Chen *et al.*, 2004). The adhesion types can be differentiated by their molecular components (Zamir *et al.*, 2000), abundance and proximity to the substratum (Chen and Singer, 1982). Focal adhesions and their precursors, focal complexes (Geiger and Bershadsky, 2001), are the strongest adhesion points, and the closest, normally within 10-20nm of the substrate (Chen and Singer, 1982; Curtis and Varde, 1964; Izzard and Lochner, 1976). They are made up of a molecularly complex and diverse group of proteins (over 50) which have been separated by their function into: cytoskeletal proteins, tyrosine kinases, serine/threonine kinases, modulators of small GTPases, phosphatases and other enzymes (Zamir and Geiger, 2001a; Zamir and Geiger, 2001b). The cytoskeletal group of proteins are the most established (in terms of published structural arrangements) and provide a basic structural outline from extracellular connection to the actin stress fibre. Integrins are a set of diverse ubiquitous, heterodimers - transmembrane proteins that attach 'head-on' to the ECM (Hynes and Bader, 1997) forming the first part of the link. Intracellularly, a variety of linker proteins, including vinculin, paxillin and talin, establish a

cascade that attaches the integrins to the capped end of F-actin fibres thus completing the link (Bershadsky and Geiger, 1999).

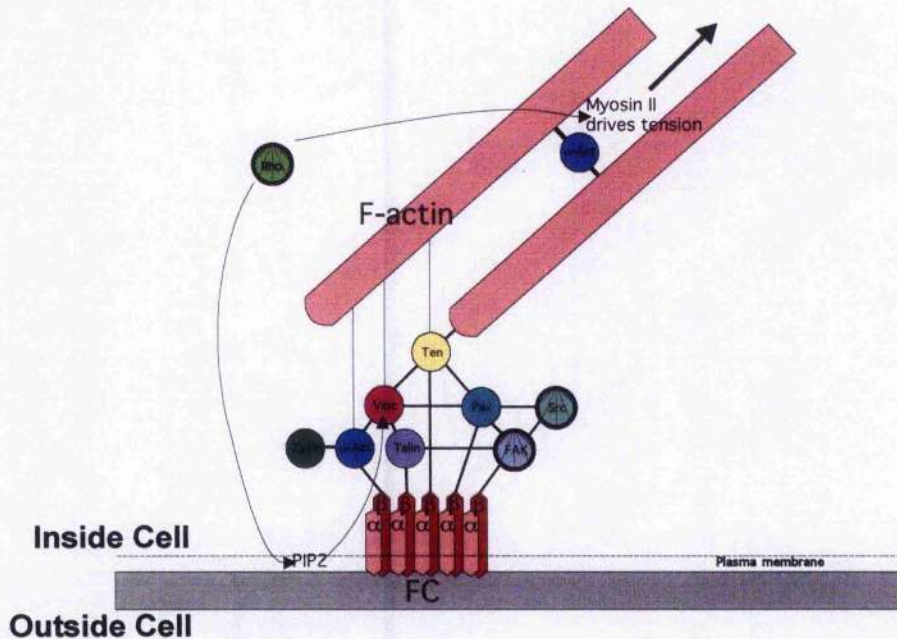


Fig 3.1 – A simplified diagram of the cytoskeletal protein structure at a focal adhesion site and demonstrating the currently assumed structure from integrins to F-actin. ‘ α ’ and ‘ β ’ integrins, present at the plasma membrane, attach to ECM ligands. Intracellularly, Talin, α -Actinin (α -Act), Vinculin (Vinc), Paxillin (Pax,) Tensin (Ten) and Zyxin form the cytoskeletal link required to complete the mechanical link from the outside of the cell to F-actin. FAK, Src and Rho are included to demonstrate the possible course of the numerous signalling cascades. Adapted from Kreis and Vale, 1999.

The control mechanisms for the formation and maturation of focal adhesions are still a ‘hot topic’ of debate, however some basic steps of the process have been elucidated. The attachment of α and β integrins subunits to ECM ligands trigger a conformational change facilitating the attachment of the integrin β -subunit to actin filaments (Bershadsky *et al.*, 2003; Burridge and Chrzanowska-Wodnicka, 1996; Kreis and Vale, 1999) through a structure containing vinculin, paxillin and phosphotyrosine (Nobes and Hall, 1995; Zimmerman *et al.*, 2004). These small structures are known as focal complexes and are the precursors for mature focal adhesions (Chen *et al.*, 2004). The signalling involved in this initial assembly is still unclear, however members of the Rho-family G-protein, Rac and Cdc42 are initially involved (Nobes and Hall, 1995; Rottner *et al.*, 1999) along with the association of Focal Adhesion Kinase (FAK) (Schen and Schaller, 1999). The maturation of

the complex into an adhesion requires the activation of Rho that in turn activates two essential pathways; myosin-II driven stress fibre contractility and local and global actin polymerisation (Chen *et al.*, 2004; Geiger *et al.*, 2001). Tension from the attached fibres pulls at focal contacts promoting the incorporation and assembly of new protein components thus increasing its size (Bershadsky *et al.*, 2003; Chen *et al.*, 1997; Geiger and Bershadsky, 2001). Again, the mechanism of this protein incorporation is subject to debate (Geiger and Bershadsky, 2002), however mature 'dash' morphology focal adhesion sites of 2-10 μm in length and 0.5 μm in width are the result (Bershadsky *et al.*, 1985).

The complex and as yet unresolved pathways of focal adhesion formation and maturation reveal some of the roles that the structure plays. In addition to anchorage of the cell, focal adhesions function as 'mechanosensors' reporting on the external chemical and physical environment through contact with the ECM (Geiger and Bershadsky, 2001; Geiger and Bershadsky, 2002). These signals are perceived through the integrin and transmitted through a signalling cascade of Src and FAK eventually leading to mitogen activated protein kinase (MAPK) cascades capable of controlling gene expression (Boudreau and Jones, 1999; Burridge and Chrzanowska-Wodnicka, 1996). This process is known as signal transduction (Chen *et al.*, 1997; Chen *et al.*, 2004). Through this intimate connection with actin filaments, focal adhesion sites are key players in the regulation of cell shape and cell cycle progression as discussed below (Burridge and Chrzanowska-Wodnicka, 1996; Chen *et al.*, 1997; Turner and Burridge, 1991).

The Cell Cycle

Dividing cells follow a pattern of behaviour called the 'cell-cycle', which consists of the progression of a cell through a set of stages (Murray and Hunt, 1993). These stages start with a growth phase (G1), followed by DNA replication (S), and a second growth phase (G2). These three stages are grouped under the term 'interphase' and prepare the cell for division by producing new cellular components and cellular DNA (Everhart and Rubin, 1974; Pardee, 1989). The cell then enters the mitotic phase where cell division results in two daughter cells which can then re-enter the cell cycle (Ohnishi, 1981).

Cell adhesion plays an important part in the regulation of the cell cycle, one aspect being the determination of cell morphology (Schoenwaelder and Burridge, 1999; Yamakita *et al.*, 1999; Zamir and Geiger, 2001b). Cell morphology and the cell cycle are intrinsically linked, to the extent that specific morphological states are indicative of cell cycle stages (Folkman and Moscona, 1978; Porter *et al.*, 1973). For example, the signature S-phase morphology is a flat well-spread cell, a morphology maintained by actin stress fibres and their associated focal adhesions (Iwig and Glaesser, 1991; Maddox and Burridge, 2003; Wang and Ingber, 1994; Zana and Albrecht-Buehler, 1989). However, at the 'S-phase' stage, morphology is not the only role for the focal adhesion/cytoskeleton complex. Both the generated intracellular tension and signal transduction of growth factor stimulation are transmitted through the complex, and both are essential to facilitate progression from G1 through to the S-phase (Huang and Ingber, 1999; Iwig *et al.*, 1995).

Summary

The investigation of cell shape, adhesion and growth provides a comprehensive basis with which to establish a material or topography's cytocompatibility, as numerous cellular 'fail-safe' measures must be overcome for the cell to function to the point of proliferation. Thus, the characteristics of cell morphology on a material allow for visual reference of the cells' behaviour while growth confirms the overall compatibility of the surface or topography.

Materials and Methods

Experiment 5 - Cell Growth and Morphology

Cell Culture

hTERT-BJ1 fibroblasts are an immortalised human fibroblast cell line. They are commercially available (Clontech Laboratories, Inc., USA) human primary foreskin fibroblasts transfected with the hTERT vector. The hTERT vector inhibits telomere shortening allowing the cells to exhibit primary cell characteristics, without entering senescence after 60-80 divisions (Clontech, 2000). Cells were cultured in 75cm² flasks to 70% confluency before subculture. Cells were incubated at 37°C in a 5% CO₂ atmosphere either in a 'hot room' or an incubator. All references to Dulbeccos Modified Eagles Media (DMEM)/199 media solution included supplementation with 10% Foetal Calf Serum (FCS).

1. DMEM/199 medium was removed from the flask and the cells were washed three times in 10ml TBSS (Tyrode's Balanced Salt Solution, see Appendix I included on the CD-ROM).
2. 3ml of 0.25% Trypsin with 0.02% EDTA in TBSS was added to the flask and the cells were incubated for 5 minutes (or until the monolayer was loosened) at 37°C.
3. 10 ml of DMEM/199 was added to the flask and the cells were collected in a centrifuge tube and centrifuged for 5 minutes at 1500 rpm.
4. The supernatant was removed, the cells re-suspended in 10 ml of DMEM/199 and centrifuged again for 5 minutes at at 1500 rpm.
5. The supernatant was removed again and the cells re-suspended in 5 ml of DMEM.
6. Cells were counted using a haemocytometer.
7. 3.0-5.0x10⁵ cells were seeded in 15ml media in 75cm² flasks.

Cell Seeding

hTERT-BJ1 cells were seeded onto 11mm sample discs of Th, SS, TE, TS, NE and NS at 5000 cells per 0.5ml of complete DMEM/199 in 4 well multidishes (Nunc, 176740). The cells were incubated at 37°C with a 5% CO₂ atmosphere for 24 hours, 5 and 10 days and the culture media was changed every 2.5 days.

Sample Fixation and Scanning Electron Microscopy Preparation

Note – it was necessary to conduct all aldehyde steps in a fume hood. All procedures were carried out at 20°C and all volumes were 0.5ml unless stated otherwise.

1. The samples were rinsed with 0.1M Piperazine-NN'-bis-2-ethane sulphonic acid (PIPES), pH 7.4 for 2 minutes.
2. The samples were fixed with 2.5% glutaraldehyde in 0.1M PIPES, pH 7.4 for 5 minutes.
3. Samples were rinsed with 0.1M PIPES, pH 7.4 three times at 2 minute intervals.
4. Samples were post-fixed and stained with 0.5% osmium tetroxide in 0.1M PIPES, pH 6.8 for 60 minutes
5. Samples were rinsed with double distilled ultrapure water three times at 2 minute intervals.
6. The samples were dehydrated through an ethanol series (50, 60, 70, 80, 90, 96, 100%) followed by a Fluorisol/Ethanol series (25, 50, 75, 100%) (Fluorisol - 1,1,2 trichloro,1,2,2, trifluoroethane).
7. The samples were critical point dried with liquid CO₂ using a Polaron E3100 critical point drier.
8. The metal discs were mounted on aluminium stubs using carbon stickers (Baltec, Balzers, FL) and sputter coated with a 10nm layer of gold/palladium (80Au/20Pd) using a Baltec MED 020 sputter coater (Baltec, Balzers, FL).

Scanning Electron Microscopy (SEM)

Cell imaging micrographs were taken using the Hitachi S4100 using both secondary electron (SE) and backscattered electron (BSE) imaging modes, with an accelerating voltage of 5kV, an emission current of 45µA, an aperture of 100µm (apt1), condenser lens set to 12, and a working distance of 10mm. Additional imaging in SE mode was taken using an Hitachi S4700 at an accelerating voltage of 5 kV and a current of 45µA. The aperture was set to 4, the condenser lens to 12, the column condition was set to 'Normal' and working distance was 10mm.

Experiment 6 - DNA Quantification of cells cultured on samples**Cell Seeding**

hTERT-BJ1 cells were seeded onto 49mm sample discs of SS, TE, TS, NE and NS at 5.0×10^4 cells per 5ml of complete DMEM/199 in 60x15mm tissue culture dishes (Falcon 353004, Becton Dickinson Labware) (Fig 3.2). Nunc™ does not manufacture Thermanox discs of 49mm diameter dimension therefore 4 squares (22x22mm) were used to provide a similar surface area of material. The cells were incubated at 37°C with a 5% CO₂ atmosphere for 24 hours, 5 and 10 days and the culture media was changed every 2.5 days. All samples were prepared in triplicate.

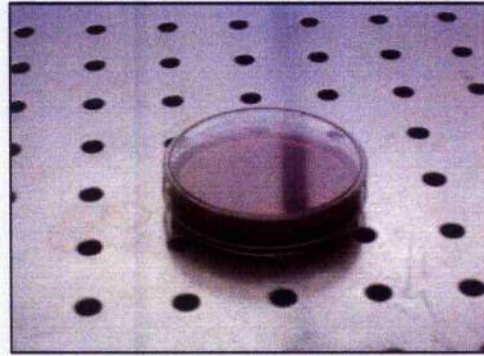


Fig 3.2 - 49mm diameter metal samples were placed in 60x15mm Petri dishes and seeded with 5.0×10^4 cells per 5ml of complete DMEM/199.

DNA Isolation**Day 0**

Three vials of 5.0×10^4 cells in 5ml were processed as Day 0 cell number references. Note that DMEM supplemented with FCS was used as it contained anti-trypsin factors (Freshney, 2000).

1. 5ml of cell suspension was pipetted into a sterile falcon tube (12ml) and centrifuged for 7 minutes at 1500rpm.
2. The supernatant was gently decanted from the cell pellet with DMEM and centrifuged.
3. The supernatant was drained, leaving 100 μ l of media above the cell pellet.
4. 100 μ l of Proteinase K solution (Roche, Cat No. 1 000 144) was added and the mix was aspirated. The falcon tubes were capped and sealed with Parafilm (America National Can Inc) and placed in a water bath set to 56°C for 14-16 hours.

5. The samples were stored at -20°C until required.

DNA isolation from samples at 24 hours, 5 and 10 days

Note that DMEM supplemented with FCS was used.

1. The samples were rinsed with 5ml of sterile TBSS.
2. The sample discs were removed and placed in new sterile 60x15mm Petri dishes. The transferred samples were rinsed with 5ml TBSS.
3. Samples were incubated with 2ml of 0.25% trypsin and 0.02% EDTA (ethylenediamine tetra-acetic acid, disodium salt) in TBSS for 20 minutes.
4. The trypsin was quenched with 5ml of media added to samples and holders. The trypsinised cells were transferred to a falcon tube. An additional 2ml of media was used to wash the discs (both sides) and then added to the falcon tube.
5. The protocol now followed the Day 0 DNA isolation.

DNA staining and cell number quantification

- The sample DNA were thawed at 20°C and centrifuged from 1 minute at 1000 rpm to ensure that all the liquid was pooled in the bottom of the tubes. The amount of liquid for each sample was accurately measured by a process of trial and error using 200µl Gilson micropipette.
- The sample DNA was plated in duplicate on a 96 well plate (Opaque White Plastic, Falcon, Cat. No. 353296) in 40µl volumes, with careful note of the sample coordinates. 160µl of 1:10,000 dilution of Hoechst 33258 (Polysciences, Inc.) in DPBS (see Appendix I on the accompanying CD-ROM) was added to each well in sequence using a multi-tip micropipette. Hoechst 33258 is very sensitive to light therefore all solution tubes were covered with foil. The plate was covered in foil and incubated at 20°C for 20 minutes.
- The plate was read using a PE HTS 7000 Bio Assay Reader (Perkin Elmer) equipped with filters to provide an excitation wavelength of approximately 360 nm and an emission wavelength at 465 nm. The htSoft 2 software application was used to operate the PE HTS 7000 Bio Assay Reader and the emission values were exported into Microsoft Excel.

- Within Microsoft Excel, the emission values for duplicate samples were averaged and the 'blank' average value was subtracted from these values. The 'day 0' and sample emission values were adjusted to take into account the original volume of isolated DNA. Sample cell numbers were then extrapolated from the known 'day 0' sample readings. The average values were plotted on an interaction plot included as Graph 3.1 in the results section of this chapter.

Statistical Analysis

Statistical analysis was performed using Statlets© (1997, NWP Associates, Inc. <http://espse.ed.psu.edu/statistics/statlets/statlets.htm>), a Java Applets programme [MW1] and Microsoft® Excel. Two-way analysis of variance (ANOVA) was utilised to determine statistically significant differences between samples with respect to sample type, time and interaction between these independent variables on cell number. F-tests were used to determine which of these factors were statistically significant from one another. Factors with P-values below 0.01 are highlighted in the ANOVA table with a double asterix (**), which corresponds to statistically significant effects. Following the identification of statistically significant differences between the independent variables using two-way ANOVA, multiple range tests using Fisher's least significant difference (LSD) procedure were applied for more sensitive detection of statistically significant differences between all the sample means.

Experiment 7 – Immunostaining of Vinculin, Tubulin, Actin and DNA, Analysis of Cell Area and Shape, and Measurement of Focal Adhesion Lengths*Cell Seeding*

hTERT-BJ1 cells were seeded onto 11mm the sample discs of Th, SS, TE, TS, NE and NS at 10,000 cells per 0.5ml of complete DMEM/199 in 4 well plates. All labelling procedures were conducted on duplicate samples. The cells were incubated at 37°C with a 5% CO₂ atmosphere for 48 hours.

Vinculin, Tubulin, Actin and DNA Immunostaining

Note – Phosphate Buffered Solution (PBS) and 4% formaldehyde were pre-warmed to 37°C. All work was carried out at room temperature (20-25°C). All volumes used were 0.5ml except where stated otherwise.

- 1) The samples were washed in (1x) PBS at 37°C.
- 2) The samples were fixed in 4% formaldehyde / PBS (with 2% sucrose) for 15 minutes at 37°C.
- 3) Samples were incubated for 5 minutes with the permeabilising buffer (see Appendix I on the accompanying CD-ROM).
- 4) The samples were blocked using 1%BSA/PBS for 5 minutes.
- 5) The samples were incubated with 0.4ml of either 1:100 mouse monoclonal anti-Vinculin (Sigma, Cat No. V9131) or 1:50 mouse anti-β-Tubulin (Sigma, Cat No. T4026) and 1:50 Phalloidin (Rhodamine conjugated, Molecular Probes, Cat No. R415) suspended in 1%BSA/PBS for 1 hour at 37°C. Note that the samples were shielded from light from this point on.
- 6) The samples were washed three times at 2 minute intervals in 0.5% Tween 20/PBS.
- 7) The samples were incubated with 0.4ml 1:50 horse biotinylated anti-Mouse (Vector Laboratories, Cat No. BA-2000) for 1 hour at 37°C.
- 8) The samples were washed three times at 2 minute intervals in 0.5% Tween 20/PBS.
- 9) The samples were incubated with 0.4ml 1:50 Fluorescein Streptavidin (Vector Laboratories, Cat No. SA-5001) for 30 minutes at 4°C.
- 10) The samples were washed three times at 2 minute intervals in 0.5% Tween 20/PBS.

11) The sample surface was immersed with Vectashield with DAPI (4',6-diamidino-2-phenylindole) (Vector Laboratories, Cat No. H-1200) and sandwiched between two 24x50mm coverslips. Samples were kept at 4°C and kept away from light until imaged.

Fluorescence Microscopy

Samples were imaged using a Zeiss Axiovert 200M inverted microscope fitted with an Evolution QEi Monochrome (MediaCybernetics, UK) camera. Fluorescent light was supplied by a HBO 100 mercury lamp (Zeiss) and reflected light by a HAL 100 (12V, 100W, Zeiss) lamp. Samples were imaged using 3 objective lenses; x5 Zeiss A-Plan (5x/0,12 Ph0, ∞), x20 Zeiss D ACHROPLAN (20x/0,40 Korr Ph2 ∞/0-1,5) and a 40x Zeiss Plan-NEOFLUAR (40x/0,75, ∞, 44 03 51). Zeiss fluorescence filter set 02 (488002-0000) was used for detecting DAPI, 10 (488010-0000) for Fluorescein and 15 (488015-0000) for Rhodamine, and a polarising AR coated neutral beamsplitter for reflected light. Images were captured using Image-Pro Plus Version 5.1 with a separate pass required for each filter and reflected light image. Pseudocoloured images were assembled using Photoshop 7.0 (Adobe, USA) in RGB mode. Reflected light images were superimposed with 50-60% opacity.

Cell Area and Aspect Ratio

Fluorescence Microscopy

Samples were imaged using the Rhodamine filter set at x20. Twenty images of each sample were taken at random.

Image Analysis

Using Photoshop 7.0 all images were edited with a criterion of splitting adjoining cells by means of a 3 pixel wide line and enhancing the contrast of the image. If any adjoining cells could not be separated satisfactorily or cell images were impaired in any way, the image was omitted from the study.

The image analysis process was then transferred to ImageJ 1.33m (National Institute of Health, <http://rsb.info.nih.gov/ij/>). Images pertaining an experiment (e.g all images of cells

cultured on SS) were imported as an 'Image Sequence' and saved as a 'Stack'. The stack was 'Inverted' changing the background to white and the majority of the cell area to black. This allowed the stack to be 'Thresholded', thus converting the image to binary and differentiating cells from the background. The stack was measured and a resulting new stack was generated representing and numbering the measured cells (Fig 3.3). The outline stack was compared with the original cell images and any cells found to be misrepresented in the outline version were omitted from the list of measured cells. The generated data were imported into Excel (Microsoft, Inc); the measurements utilised were cell area and shortest and longest axis. The cell aspect ratio provides numerical information on the morphology of the cell and was calculated by dividing the longest measured axis with the shortest. A perfect circle would return a value of 1 as both axes were identical while the longer and narrower a cell is the larger this ratio becomes.

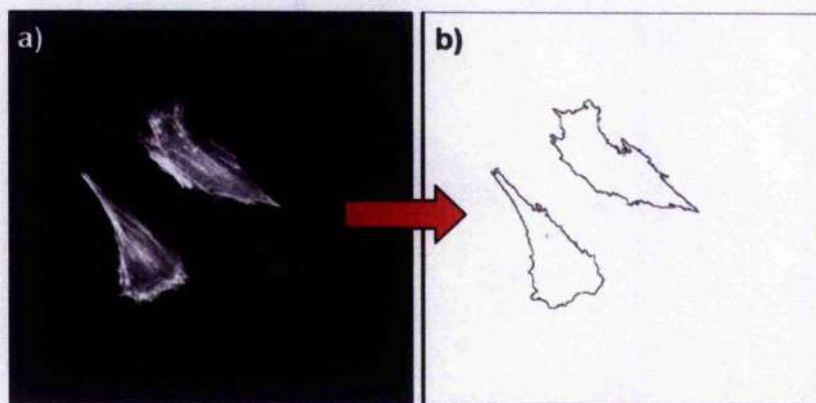


Fig 3.3 – Image analysis procedure. (a) Low magnification cell image prior to image analysis. (b) Image of the outline of measured cells generated using the image analysis procedure.

Statistical Analysis of Cell Area and Cell Aspect Ratio

Statistical analysis was performed using Statview© 4.02 (Abacus Concepts, Inc) and Microsoft® Excel. Measurements on all samples were positively skewed and required logarithmic transformation to allow parametric analysis. One-way analysis of variance (ANOVA) was utilised to determine statistically significant differences between samples with respect to cell area and sample type. Factors with P-values below 0.01 are highlighted in the ANOVA table with a double asterix (**), which corresponds to statistically significant effects. Following the identification of statistically significant differences using one-way ANOVA, multiple range tests using the Bonferonni/Dunn interaction procedure

were applied for more sensitive detection of statistically significant differences between all the sample means. An identical procedure was carried out on the cell ratio data. Data were presented in the form of box plots (see Graph 3.2 for example). The box represents the interquartile range (25%-75% percentile) of areas measured on a specific sample, while a line separating the box is representative of the median (the number that halves a population of observations). A solid line either side of the box, similar to error bars, represents the smallest and largest values that are not considered outliers, while the dots represent the outliers.

Measurement of Focal Adhesion Lengths

Fluorescence Microscopy

12 cells divided between the duplicate samples were imaged per sample type using the Fluorescein filter set at x40.

Image Analysis

Using Photoshop 7.0 all samples were converted to RGB, with the Red and Blue channels blacked out to provide a Green channel image only (Fig 3.4a). Utilising the 'transparent layer' function, the length of each focal adhesion was traced by drawing a white 2 pixel thick line across the long axis of the adhesion site. The contrast of the white line and green cell allowed for a progressive elimination of each site. The 'virtual tracing' generated was imported into ImageJ and measured (Fig 3.4b). The long axis measurements were converted into μm and consequently utilised for statistical analysis performed using the same procedure documented for Cell Area and Aspect Ratio.

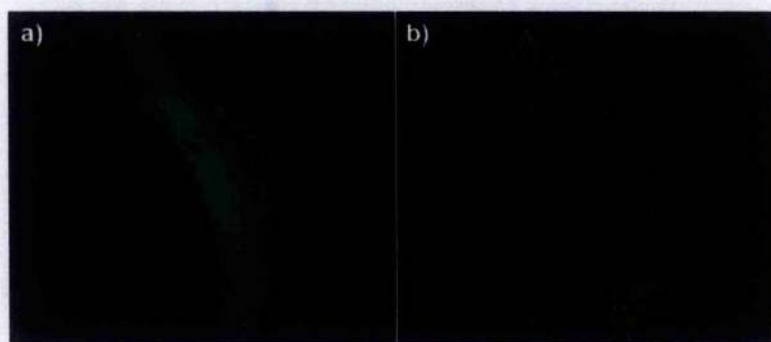


Fig 3.4 – Focal adhesion measurement procedure. (a) A green channel image of the focal adhesion stain was prepared. (b) The 'tracing' of the focal adhesion lengths.

Results

The results have been organised into 'Cell Growth' and 'Cell Morphology and Adhesion', with the relevant results documented within each section. SEM provided qualitative cell growth data and cell morphology, while fluorescence microscopy was utilised for qualitative and quantitative morphology.

Cell Growth

Cells were cultured on all the sample types for a period of 10 days with samples fixed at 24hr, 5 and 10 day timepoints. Cell growth was qualitatively examined using low magnification SEM images. Low magnification imaging of cells on the surfaces was performed in backscattered electron (BSE) mode (with the exception of Th) as it provided an adequate compositional contrast between the biological tissue and metal substrate.

Qualitative Cell Growth - SEM

At low magnification, cells on Th, SS, TE, TS and NE were all observed to follow similar trends. At 24hr a scattering of spread cells was observed on all samples. At 5 days the number of cells had increased considerably, however their morphology remained similar to 24hr. At 10 days cell morphology had changed considerably to an elongated shape due to the proximity of the neighbouring cells in confluent monolayers (Fig 3.5). Cell behaviour on NS differed considerably; at low magnification it was very difficult to resolve cells at 24hr, 5 and 10 days (Fig 3.6,abc). At 24 hours the cells were scattered sparsely and were generally not spread (Fig 3.6a). At 5 and 10 days the number of cells did not seem to increase, nor did they increase in their spreading (Fig 3.6b,c).

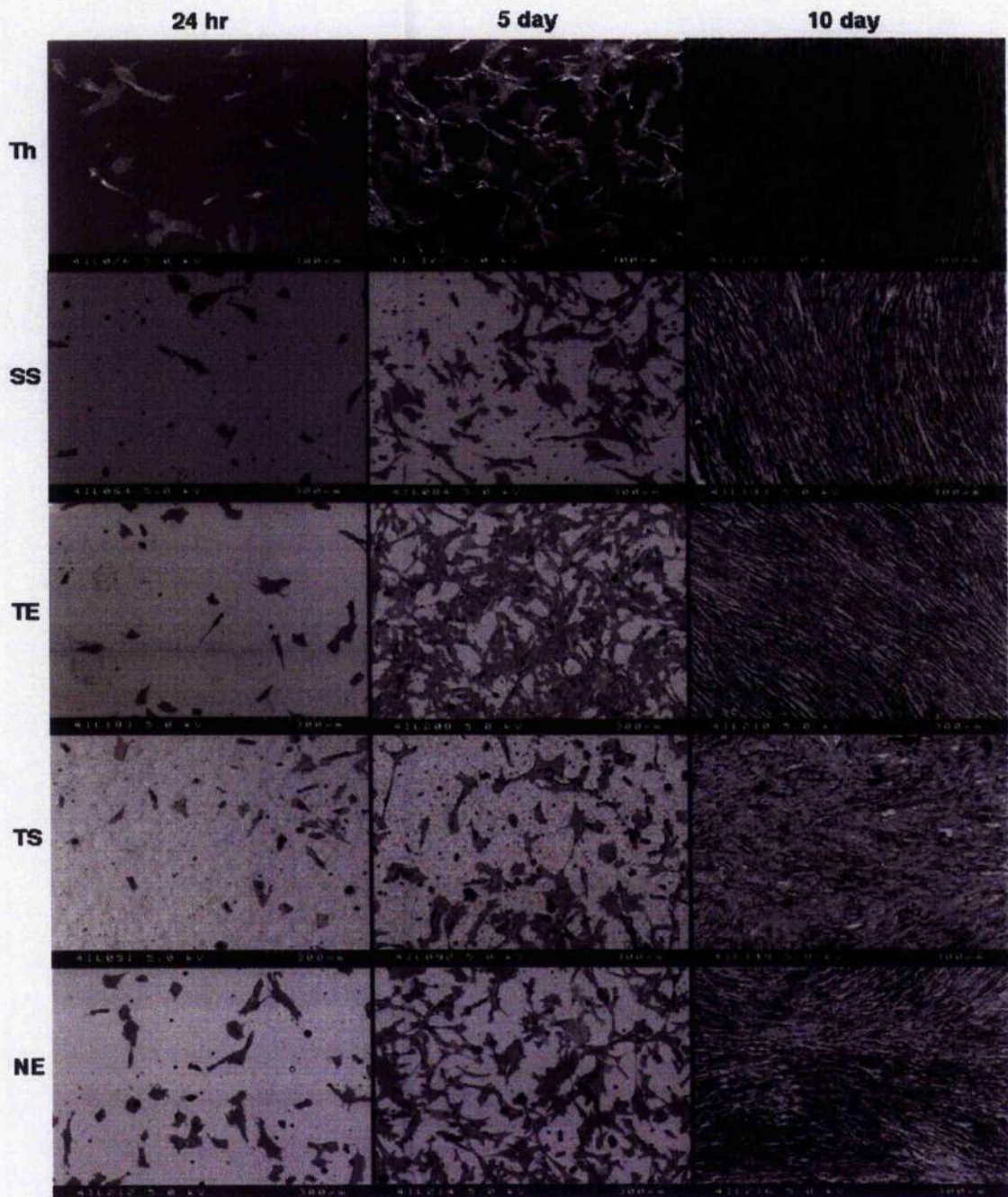


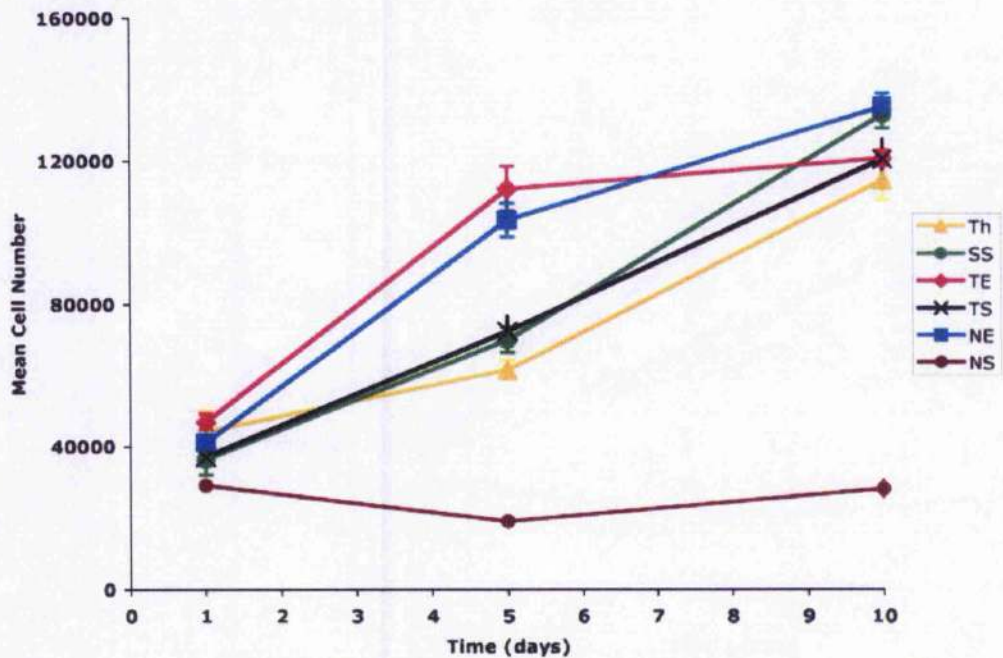
Fig 3.5 - SEM micrographs (BSE mode) of hTERT fibroblasts cultured on Thermanox (Th), Stainless Steel (SS), Electropolished Titanium (TE), Standard Titanium (TS) Electropolished TAN (NE) for 24hr, 5 and 10 day time periods. BSE mode was utilised to enhance the contrast between the biological material and metal substrate.



Fig 3.6 –hTERT fibroblasts cultured on Standard TAN (NS) for (a) 24hr, (b) 5 days and (c) 10 days. The low cell numbers at all timepoints and their unspread morphology coupled with the rough topography made it difficult to resolve them from the background.

Quantitative Cell Growth

This experiment was used to confirm the SEM observations of cell growth, with quantitative cell data.



Graph 3.1 – A plot of the mean cell number ($n=3$, per sample, per timepoint) quantified per sample area (1885mm^2) at the three timepoints. All samples follow a general trend of cell number increase with time with the exception of cells on NS which had persistently low numbers.

The means of the cell numbers quantified on the samples at the three timepoints were plotted in an interaction plot (Graph 3.1). Day 1 numbers were lower than the initial seeding number due to a loss of a number of cells to the exposed space between the edge of the sample and the wall of the holders. All samples follow a general trend, namely cell number increases with increasing time. One exception was noted however on NS where persistently low numbers of cells were observed at all time points.

Statistical Analysis

The sample type, time and interaction were found to have statistically significant effects on the number of cells adhering to a surface ($P < 0.01$) (Table 3.1). Using multiple range tests to compare the sample means, 11 of 15 comparisons were statistically significant (99% confidence level), summarised in Table 3.1. Comparisons of Th, SS, TE, TS or NE with NS produced very large estimated differences between each pair of means ranging from 47815 to 67761.5. The other 6 significant comparisons were Th-TE, Th-NE, SS-TE, SS-NE, TE-TS and TS-NE, however the differences between these means were much lower, ranging from 13532.4 to 19946.5. Only Th-SS, Th-TS, SS-TS and TE-NE returned mean differences of no statistical significance.

<i>Source of Variation</i>	<i>Sum of Squares</i>	<i>Degrees of freedom</i>	<i>Variance</i>	<i>F-Ratio</i>	<i>P-Value</i>
Sample Type (Variable A)	2.7×10^{10}	5	5.4×10^9	122.53	** 1.0×10^{-4}
Timepoint (Variable B)	4.0×10^{10}	2	2.0×10^{10}	457.80	** 1.0×10^{-4}
Interaction	1.1×10^{10}	10	1.3×10^9	25.64	** 1.0×10^{-4}
Residual	1.4×10^9	32	4.4×10^7		
Total (corr.)	8.0×10^{10}	49			

Table 3.1 – ANOVA table (Type III Sums of Squares). **P-Values are < 0.01 and statistically significant.

<i>Sample Comparison</i>	<i>Significant Difference</i>	<i>+/- Limits</i>
Th - TE	-19946.5	6576.77
Th - NE	-19941.2	6576.77
*Th - NS	47815	6767.44
SS - TE	-13537.8	6576.77
SS - NE	-13532.4	6576.77
*SS - NS	54223.7	6767.44
TE - TS	16581.4	6576.77
*TE - NS	67761.5	6576.77
TS - NE	-16576.1	6576.77
*TS - NS	51180.1	6767.44
*NE - NS	67756.2	6576.77

Table 3.2 – Statistically significant (99% confidence level) differences between each pair of means. * The estimated mean differences of all samples in comparison with NS are considerably larger than the other significant mean differences.

Cell Morphology and Adhesion

Qualitative Cell Morphology - SEM

With the exception of NS, higher magnification imaging of cells was performed using secondary electron mode (SE). For NS, both SE and BSE was used, SE for morphology and BSE for differentiating the surface from the cells.

Th – Thermanox

At higher magnifications it was possible to see that the cell morphology did not change between the 24hr and 5 day timepoints (Fig 3.7a,b). At both timepoints cells had relatively smooth featureless membranes, due to their degree of spreading, with lamellapodia present at 24hr (Fig 3.7a) and filopodia at 5 days (Fig 3.7b). At 10 days the morphology had changed radically into an elongated fibular shape with a rough membrane and apparent cross-linking possibly by means of filopodia (Fig 3.7c).

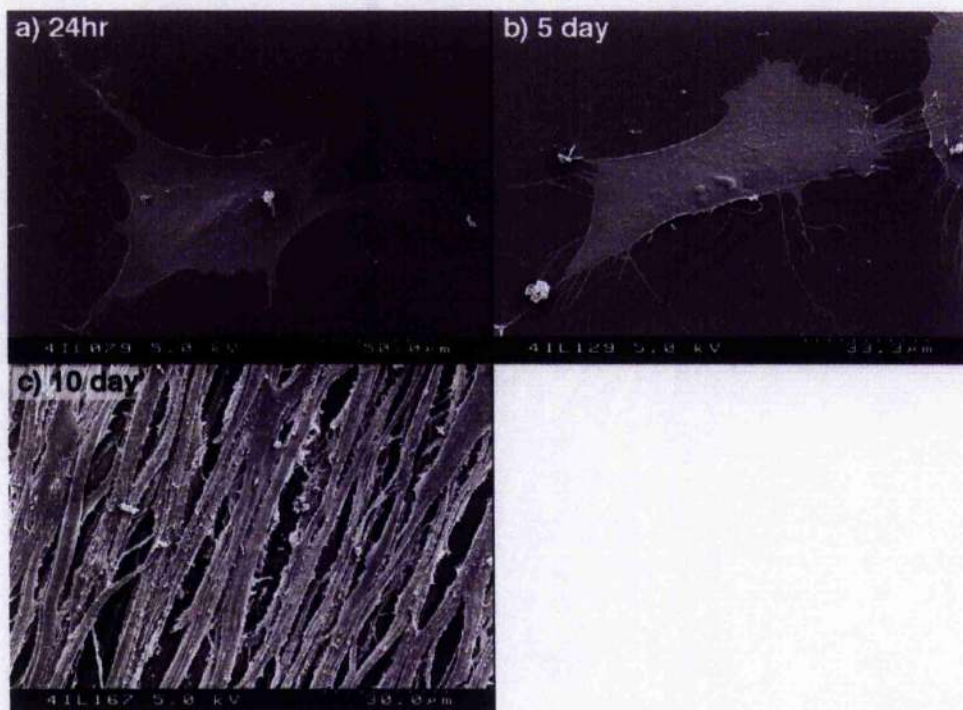


Fig 3.7 – SEM micrographs (SE mode) of hTERT fibroblast morphology for cells cultured on Th. (a) 24hr, cells are well spread with lamellapodia extending at the periphery. (b) At 5 days cells were still well spread with numerous filopodia present at the periphery. (c) At 10 days, cell morphology was elongated due to the proximity of neighbouring cells.

SS - Stainless Steel

The cells were very well spread at 24hr with only a few filopodia at the cell edges (Fig 3.8a,b), and by day 5 the number of filopodia at the cell edges had increased (Fig 3.8c,d). After 10 days the cell morphology was elongated and cell borders with parallel neighbouring cells were difficult to resolve. The cell membranes were considerably smoother than those of cells on Th for 10 days, and there was evidence of multiple cell layers (Fig 3.8e).

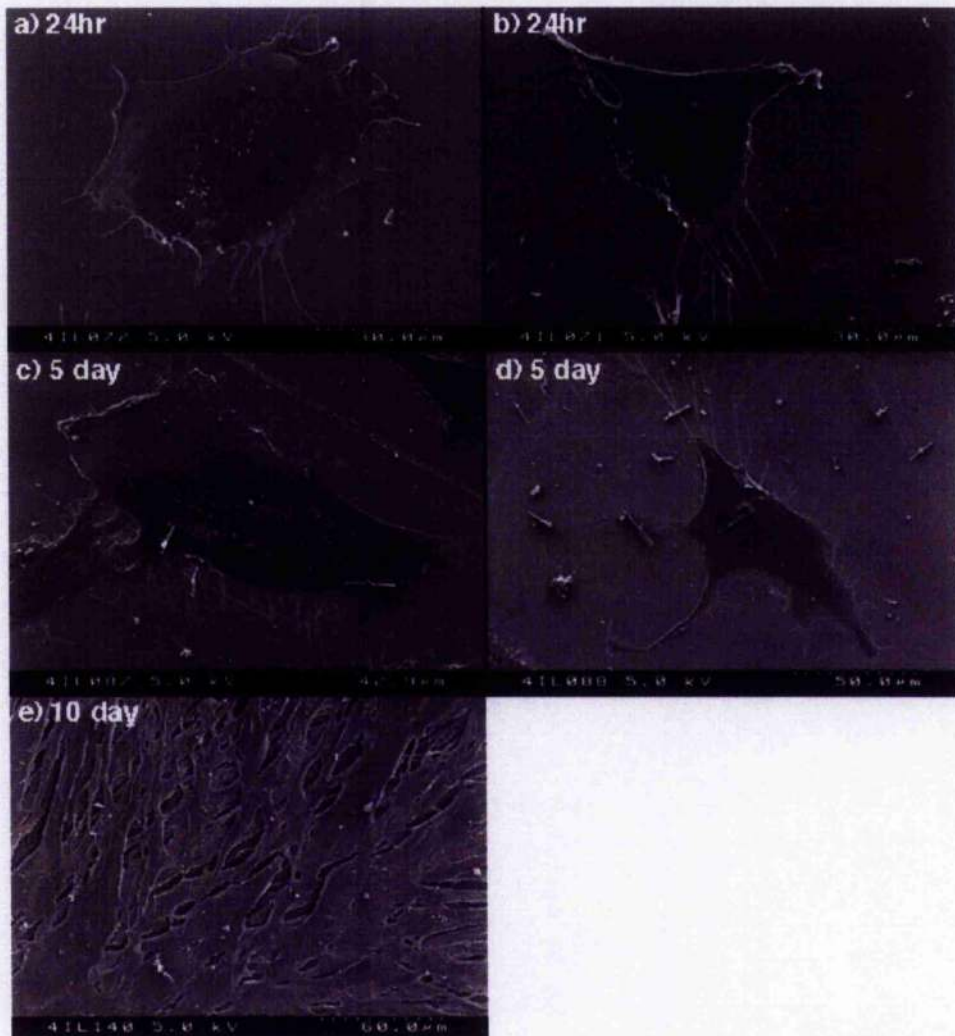


Fig 3.8 - hTERT fibroblast morphology for cells cultured on SS. (a & b) At 24hr, cells were very well spread with only a few filopodia at the cell edges. (c & d) At 5 days, cells had an increased number of filopodia at the cell edges, possibly due to the closer proximity of neighbouring cells. (e) At 10 days the cell morphology had changed considerably to accommodate the proximity of neighbouring cells.

TE – Electropolished Titanium

At 24hr and 5 days, a higher magnification showed that the cells were spread so thinly that it was possible to trace the ‘nano-hill’ surface detail on the cell membrane itself (Fig 3.9a,b,c,e). The cells at 24hr and 5 day had some filopodia at the cell periphery, and also at 5 days the cells were in closer proximity to each other due to the higher numbers (Fig 3.9c,d). By day 10 the cell morphology had become elongated due to the close proximity of neighbouring cells (Fig 3.9f).

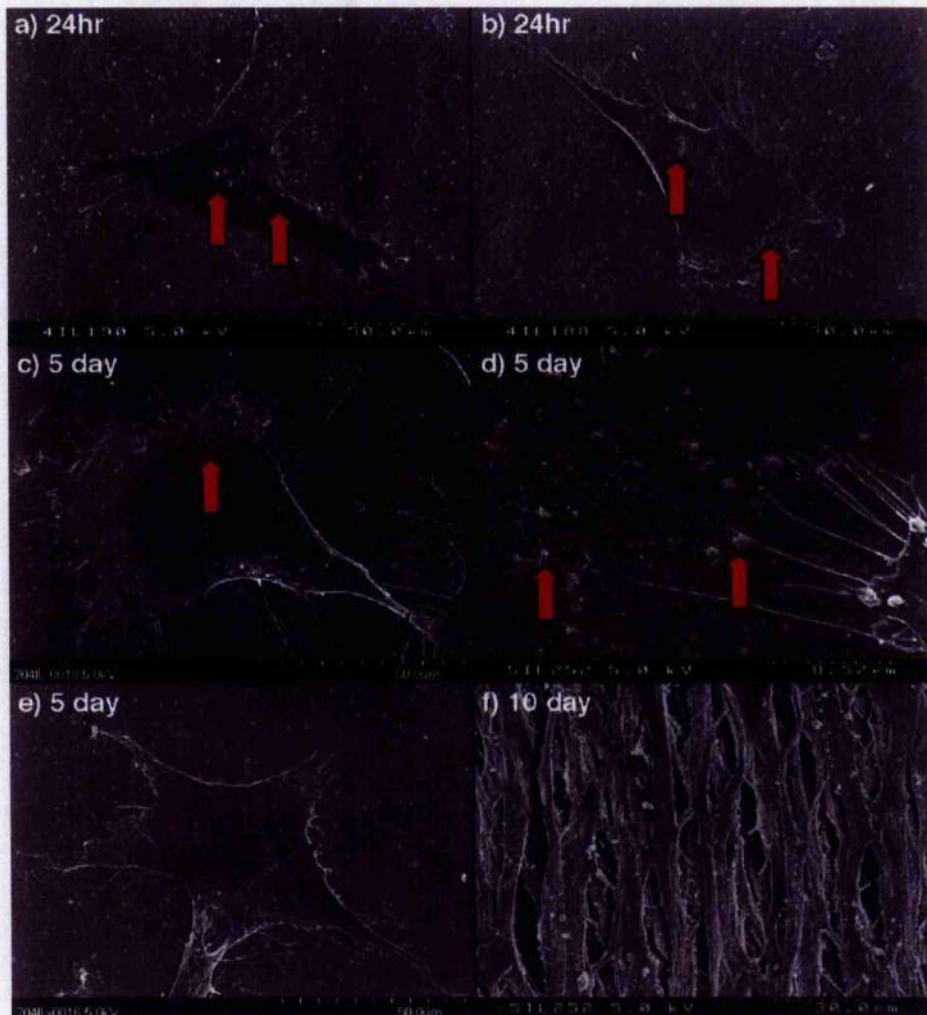


Fig 3.9 – hTERT fibroblast morphology for cells cultured on TE. (a & b) At 24hr it was possible to trace the nano-hill surface detail through the surfaces of the spread cells (examples of these protrusions are indicated at the tip of the red arrows). (c & e) At 5 days, the topographical surface detail was again visible through the spread cell surface (red arrow). (d) Filopodia were observed occasionally interacting with the ‘nano-hill’ surface features (red arrows). (f) At 10 days cells displayed an elongated morphology.

TS – Standard Titanium

Imaging the cells at higher magnification at 24hr demonstrated clear differences in cell spreading in comparison with those on the smoother titanium surface. These differences included surface ruffling above the cell's nucleus and an increased number of filopodia extending from much further in the main cell body, occasionally even from above the nucleus (Fig 3.10a,b). At day 5, cells were generally more spread in the non-confluent areas, although filopodia were still observed extending from further within the cell body (Fig 3.10c,e). The filopodia did not attach to any specific surface features, as with TE, but randomly probed the surface discontinuities (Fig 3.10d). Occasional cells could be found to have spread to the same proportions as on TE where ruffling was absent and the underlying topography could be traced through the cell membrane and, in addition, filopodia extended from the periphery (Fig 3.10e). The morphology changed again by day 10 to favour a generally elongated appearance, however some cells could be observed to be well spread filling any spaces in the confluent monolayer (Fig 3.10f).

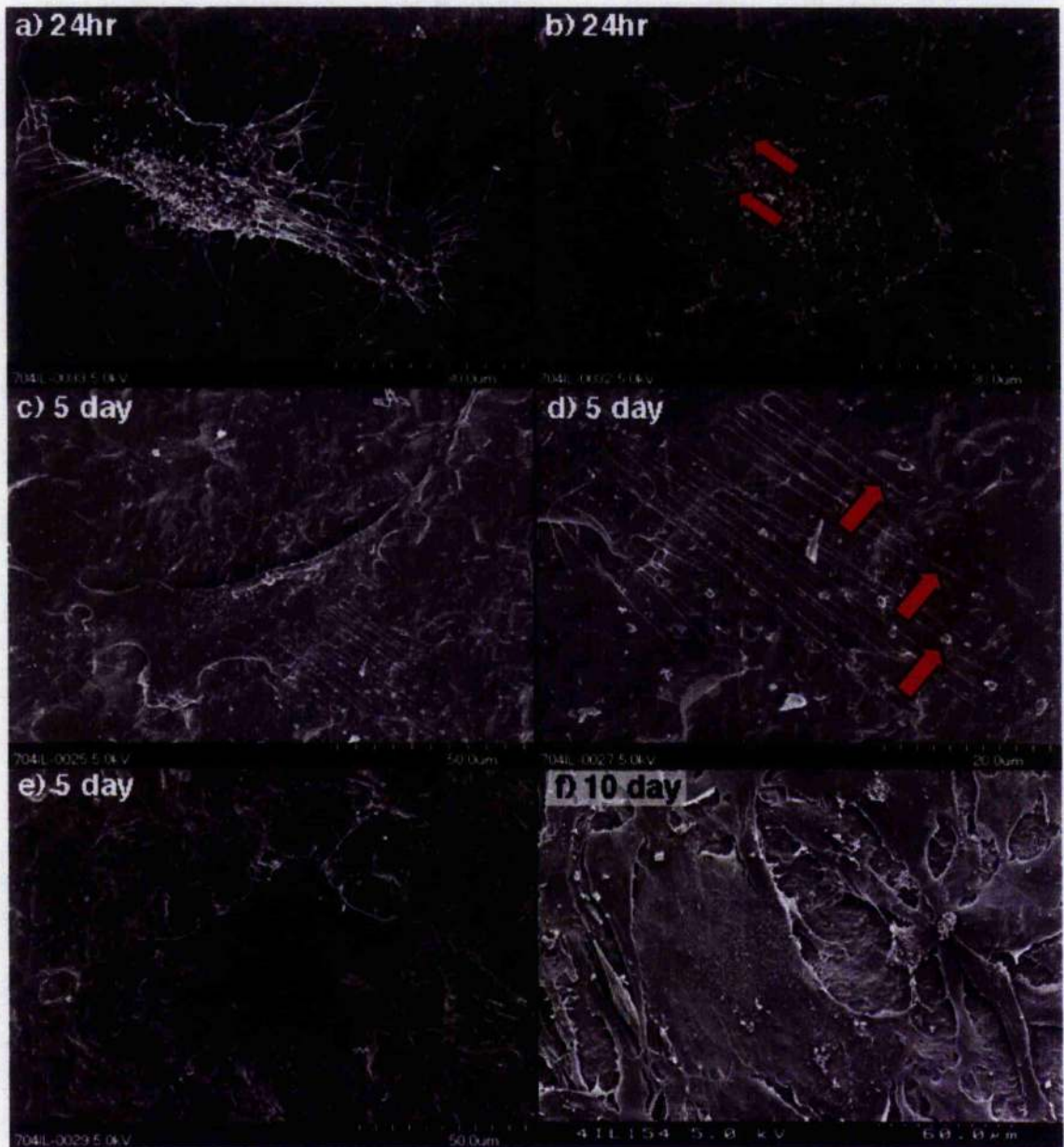


Fig 3.10 – hTERT fibroblast morphology for cells cultured on TS. (a & b) At 24hr cells displayed prominent surface ruffling above the nucleus of cells and increased filopodia extending from much further in the cell membrane (red arrows). (c & e) At 5 days, cells were generally more spread in the non-confluent areas, although filopodia still extended from further within the cell body. (d) While not attaching to any specific features, filopodia could be observed probing the surface (red arrows). (f) Cells spread to fill any spaces of uncovered topography.

NE – Electropolished TAN

At 24hr the cells were spread and demonstrated occasional ruffling, however no more than on the other electropolished surfaces. Filopodia also extended from the cell periphery exploring the surface (Fig 3.11a,b). By day 5 cells were spreading to a degree that there was no ruffling and it was possible to trace the microtopography through the cell membrane (Fig 3.11c,d). The undulating appearance of the material did not appear to affect the cells, nor did the small metal particles present on the surface (confirmed in the previous chapter to be β -phase particles), as filopodia could not be observed primarily attaching to these features (Fig 3.11e). By day 10 the morphology had changed to an elongated form with individual cells hard to distinguish. The cell membrane was smooth and there was evidence of multiple cell layers (Fig 3.11f).

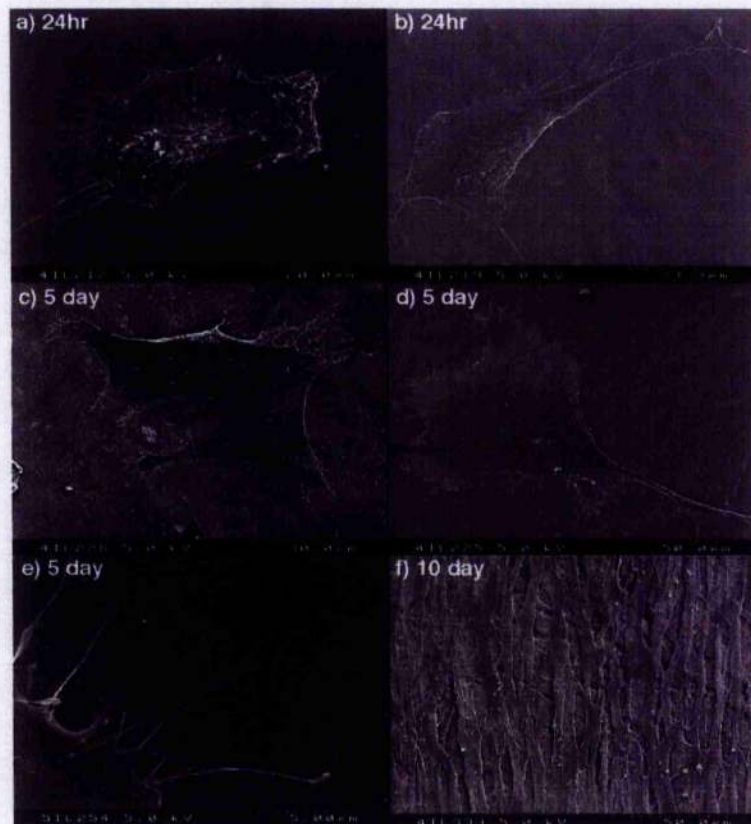


Fig 3.11 – hTERT fibroblast morphology for cells cultured on NE. (a & b) At 24 hr, cells were spread and occasional ruffling was visible on the cell membranes, however filopodia extended from the cell periphery exploring the surface. (c & d) At 5 days cells were spreading sufficiently that there was no ruffling and it was possible to trace the microtopography through the cell membrane. (e) No specific interaction of the filopodia and surface topography was observed. (f) At 10 days cell morphology was elongated and in multiple layers.

NS – Standard TAN

At higher magnification cells seeded for 24hr cells were not spread and had highly ruffled membranes (Fig 3.12a). The unspread morphology occasionally made it difficult to distinguish cells from other surface features using SE, therefore BSE was utilised to distinguish metal from the organic material based on elemental composition (Fig 3.12b). Some cells were found to have elongated bipolar morphologies; however they still remained unspread. By day 5 cell morphology did not differ with only unspread or elongated cells present (Fig 3.12c,d). Cells displayed some filopodia which emanated from the cell periphery and others extending from more central parts (Fig 3.12e,f). Some of these filopodia could be observed to attach to the metal particles present on the surface (Fig 3.12g). Since the morphology of the metal particles on the surface made it perceivable that the cells could in some cases remove them by ingestion, higher accelerating voltage (kV) BSE imaging was utilised to penetrate further into the cell, thus resolving these particles within the cell. Unfortunately it was still not possible to confirm if these particles were within the cell body or underneath (Fig 3.12f). By day 10 the cells, still unspread, had retracted their filopodia and appeared to have ceased exploring the surface. On some cells the membrane integrity was reduced with a much coarser texture (Fig 3.12h).

Fig 3.12 - SEM micrographs in SE mode (left) and BSE mode (right) of hTERT cells cultured on NS fixed at varying timepoints. (a) At 24hr cells were unspread and had a highly ruffled membrane. (b) In BSE mode the compositional contrast allowed for the biological material to be differentiated with more ease from the underlying metal. (c) At 5 days some cells displayed an elongated morphology. (d) The elongated cell could be differentiated from the underlying metal topography with more ease in BSE mode. (e) At a higher magnification of cell 'd', small filopodia could be seen to extend from the cell periphery. (f) Utilising high kV BSE mode, it was possible to resolve β -phase particles through the cell body, although these particles could not be confirmed to be within the cell or underneath. (g) Filopodia could also be observed to attach to the β -phase particles present on the surface. (h) At 10 days cell membrane integrity seemed to be reduced with a much coarser texture.

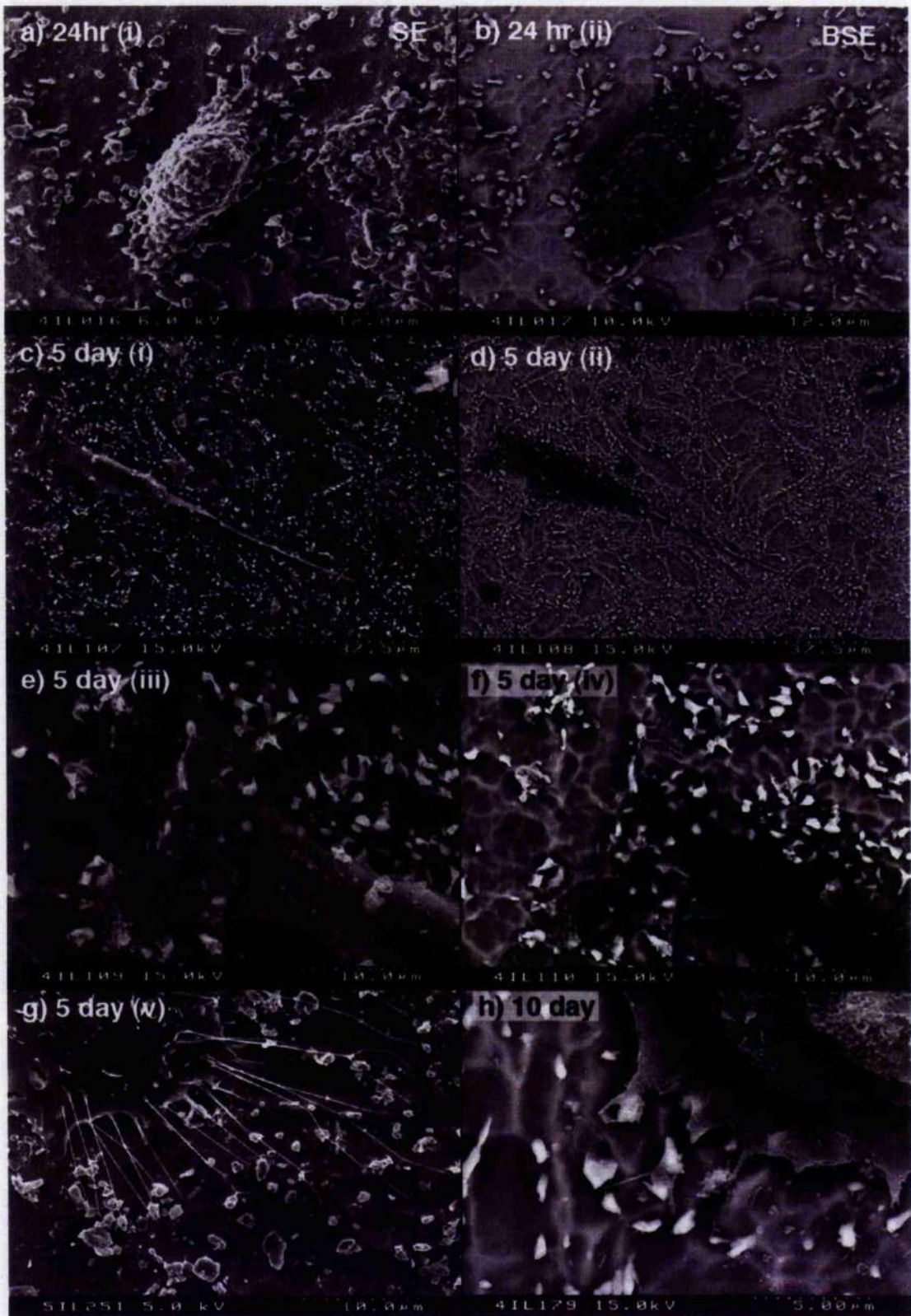


Fig 3.12 – (legend on opposite page)

Quantitative Cell Morphology – Fluorescence Microscopy

Note that cells were seeded at higher concentrations for these experiments (in comparison to the qualitative morphology studies) to enable a higher proportion of non-contact cells to be imaged within the field of view. The average number of cells measured for each sample type was 500-580. This produced a high amount of variation, however it also increased the significance of the test. Similar to most biological data all datasets were positively skewed and required logarithmic transformation to normalise their distribution thus enabling the use of parametric tests. All statistical comparisons were made using one-way ANOVA at a 99% level of significance ($p < 0.01$) and a Bonferonni/Dunn multiple range test was used to compare the sample means.

Cell Area

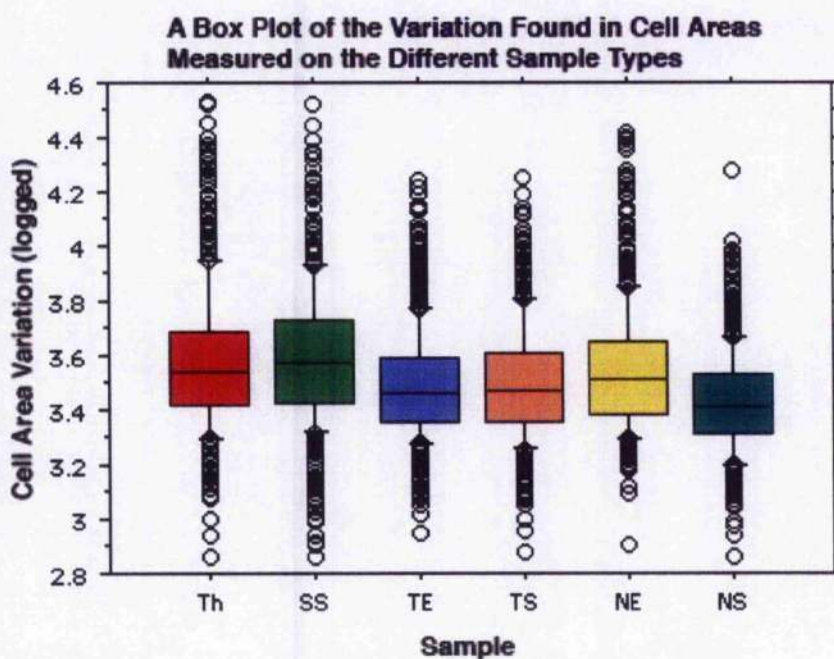
Sample types were found to have statistically significant effects on cell area ($P < 0.01$) (Table 3.3). 10 of 15 comparisons of the sample means were statistically significant (99% confidence level), summarised in Table 3.4. The lowest mean area was found on NS and this was statistically different from all the other substrates. Interestingly, the mean cell areas for SS and Th were higher than for the remaining TE, TS and NE. SS was found to be statistically higher than TE, TS and NE, while Th was found to be higher than TE and TS. A box plot demonstrates the complete range of areas measured on the surfaces; this was vast as the number of measured cells was high ($n > 500$), but this increased the confidence of the results obtained, indicating they were more representative of the cell area distribution (Graph 3.2). NS was demonstrated to have the lowest median (the number that halves a population of observations) and first quartile (25%), which meant that at least 25% of cell areas measured on NS were lower than on the other sample types - a significant number.

<i>Source of Variation</i>	<i>Sum of Squares</i>	<i>Degrees of freedom</i>	<i>Mean Square</i>	<i>F-Ratio</i>	<i>P-Value</i>
Sample Type	10.4	5	2.1	39.9	**<0.0001
Residual	166.6	3209	0.052		

Table 3.3 – ANOVA table. **P-Values are <0.01 and statistically significant.

<i>Sample Comparison</i>	<i>Mean Diff.</i>	<i>P-Value</i>
Th - TE	0.088	<0.0001
Th - TS	0.082	<0.0001
Th - NS	0.157	<0.0001
SS - TE	0.097	<0.0001
SS - TS	0.091	<0.0001
SS - NE	0.051	0.0002
SS - NS	0.166	<0.0001
TE - NS	0.069	<0.0001
TS - NS	0.075	<0.0001
NE - NS	0.115	<0.0001

Table 3.4 – Bonferonni/Dunn interaction table. Statistically significant (99% confidence level) differences were observed between each pair of means highlighted.



Graph 3.2 – Box plot of cell area variation on the samples. Note that the values have been logged. The box represents the interquartile range (25%-75% percentile) of areas measured on a specific sample, while the line separating the box is representative of the median (the number that halves a population of observations). The solid line either side of the box represents the smallest and largest values that are not considered outliers, while the dots represent the outliers. Cell area measured on NS was demonstrated to have the lowest median in comparison to other samples.

Cell Aspect Ratio

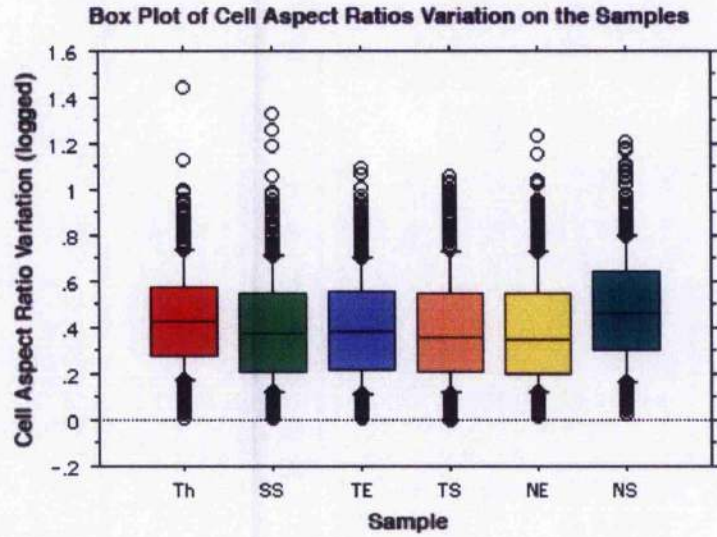
Sample types were found to have statistically significant effects on cell aspect ratios (length/width: $p < 0.01$) (Table 3.5). 7 of 15 comparisons of sample means were statistically significant (99% confidence level), summarised in Table 3.6. The highest mean aspect ratio was found for cells on NS and was statistically different from all the other substrates, except for Th. Th was also found to be significantly higher than SS, TS and NE. The higher ratio indicates the cells were more elongated on NS and Th in comparison with the other samples. A box plot maps the range of ratios measured on the surfaces and demonstrates how similar the ranges for SS, TE, TS and NE are (Graph 3.3). The proportion of cells displaying higher ratios on NS and Th are also visible in the plot.

<i>Source of Variation</i>	<i>Sum of Squares</i>	<i>Degrees of freedom</i>	<i>Mean Square</i>	<i>F-Ratio</i>	<i>P-Value</i>
Sample Type	3.7	5	0.7	13.9	**<0.0001
Residual	171.498	3268	0.052		

Table 3.5 – ANOVA table. **P-Values are <0.01 and statistically significant.

<i>Sample Comparison</i>	<i>Mean Diff.</i>	<i>P-Value</i>
Th - SS	0.048	0.0006
Th - TS	0.050	0.0004
Th - NE	0.054	0.0001
SS - NS	-0.083	<0.0001
TE - NS	-0.081	<0.0001
TS - NS	-0.085	<0.0001
NE - NS	-0.090	<0.0001

Table 3.6 – Bonferonni/Dunn interaction table displaying the statistically significant differences identified between each pair of sample medians (99% confidence level).



Graph 3.3 - Box plot of cell ratio variation on the samples. Note that the values have been logged. The ranges plotted for SS, TE, TS and NE were very similar. The proportion of cells displaying higher ratios on NS and Th could also be observed, notably more so for NS.

Cell Morphology – Intracellular Labelling

Preceding experiments demonstrated that cells were affected by the various topographies, especially the roughened and protruding morphology of the standard materials (TS and NS). To extend upon these observations, actin, vinculin and tubulin and DNA were stained on cells cultured on all the sample types. As illustrated in the 'Introduction' section, these stains help to visualise adhesion and the structural integrity of cells on the various surfaces.

Th - Thermanox

Cells were well spread on Thermanox with a clearly discernible actin cytoskeleton, each individual filament terminated at both ends by 'mature' dash morphology focal adhesion sites (Fig 3.13a). Although the representative cell adhesion sites were located at closer proximity to the cell periphery rather than its nucleus, this was not observed in all cells. The microtubule network extended to all areas of the cell body from a point, probably the microtubule-organising centre (MTOC), located off-centre near the cell's nucleus (Fig 3.13b).

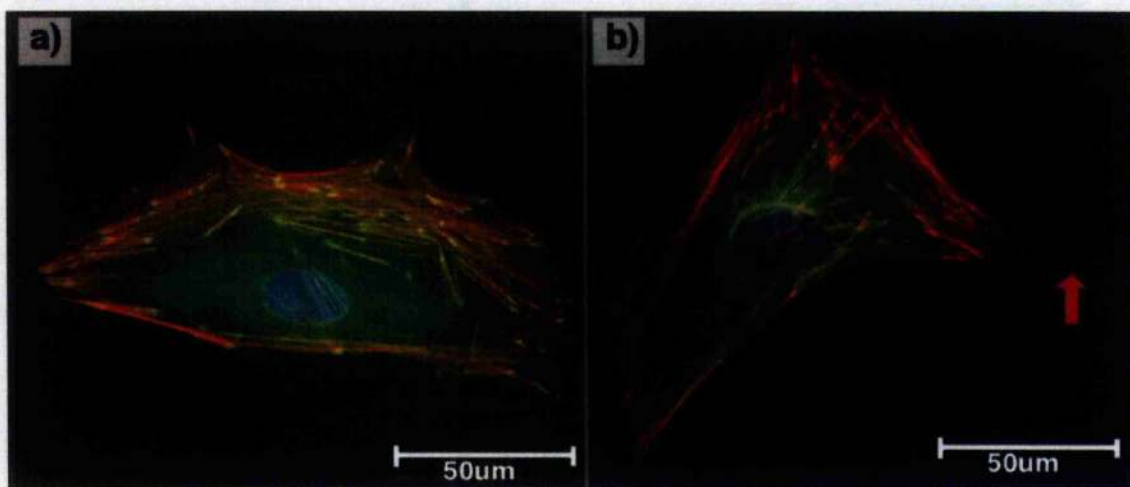


Fig 3.13 - Cells cultured on Th. (a) Triple labelled for ● Vinculin, ▼ Actin and ◆ DNA – Well spread cells with an abundance of focal adhesion/actin cytoskeleton complexes generally located at the cell periphery (b) ● Tubulin, ▼ Actin and ◆ DNA – The microtubule network radiated to all areas of the cytoplasm including extending lamellapodia without the presence of actin (red arrow).

SS – Stainless Steel

Cells cultured on SS were well spread; the actin cytoskeleton was again stretched to considerable lengths across the cell and terminated by mature dash morphology focal adhesion sites (Fig 3.14a). On very spread cells it was possible to resolve both the mature 'dash' type further in the cell body and also immature 'dot' focal adhesion sites not yet attached to actin (Fig 3.14c). Focal adhesions could be observed to align to surface features such as scratches, however this did not affect overall cell spreading, or orientation (Fig 3.14d). The microtubule network formed a dense network stretching to all areas of the cell cytoplasm (Fig 3.14b).

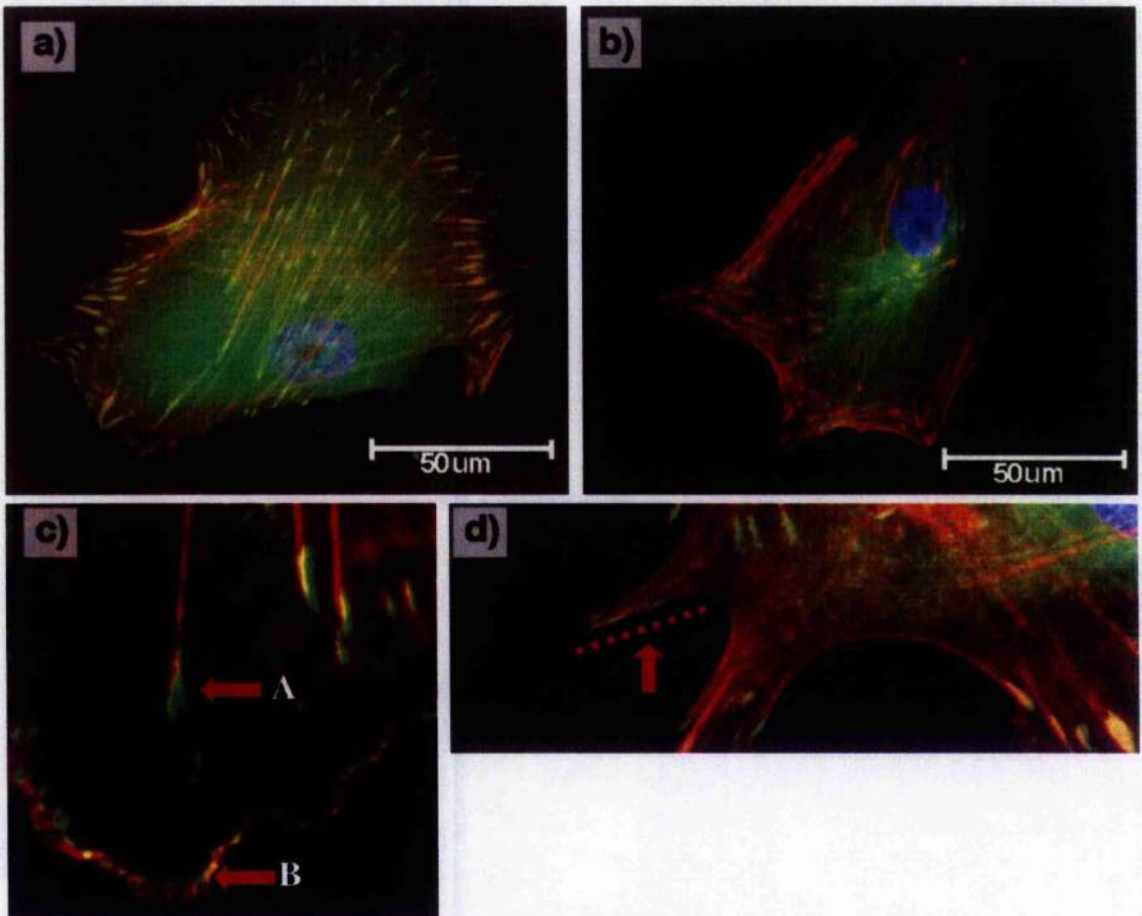


Fig 3.14 – Cells cultured on SS. (a) Triple labelled for ●Vinculin, ▼Actin and ◆DNA – Cells were well spread with large mature focal adhesion sites and associated actin cytoskeleton (b) ●Tubulin, ▼Actin and ◆DNA – The microtubule stain demonstrated a dense network reaching all areas of the cytoplasm. (c) Cells were spread enough to distinguish between 'mature' focal adhesions and associated actin filaments (A), and immature dot adhesion sites (B). (d) Cells were sensitive to any surface blemishes as the focal adhesion/actin complexes aligned with surface scratches (red line indicates scratch orientation).

TE – Electropolished Titanium

Cells were well spread on TE, again demonstrating mature focal adhesion sites attached to an organised cytoskeleton, and this structure could be observed to transect considerable portions of the cell body. Although the surface was very smooth, cells could be observed sensing and interacting with the surface detail. As observed in SEM, the filopodia could be seen interacting with the nodule surface detail, but this was not exclusively interaction for the filopodia as they also probe the surface undulations (Fig 3.15a(i)). Focal adhesions sites could also be observed aligning to these small undulations present on the surface (Fig 3.15a(ii)). The microtubule network was well conserved and radiated into all areas of the cell cytoplasm, however, close up the individual filaments could be observed occasionally avoiding the nodule features, indicated by the darker spots on the reflected light overlay (Fig 3.15b).

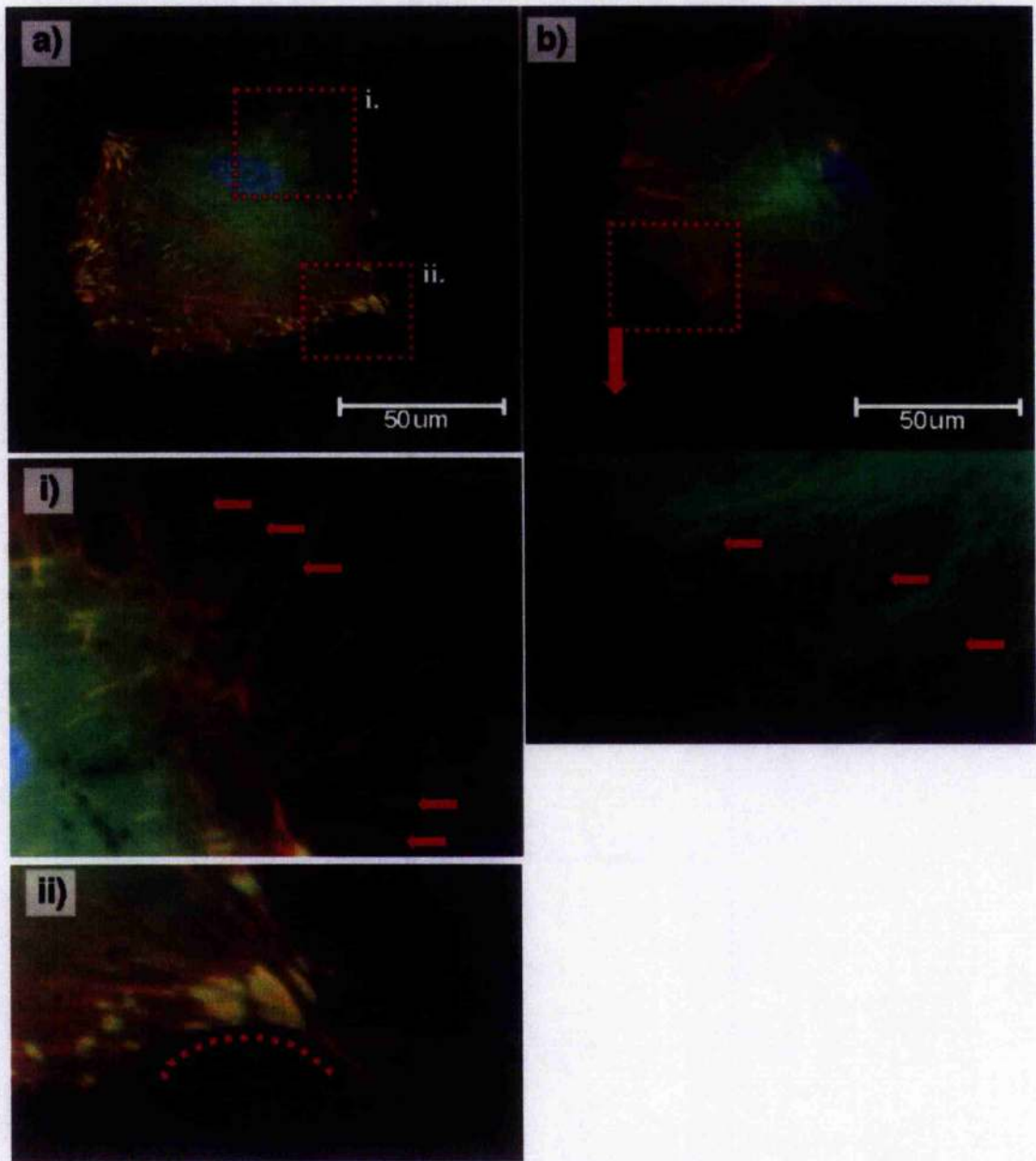


Fig 3.15 – Cells cultured on TE. (a) Triple labelled for ●Vinculin, ▼Actin and ◆DNA - Cells were well spread with mature ‘dash’ focal adhesion sites (vinculin) stain and associated actin fibres. Magnification (i) demonstrates filopodia probing the surface (red arrows). Inset (ii) demonstrates the alignment of the cell periphery and adhesion with the surface topography (dotted line). (b) ●Tubulin, ▼Actin and ◆DNA – Microtubules extended centrally to all areas of the cytoplasm. Inset demonstrates the nano-hill surface causing occasional avoidance of the microtubules (red arrows).

TS – Standard Titanium

Interaction with the rougher TS surface left cells with the appearance of being less spread compared with other surfaces. The focal adhesion sites appeared generally smaller in size however they were still connected to the actin cytoskeleton (this was confirmed quantitatively - see following section). Although not measured quantitatively, the actin cytoskeleton did not appear to transect such distances of the cell body as compared with smoother surfaces. The actin filaments were generally located at the cell periphery and contributed to considerable arching observed, possibly an indicator of the rougher surface (Fig 3.16a). Closer up it was possible to observe how the cells utilised straight actin fibres to produce the illusion of a curve at the cell periphery (Fig 3.16c). When the periphery was not arched its shape could often be dictated by features of the surface topography (Fig 3.16a). While cell shape was affected, the microtubule network was not, present at all areas of the cell and did not appear to be impaired by the rough surface (Fig 3.16b).

Fig 3.16 - Cells cultured on TS. (a) Triple labelled for ●Vinculin, ▼Actin and ◆DNA – The surface roughness of TS appeared to restrict the focal adhesion size and limit the lengths of the actin filaments transecting the cell. At the cell periphery, actin dependent arching was observed (red arrow 'A') and well as topography dependent spreading (red line on the inset magnification). (b) ●Tubulin, ▼Actin and ◆DNA – the rough topography had no influence on the microtubule structure. (c) Probable arrangement for the formation of the actin arching observed on the rough surfaces, involving the grouping of numerous filaments at different angles.

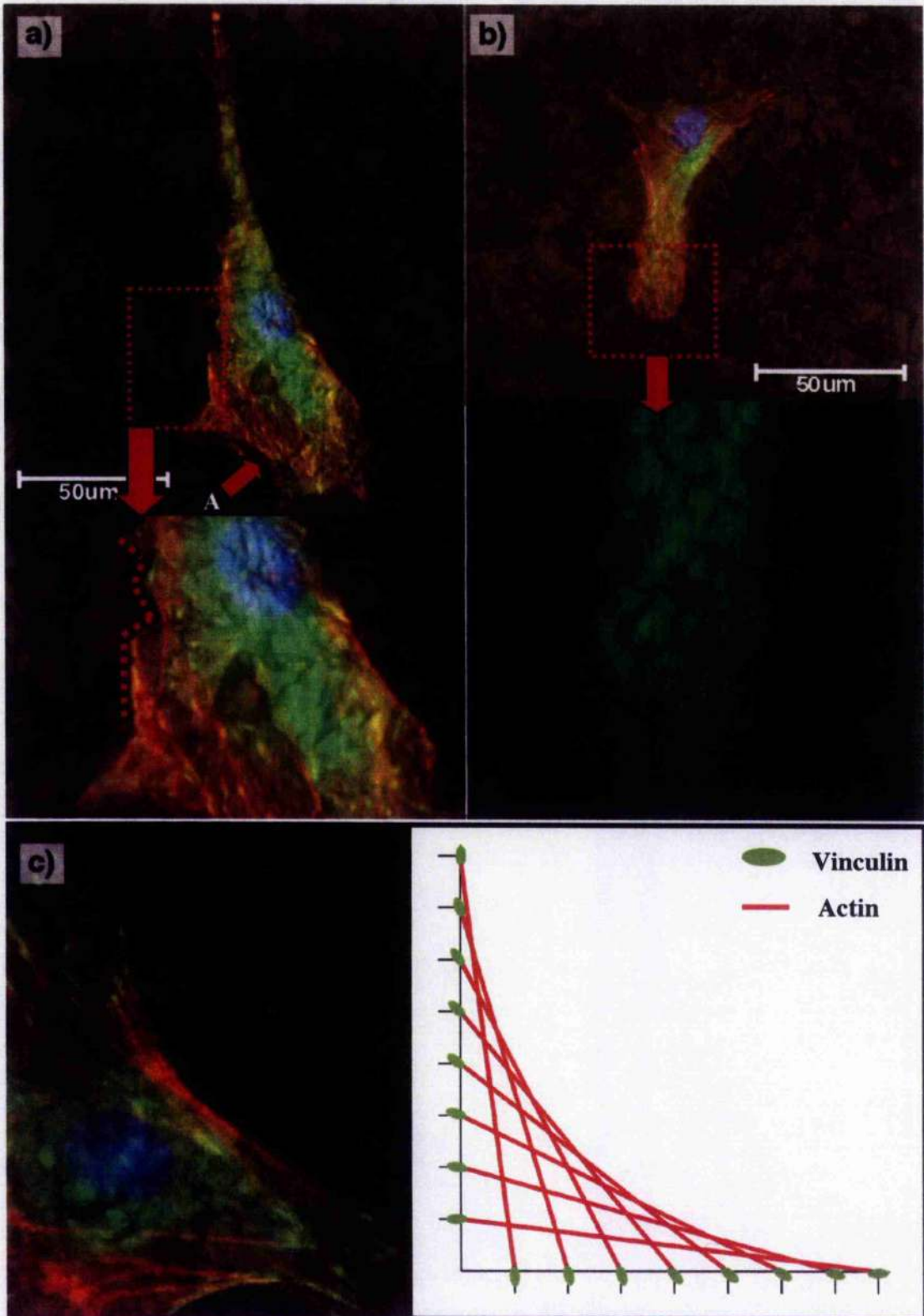


Fig 3.16 – (legend on opposite page)

NE - Electropolished TAN

Cells were well spread on NE with an organised actin cytoskeleton terminated by mature 'dash' focal adhesion sites generally located at the cell periphery. Cells were again sensitive to the minimal surface topography, as concluded from areas of the cell periphery and focal adhesion aligning to the surface undulations, however this surface detail did not restrict the size of the focal adhesion sites (see next section) (Fig 3.17a). The microtubule network was unaffected throughout the cell body, but was impeded indirectly by the surface topography due to its influence on peripheral spreading (Fig 3.17b).

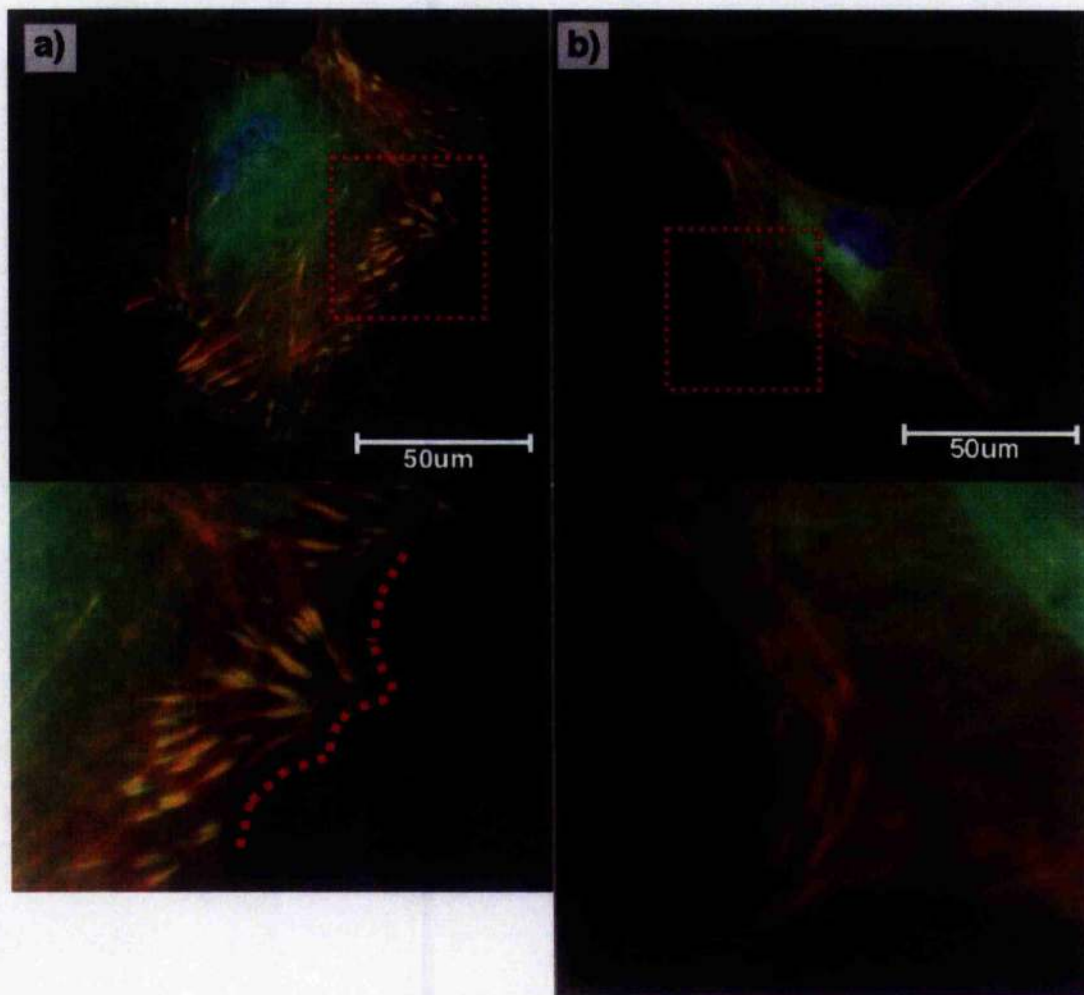


Fig 3.17 - Cells cultured on NE. (a) Triple labelled for ●Vinculin, ▼Actin and ◆DNA – Cells were well spread and produced mature adhesion sites associated with actin filaments. The inset demonstrates that the surface topography did influence the cell periphery and adhesion (red dotted line). (b) ●Tubulin, ▼Actin and ◆DNA – The surface topography demonstrated little influence on the microtubule network.

NS – Standard TAN

As observed previously with SEM, cells were generally unspread or elongated on NS (Fig 3.18a). The focal adhesion sites were small but were generally attached to the actin cytoskeleton. The adhesions were also observed avoiding the protruding particles on the surface – as discussed previously (Chapter 2, Discussion) the particles are the β -phase of the TAN alloy (Fig 3.18a). Actin arching at the cell periphery was also common for cells on the surface, an indication that this reaction might possibly be due to the rough topography. Due to the sizes of the cells the microtubule network could occasionally be difficult to resolve at low magnification (Fig 3.18b). Although, even at the low magnification it was apparent that there were breaches in the cell microtubule network throughout the cell body, and the microtubule filaments could be observed around, but not above the β -phase particle protrusions (Fig 3.18b(i)&(ii)).

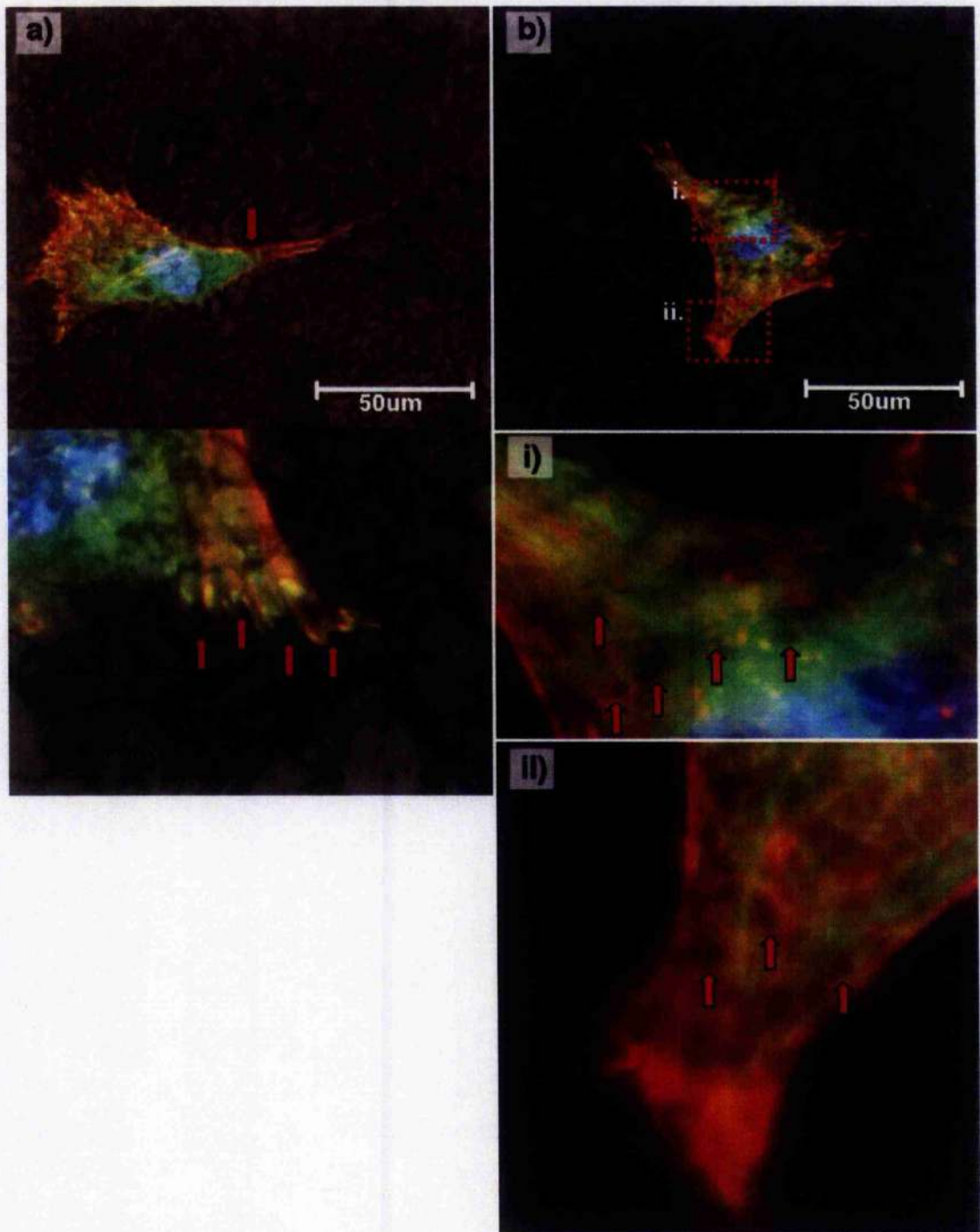
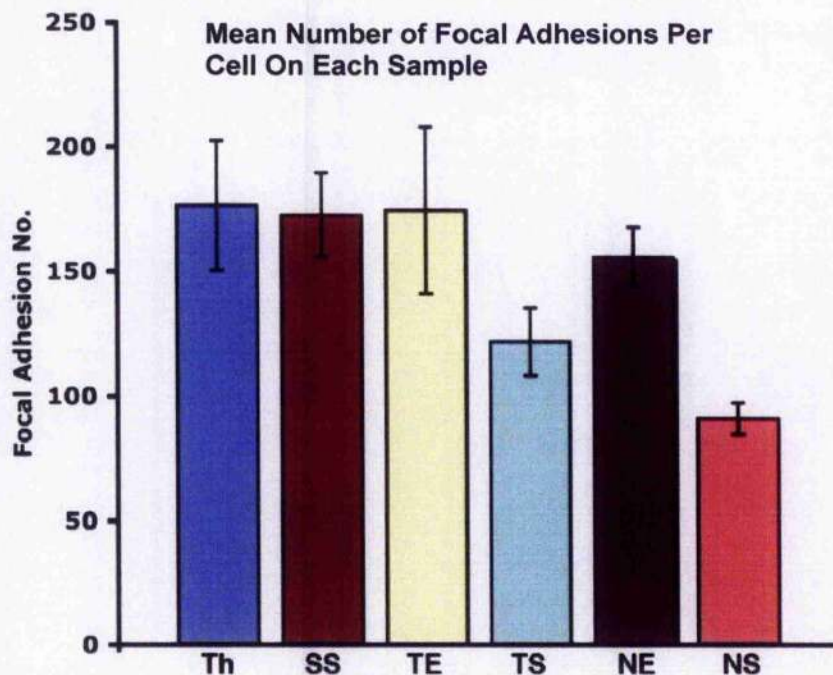


Fig 3.18 - Cells cultured on NS. (a) Triple labelled for ● Vinculin, ▼ Actin and ◆ DNA. Cells were generally unspread or elongated. Actin arching at the cell periphery was also common (red arrow). The rough topography of NS elicited small focal adhesion sites that were observed (inset) to avoid protruding β -phase particles on the surface (red arrows). (b) ● Tubulin, ▼ Actin and ◆ DNA – The protruding β -phase element of NS produced breaches in the microtubule network throughout the cell body. Insets (i) and (ii) demonstrate the occurrence of these breaches (red arrows),

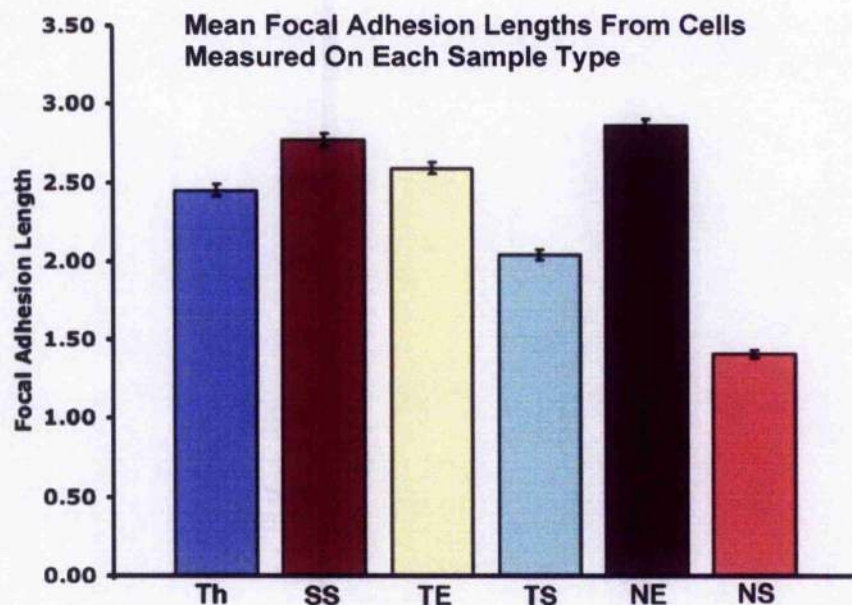
Focal Adhesions (FA) Measurement

Cells for measuring were chosen at random; therefore there was considerable variation in cell shape and area. This was reflected in the large standard error for most mean FA numbers. However, an average of 1700 adhesion sites were measured on each sample from 12 measured cells. This number provided a consistent mean number of FA's for cells on all the smooth surfaces – Th, SS, TE and NE (Graph 3.4). Both TS and NS were lower in numbers, with a lower standard error for NS indicating a more constant FA number from cell to cell (Graph 3.4).



Graph 3.4 – Summary of mean focal adhesion numbers per cell counted on each material. Error bars denote Standard Error

Similar to FA numbers, there was considerable deviation in the mean lengths of FA. This was expected, as the focal adhesion is a dynamic structure constantly changing. Again, the mean length per cell was consistent for cells on the smooth surfaces, Th, SS, TE and NE (Graph 3.5). FA lengths were smaller for TS and NS but a lower standard error suggested a more uniform FA length, especially for cells on NS.



Graph 3.5 - Summary of mean focal adhesion lengths measured from cells cultured on each sample type. Error bars denote Standard Error

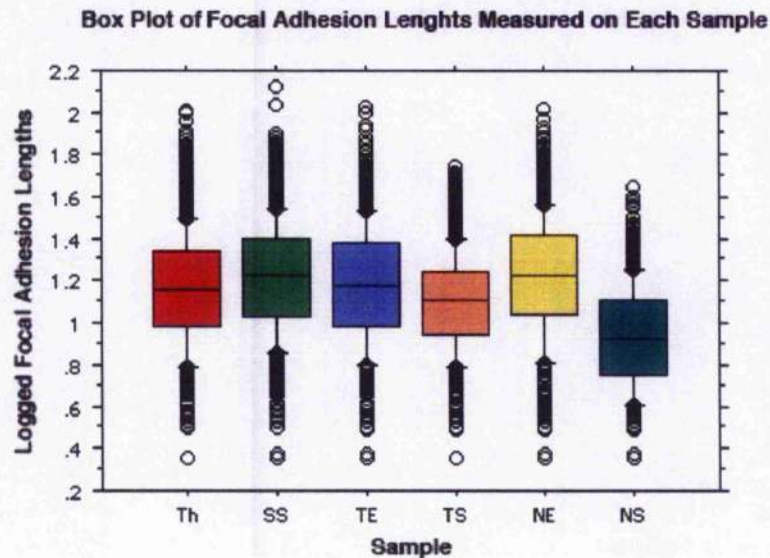
Utilising One-way ANOVA, the sample types were found to have statistically significant effects on focal adhesion length ($P < 0.01$) (Table 3.7). 13 of 15 comparisons of sample means were statistically significant (99% confidence level), summarised in Table 3.8. For cells on NS, FA length was confirmed to be significantly smaller than on any of the other substrates. However, the test also demonstrated that FA's on TS was significantly larger than NS, but smaller than for the other four samples. A box plot demonstrates the range of FA's measured on the surface, and indicated that for TS the focal adhesion length was not shorter than that found on the smooth surfaces, however they were stunted in producing longer adhesion sites. For NS, the whole distribution of FA lengths was much lower than on the other samples (Graph 3.6).

Source of Variation	Sum of Squares	Degrees of freedom	Mean Square	F-Ratio	P-Value
Sample Type	72.4	5	14.5	200.1	**<0.0001
Residual	751.5	10381	.072		

Table 3.7 - ANOVA table. **P-Values are <0.01 and statistically significant.

<i>Sample Comparison</i>	<i>Mean Diff.</i>	<i>P-Value</i>
Th - SS	-0.057	<0.0001
Th - TS	0.059	<0.0001
Th - NE	-0.058	<0.0001
Th - NS	0.225	<0.0001
SS - TE	0.039	<0.0001
SS - TS	0.116	<0.0001
SS - NS	0.282	<0.0001
TE - TS	0.077	<0.0001
TE - NE	-0.039	<0.0001
TE - NS	0.244	<0.0001
TS - NE	-0.0117	<0.0001
TS - NS	0.166	<0.0001
NE - NS	0.283	<0.0001

Table 3.8 – Bonferonni/Dunn interaction table. Statistically significant (99% confidence level) differences between each pair of means.



Graph 3.6 - Box plot of focal adhesion length variation measured on the sample types - note that the values have been logged. TS's lower quartile range (bottom edge of the box) does not dip below that of the smooth samples, however, its higher quartile does not extend as high, indicating a lower limit on focal adhesion lengths. The plot for NS demonstrates that the whole distribution of focal adhesions on NS is lower than for the other samples.

Sample Type	Cell Growth	Cell Morphology				Intracellular Staining			
		Spreading	Area	Elongation	Filopodia	Actin Cytoskeleton	Microtubules	Focal Adhesions Numbers	Length
Th	+/+	Variation of well spread and elongated cells	+/+	+/-	Present in close proximity to other cells	√	√	+/+	+/+
SS	+/+	Well spread cells	+/+	-/-	Present in close proximity to other cells	√	√	+/+	+/+
TE	+/+	Well spread cells. Some alignment to the topography	+/-	-/-	Utilised to sense topography and neighbouring other cells	√	√	+/+	+/+
TS	+/+	Cell were initially unspread at 24 hrs but by 48 were well spread. Visible alignment to the topography	+/-	-/-	Highly prominent on cells at 24 hrs and 5 days. Typically utilised to sense the topography	√	√	+/-	+/-
NE	+/+	Well spread cells. Some alignment to the topography	+/-	-/-	Present, but could not be observed sensing the topography	√	√	+/+	+/+
NS	-/-	Unspread or elongated cells. Some alignment to topography.	-/-	+/+	Highly visible on the surface, primarily interacting with the particulate topography	√	Network punctuated with holes at the sites of protruding particulates	-/-	-/-

Table 3.9 – Summary table of all qualitative and quantitative observations for hTERT cells cultured on the various sample types. All qualitative observations are described apart from '√' which denotes that the surface did not affect the labelled structure. For quantitative measures; '+/+' indicates a high value, '+/-' intermediate and '-/-' low.

Discussion

Cell Growth

Quantitative and qualitative cell growth demonstrated that the smooth metal topographies of SS, TE and NE, in addition to Th, allowed for favourable cell growth on the surfaces. Quantitatively, there were significant differences in cell growth generally split between two groups, Th, SS and TE, NE. Cell growth at the midpoint (5 days) was significantly higher for TE, NE compared to Th, SS, indicating that the nanoscale topography interaction was possibly advantageous for cell proliferation. However, over the timescale the final levels attained were similar, indicating that the various surface chemistries and minimal topographies did not have an adverse effect on cells.

For TS, the roughened topography was not inhibitory to cell growth on the surface with qualitative and quantitative levels comparing favourable with the smooth topographies. There were significant differences expressed in cell growth between TE and TS at the mid culture timepoint, with cell growth on TE higher than on TS. However, as with the electropolished samples, the final levels attained were similar. It would appear that for titanium a change in topography was not a cause for concern with respect to fibroblastic cell growth.

Cell growth on NS was consistently low at all timepoints, being visibly difficult to resolve cells with SEM and confirmed with quantified low cell numbers. NS was the only sample where its cell growth numbers were significantly different compared to all the other samples types. It is interesting in this instance that there was such a difference between cell growth on NS and its smoothed counterpart, NE, as both are produced from the same bulk material. While this might be a good indication that the topography of NS is the contributory factor, this was not a problem with TS and TE and numerically the roughness of TS was very similar to NS.

Cell Morphology

The qualitative morphology of cells cultured on the electropolished samples (SS, TE and NE), and that of Th, was quite similar in that the cells were very well spread, indicating

favourable adhesion to the surfaces. Quantitatively, the mean cell area of SS and Th was significantly higher than on the other electropolished surfaces. This would indicate that the cell spreading was higher on SS and Th, however the cell aspect ratios demonstrated that only cells on SS were well spread while cells on Th had large areas but over a more elongated morphology. It is possible that the micro and nano-topography of TE and NE did influence cell spreading, as cells appeared to detect certain topographical aspects. As discussed later, fluorescence labelling of intracellular features demonstrated alignment to surface features on both TE and NE, and filopodia were observed with SEM to be exploring the nano-hill topography of TE.

Cells, cultured on TS, morphologically differed from counterpart cells cultured on TE. At 24hr the cells on TS were visibly less spread with numerous surface ruffles. Ruffling is considered as storage compartments for excess membrane, and in unspread cells this would logically appear increased (O'Neill *et al.*, 1986; Rubin and Everhart, 1973). This lesser spread morphology could be due to the rougher topography; this is indicated by the exploratory nature of the filopodia emanating from more central regions of the cells (Clark *et al.*, 1990; Dalby *et al.*, 2004a; Dalby *et al.*, 2004b; Wood and Martin, 2002). However, by 5 days cell growth demonstrated that cells were viable on the surface, and better spread cells were observed. These differences were also diminished at 48hr as quantitatively there were no differences in cell area or aspect ratio between TS and TE.

Cells cultured on NS displayed a remarkable contrast to those cultured on the other five substrates. Qualitatively, at 24hr, cells were less spread with a rounded or thin and elongated morphology. Shadowing surrounding the cells indicated that they did not favour adhesion on the surface and appeared to be retracting. The emergence of filopodia at 5 days suggested that the cells were exploring the surface, generally found attached to the protruding β -phase particles surrounding the settling site of the cell. High current BSE imaging was used in an attempt to examine the cells' relationship with the underlying β -phase particles. However, it could not be elucidated from this method if the cells were attempting to endocytose the particles in a possible attempt to create a more favourable underlying topography. Quantitatively, the cell morphology findings were confirmed with

cell areas on NS being significantly different from all other sample types, and the cell aspect ratio suggested that cells were more elongated compared to cells on all other samples with the exception of Th.

At this point it could be speculated that the cell morphology and stalemated cell growth on NS might indicate that the cells have entered senescence (Campisi, 1997) or a form of cell death. Lack of spreading has been associated with initiating apoptosis (Chen *et al.*, 1997). However, in the occurrence of apoptosis (programmed cell death) the cell membrane remains intact, while a loss of membrane integrity is associated with increased permeability characteristics of cell necrosis (Dartsch *et al.*, 2002; Gjertsen *et al.*, 1994). The change in membrane integrity and rounded cell morphology of cells cultured for 10 days on NS would indicate possible necrosis (Sen *et al.*, 1998; Zislis *et al.*, 1989).

Cell Adhesion and Measurement

There are numerous methodologies for the measurement of focal adhesions; indeed the author has been involved in studies developing SEM immunolabelling and quantification for biomaterials purposes (Meredith *et al.*, 2004; Owen *et al.*, 2001; Owen *et al.*, 2002). However, while vinculin is an adequate choice for labelling focal adhesion sites (Owen *et al.*, 2005), total quantification of focal adhesion sites is difficult. Theoretically, permeabilisation treatments should remove a significant portion of the unbound cytoplasmic vinculin pool leaving only focal adhesion bound vinculin, however, in practice a considerable amount of background remains. For the analysis of fluorescence images this is a problem as it can be difficult to successfully separate the sites from the background (Hunter *et al.*, 1995). While SEM quantification can omit the background more easily due to the particulate nature of the label allowing size omission, it is not accurate enough to assess focal adhesion numbers and length (Fig 3.19a). Although the length of a mature focal adhesion site has been reported up to 10 μ m (Bershadsky *et al.*, 1985), when examining numerous larger sites with fluorescence it becomes obvious that there are actually numerous sites present (Fig 3.19b). Image analysis of SEM nor fluorescence can elucidate this and therefore, although time consuming, the most accurate focal adhesion measurements and counts should be done manually (Diener *et al.*, 2005).

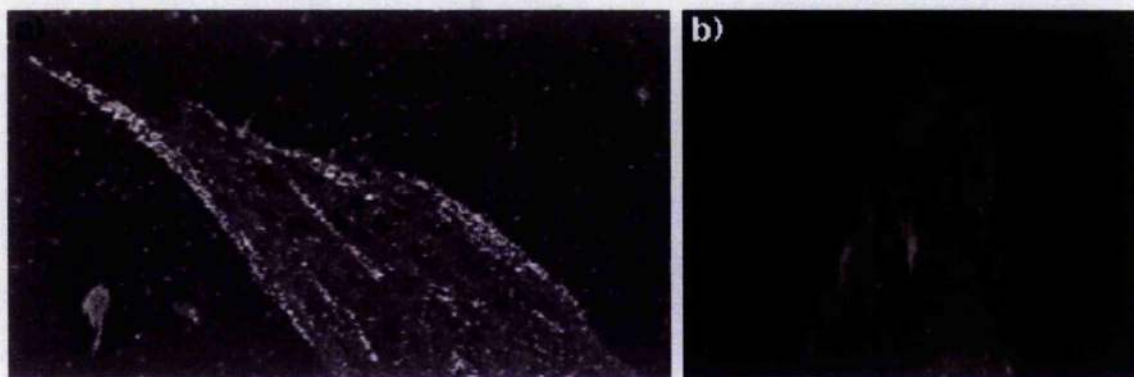


Fig 3.19 – (a) Example of immunogold vinculin label demonstrating mature 'dash' focal adhesion sites. While adhesion area can be calculated, the number and length is difficult to measure. (b) Fluorescence image of vinculin labelled focal adhesion sites confirms that numerous large focal adhesions are in fact comprised from multiple 'dash' adhesions.

For cells on the smooth electropolished surfaces (SS, TE and NE) and Th, qualitatively, there was an abundance of mature 'dash' morphology focal adhesion sites with associated stress fibres stretching considerable lengths over the surface. On SS, the adhesions were only sensitive to surface blemishes such as micron dimension scratches. The topography on TE and NE did provide alignment cues for cell spreading with focal adhesion sites aligning to the ridges. As mentioned previously, this might be a contributing reason for the lower cell area on TE and NE compared to SS and Th. Quantitatively, the mean number of focal adhesions and their lengths on each surface were surprisingly consistent, indicating that the minimal topographies do not clearly prevent focal adhesion formation and maturation. The large standard deviations indicated that when there was no visible topographical restriction, the constant dynamic remodelling of adhesion sites produced a natural range of sizes (Davies *et al.*, 1993). However, it must be noted that the differences between the focal adhesion sizes on each of the surface were statistically significant.

Qualitatively, both cell spreading and focal adhesion formation appeared restricted by the rough topography on TS. Mature 'dash' focal adhesion sites were observed with associated actin cytoskeleton on the surface, however, quantitatively, the mean focal adhesion number and length was lower than those on the smoother surfaces. This did not translate into a difference in cell growth, nor in mean cell area. While the mean focal adhesion length was less than the on smooth surfaces, its mean length was still within the minimal $2\mu\text{m}$ range for categorising a mature focal adhesion site (Bershadsky *et al.*, 1985).

Cells on NS retained some similar characteristics with TS such as restricted focal adhesion formation and spreading. Focal adhesion sites were also restricted in their formation by the protruding β -phase particle topography, and quantitatively, focal adhesion numbers and lengths were the lowest of any cells measured on all the samples. The variability (standard deviation) was also lower, indicating that there was only a small range of sizes measured on the topography. The mean size dipped below Bershadsky's minimum measurement at 1.4 μ m and was significantly lower than that on TS and the smooth samples. This could possibly serve as an indication that the lower number and length of the focal adhesions of cells on NS compared to TS might dip below a certain threshold value required for spreading and proliferation on the surface.

Microtubules

Microtubules are the larger filaments of the cell cytoskeleton (25nm) and form a cytoplasmic-wide network extending outwards from a microtubule-organising centre (MTOC) or centrosome (Cleveland, 1999; Lodish *et al.*, 1999). They are found to be responsible for an ever-increasing number of functions within cells. A well-documented function is the production of the mitotic spindle required to separate the duplicated chromosomes during mitosis, thus allowing the formation of two daughter cells (Cleveland, 1999). Apart from this central role they have been found to have a considerable influence in establishing cell shape (Etienne-Manneville, 2004) and are utilised as transport networks to move essential organelles, such as mitochondria (Tanaka *et al.*, 1998), and mRNA (Chou *et al.*, 1995) to various areas of the cell cytoplasm as required. Recent discoveries have identified their involvement in the maintenance of focal adhesion sites, specifically the transport of components and also the regulation of internal stress (Geiger and Bershadsky, 2001). Disruption of the microtubule network increases intracellular tension and focal adhesion growth, while its presence relaxes the tension and formation (Ezratty *et al.*, 2005; Small *et al.*, 2002). It is speculated that the system is important for cell migration (Geiger and Bershadsky, 2001).

While there was a possible disruption of the microtubule network on cells on NS, the lower focal adhesion size would suggest that this did not affect cell adhesion. A more probable

theory is that the disruption of the network might have influenced protein, organelle and mRNA distribution. A light microscopy study examining mitochondria distribution in comparison with the microtubule network was attempted, however mitochondrial labelling was unsuccessful, possibly due to the presence of the metal substrates interfering with the labelling method. Due to time constraints this investigation could not be explored further.

Summary

These initial studies have demonstrated that for the smooth materials, Th, SS, TE and NE the variation in their surface chemistry and micro and nano-topography did not have an adverse influence on cell adhesion, spreading or subsequent cell growth. The morphology observed is common to that on smooth surfaces (Brunette and Chehroudi, 1999) and corresponds with previously reported osteoblast reactivity to smooth SS, Ti-6Al-4V and Thermanox (Anselme *et al.*, 1999). For titanium the standard roughened topography also presented no problems for cells, indicating the overall cytocompatibility of titanium as a biomaterial. This is a more surprising result as it is commonly reported that variation in titanium roughness can have an effect upon spreading and proliferation (Kononen *et al.*, 1992), and the poor performance of NS is more in keeping with these observations. Focal adhesion site length has been found to be dependent on surface roughness (Diener *et al.*, 2005) although the context of their observations has generally leaned towards aspects of motility and anchorage rather than what is proposed here; that the impairment of focal adhesion maturation and cell spreading to a possibly sufficient threshold blocks cell cycle progress and eventually cell growth (Baharloo *et al.*, 2005; Diener *et al.*, 2005).

While favourable cell growth on NE would indicate that the roughened topography is the contributing factor, this cannot be certain as the surface treatments of both NS and NE produce heterogeneous oxide layers of stoichiometrically different compositions (Brunette *et al.*, 2001; Sittig *et al.*, 1999). As discussed in Chapter 2, this could influence the surface isoelectric point and thus protein absorption. Additionally, studies with Ti-6Al-4V of various roughness suggest this as a possible reason for an observed decrease in osteoblast proliferation (Anselme *et al.*, 2000b). Simply a roughened topography is also insufficient as an explanation as cell growth was adequate on TS, a numerically similar roughness to NS.

Only through visual surface characterisation is it apparent that there is considerable difference between TS and NS that might explain the differences observed. Through a culmination of studies, Bigarelle and Anselme have concluded that surface ‘morphology’ and not numerical roughness influence cell proliferation (Bigarelle and Anselme, 2005). This definition is based on the correlation of numerous measurements, such as roughness organisation rather than simple height averages; these measures were observed to elicit significant osteoblast reactivity (Anselme *et al.*, 2000a; Anselme *et al.*, 2002; Bigarelle *et al.*, 2002). A prominent characteristic of NS is the protruding β -phase particles observed to elicit filopodia probing, focal adhesion avoidance and microtubule network interference. Cell reactivity to the particles might solely be due to the topography they produce, their oxide chemistry or possibly a combination. Additionally, a practical observation of the apparent looseness of some of the particles and SEM images of cellular interaction might indicate attempted cellular endocytosis of these particles. A final factor generally put forth in biomaterials studies is the possibility of harmful metal ion diffusion from the surface (Okazaki and Gotoh, 2005). This could be disproved by the favourable reaction of cells on NE and evidence from recent studies have also demonstrated that even if present, Al and Nb ions are not detrimental to the cells (Hallab *et al.*, 2005; Okazaki *et al.*, 1998).

Chapter 4 - β -Phase Particles

Abstract

In the previous chapter, considerable cellular interaction was suspected to occur in relation to the protruding β -phase particles on NS. A practical observation of the apparent looseness of some of the particles on NS led to the notion that the cells might possibly endocytose or at least attempt to endocytose the loosened particles from the surface. Cells recovered from the surface of NS were demonstrated to have internalised particles which were confirmed to originate from NS. However, clathrin staining of cells on NS failed to demonstrate any visible signs of endocytosis on the surface. Cells cultured in the presence of NS displayed endocytosed particles but their growth was not significantly inhibited, suggesting that even if endocytosis occurred on the surface of NS, this was not the cause of the suppressed cell growth observed. This also ruled out ion leeching affecting the cells, and further confirmed the influence of NS topography or chemistry or a combination of both on cell growth.

Chapter 4 - β -Phase Particles

Introduction

In Chapter 3, the initial SEM and fluorescence microscopy investigations of cells on NS demonstrated considerable cellular interaction with the protruding β -phase particles; such as they were being probed by filopodia, avoided by focal adhesions and interfered with the microtubule network. In addition, a practical observation of the apparent looseness of some of the particles on NS led to the notion that the cells might possibly endocytose (Osano *et al.*, 2003), or at least attempt to endocytose (Dalby *et al.*, 2004c), the loosened particles. In Chapter 3, higher current BSE was utilised to examine cell interaction directly over the particles, however this did not elucidate any specific interaction.

Endocytosis is a mechanism of transporting macromolecules and particles of various sizes into the cell. The term encompasses two separate types of ingestion; pinocytosis and phagocytosis. Pinocytosis, or 'cellular drinking', allows sub-100nm particles such as solutes and fluids to be ingested. Phagocytosis, or 'cell eating', allows the ingestion of objects above 250-500nm - these can be diverse including apoptotic cell bodies, pathogens or food particles (Alberts *et al.*, 1994; Conner and Schmid, 2003; May and Machesky, 2001). Pinocytosis occurs in all cells while apart from food ingestion and apoptotic cell bodies, phagocytosis is generally present only in specialised cells. Macrophages, neutrophils and dendritic cells are classed as 'professional' phagocytes, however other cells including fibroblasts, endothelia and epithelia are termed 'non-professional' phagocytes and display facultative phagocytosis (Alberts *et al.*, 1994; Fadok and Henson, 1998). The mechanism of endocytosis (both phagocytosis and pinocytosis) involves utilising the cell membrane, pinocytosis by membrane invagination, and phagocytosis by extension of pseudopodia, that progressively engulfs the macromolecule until it is completely internalised in the cell (Conner and Schmid, 2003). The internalised macromolecule is contained in a pinched-off sac lined with membrane – this is termed an endocytic vesicle (Alberts *et al.*, 1994). For internalisation, the membrane is lined on the inside with the cytoskeletal element, clathrin, which cross-links to eventually produce a spherical fullerene-like net that engulfs the particle (Conner and Schmid, 2003; Cooper and

Hausman, 2003; Qualmann and Kessels, 2002). Dynamin completes the internalisation process by pinching-off the neck of the vesicle, thus releasing the structure from the cell membrane (Alberts *et al.*, 1994; Hinshaw, 2000). Another important component is the actin cytoskeleton which is involved in the initial pseudopod extension followed by giant membrane ruffles that enable particle ingestion (Ellis and Mellor, 2000; May and Machesky, 2001; Qualmann and Kessels, 2002; Qualmann *et al.*, 2000).

There are no studies currently in the literature examining fibroblast behaviour towards titanium and niobium β -phase particles, or TAN particles, but reactivity to titanium particles has been documented (Chapter 1: Section 2.7). Cells cultured *in vitro* exposed to titanium particles have been observed to display reduced viability (Osano *et al.*, 2003) and occasional necrosis (Mostardi *et al.*, 1999; Mostardi *et al.*, 2002). It would seem plausible that, as these β -phase particles are primarily titanium, they might elicit similar effects.

In the following chapter, the possibility was investigated that fibroblast endocytose β -phase particles on NS. Due to sample limitations, electropolished samples of TE and NE were not included in these studies. Controls for NS were the other standard materials, SS and TS, and Thermanox.

Materials and Methods

Experiment 8 - β-phase particle X-ray microanalysis

Cell Seeding

hTERT-BJ1 cells were seeded onto 11mm NS sample discs at 5000 cells per 0.5ml of complete DMEM/199 in 4 well plates. The cells were incubated at 37°C with a 5% CO₂ atmosphere for 48 hr.

Cell Removal from NS

The samples were transferred to a new container, washed with TBSS and detached with 0.25% trypsin and 0.02% EDTA in TBSS. Cells were then seeded on Thermanox and cultured for a further 24 hr.

Sample Fixation and SEM Preparation

The Thermanox samples were fixed for SEM (see Chapter 3: Experiment 5) with the omission of the osmium tetroxide post-fixation. Samples were coated with 15nm carbon using a Bal-Tec Carbon Evaporator (CED 030).

Resin Embedding of NS particles

NS samples were immersed in un-polymerised liquid LR White Acrylic Resin (London Resin Company), of medium hardness. 3 drops of paraffin were suspended on the liquid resin surface to seal the resin from contact with air and the sample was polymerised for 12 hours at 55°C. The NS embedded resin bloc was ground to expose the disc edges and lower side while leaving a column of resin attached to the topmost surface of the metal. A copper block was cooled using liquid nitrogen slush (produced by a high vacuum), and the NS bound resin placed on the block. By pressing down the metal cooled quicker than the resin and parted from the resin. The resulting resin column was mounted on an EM stub, oriented so that the newly exposed surface was the samples' focal point. The resin was lined with silver paint and carbon coated for electrical conductivity (Richards *et al.*, 1995).

BSE and X-Ray Microanalysis

Samples were imaged on the Hitachi 4100 in both SE and BSE detection mode at between 10-20 kV. These samples were also analysed using an energy dispersive X-ray microanalysis system (EDX) fitted with a Pentafet Silicon (lithium) detector with 1024 channels and 20keV range detector (Link Isis 300, Oxford Instruments, Witney, U.K.) attached to the microscope. X-ray analysis of cell particular uptake was conducted using 'spot' analysis where elements from a specifically selected spot were measured. Resin samples were imaged using 'mapping' of a whole image to observe the location of specific elements.

*Experiment 9 - Clathrin Immunostaining**Cell Seeding*

hTERT-BJ1 cells were seeded onto 11mm sample discs of SS, TS, and NS (in duplicate) at 5000 cells per 0.5ml of complete DMEM/199 in 4 well plates. The cells were incubated at 37°C with a 5% CO₂ atmosphere for 48 hr.

Clathrin and Actin Immunostaining

The fluorescence immunostaining was conducted following the procedure listed in Chapter 3: Experiment 7 with some minor modifications. In step 5 the primary antibody applied was anti-Clathrin at 1:100 (Biogenesis, Cat No. 2115-5004).

Experiment 10 - DNA Quantification of cell growth in the presence of Th, SS, TS and NS

hTERT-BJ1 cells were seeded onto 49mm sample discs of SS, TE, TS, NE and NS at 5.0 x10⁴ cells per 5ml of complete DMEM/199 in 60x15mm tissue culture dishes. The cells were incubated at 37°C with a 5% CO₂ atmosphere for 24 hours, 5 and 10 days and the culture media was changed every 2.5 days. All samples were prepared in triplicate and samples were processed using a similar protocol to Chapter 3: Experiment 6, although in this instance the sample holders were processed.

Results

Experiment 8 - β -phase particle X-ray microanalysis

From the SEM observations of cells on NS, it was hypothesised that cells could be endocytosing loose β -phase particles from the surface of NS. In order to investigate whether the cells had indeed ingested the metal particles, cells were seeded and then recovered from NS and reseeded on Thermanox. Locating cells on the Thermanox was difficult due to the observed lack of cell adhesion and proliferation on NS, lowering the number of recoverable cells and also due to the required omission of the osmium tetroxide postfix. The osmium tetroxide stain was omitted to lower the number of expected elements found in the X-ray microanalysis. The recovered cell seemed similar in morphology, viewed with SE imaging, to cells cultured on other smooth substrates, and there were no visible particles on the surface (Fig 4.1a). When the cell was examined in BSE mode, it became apparent by the difference in compositional contrast that the cells contained foreign material particles (Fig 4.1b,c). These particles were examined using spot analysis mode on the X-ray microanalysis detector and were confirmed to be primarily composed of titanium and niobium, indicated by the spectrum peak identification (Fig 4.1c).

To confirm that the surface particles evident on NS could be removed from the surface by a cell and to identify them, a standard NS surface was embedded in LR White resin and peeled away. A BSE image of the resin demonstrated the presence of electron dense particles (Fig 4.2a). An X-ray map confirmed that these particles contained titanium and niobium (Fig 4.2b). This confirmed that the particles found within the cell originated from the NS surface. The stringent washing regime carried out during the trypsinisation step and consequent seeding supports the argument that the cells must have actively endocytosed the particles whilst on the NS surface, prior to removal.

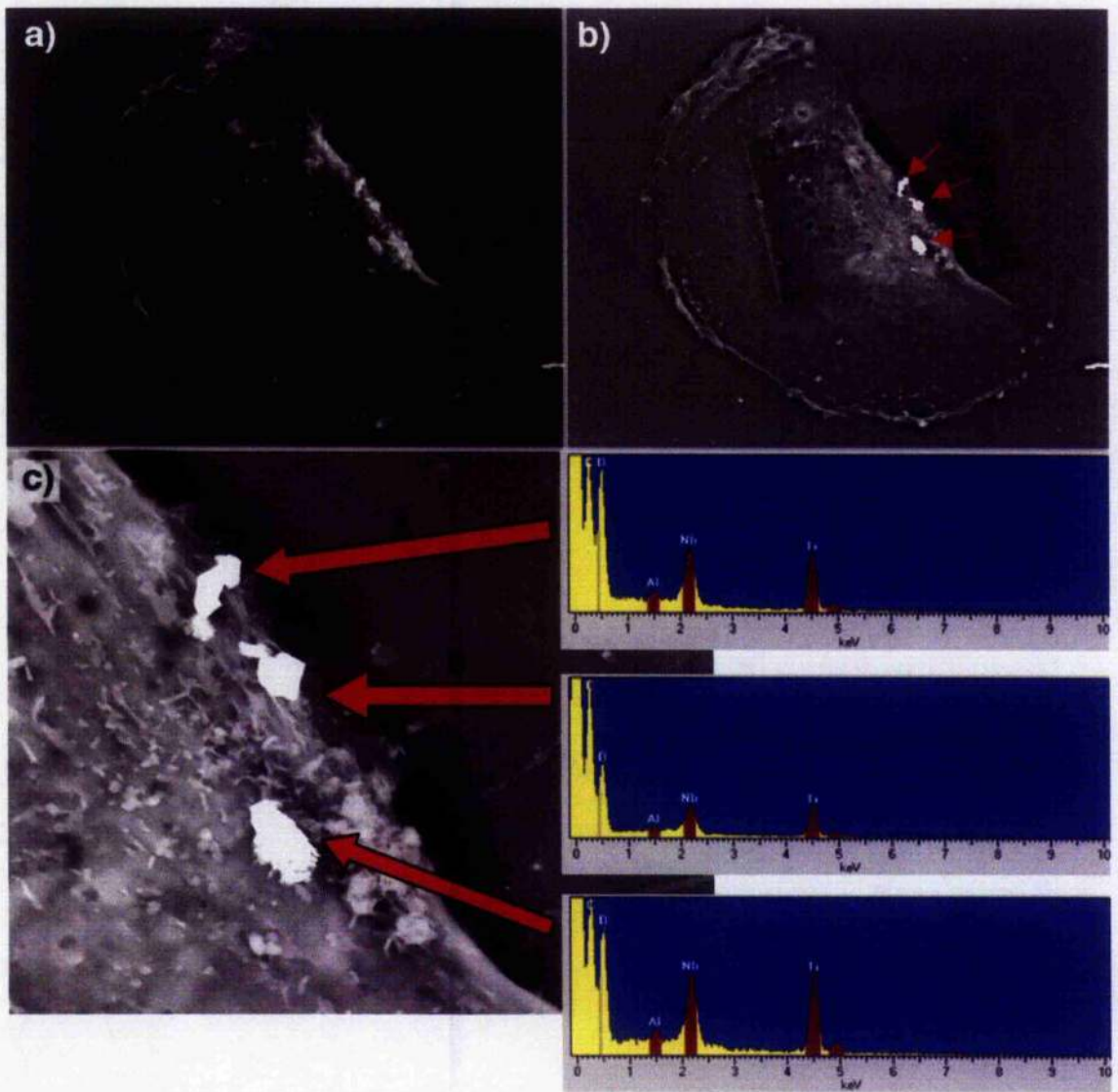


Fig 4.1 - Cells were removed from Standard TAN (NS) after culturing for 48hr and subsequently seeded onto Thermanox and cultured for a further 24hr prior to fixing. (a) An SEM micrograph in SE mode indicated no visible particles on the cell surface. (b) BSE mode demonstrated with compositional contrast that the cells contained foreign material particles labelled A., B. and C. (c) A higher magnification of the foreign material particles. X-ray microanalysis spectrums (spot analysis) for the corresponding particles confirmed them to be primarily titanium and niobium in composition, originating from NS surface.

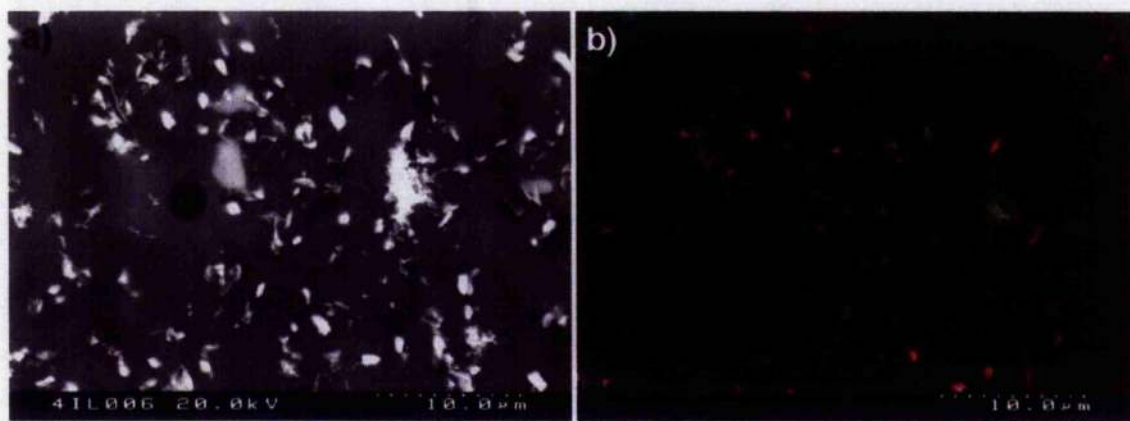


Fig 4.2 (a) BSE image of a resin sample removed from the surface of NS. The bright particles are loose β -phase particles of TAN embedded in the resin. (b) Pseudo-coloured X-ray map composite with the BSE signal in red, Nb signal in Green and Ti in Blue.

Experiment 9 – Clathrin, Actin and DNA Immunostaining

As removal and endocytosis of particles by fibroblasts on NS was a possibility, evidence was sought of this interaction directly on the surface. The possible endocytosis of β -phase particles by cells cultured on the NS surface was investigated utilising a Clathrin and Actin stain, as both proteins are known to be involved in endocytosis. SS and TS were utilised as controls for staining on NS.

SS - Stainless Steel

For cultured cells on SS, the actin staining demonstrated an organised cytoskeleton throughout the well spread cells. The immunostaining of clathrin demonstrated it to be diffuse throughout the cell cytoplasm without condensing in any particular areas (Fig 4.3).

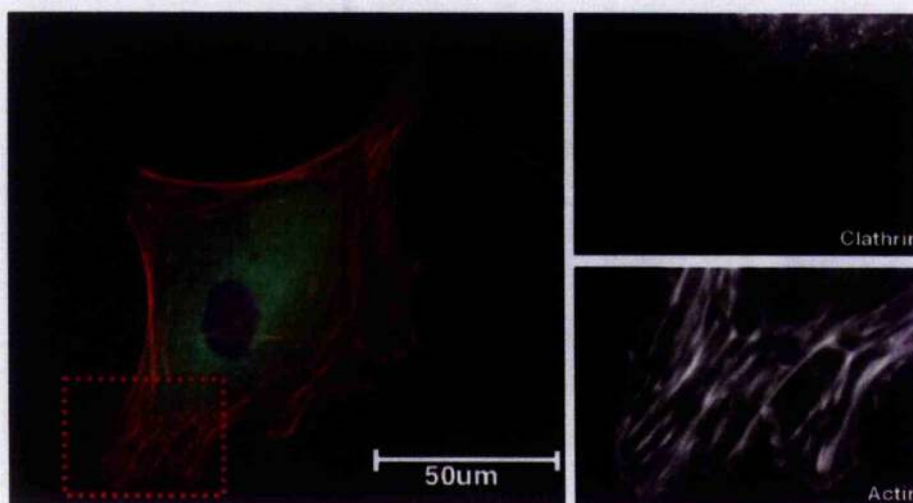


Fig 4.3 – ● Clathrin, ▼ Actin and ◆ DNA. The actin cytoskeleton was organised into filaments generally located at the cell periphery on SS. Clathrin was observed to be diffuse throughout the cytoplasm stained as small globules, apparently most concentrated in the cell centre. The inset pictures demonstrated no specific organisation of clathrin while actin filaments had a high level of organisation of the surface.

TS – Standard Titanium

For cells cultured on TS, the cell periphery appeared more undulating with lamellapodia extending into numerous directions. The actin cytoskeleton was organised throughout the cell with no indication of its utilisation for any purpose apart from a structural role. The clathrin staining was diffuse throughout the cell cytoplasm with no apparent condensation towards any particular surface roughness characteristics. (Fig 4.4)

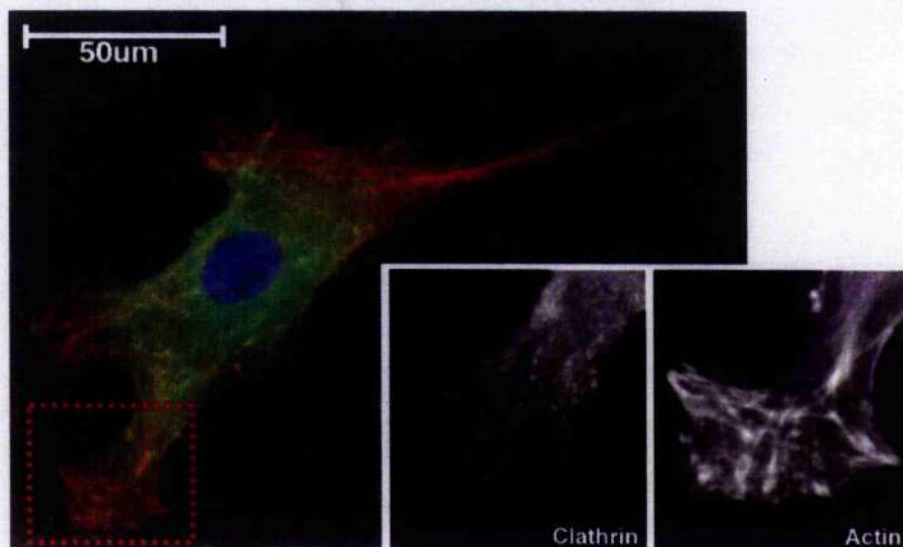


Fig 4.4 - ●Clathrin, ▼Actin and ◆DNA. Actin filaments were visible and did not appear to be affected by the rougher topography of TS. Clathrin staining was most concentrated at the centre of the cell however no specific organisation could be observed. The inset images demonstrate the diffused clathrin at the extending lamellapodia, while the actin is organised in filaments orientated in numerous directions.

Fig 4.5 – (opposite page) ●Clathrin, ▼Actin and ◆DNA. (a & b) Elongated cells NS, possibly under tension demonstrated by the large actin bundling visible at the cell periphery (red arrows). Breaches in the cytoplasm could be observed at low magnification attributed to β -phase particle protrusion. Inset on both cells demonstrate that while there were breaches in the clathrin staining (red arrows), no extra condensation of the labelled globular protein could be observed surrounding them. In addition, an actin filament production was unperturbed at the areas of the protrusions (red arrows).

NS – Standard TAN

On NS cells were generally unspread or elongated. As the cytoplasm made the labelling too dense to resolve any detail in unspread cells, elongated cells were imaged as examples. A visible detail of cells on NS was apparent with breaches in the cell cytoplasm at various points in the cell body, generally corresponding with protruding β -phase particles. Cells were apparently under tension on the surface with large bundling of actin at the cell periphery (Fig 4.5a,b). Apart from this the cytoskeleton was organised and unperturbed by the presence of these protrusions. The clathrin was diffuse throughout the cell cytoplasm with the exception of the observed breaches. However, no apparent condensation of clathrin could be observed surrounding these areas nor were there any indications of the formation of specific endocytosis related structures.

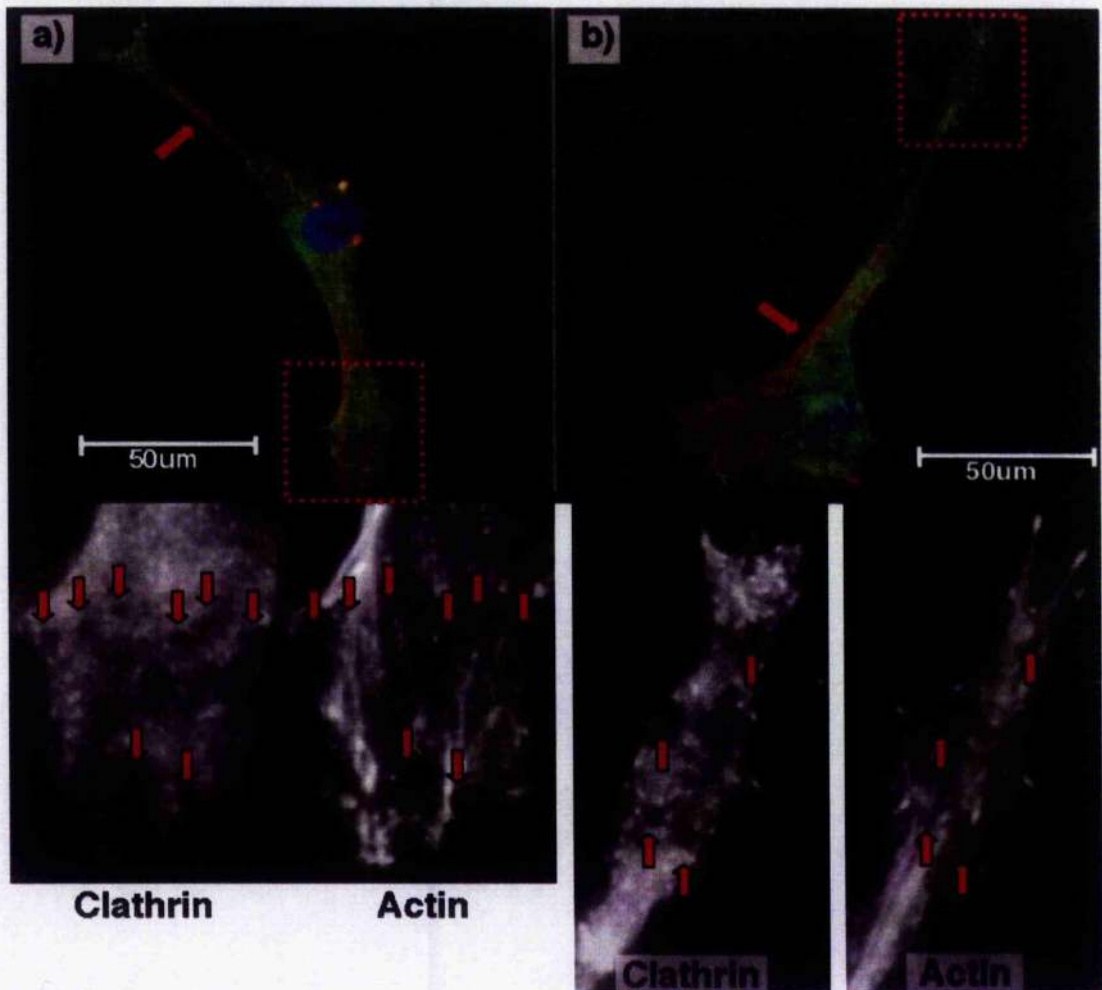


Fig 4.5 – (legend on opposite page)

Experiment 10 - DNA Quantification of cell growth in the presence of Th, SS, TS and NS

While endocytosis could not be confirmed on the surface of NS, this raised the question of the involvement of loose particles in the previous observations of arrested cell growth. It had been observed during culturing on NS that cells cultured in the presence of the material were frequently contaminated with material now known to be loose β -phase particles from the surface (Fig 4.6). To investigate this, cell growth was measured over a 10 day timeperiod, measured by means of DNA quantification.

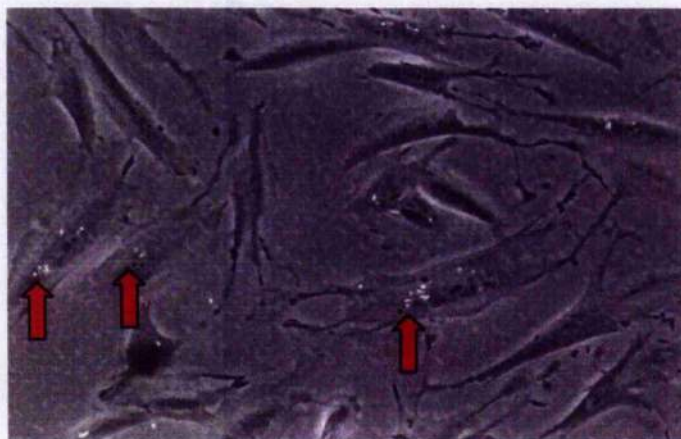
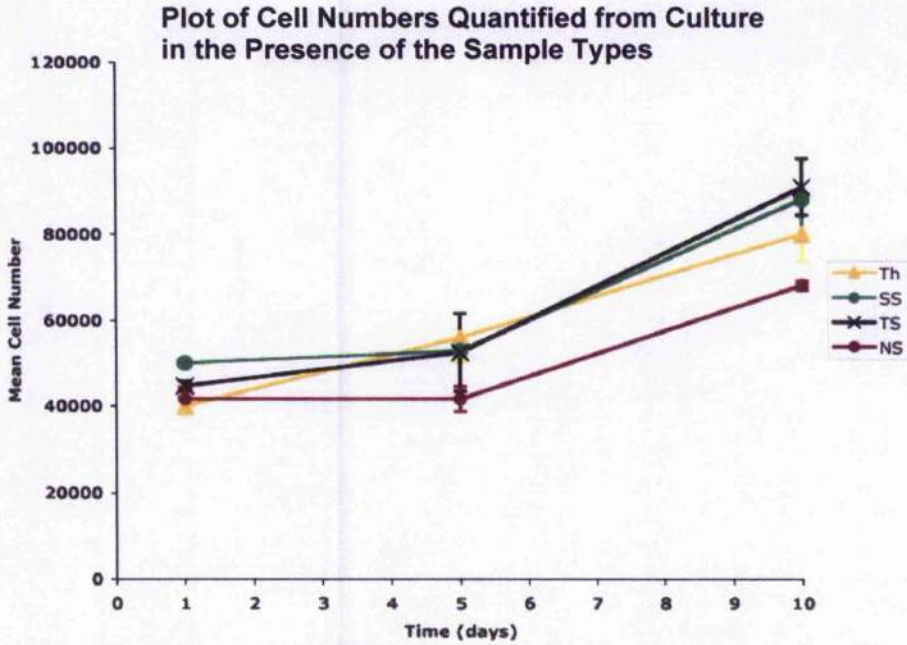


Fig 4.6 – ‘Contaminated’ cells cultured in the presence of NS demonstrated possible endocytosis of metal particles.

The means of the cell numbers quantified in the presence of samples at the three time points were plotted on Graph 4.1. Cell growth in the presence of Th, SS and TS demonstrated similar numbers for all timepoints. For cells in the presence of NS, the cell numbers at 5 and 10 days were lower in comparison, but overall cell exhibited growth by day 10. Utilising 2-way ANOVA, statistically the only significant differences in cell numbers occurred between the timepoints, while none was identified for between different sample types ($p < 0.01$) (Table 4.1).



Graph 4.1 – A plot of the mean cell number ($n=3$, per sample, per timepoint) quantified per sample area (1885mm^2) at the three timepoints. All samples follow a general trend of mean cell number increase with time on the sample discs although the cell numbers on NS were lower.

Source of Variation	Sum of Squares	Degrees of freedom	Variance	F-Ratio	P-Value
Timepoint (Variable A)	8.9×10^9	2	4.4×10^9	57.52	$**1.0 \times 10^{-4}$
Sample Type (Variable B)	8.1×10^8	3	2.7×10^8	3.51	0.0298
Interaction	4.0×10^8	6	6.6×10^7	0.83	0.5637
Residual	1.5×10^9	19	8.0×10^7		
Total (corr.)	1.2×10^{10}	49			

Table 4.1 – ANOVA table (Type III Sums of Squares). **P-Values are <0.01 and statistically significant.

Discussion

The removal of cells from NS, and the subsequent confirmation of internalised particles originating from NS, strongly suggested the possibility of endocytosis occurring on the surface. In addition, the removal of particles by the resin also confirmed that particle displacement was feasible. Any possible contamination during treatment was minimised by media changes and processing washes.

To confirm that endocytosis occurred on the NS surface, cells were stained for clathrin and actin, with SS and TS utilised as control surfaces. No difference in the staining on any of the surfaces could be observed, as the clathrin staining was diffuse throughout the cells. Notably on NS, the cytoplasm was punctuated with breaches thought to be the site of protruding β -phase particles. These breaches were considered to possibly be vacuoles containing ingested particles, however, no specific clathrin condensation was observed at these sites. Similarly, the actin cytoskeleton was unperturbed by the presence of the particles. These results suggested that cells were not actively reacting to the particles, as they did not demonstrate evidence of endocytosis of the surface, nor were the cells attempting to do so.

Quantitative cell numbers for cells cultured in the presence of NS further questioned the involvement of particle endocytosis as a contributory cause. In the presence of NS, contamination of cells with small particles was observed, in a similar manner to cells removed from its surface. Endocytosis of the particles was indicated due to the proximity of the particles to the cell nucleus as endocytic vesicles are typically transported towards the centre of the cell. Even having observed this, cell numbers still increased at the later timepoints in the presence of NS and while mean cell numbers appeared to be lower, no significant differences were observed statistically.

Summary

The initial indication of endocytosis could not be confirmed to occur on the surface of NS; however, cells isolated from its surface were demonstrated to occasionally internalise particles. This was not important in the overview of cell behaviour, as even with

endocytosed particles, cell growth was not significantly inhibited and thus rules out endocytosis as a contributory factor. In addition, cell growth in the presence of NS discounts the possibility of ion leeching contributing to a significant effect on the cells. From the previous chapter's initial identification of four NS associated surface aspects controlling cell growth, the influence of loosened β -phase particles and ion leeching could now be ruled out. This resolves surface chemistry, topography or a combination of the two as being the main contributory cause of NS's non-cytocompatibility.

Chapter 5 – Gene Expression Analysis

Abstract

Gene expression analysis was conducted to further elucidate cell reactivity on the surfaces. As all the sample types were different, mRNA from cells cultured on Thermanox was utilised as the baseline control with which all the metal surfaces were compared. Of the smooth electropolished samples, only SS demonstrated a few low expression changes while TE and NE demonstrated no significant differences compared to Th. These results confirmed that the surface chemistry and minimal changes in topography of these samples did not affect cell behaviour in the time period studied *in vitro*. Gene expression on TS was significantly more reactive with 274 regulation changes and while not directly comparable with TE, observed changes related to extracellular matrix production, increased cell replication and proliferation, and cell signalling, and were probably due to the rougher surface topography. The lack of cell growth on NS meant that it was difficult to extract sufficient RNA from cells cultured on the surface, and the introduction of amplification steps resulted in indicative rather than quantitative changes, however, indications of apoptosis were observed. Following on from the gene expression data, extracellular matrix remodelling was examined by means of labelling cellular fibronectin produced by cells at different timepoints on all the surfaces. At the earlier timepoints of 24hr and 5 days, cells on the smooth surfaces demonstrated fibronectin condensation sites scattered over the cell body and by 10 days the confluent cells had produced a fibrillar network over the surface. On the rougher surfaces, fibrillar fibronectin was observed at earlier timepoints, however, for TS a fibrillar network was produced at 10 days, thus there is no real difference from the smooth surface. Fibronectin production on NS was only thought to be less due to the lower cell numbers on the surface. Another follow on from the gene expression studies was the possibility of apoptosis on NS. Cell viability was examined at 24hr, 5 and 10 days for all the surfaces but no evidence of apoptosis was found on NS, nor any other surface with the exception of TS, however this was only one instance.

Chapter 5 – Gene Expression Analysis

Introduction

In an attempt to expand on the observations of cell reactivity to the materials and to identify any activity in other regulatory systems, gene expression profiling was analysed on cells cultured on SS, TE, TS, NE and NS, with Thermanox utilised as the control. The most interesting results were then further investigated by subsequent analysis.

Gene Expression Profiling

Gene expression profiling is a tool for quantitatively and simultaneously assessing the regulatory states of multiple genes. The method is known under many names such as microarrays, DNA or gene arrays – however, these terms refer to the methodology rather than the resulting information gathered. The microarray consists of a ‘support’ substrate that has been spotted with an array of different surface bound 20-30mer DNA with selected gene specific sequences in order to fish for specific cDNA targets, each spot (often repeatedly spotted) corresponds to a specific gene. It is far from a standardised method with polymers, silicon and glass utilised as support substrates, and target gene sequences supplied by replicated cDNA or sequenced oligonucleotides (Barrett and Kawasaki, 2003; Granjeaud *et al.*, 1999; Lipschutz *et al.*, 1999).

The procedure starts with mRNA extracted from the experimental tissue or cell sample which is transcribed into cDNA before hybridisation onto the microarray where it specifically attaches to the target gene spots (Duggan *et al.*, 1999). This cDNA is termed a ‘probe’ and its visualisation and quantification, once hybridised onto the array, is also far from standardised. Both fluorescence and radioactivity have been utilised to label the probes, this is generally incorporated into the probe during the reverse transcription of the mRNA into cDNA by means of a nucleotide labelled with ^{33}P , fluorochromes or biotin (Granjeaud *et al.*, 1999). The intensities of the hybridised probe labels are recorded for each spot; for instance fluorescence intensities are recorded by confocal laser scanner, and are processed to quantitatively demonstrate gene regulation.

In its infancy in the late 1990's both glass microarrays and oligonucleotide chips were restricted to industrial research due to the prohibitive cost of both apparatus and consumables. In more recent times the commercial marketing of relatively low-cost glass microarrays and the increased funding of genomics laboratories has allowed for specific microarray suites to become available to academic researchers.

In this study, the gene expression of each sample type was compared to a control substrate of Thermanox. In this manner, not only was topography, but also surface chemistry investigated. The spotted cDNA glass arrays utilised in the study employ a competitive hybridisation method where both the experimental and control cDNA's are mixed and washed over the microarray slide. The two sets of cDNA are differentiated by the incorporation of either Cy3 (green fluorescence) or Cy5 (red fluorescence) fluorochromes that are scanned at different wavelengths.

Materials and Methods

Experiment 11 - Gene Expression Analysis

Gene expression analysis is a complex process with numerous practical steps and computational analysis. The major steps are included in the flow chart below and each numbered step is covered in the following sections.

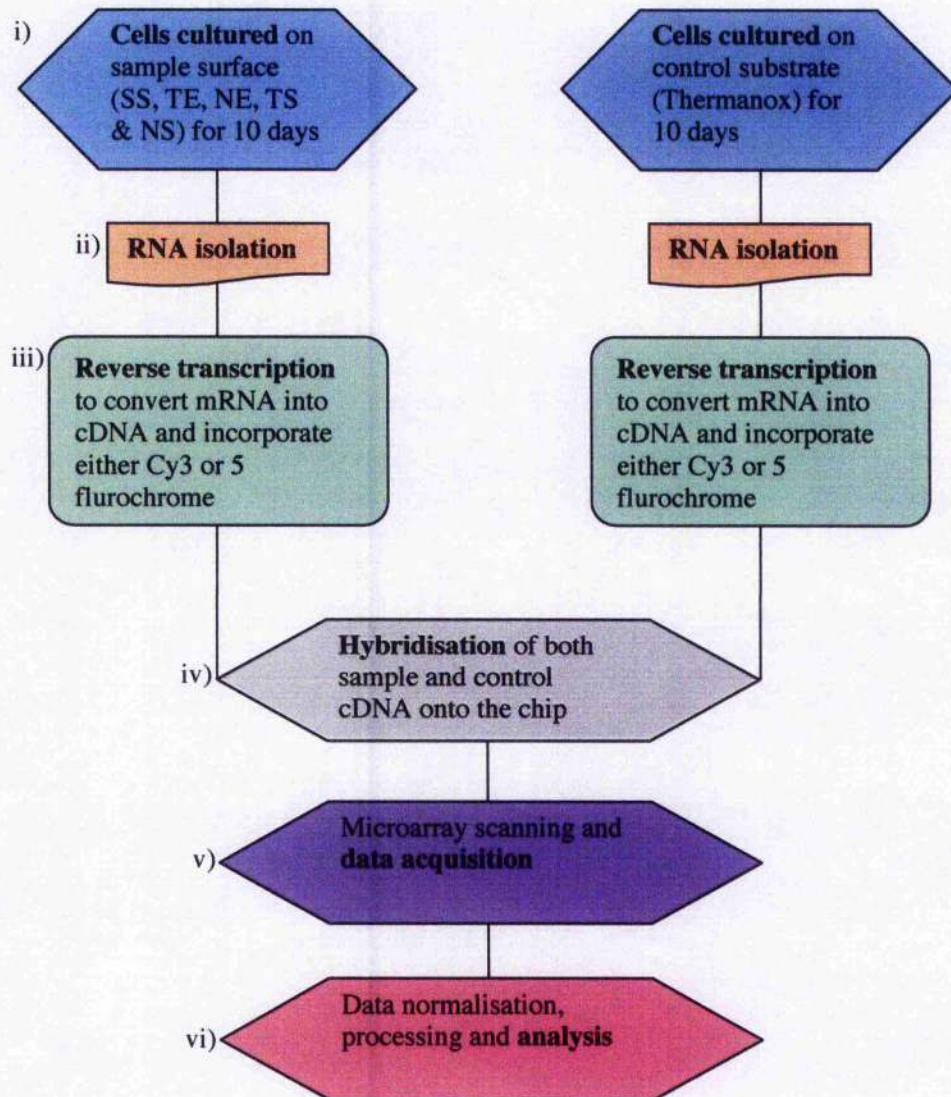


Chart 5.1 – Flow chart demonstrating the major steps (bold text) involved in a microarray experiment from cell culture to final analysis.

Each array experiment consisted of a sample RNA collected from cells cultured on test material (SS, TE, TS, NE, or NS) and control RNA collected from cells cultured on Thermanox. Each experiment was conducted using 4 Human 1.7k cDNA Array (Microarray Centre, University Health Network, Ontario, Canada¹). The RNA amounts used varied from 1-5 μ g due to the manufacturer's revision of protocol. However, within an experiment the total RNA amounts were uniform (for both sample and control).

(i) Cell Culture

hTERT-BJ1 cells were seeded onto 49mm the sample discs of SS, TE, TS, NE and NS at 5.0×10^4 cells per 5ml of DMEM/199 in 60x15mm tissue culture dishes. For the control, 4 Thermanox squares (22x22mm) were used to provide a similar surface area of material. The cells were incubated at 37°C with a 5% CO₂ atmosphere for 10 days and the culture media was changed every 2.5 days. Six replicates were prepared for each substrate as to allow for a selection of the most favourable RNA amounts.

(ii) RNA isolation

RNA extraction was conducted using 2 commercially available kits: RNeasy (Qiagen, Cat No. 74104) and Absolutely RNA[®] (RT-PCR Miniprep Kit, Stratagene, Cat No. 400800). Both methods utilise β -Mercaptoethanol (β -ME) for cell lysis and silica-based fibre spin columns to bind the RNA for washing and finally eluting it in a purified form. As trypsinisation of the cells prior to lysis might affect the gene expression of cells, the lysis buffer was applied directly to the samples (600-1000 μ l) and cellular material loosened with a cell scraper (Falcon, Cat No. 3085). After 10 minutes the cell/lysis buffer mixture was collected and processed following the kit's instructions.

RNA Quantification²

Isolated sample quality and quantity was assessed using the RNA 6000 Nano LabChip[®] Kit (Agilent Technologies) kit.

¹ <http://www.microarrays.ca>

² Step conducted by the Sir Henry Wellcome Functional Genomics Group, University of Glasgow

(iii) Reverse Transcription

On each chip, one set of experimental and control RNA were combined for hybridisation, once they had been reverse transcribed to allow the incorporation of the applicable fluorochrome. Reverse transcription involved 'writing' a complementary single stranded cDNA copy of the isolated RNA stands using a reverse transcriptase enzyme (Superscript II Reverse Transcriptase) incorporating available free nucleotides, dATP, dTTP, dGTP and dCTP. dCTP was an exception in that it had a fluorochrome conjugated to it, thus making cDNA transcribed with it fluorescent. For the gene analysis experiments two types of dCTP were utilised, Cy3 and Cy5, to differentiate between the sample and control cDNA. In an experiment containing 4 slides, two sets of sample RNA were incorporated with Cy3 and the other two with Cy 5. This was also carried out for the control RNA. When the sample and control RNA's were hybridised, two of the chips had identical fluorochrome types, while the other two were flipped. This is known as the 'fluor-flip' or 'dye-swap' and offsets any artefact from differences in the fluorochrome intensities.

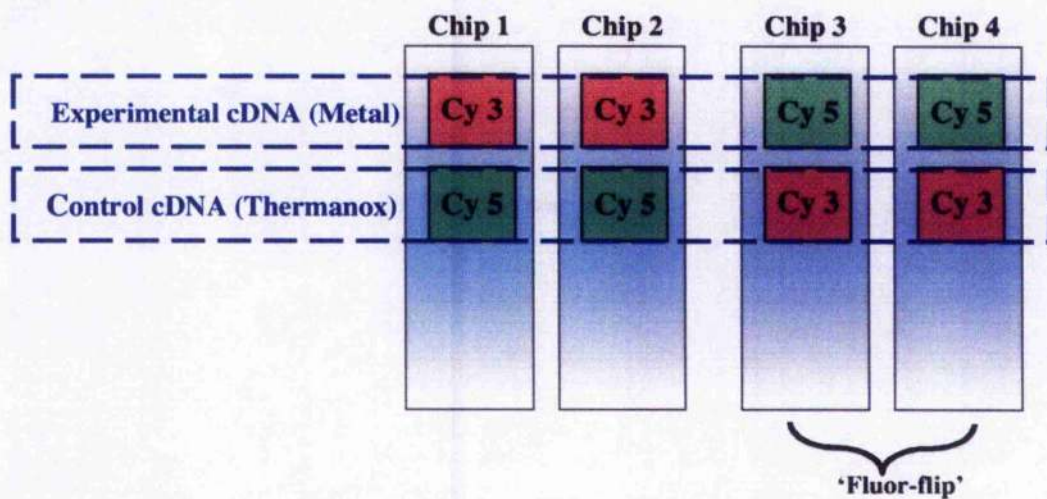


Table 5.1 – Arrangement of dCTP dyes for the hybridisation of cDNA onto each chip. Chips 3 and 4 are the 'Fluor-flip' chips.

mRNA to cDNA

Until indicated, each set of mRNA, control or experimental, is considered a separate sample. As the liquid volumes used in the transcription process are very small, the samples

are routinely centrifuged for 2-3 seconds at 10,000 rpm after the addition of every reagent using a Minispin centrifuge (Eppendorf).

- Two reagent 'master-mixes' with either Cy3 or Cy5 dCTP are initially created. For each sample the mix contains 8.0 μ l 5 x first strand buffer, 4 μ l 0.1M DTT (both included with Superscript II Reverse Transcriptase – Gibco, Cat No. 18064-022), 1.5 μ l Oligo (dT)12-18 mRNA primer (Gibco, Cat No. 18418-012), 3.0 μ l of a 20mM dATP, dTTP, dGTP mix (dNTP set, Promega, Cat. No U1240), 1.0 μ l of dCTP (included in the dNTP set) and 1.0 μ l of either Cy 3 or Cy 5 dCTP (PerkinElmer). All reagents and RNA are kept on ice until they are incubated.
- 18.5 μ l of the master mix was placed in each PCR tubes (either Cy mix per tube, 1 tube per reaction). The measured mRNA was added to the tube and the volume was topped up to 40 μ l with ddH₂O and centrifuged for 5 seconds
- The mix was incubated using a thermocycler (Mastercycler Personal, Eppendorf) at 65°C for 5 min followed by 42°C for another 5 min.
- 2 μ l of Superscript II reverse transcriptase was added to each tube and centrifuged, then incubated at 42°C for 2-3 hours.
- Placing the samples on ice stopped the reverse transcription reaction. 4 μ l of 50mM EDTA (pH 8.0) and 2 μ l of 10N NaOH were added and the samples were incubated for 20 min at 65°C.

iv) Hybridisation

- After 4 μ l of 5M acetic acid was added to each sample, the experimental and control material were combined into one tube. 100 μ l of isopropanol was added to each tube and left to precipitate on ice for 30min. The tubes were centrifuged at 10,000 rpm, 4°C, for 10min.
- The isopropanol was poured away leaving a dark pellet at the bottom of the PCR tube. The pellet was gently rinsed with 50 μ l ice-cold 70% ethanol taking care not to dislodge to pellet. The ethanol was poured off and the tube mouth blotted with tissue, and the pellet resuspended with 5 μ l of ddH₂O.

- In the extended precipitation time-period, the hybridisation solution was prepared. Each sample requires 30µl of EasyHyb™ solution (Roche Diagnostics, UK) containing 1.5µl yeast tRNA (10 mg/ml, Gibco, Cat. No 15401-011) and 1.5µl salmon sperm DNA (Gibco, Cat. No 15632-011). The mixture was incubated at 65°C for 2 min and then left to cool at room temperature.
- 30µl of the hybridisation solution was added to the sample tube and the mixture was pipetted onto the array area of the slide. This area can be determined prior by holding the slide to the light. A large coverslip (24 x 50mm) was placed over the array taking care to eliminate all air pockets. The arrays were kept in a light-tight box containing some ddH₂O, to ensure the hybridisation solution does not dry out, and were incubated for 16 hr at 37°C.
- After the incubation period, the slides were immersed in saline sodium citrate (1x SSC) solution warmed to 50°C to remove the coverslips. Once removed, all the slides were placed in a histological staining rack and immersed in 1x SSC with 0.1% sodium dodecyl sulfate (SDS) warmed to 50°C for 10 min. The solution was changed and the process was repeated a following two times. The slides were then washed by plunging 6 times in 1x SSC before air drying and blotting without touching the array area, and storing in a light-tight slide box.

(v) Slide Scanning and Data Acquisition

The slides were scanned using a 'ScanArray Lite Microarray Analysis System' (Packard Biochip Technologies) scanning at a wavelength of 543nm for Cy 3 and 633 nm for Cy5. The resulting images were imported into a Quantarray (GSI Lumonics) program where the array spots are aligned (manually) and analysed. The resulting file containing all the regulation information in a basic form was exported.

(vi) Data Processing and Analysis

For each experiment four datasets were obtained for the chip repeats. These were imported into Genespring (Agilent Technologies) under one experiment, for instance SS-Th. Each dataset was then normalised using 'Intensity Dependent (Lowess)' normalisation. This

function plots 20% of the datapoints, taken at random, on a scatter plot. A 'best-fit' line and equation was then calculated from these datapoints, and applied the remaining 80% of the data. As only a change in regulation is of interest the data was then filtered. The parameters applied were that a significant change in regulation was either below 0.7 or above 1.3 in the logarithmic expression scale, where the value 1 demonstrated no change. In addition, the significant change in regulation had to be present in 3 of the 4 datasets of the experiment for it to be noted. Once these parameters were applied the resulting filtered dataset was exported into Excel to allow sorting of the genes of interest. Information for the genes of interest was obtained from SOURCE, a scientific database unification tool (Diehn *et al.*, 2003) (<http://source.stanford.edu/cgi-bin/source/sourceSearch>).

(vii) NS – Standard TAN

Due to difficulties obtaining sufficient amounts of RNA from cells cultured on NS, the culture period was extended to 20 days and an RNA amplification step was utilised³. This process involved using a high yield transcription kit (MEGAscript T7, Ambion) in conjunction with a One-Cycle Eukaryotic Gencchip® Target Labelling Assay (Version 2, Affymetrix). Theoretically, the amplification should be linear resulting in significant regulatory changes becoming less significant, however in practice it also results in some of the subtler changes being lost altogether. Unfortunately, the NS experiment now became more of an assessment of gene activity rather than an assay of up or downregulation of genes. The control samples were also amplified to help normalise some of the amplification artefacts.

³ Step conducted by the Sir Henry Wellcome Functional Genomics Group, University of Glasgow

Experiment 12 - Fibronectin Immunostaining

hTERT-BJ1 cells were seeded onto 11mm sample discs of Th, SS, TE, TS, NE and NS at 5000 cells per 0.5ml of DMEM/ Media 199 in 4 well multidishes. The cells were incubated at 37°C with a 5% CO₂ atmosphere for 24 hr, 5 and 10 days and the culture media was changed every 2.5 days. All sample types were in duplicate for each timepoints. The fluorescence immunostaining was conducted following the procedure listed in Chapter 3: Experiment 7 with some minor modifications. In step 5 the primary antibody applied was anti-Fibronectin at 1:100 (Sigma, Cat No. F0916).

Experiment 13 – Apoptosis and Necrosis

hTERT-BJ1 cells were seeded onto 11mm sample discs of Th, SS, TE, TS, NE and NS at 5000 cells per 0.5ml of DMEM/199 in 4 well multidishes. The cells were incubated at 37°C with a 5% CO₂ atmosphere for 24 hr, 5 and 10 days and the culture media was changed every 2.5 days. All sample types were in duplicate for each timepoints.

Apoptosis was assayed utilising an Annexin V-Cy3 Apoptosis Detection Kit (Sigma, APOAC-1KT). The kit includes two dyes, a cell viability stain, 6-carboxyfluorescein diacetate (6-CFDA), and the apoptosis marker Annexin V conjugated to the Cy3.18 fluorochrome. Viable cells hydrolyze the non-fluorescent 6-CFDA into a fluorescent 6-carboxyfluorescein (green) and Annexin V-Cy3 attaches to the membrane of apoptotic cells (red). The assay was advantageous as it could demonstrate early apoptosis by the presence of both dyes, and necrosis by sole presence of Annexin V-Cy3.

Results

Experiment 11 - Gene Expression Analysis

Cell morphology and staining demonstrated considerable differences in the reactions of cells cultured on the various standard and electropolished surfaces. In an attempt to elucidate further, with respect to cell reactivity on the surface, gene microarray analysis was conducted on cellular mRNA harvested from cells cultured on all the surfaces. As all the samples were different, mRNA recovered from cells cultured on Thermanox was utilised as competitor cDNA (after reverse transcription) with which all the metal surfaces were compared. Due to the difficulty of obtaining mRNA from cells cultured on NS, these cells were cultured for 20 days rather than the 10 days time period used for the other surface and the recovered mRNA also had to be amplified to increase the amount of material which was required to meet the manufacturers guidelines for newer versions of the utilised microarrays.

SS- Stainless Steel

From an arrayed 1718 genes only 14 genes were up or down regulated on SS compared to Th, although the role of 3 were unknown leaving just 11 changes. A normal procedure in documenting microarray data would be to establish a threshold for $\Delta\%$ gene regulation after the initial filtering, however with such a small number, all changes were included in Table 5.2 (means of the 4 chip values). These changes have been classed under general headings derived from the classification used on the SOURCE website and considered relevant to cell/material observations.

<i>Gene</i>	$\Delta\%$	<i>Gene</i>	$\Delta\%$
<i>ECM (Extracellular Matrix)</i>		<i>Cell Signalling</i>	
Matrix metalloproteinase 7 (MMP7)	22	Cytochrome P450, subfamily IVA	24
Extracellular matrix protein 1	-44		
		<i>Replication</i>	
		Zinc finger protein 151	31
<i>Cell Proliferation</i>			
Insulin-like growth factor binding protein 2	22		
Spindlin-like:LOC54466	29		
		<i>Cell Adhesion</i>	
		Tumour-associated calcium signal transducer 1	27

Table 5.2 – Details of gene regulation changes observed on SS in comparison with Th. Genes highlighted grey are downregulated.

TE – Electropolished Titanium

Electropolished titanium was demonstrated to be very inert with no significant up or downregulation of any genes in comparison to Thermanox.

TS – Standard Titanium

274 separate up or downregulations were observed on TS, the highest of any of the samples types tested. These $\Delta\%$ changes were also considerably higher than on any of the other surfaces, therefore a filter of $>40\%$ was applied to reduce the number of regulated genes displayed. These genes are listed and included under general headings in Table 5.3.

NE – Electropolished TAN

No significant up or downregulations were observed for cells cultured on NE in comparison with Thermanox.

<i>Gene</i>	$\Delta\%$	<i>Gene</i>	$\Delta\%$
<i>ECM</i>		<i>Cell Signalling</i>	
Serine (or cysteine) proteinase inhibitor, member 6	127	Cytochrome P450/ and subfamily IVA	59/112
Matrix metalloproteinase 7 (MMP7)	80	Complement component 1, subcomponent	99
Fibrillin 2	46	ELK3, ETS-domain protein (SRF accessory protein 2)	94
Decorin	44	Ras homolog gene family, member C	87
Collagen, type VI, alpha 1	-40	Purinergic receptor (family A group 5)	68
		RAP1B, member of RAS oncogene family	62
		Signal sequence receptor, alpha (translocon-associated protein alpha)	59
<i>Cell Proliferation</i>		GTP binding protein overexpressed in skeletal muscle	47
Insulin-like growth factor binding protein 6	124	3wingless-type MMTV integration site family, member 5A	43
Protein phosphatase 1, catalytic subunit, beta isoform	115	Ciliary neurotrophic factor receptor	-42
Thioredoxin	81		
Insulin-like growth factor binding protein 2	79		
Spindlin-like:LOC54466	75		
		<i>Replication</i>	
S100 calcium binding protein A6 (calcylin)	61	Ribosomal protein L39-like/L37a/S28/151	124/ 116/ 75/ 44
Cysteine and glycine-rich protein 2	58	Zinc finger protein C3HC4/35/151	90/ 50/ 44
Ferritin, heavy polypeptide	43	Cleavage and polyadenylation specific factor 1, 160kD subunit	88
Interferon, gamma-inducible protein 16	-42	RNA polymerase II	88
		Thyroid hormone receptor alpha	50
		Forkhead box F2	50
<i>Apoptosis</i>		Myeloid/lymphoid or mixed-lineage leukemia	42
TIA1 cytotoxic granule-associated RNA binding protein	107/ 70	Eukaryotic translation initiation factor 4 gamma	40
<i>Cell Adhesion</i>		Heterogeneous nuclear ribonucleoprotein D	-40
Tumor-associated calcium signal transducer 1	65	ISL1 transcription factor, LIM/homeodomain, (islet-1)	-41
		GATA binding protein 3	-47
		Nucleosome assembly protein 1-like 4	-51
		Zinc finger protein 76	-40

Table 5.3 – Details of gene regulation changes observed on TS in comparison with Th. Genes highlighted grey are downregulated.

NS – Standard TAN

Although incomparable with the other samples, the amplified RNA extracted from cells on NS did demonstrate 42 gene regulation changes. The regulation values were quite low, however these values cannot be taken as being quantitative due to the amplification process interfering with both the larger and more subtle upregulations. These changes have been classed under general headings considered relevant to cell/material observations in Table 5.4.

<i>Gene</i>	$\Delta\%$	<i>Gene</i>	$\Delta\%$
<i>Cell Proliferation</i>		<i>Cell Signalling</i>	
Transforming growth factor, beta 2 (TGF β 2)	21	G protein-coupled receptor	34
CDC10 cell division cycle 10 homolog	20	RAB27A, member RAS oncogene family	29
Insulin-like growth factor binding protein 3	-15		
secreted protein, acidic, cysteine-rich	-19	<i>Replication</i>	
		MAP/microtubule affinity-regulating kinase 3	40
<i>Apoptosis</i>		Polymerase (RNA) II (DNA directed) polypeptide G	30
Apoptosis inhibitor 5	-28	5'-nucleotidase, ecto (CD73)	30
		DNA cross-link repair 1C (PSO2 homolog, <i>S. cerevisiae</i>)	24
<i>Cell Adhesion</i>		Ribosomal protein L15	23
Tumour-associated calcium signal transducer 2	29	Zinc finger protein 195	16

Table 5.4 – Details of gene regulation changes observed on NS in comparison with *Th*. Genes highlighted grey are downregulated.

Comparisons

The labour intensive nature of the study meant that the samples were processed in batches, TE and NE, SS and TS and it was only these experiments that were comparable due to the use of the same batches of control mRNA (Thermanox) and the same chip generation. As there were no significant regulation changes for either TE or NE a comparison yielded no differences, which in itself was an interesting result. When SS and TS experiments were compared, 6 genes were found commonly upregulated in both, although always higher on TS (Table 5.5).

<i>Gene</i>	<i>SS ($\Delta\%$)</i>	<i>TS ($\Delta\%$)</i>
<i>ECM</i>		
Matrix metalloproteinase 7 (MMP 7)	22	80
<i>Cell Proliferation</i>		
Insulin-like growth factor binding protein 2	22	79
Spindlin-like:LOC54466	29	75
<i>Cell Signalling</i>		
Cytochrome P450, subfamily IVA	24	112
<i>Replication</i>		
Zinc finger protein 151	31	44
<i>Cell Adhesion</i>		
Tumour-associated calcium signal transducer 1	27	65

Table 5.5 – Common gene upregulations found in cells cultured on SS and TS.

Experiment 12 – Fibronectin Immunostaining

Following on from the microarray data there was an indication of possible changes to the production of extracellular matrix (ECM) proteins on TS compared to other standard materials. The rationale for this investigation is covered in depth in the 'Discussion' section of this chapter. In an initial attempt to investigate ECM production, endogenous fibronectin (Fn) was labelled at 24hr, 5 and 10 days on all the surfaces. The general trend for staining on the smooth surfaces was similar at the different timepoints, therefore SS was included as an example for these to save space - Th, TE, NE are included on the accompanying CD-ROM. Apart from the lack of confluency on NS at day 10, Fn production was similar on both the rough surface of TS and NS. The gene expression data flagged TS, therefore this was included as representative of Fn production on a rough surface while NS can be found on the CD-ROM.

On the smooth surfaces of Th, SS, TE and NE at 24hr, there were many 'dot morphology' Fn condensation sites scattered over the cell body, assumed to be nucleation sites for Fn production. Some fibrillar Fn production was observed around the nucleus and occasionally extracellularly, however this was a commonly observed feature at 24hr and assumed to be the initial site of adherence of the cells to the surface and the original morphology prior to spreading (Fig 5.1a). At 5 days there was evidence of Fn production for other areas of the cell, present as either dot condensations or fibrillar structures. There was also evidence of cell motility on the generally featureless surfaces as cells could occasionally be observed leaving trails of fibrillar Fn (Fig 5.1b). A broad observation for the hTERT cell type was that the Fn labelling was concentrated around the nucleus and thinned out further towards the cell periphery where only condensations were present. (Fig 5.1a,b). By day 10, the confluent monolayer obscured the material surface and the Fn had formed a dense fibrillar network (Fig 5.1c).

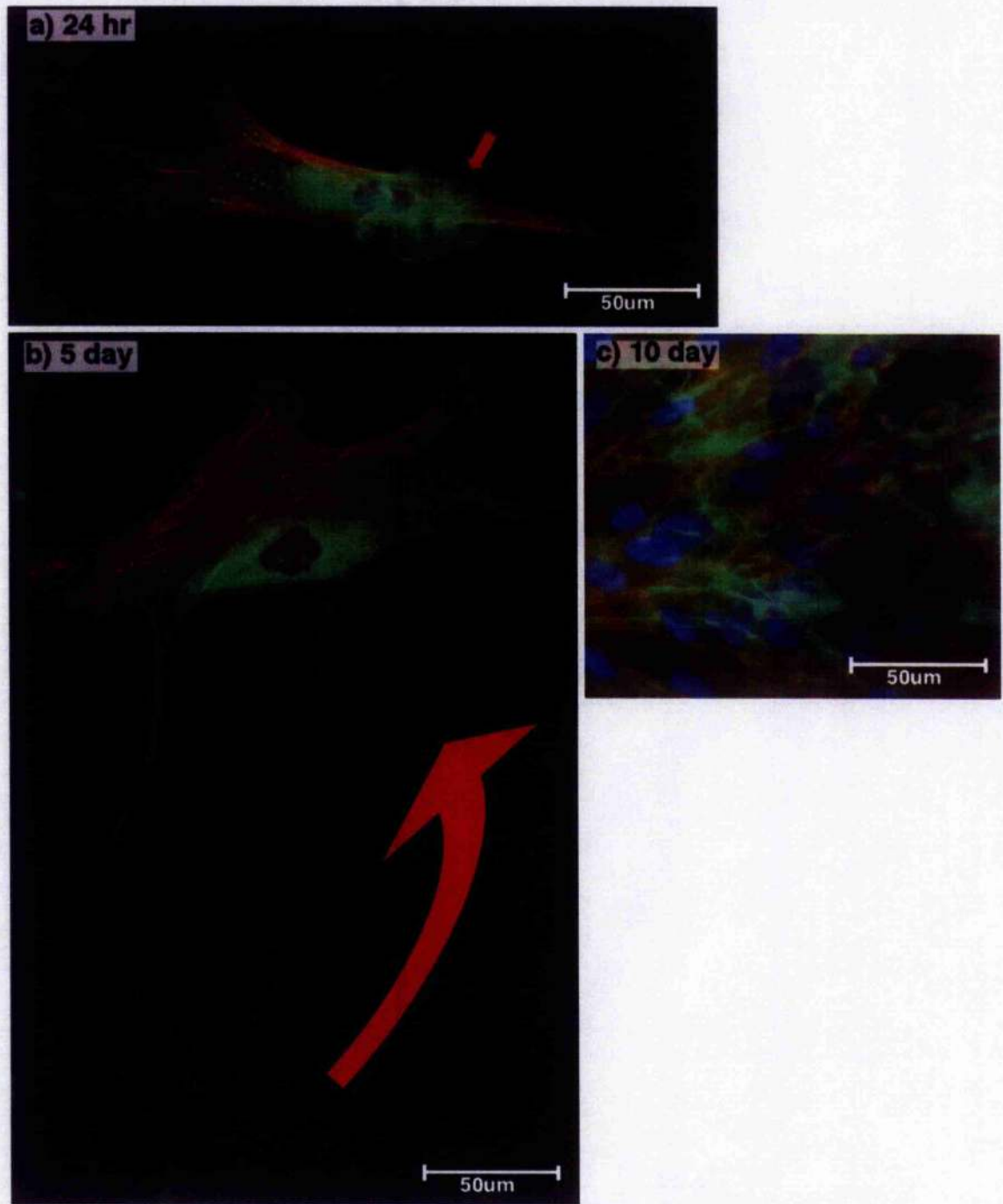


Fig 5.1 - Cells cultured on SS and triple labelled for ●Fibronectin, ▼Actin and ◆DNA. (a) 24hr. A dense fibrillar network (red arrow) indicated the site and morphology of the initially adhering cell. The cell was now spread and demonstrated dot fibronectin nucleation sites throughout its cell body. (b) 5 days. Evidence of fibronectin production by a motile cell leaving a trail of fibrils on the SS surface (the red arrow suggests the general direction of cell movement). The cell itself demonstrated dense fibronectin labelling near the nucleus and scattered nucleation sites further towards the cell periphery. (c) At day 10 a confluent monolayer accompanies a dense fibrillar network masking the surface.

On the rougher surfaces of TS and NS, the cells were generally less spread at 24hr, however, they did demonstrate similar characteristics to those on the smoother surfaces such as the Fn becoming more organised into dot condensations further away from the nucleus (Fig 5.2a). At 5 days there was considerable change as the Fn was arranged into thick fibrils generally contained within the area of the cell body, around the site of the nucleus (Fig 5.2b). Less prominent at this timepoint, was the presence of the condensed dot nucleation sites around the cell periphery; however, they could have been masked by the fibrillar Fn (Fig 5.2c). At 10 days TS and NS differed, with cells on TS becoming confluent on the surface with a fibrillar Fn network (Fig 5.2d), while cells on NS no change was observed from 5 days in the Fn organisation.

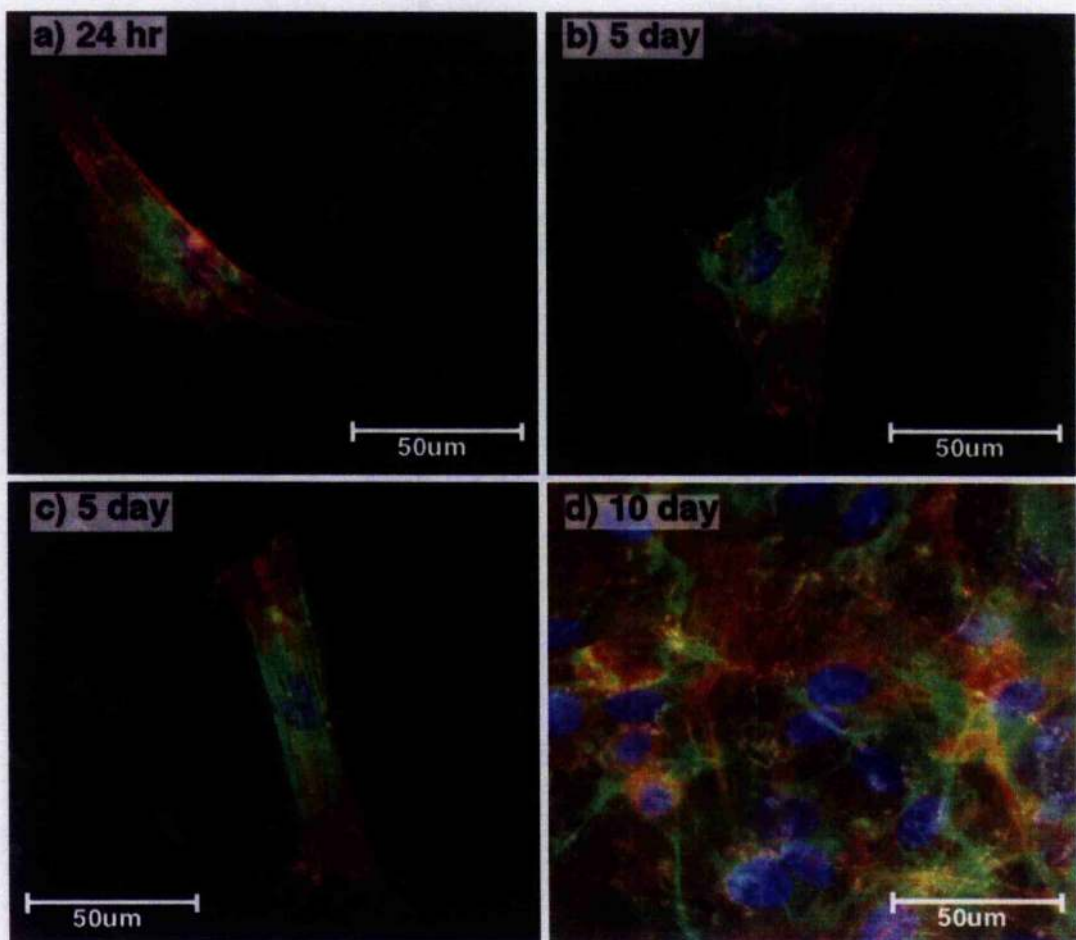


Fig 5.2 - Cells cultured on TS and triple labelled for ● Fibronectin, ▼ Actin and ◆ DNA. (a) 24hr, cellular production of Fn was similar to the smooth surfaces with condensation surrounding the nucleus and dot nucleation located further out towards the cell periphery. (b) At 5 days, thick Fn fibrils were present around the cell centre and nucleus. (c) At 10 days the cells were confluent and a dense network of fibrillar Fn had been produced covering the whole surface.

Experiment 13 – Apoptosis

The suggestion of necrosis (by SEM, Chapter 3) or apoptosis (by gene expression studies, this chapter) would correspond to the lack of growth of cells on NS. To explore this, cell viability at 24hr, 5 and 10 days was examined on all surfaces. The test utilised coupled a viability stain (green) and an apoptosis stain (red) so the presence of viable and dead or dying cells could be ascertained.

All samples, including NS, demonstrated viable cells indicated by the green fluorescence stain. The only indication of possible apoptosis was observed on TS at 10 days, however, this was only one instance and other areas on the sample and the repeat did not demonstrate any further evidence of apoptosis on TS.

Th - Thermanox



Fig 5.3 – Viable cells were observed at all timepoints, with no evidence of apoptosis or necrosis. Occasional autofluorescence was observed on Th (a).

SS – Stainless Steel



Fig 5.4 – Cells were viable at all timepoints on SS.

TE – Electropolished Titanium

Fig 5.5 – Cells on TE were viable at all timepoints.

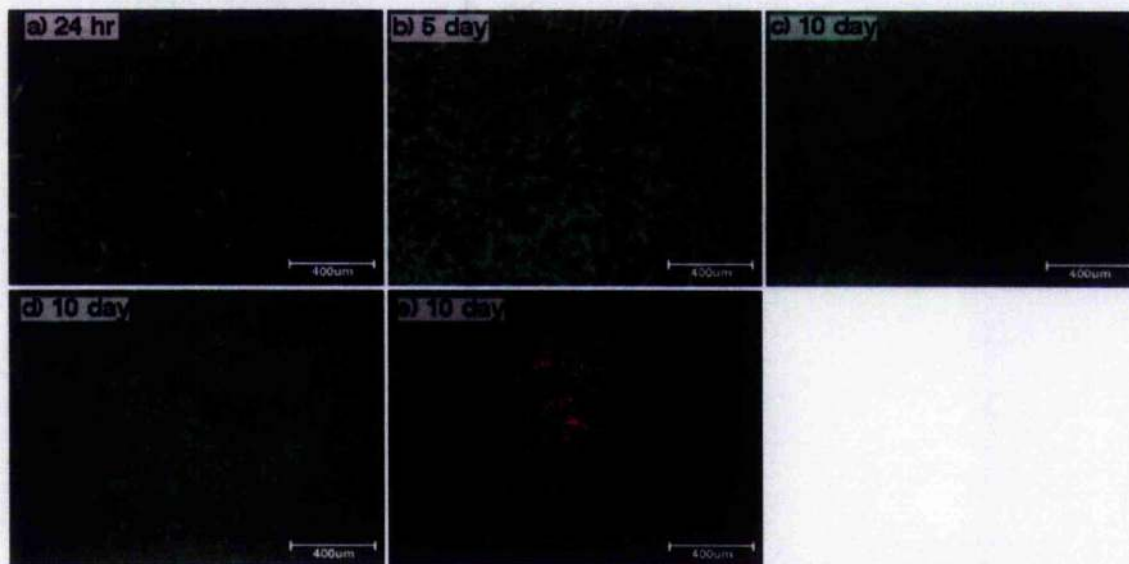
TS – Standard Titanium

Fig 5.6 – Generally, cells on TS were viable at all timepoints although confluent cells on one 10 day sample (d) demonstrated small breaches in the confluent cell monolayer. (e) Utilising the apoptosis stain cells at this time point stained positive for apoptosis indicating cells entering the early stages of apoptosis.

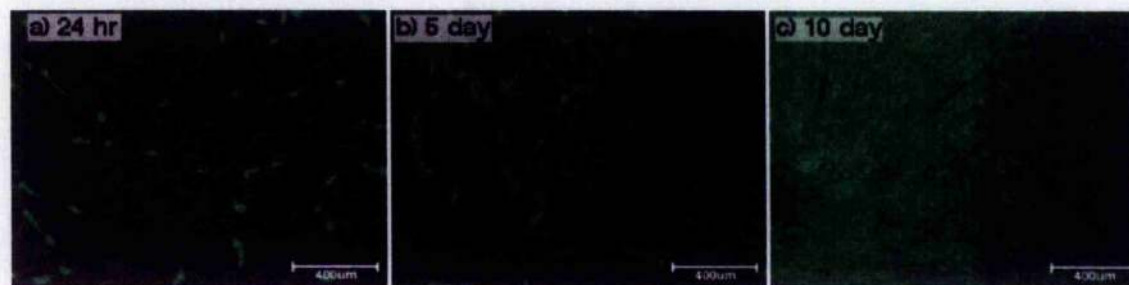
NE - Electropolished TAN

Fig 5.7 - Cells on TE were viable at all timepoints.

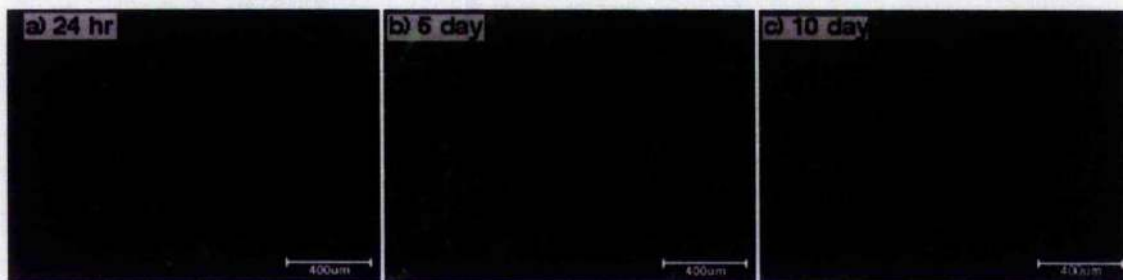
NS – Standard Titanium

Fig 5.8 – While lower in number than on the other surfaces cells on NS were viable at all timepoints and no evidence of apoptosis was observed.

Discussion

Gene Expression

The gene expression results were interesting in suggesting that for implant metals, the primary cause of gene regulation changes was topography. Of the smooth electropolished samples, only SS demonstrated a few low changes, and of these only the identity of eleven is currently known. TE and NE demonstrated no significant differences compared to Th. These results confirmed what was previously indicated by cell growth studies, in that the surface chemistry and minimal changes in topography on these samples did not affect cell behaviour. This was somewhat surprising as gene expression changes have been observed towards nanotopographies (Carinci *et al.*, 2004; Dalby *et al.*, 2005; Dalby *et al.*, 2002), of which Th, SS, TE and NE possess, however these changes were generally confined to feature sizes below 30nm. To the author's knowledge, there have been no published studies observing gene expression changes solely based on metal surface chemistry, although based on my results this would not make an exciting, but nevertheless necessary, study.

Gene expression on TS was significantly more reactive with 274 genes differentially regulated. While not directly comparable with TE, the utilisation of mRNA from cells on Th suggests that the observed changes related to extracellular matrix (ECM) production, increased cell replication and proliferation, and cell signalling are due to the rougher surface topography. As the control mRNA and chips used for the SS and TS experiments were identical, the gene changes could be compared and 6 genes on both materials were found commonly upregulated, although always more so on TS. This might suggest some common ground for cellular interaction towards metals. Of these genes, Matrix Metalloproteinase 7 (MMP 7) was the most notable. MMP's are a family of metal ion-requiring enzymes found at sites of tissue remodelling and wound healing and are involved in extracellular proteolysis (Cawston, 1995; Mott and Werb, 2004; von Bredow *et al.*, 1995). MMP 7 is also known as matrilysin and has been noted to degrade extracellular components such as the collagens type IV (Miyazaki *et al.*, 1999; Murphy *et al.*, 1991) and type X (Sires *et al.*, 1995), however, its assumed natural substrates are fibronectin and laminin (Cawston, 1995; Miyazaki *et al.*, 1999; von Bredow *et al.*, 1995).

NS illustrated a unique problem; microarray is a technique that requires a large amount of mRNA and is a method that does not lend itself well to substrate surfaces that are non-cytocompatible or of low adhesion for cells. However, these 'lower mRNA yield' surfaces are of particular interest as they demonstrate surface characteristics that are clearly influential for cell adhesion and growth. This problem was encountered on NS and solved using mRNA amplification. Analysis of the gene changes suggested a possible degree of interference in expression data by the amplification step, however, 42 changes were still apparent. The most interesting of these were the downregulation of an apoptosis inhibiting gene and upregulation of transforming growth factor beta (TGF- β 2). The suggestion of apoptosis was interesting as it was first considered in Chapter 3, solely based on the morphological features of the cells. TGF- β 2 is one of three isoforms of TGF- β , part of a super-family of growth factors. While generally associated with cell proliferation and ECM production, especially in osteoblastic cells (Wrana *et al.*, 1988), they have also been associated with inhibition of proliferation in growth plate chondrocytes (Ballock *et al.*, 1993) as well as endothelial cells in maturing blood vessels (Brogi *et al.*, 1994). The TGF- β growth factors are regarded an essential component of wound healing (Leask and Abraham, 2004).

There are only a handful of gene expression studies related to orthopaedic metals in the literature and these generally utilise osteoblasts. While Carinci demonstrated that rough titanium activated a small number of genes compared to cell culture plastic (Carinci *et al.*, 2003b) most other studies in fact only investigate the effect of surface roughness in relation to titanium materials. All of the studies noted differences extrapolated to the increase of roughness, however, the use of cells was paramount as cell lines such as MG-63 osteoblast-like cells demonstrated the least differences (Carinci *et al.*, 2003a; Carinci *et al.*, 2003b; Kim *et al.*, 2004), while for primary bone cells up to 25% of the total gene numbers assayed showed significant changes (Brett *et al.*, 2004; Brett *et al.*, 2003; Harle *et al.*, 2004).

Titanium alloy surface roughness has also been demonstrated to modulate expression of genes associated with multiple differentiation pathways in bone marrow stromal cells (Leven *et al.*, 2004). Conspicuous by their absence are a lack of studies investigating

fibroblast activity to titanium surfaces, and in none of the other studies' did expression gene-sets bare any resemblance to the one presented here. When compared with nanoparticle and topography related studies using similar cells and arrays, some notable genes such as MMP 7, cytochrome P450 and zinc finger proteins could be observed with altered expression (Berry *et al.*, 2003; Dalby *et al.*, 2005; Dalby *et al.*, 2003). This leads to an obvious point that the outcome of a gene expression experiment hinges on the choice of cells, be they primary or a cell line, and the choice of array utilised as this influences the genes that are assayed.

The profiling of gene expression by microarrays is still very much a technique in its infancy and this was illustrated by some of the drawbacks encountered utilising the method. The accelerated development in the field was reflected by the frequency of chip upgrades, which are not directly comparable with past chip versions. In an attempt to combat this, the control mRNA was kept constant for all experiments, therefore while direct comparison was not always possible observations could be inferred. This also brings into question a general molecular biology observation of the validity of the control source. Ideally, a section of healthy connective tissue would provide the ideal control, however numerous problems arise from this. Primarily it is a question of availability, especially if human tissue is required. Also, primary fibroblasts from the connective tissue would have to be isolated and cultured prior to seeding on the biomaterials. In this study, Th has been used as it is a tried and tested cell culture plastic for many years and therefore was considered a reliable control.

The variety of manufactured chips coupled with high costs mean that most published studies utilise different chips with different analysis methods thus making comparisons with published data unreliable. Furthermore, it has been demonstrated that this is also influenced by the choice of cell type and more surprisingly the laboratory. This was highlighted in a recent 'multi-laboratory' study where relatively large differences in the data acquired from identical mRNA was demonstrated (Irizarry *et al.*, 2005). However, the drawbacks listed do not significantly diminish the benefits of this method; microarrays allow for the opportunity of measuring and analysing vast amounts of gene regulation data

with comparative ease. The cumulative benefit, in the instance of this study, has resulted in the formation of a comprehensive database of gene regulation for fibroblasts cultured on numerous orthopaedic grade materials in standard and modified forms – something previously impossible, or at the very least taking years to compile.

The 10 day timepoint was chosen to allow an extended period of culturing and proliferation relative to the various surfaces, and to obtain sufficient mRNA. This proved sufficient for all materials with the exception of NS where mRNA amounts were far from optimal. The author believes there to be considerable potential in extending this study utilising a higher number of cells for a shorter time period of 48hr, this would benefit studies into NS considerably. It was the intention of utilising gene-chips as a screening method to identify a gene set for more in depth gene expression analysis with gene specific PCR (polymerase chain reaction). However, the lack of consistent gene changes between the surfaces indicated that no particular genes could be focused upon. Two changes that were of considerable interest was the possibility of extracellular matrix remodelling and apoptosis, however, it was believed that these two reactions could be investigated more effectively by other methods.

Fibronectin

The observation of elevated MMP 7 expression on TS raised the question: what purpose could more ECM degrading enzyme, not accompanied by a higher amount of fibronectin expression serve? Composition and organisation of the ECM surrounding a cell can regulate expression of matrix remodelling genes (Huhtala *et al.*, 1995). Chou observed that the expression of fibronectin (Fn), a substrate of MMP 7, on smooth titanium fluctuates in comparison with tissue culture plastic, initially increasing at 16hr and then decreasing at 90hr (Chou *et al.*, 1996). However, he also noted elevated Fn levels on grooved titanium compared to smooth titanium, suggesting roughness was an important regulating factor (Chou *et al.*, 1995).

Studies have demonstrated an interesting relationship between Fn and titanium, as Fn absorption was preferred to other ECM molecules such as vitronectin (Ku *et al.*, 2005), and

Fn absorption was higher on titanium compared to other metal oxides (Voros *et al.*, 2001). It was therefore possible to speculate that TS could be influencing fibronectin absorption or production. It is worth noting that no evidence of upregulated Fn levels were observed on any of the surfaces, however, a possible reason might be the reduced half-life of Fn mRNA on titanium (Chou *et al.*, 1996). Separate studies have demonstrated a 'mat' of absorbed plasma Fn on titanium from serum with no visible differences (MacDonald *et al.*, 1998; Scotchford *et al.*, 2003). Rather more revealing studies have examined cellular Fn production; Abiko and Brunette observed that cells guided by grooves on titanium left fibrillar Fn tracks (Abiko and Brunette, 1993), while Luthen observed both aligned fibrillar and dot (punctiform) FN structures on various roughness of titanium (Luthen *et al.*, 2005). Utilising an anti-human fibronectin monoclonal antibody, the endogenous cell production of fibronectin on the surface could be examined (Hynes, 1999).

Fibronectins (Fn) are high molecular weight glycoproteins (440,000 Da) essential for cell adhesion (Hynes, 1999). *In vivo* and *in vitro*, their primary role is as a site of attachment for cells; *in vivo* Fn also attaches to other ECM components such as collagen (Hynes and Yamada, 1982), while *in vitro* it adsorbs onto the substrate surface facilitating cell adhesion (Miller and Boettiger, 2003). It possesses a hierarchy of structures, the basic subunits of which are bonded together to form a polymeric fibril. This basic Fn subunit is made up of varying numbers of three module types, I, II and III. The modules are repeating units, with variations in the sequence making different types of modules; type I has 12 different types, type II has two and type III has 15-17 (Hynes, 1999; Hynes and Yamada, 1982). The tenth variation of type III contains the RDG (Arg-Gly-Asp) sequence identified as being the cell binding domain for $\alpha_5\beta_1$ integrin binding (Miller and Boettiger, 2003; Schwarzbauer and Schler, 1999).

Initial Fn is secreted in a soluble form of two subunits held together by disulphide bonds. Fibrillar Fn is assembled from this form by the addition of more disulphide bonds and becomes insoluble (Hynes, 1999). A mechanism for the formation of fibrils has been suggested as nucleating at the end of actin filaments followed by stretching towards the cell centre by the continuous attachment of new Fn molecules (Ohashi *et al.*, 2002).

Cells on the entire range of test surfaces demonstrated some common features for the labelling of Fn. Primarily, most of the label was confined around the cell nucleus. This was also observed for other fibroblastic cell types such as 3T3's (Ohashi *et al.*, 2002), however, osteoblasts produce a much cleaner Fn staining (Luthen *et al.*, 2005). Secondly, further out from the cell centre the Fn labelling became more globular or punctiform; this was better observed on the well spread cells found on the smooth surfaces of Th, SS, TE and NE. The fibrillar formation of Fn is reliant on the development of cell tension dependent actin cytoskeleton as an initiation site and guide for its extension towards the cell centre (Ohashi *et al.*, 2002). These globular structures are probably sites of new Fn fibrillar formation that will eventually develop into the network observed at 10 days, although it has been noted that fibronectin adsorbed onto titanium tends to demonstrate a globular structure (MacDonald *et al.*, 1998). The visible differences in Fn staining are only apparent when comparing rougher surfaces with smooth, where fibrillar Fn appears to be better developed at an earlier timepoint on the rougher surfaces, however this could be due to the cells being less spread.

No alignment to any specific surface detail could be observed on the rougher surfaces. For all surfaces, with the exception of NS, the confluent monolayer also exhibited a dense network of Fn fibrils and even cells cultured on NS for 10 days demonstrate some fibril production. For the upregulation of MMP 7 observed at 10 days on TS and to a lesser extent on SS, the confluent cell layer and visible Fn network might be the only possible reason for the change. It would be interesting in this instance to label cells at the timepoints between 5 and 10 days to examine if the development of the surface-wide Fn network might differ on the various sample surfaces.

Apoptosis and Necrosis

The rationale of apoptosis or necrosis as a possible explanation for the lower cell growth on NS was first suggested in Chapter 3, and again in the gene expression section of this chapter.

Cell death can be divided into two general types, apoptosis and necrosis. Apoptosis, also known as programmed cell death, is an important physiological phenomenon involved in growth and maintenance of both vertebrates and invertebrates (Clarke, 1990; Heroux *et al.*, 2004). It is an efficient method of cell recycling, methodically breaking down cell contents into manageable packets known as apoptotic bodies which are consequently phagocytosed by macrophages and neighbouring cells (Gjertsen *et al.*, 1994). From a morphological viewpoint, the first signs are changes in the cell membrane as it becomes convoluted and eventually detaches in large sections (Clarke, 1990; Schwartzman and Cidlowski, 1993). At the intracellular level, the DNA condenses into dense regions and the nucleus breaks down. There are also alterations in the cell membrane as phosphatidylserines, normally confined to the inner cytoplasmic section, translocate to the extracellular section. In the *in vivo* environment this translocation is a marker for the ensuing phagocytosis of the dead cell (Verhoven *et al.*, 1995), however it can also be utilised for bioassays (Vermes *et al.*, 1995).

While apoptosis inflicts minimal damage on neighbouring cells, necrosis is a far more destructive form of cell death. It is pathological rather than a physiological type of cell death resulting from the cell's exposure to numerous harmful conditions (Schwartzman and Cidlowski, 1993). Generally, the cell membrane loses its integrity becoming leaky while the cell becomes swollen before finally rupturing (Dartsch *et al.*, 2002; Vermes *et al.*, 1995). During this time enzymes and eventually cell contents are spilled out and can elicit inflammatory reactions and damage neighbouring cells.

A combination of a cell viability marker and Annexin 5, an apoptosis marker was used to look for evidence of cell death. None of which was observed on NS and all other sample types performed as expected with the exception of TS. Apoptosis in small parts of the confluent monolayer on TS were observed, but only in one instance. This might help explain the upregulation of apoptosis related genes observed in the gene array data found on TS. A possible explanation for this apoptosis might be nutrient depletion of the media, and especially in the lower cell layers at the late timepoint due to the high number of cells. For NS, the observed lack of cell growth did not initiate the cell towards any seemingly destructive pathways.

Conclusion

Gene expression screening confirmed initial observations from Chapter 3; for a smooth surface, a change in chemistry between a polymer (Th) and three separate metal types, stainless steel, titanium and alloyed titanium, did not cause any significant changes in cell reactivity on the surfaces at the later timepoints. Indeed, it could be inferred that any genetic changes observed on TS were due to the change in topography on the surface and similarly for NS. Follow-up studies for the observed up-regulated were logical in terms of the foreign body reaction however they failed to uncover any noteworthy differences. The absence of cell death on NS was also interesting, however, not entirely unexpected as prolonged cell culture on the surface was possible although RNA amounts were still low.

Chapter 6 – Surface Chemistry

Abstract

This chapter concerns the involvement of surface chemistry in the cellular reactions observed on NS. In attempting this, two separate surface chemistry models were created by masking NS and also Th, SS, TS, with either gold or titanium. Cell growth, measured by means of cell counts, demonstrated no significant differences between the cells on uncoated or coated versions of each surface. This meant that cells could be cultured to confluency on coated versions of Th, SS and TS, while cell numbers were consistently low on coated NS. This demonstrated that the surface topography was probably the sole cause of the cell reactions observed on NS. An interesting observation on nearly all the coated surfaces was that cells aligned to the border between the coated and original surface. This could be due to a difference in surface chemistry or topography.

Chapter 6 – Surface Chemistry

Introduction

The initial identification of four features of Standard TAN (NS) that could possibly result in the observed greatly reduced cell growth; β -phase particle endocytosis, ion leeching, surface chemistry and surface topography, have been narrowed down to the latter two (Chapters 3 and 4). This chapter seeks to primarily elucidate the influence surface chemistry has on the cellular reaction towards NS and the other 'standard' surfaces.

Surface Chemistry

As discussed in Chapter 2, the surface chemistry of NS is a heterogeneous mix of titanium, aluminium and niobium oxides found at the surface in relation to the underlying α and β phase composition of the bulk alloy (Disegi, 1997; Sittig *et al.*, 1999b). For pickled (acid etched) TAN, the concentration of Nb_2O_5 on the surface was generally higher. This, as was previously noted in Chapter 3, brings into question the validity of using NE as topographical control for NS as the chemistries might not be the same (Sittig *et al.*, 1999a; Textor *et al.*, 2001). The cellular effect of TAN's component oxides has been studied previously using a fabricated topography mimicking the distribution of the various oxides, based upon on the relation of the bulk $\alpha+\beta$ phases (Scotchford *et al.*, 2003; Winkelmann *et al.*, 2003). In this instance, it was observed that cells were sensitive to the varying oxide chemistries and that topography was not a contributing cause. However, the outcome of my earlier study (see Chapter 3) was that NE was a compatible surface for cells. This indeed brings into question the validity of isolating surface chemistry as the sole cause for poor cell compatibility. While the amount of niobium oxide on the NS surface might be higher than on NE, this material has not previously been shown to be cytotoxic (Eisenbarth *et al.*, 2004; Khan *et al.*, 1999; Velten *et al.*, 2004). It is therefore a more plausible hypothesis that the surface topography was the main cause for the observed poor cell adhesion and growth – a point also indicated by Chapter 5's gene regulation results.

Kasemo and Lausmaa noted that the biochemical interaction of a metal surface with biological material was limited to the top layer with a maximum thickness of 1 nm (Kasemo

and Lausmaa, 1988). As the naturally forming titanium oxide layer is between 2-5nm, and in the case of industrial anodisation up to 50nm (Disegi, 1997), the cells will never interact with the underlying bulk metal (Kasemo, 1983; Kasemo and Lausmaa, 1988). Coating titanium onto materials is a commonly utilised method to create surfaces to attempt to mimic implants. This overlying homogenous metal chemistry has been exploited in numerous biomaterial studies using epoxy-resin metal surface replicas (Wieland *et al.*, 2002; Wieland *et al.*, 2005) and microtopographies amongst others (Brunette *et al.*, 2001; Jain and von Recum, 2003; Tan and Saltzman, 2002), and it effectively masks the underlying surface chemistry from any biological interaction.

The hypothesis put forth is that the surface topography of NS was the sole cause of the cellular reactions observed. To test this hypothesis the surface chemistry of the NS topography was masked by coating the surface with either 50nm gold or 50nm titanium. Gold is considered bioinert and biocompatible (Tan and Saltzman, 2002) and titanium is biocompatible as it forms an inert titanium-oxide upon contact with air (Brunette *et al.*, 2001; Dee *et al.*, 2002). By using two separate metals, two different surface chemistry models could be studied in relation to the characteristic NS topography. As the overall study included two other standard orthopaedic topographies of steel (SS) and titanium (TS), both these materials were included in the study and also coated with gold or titanium. After surface characterisation, cellular reactivity was studied on the two different sets of standard topographies with homogenous, biocompatible surface chemistries. Thermanox was included as a control, however as electropolished Titanium (TE) and TAN (NE) have a similarly flat surface topography compared to SS both were omitted. While all materials were investigated, the focus of the study was on NS and its coated counterparts.

Chapter 6 – Surface Chemistry

Introduction

The initial identification of four features of Standard TAN (NS) that could possibly result in the observed greatly reduced cell growth; β -phase particle endocytosis, ion leeching, surface chemistry and surface topography, have been narrowed down to the latter two (Chapters 3 and 4). This chapter seeks to primarily elucidate the influence surface chemistry has on the cellular reaction towards NS and the other 'standard' surfaces.

Surface Chemistry

As discussed in Chapter 2, the surface chemistry of NS is a heterogeneous mix of titanium, aluminium and niobium oxides found at the surface in relation to the underlying α and β phase composition of the bulk alloy (Disegi, 1997; Sittig *et al.*, 1999b). For pickled (acid etched) TAN, the concentration of Nb_2O_5 on the surface was generally higher. This, as was previously noted in Chapter 3, brings into question the validity of using NE as topographical control for NS as the chemistries might not be the same (Sittig *et al.*, 1999a; Textor *et al.*, 2001). The cellular effect of TAN's component oxides has been studied previously using a fabricated topography mimicking the distribution of the various oxides, based upon on the relation of the bulk $\alpha+\beta$ phases (Scotchford *et al.*, 2003; Winkelmann *et al.*, 2003). In this instance, it was observed that cells were sensitive to the varying oxide chemistries and that topography was not a contributing cause. However, the outcome of my earlier study (see Chapter 3) was that NE was a compatible surface for cells. This indeed brings into question the validity of isolating surface chemistry as the sole cause for poor cell compatibility. While the amount of niobium oxide on the NS surface might be higher than on NE, this material has not previously been shown to be cytotoxic (Eisenbarth *et al.*, 2004; Khan *et al.*, 1999; Velten *et al.*, 2004). It is therefore a more plausible hypothesis that the surface topography was the main cause for the observed poor cell adhesion and growth – a point also indicated by Chapter 5's gene regulation results.

Kasemo and Lausmaa noted that the biochemical interaction of a metal surface with biological material was limited to the top layer with a maximum thickness of 1nm (Kasemo

and Lausmaa, 1988). As the naturally forming titanium oxide layer is between 2-5nm, and in the case of industrial anodisation up to 50nm (Disegi, 1997), the cells will never interact with the underlying bulk metal (Kasemo, 1983; Kasemo and Lausmaa, 1988). Coating titanium onto materials is a commonly utilised method to create surfaces to attempt to mimic implants. This overlying homogenous metal chemistry has been exploited in numerous biomaterial studies using epoxy-resin metal surface replicas (Wieland *et al.*, 2002; Wieland *et al.*, 2005) and microtopographies amongst others (Brunette *et al.*, 2001; Jain and von Recum, 2003; Tan and Saltzman, 2002), and it effectively masks the underlying surface chemistry from any biological interaction.

The hypothesis put forth is that the surface topography of NS was the sole cause of the cellular reactions observed. To test this hypothesis the surface chemistry of the NS topography was masked by coating the surface with either 50nm gold or 50nm titanium. Gold is considered bioinert and biocompatible (Tan and Saltzman, 2002) and titanium is biocompatible as it forms an inert titanium-oxide upon contact with air (Brunette *et al.*, 2001; Dee *et al.*, 2002). By using two separate metals, two different surface chemistry models could be studied in relation to the characteristic NS topography. As the overall study included two other standard orthopaedic topographies of steel (SS) and titanium (TS), both these materials were included in the study and also coated with gold or titanium. After surface characterisation, cellular reactivity was studied on the two different sets of standard topographies with homogenous, biocompatible surface chemistries. Thermanox was included as a control, however as electropolished Titanium (TE) and TAN (NE) have a similarly flat surface topography compared to SS both were omitted. While all materials were investigated, the focus of the study was on NS and its coated counterparts.

Materials and Methods

Experiment 14 – Coated Metals

Sample Evaporation

11mm samples of the test metals were evaporated with either 50nm of gold or 50nm of titanium. Evaporation was performed using an e-beam evaporator (MEB450, Plassys) utilising pure gold or titanium plate source material for evaporation. Samples were held in a specially designed holder, which resulted in a 1mm rim of bulk material left as the original surface. Sample notation and treatment is noted in Table 6.1.

Denoting Symbol	Evaporation Treatment	Layer Thickness	Original Material
ThG ThT	Gold Titanium	50nm 50nm	Th - Thermanox
SG ST	Gold Titanium	50nm 50nm	SS - Stainless Steel
TG TT	Gold Titanium	50nm 50nm	TS - Titanium
NG NT	Gold Titanium	50nm 50nm	NS - TAN

Table 6.1 – Summary of evaporation treatments for the 'standard materials' and Thermanox controls.

Scanning Electron Microscopy

Samples were assessed using same operating conditions optimised in Chapter 2: Experiment 2. Generally BSE detection was utilised at 5kV.

White Light Profilometry

Samples were assessed using the same parameters set out in Chapter 2: Experiment 1. Six separate points were scanned split between two samples of each surface.

Experiment 15 - Cell Growth and Morphology

Cells were seeded, fixed and prepared for SEM imaging as described in Chapter 3: Experiment 5. To summarise, cells were seeded on the materials (in duplicate) and cultured for 24hrs, 5 and 10 days before fixing and drying in preparation for SEM viewing.

Experiment 16 – Cell Counts

Cells were seeded on the uncoated and coated sets of samples; Th, ThG, ThT, SS, SG, ST, TS, TG, TT, NS, NG and NT in triplicate for each sample type and for the three timepoints – 24hr, 5 and 10 day. For the 5 and 10 day samples, the media was changed every 2.5 days. In a method modified from Chapter 3; Experiment 7, the cells were fixed, permeabilised, incubated with rhodamine conjugated phalloidin and mounted with DAPI. For each sample a minimum of 15 images at x10 magnification (Zeiss Axioplan 2 imaging fluorescence microscope equipped with an Axiocam and a Plan-NEOFLUAR 10x/0,30, ∞/0,17) were taken randomly on the surface, thus for each triplicate over 45 images were taken. This was repeated for all sample types at all timepoints. Cell counts were conducted using ImageJ to process the DAPI images by counting the nuclei. Statistical analysis was conducted in batches e.g SS, SG and ST, as the question posed was if there is any difference in cell numbers with regards to the surface coating and not between the original sample types. Due to the nature of cell seeding, variation on a single replicate was high, therefore the means of the three replicates per sample type were utilised for the analysis. For each sample batch a two-way analysis of variance (ANOVA) was conducted at $p < 0.01$ using Statlets© to examine for any significant differences. Cell area measurements for NS, NG and NT were conducted by imaging the phalloidin stain at x10 magnification, 15 images per sample replicate, and analysed as described in Chapter 3; Experiment 7.

Experiment 17 - Vinculin, Tubulin and Actin Immunostaining

Cells were seeded and cultured for 48hr and then fixed and stained as described in Chapter 3: Experiment 7.

Results

Experiment 14 – Coated Metals

Standard materials (11mm discs) were coated with 50nm of either gold or titanium to mask the original surface chemistry while maintaining the original topography. The effectiveness of the mask was assessed using SEM in BSE mode to determine the homogeneity of the coating and ensure the maintenance of notable surface features with reference to their uncoated counterparts characterised in Chapter 2. Profilometry was utilised to ensure there were no larger scale modifications to the topography. During coating, the disc holder obstructed the outer 1mm of the sample thus allowing a direct visual comparison between the original surface and the coated surface. This border is related to in the following as the 'mask border'.

Thermanox

The gold coated thermanox (ThG) had a rippled and scratched surface that at a higher magnification demonstrated some nanotopographical features. This topography has been previously observed on Thermanox (Th) and was probably caused by the heat generated during the coating procedure melting the polymer surface (Fig 6.1a). The mask border clearly demonstrated the compositional difference between the original and coated surfaces and showed the coating thickness (Fig 6.1b). Titanium coated Th (ThT) was thought to have a homogenous surface coating thickness, as the underlying surface blemishes of Th were still apparent with the titanium coating (Fig 6.1c). The homogeneity of the coating was further confirmed at the mask border; on the coated area there were no breaches exposing the underlying Thermanox surface, however, the mask border was more of a transition than a step (Fig 6.1d). Profilometry confirmed that the numerical roughness values were similar to the uncoated examples measured in Chapter 2: Experiment 1. The original measurement for Th was $0.14 \pm 0.045\mu\text{m}$ while for ThG the Ra was $0.23 \pm 0.029\mu\text{m}$ and for ThT it was $0.04 \pm 0.001\mu\text{m}$. It was possible that the low value for ThT was an artefact due to its highly reflective surface interfering with the profilometry readings, however gold is also highly reflective and did not impede upon the measurements. Examples of three-dimensional (3D) reconstructions of the treated samples (Fig 6.5) demonstrated them to be indistinguishable to the uncoated Th.

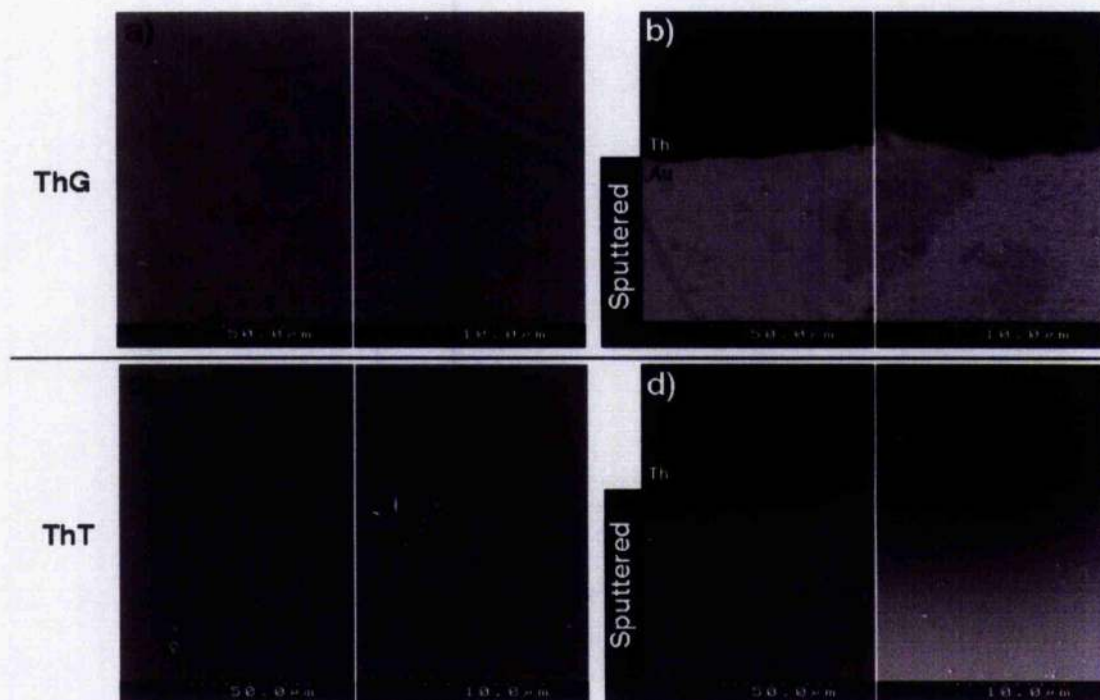


Fig 6.1 – (a) and (b) are Th samples evaporated with 50nm gold (ThG). Image (a) demonstrates a rippled and scratched surface with nanotopographical features. (b) The mask border clearly demonstrates the compositional difference between the original and coated surfaces and demonstrates the effectiveness of the coating thickness. (c) and (d) are Th samples evaporated with 50nm titanium (ThT). (a) Surface blemishes are still visible with the titanium coating indicating a homogenous coating. (d) The uniform coating was confirmed at the mask border with no breaches exposing the underlying Thermanox surface, however the mask border was more of a transition than a step.

SS - Stainless Steel

The SS surface evaporated with 50nm gold (SG) had a homogeneous coating with no visible traces of the underlying alloy surface (Fig 6.2a). The difference in surface composition was again clearly demonstrated at the mask border (Fig 6.2b). The minimal surface topography in the form of small scratches was barely visible due to the high atomic number contrast (Chapter 2; Introduction) (Fig 6.2a). Titanium coating of SS (ST) was equally efficient, although the lower atomic number contrast enhanced the resolution available for the surface detail (Fig 6.2c). The mask border clearly demonstrated the compositional difference between the chemical heterogeneity of the underlying original surface and the homogeneity of the coated surface (Fig 6.2d). Profilometry confirmed no significant changes in numerical surface roughness values due to the treatment. With reference to Chapter 2, SS was $0.19 \pm 0.022\mu\text{m}$ while for SG the Ra was $0.17 \pm 0.022\mu\text{m}$ and for ST it was $0.18 \pm 0.008\mu\text{m}$. 3D reconstructions (Fig 6.5) demonstrated them to be indistinguishable to the uncoated SS.

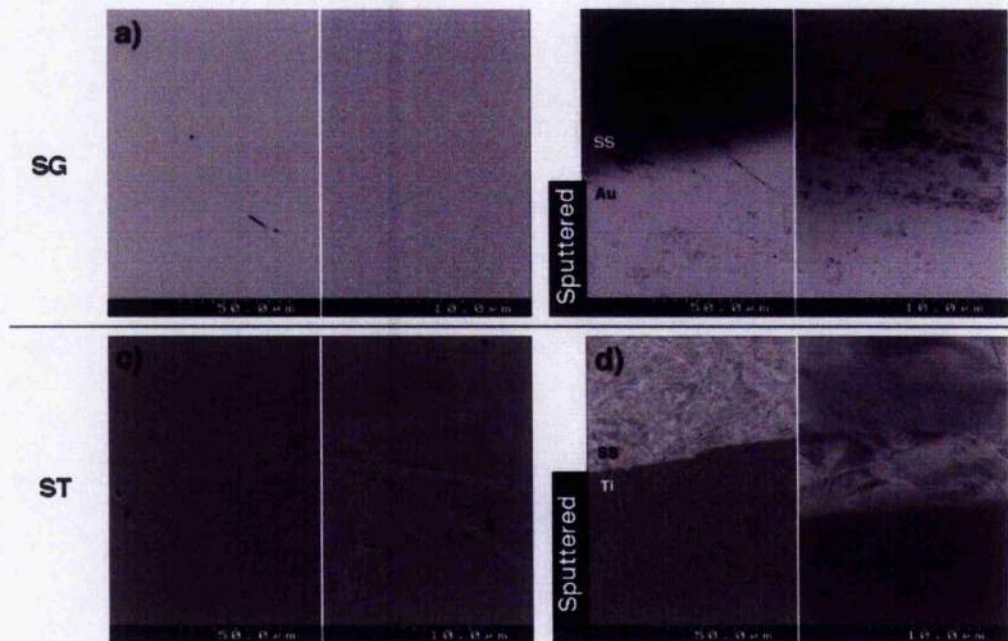


Fig 6.2 – (a) and (b) are SS samples evaporated with 50nm gold (SG). Image (a) demonstrates a homogenous covering of gold over the underlying stainless steel. (b) The mask border clearly demonstrates the compositional difference of the original and surface coatings. (c) and (d) are SS samples evaporated with 50nm titanium (ST). Image (c) demonstrates that the titanium coating was equally efficient in masking the surface. (d) The mask border demonstrates a clear border between the chemically heterogeneous original surface and homogenous coating.

TS – Titanium

Coating the rugged surface of TS with 50nm gold (TG) resulted in a uniform surface coating with characteristic TS surface features, however, lower magnifications reveal some surface contamination (Al_2O_3 ceramic) was present as dark areas on the surface (Fig 6.3a). This contamination was observed to be present on uncoated TS and therefore is an artefact of the material and not the coating. At the mask border, the difference in atomic number contrast of the gold-coated surface and the original titanium surface demonstrate the efficacy of the coating (Fig 6.3b). The evaporated titanium also produced a uniform coating (Fig 6.3c), and again this became more apparent at the mask border where the coating could be compared to the original surface (Fig 6.3d). Although both the original surface and the coating were titanium, the atomic number contrast demonstrates some compositional difference. The border was also not as defined a line compared to the titanium coating of TS. Profilometry measurements gave a Ra value of $0.88 \pm 0.017\mu\text{m}$ for TG and $0.85 \pm 0.029\mu\text{m}$ for TT, this compares well with uncoated TS, which had a Ra of $0.90 \pm 0.027\mu\text{m}$ and suggests that the coating did not modify the topography. This is further supported by the similarity of the 3D representations of the coated surfaces to the uncoated ones (Fig 6.5).

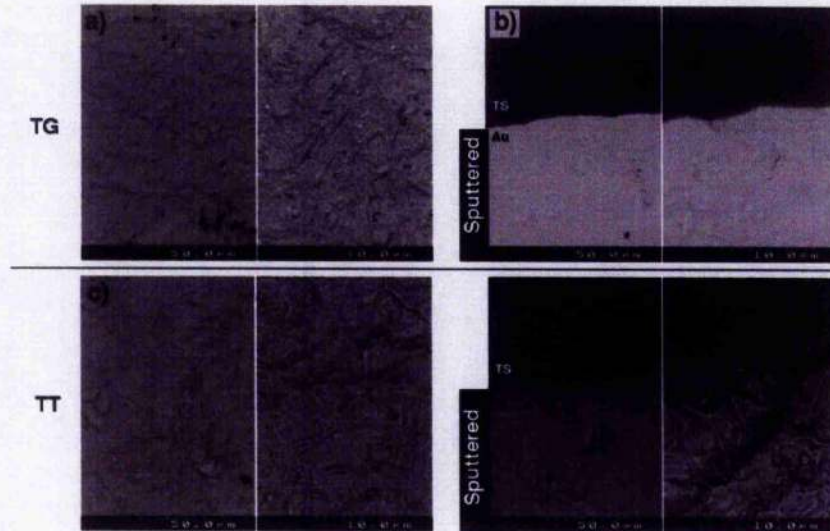


Fig 6.3 – (a) and (b) are TS samples evaporated with 50nm gold (TG). Image (a) demonstrates a uniform surface coating of TS characteristic surface features. (b) At the mask border, the considerable difference in Z-contrast of the gold coated surface and the original titanium surface demonstrate the efficacy of the coating. (c) and (d) are TS samples evaporated with 50nm titanium (TT). Image (c) demonstrates that TT has a homogenous titanium coating. (d) Compositionally the titanium coat was different from the underlying titanium surface.

NS – TAN

The original, elementally heterogeneous NS surface was effectively masked by the 50nm gold coating (NG) (Fig 6.4a). The mask border demonstrated clearly that the coating uniformly masked both the β -phase particular features and the general undulating topography of the surface in comparison to the original surface (Fig 6.4b). The reduction in atomic number contrast between the β -phase particle and the underlying surface on NS with a 50nm titanium coating (NT) would suggest that this was also a homogenous coating of the surface. At the mask border, the particles present on the coated and original surfaces were of similar greylevels suggesting a coating inconsistency (Fig 6.4c). However the atomic number contrast of the non-particulate coated surface demonstrated that this was the greylevel of the titanium mask and the uncoated particles. The roughness of NG was measured as $0.83 \pm 0.018\mu\text{m}$ and NT was $0.82 \pm 0.056\mu\text{m}$. If compared with uncoated NS of $0.77 \pm 0.076\mu\text{m}$, it suggests that the coating did not modify the topography, further confirmed by 3D representations of the coated surfaces (Fig 6.5).

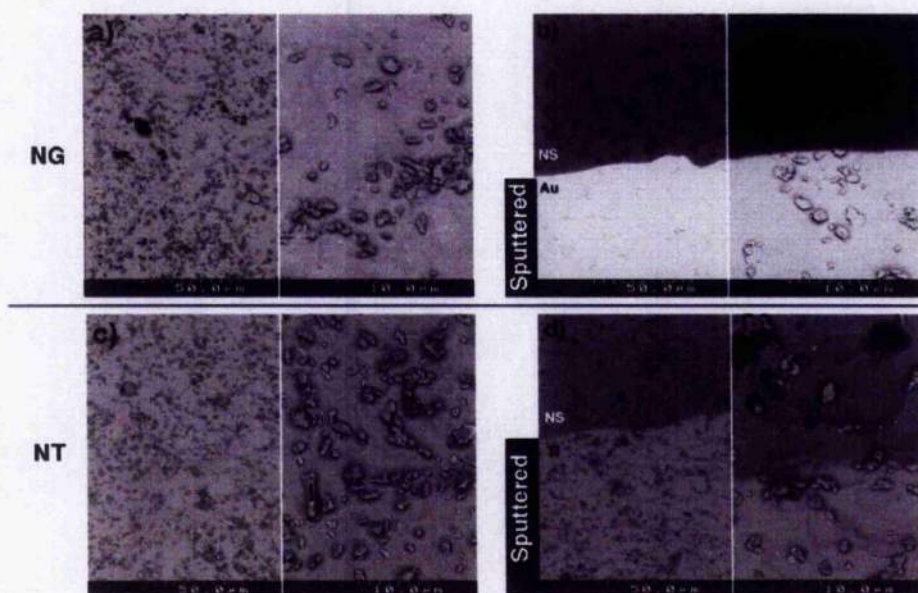


Fig 6.4 – (a) and (b) are NS samples evaporated with 50nm gold (NG). (a) The original, elementally heterogeneous NS surface was effectively masked by the 50nm gold coating (b) The mask border demonstrated clearly that the coating uniformly masked both the β -phase particular features and the general undulating topography of the surface in comparison to the original surface. (c) and (d) are NS samples evaporated with 50nm titanium (NT). (c) A reduced atomic number contrast between the particles and the underlying surface indicated a homogenous coating of both. (d) At the mask border, the particles present on the coated and original surfaces are of similar greylevels, however the atomic number contrast of the non-particulate coated surface demonstrates that this was the grey level of the titanium mask and the uncoated particles.

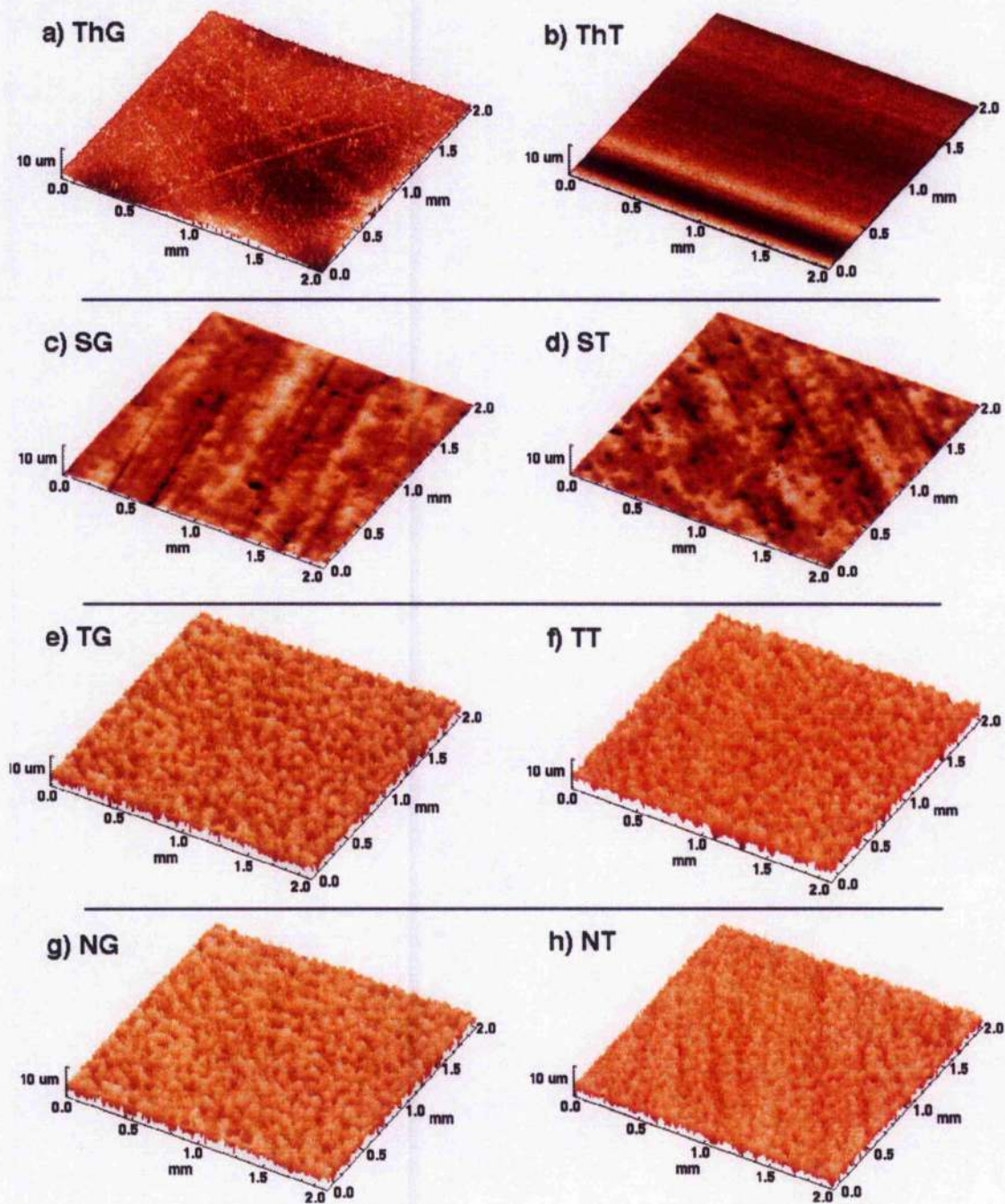


Fig 6.5 – 3D reconstructions of white-light profilometry measurements of all the coated surfaces.

Experiment 15, 16 and 17 - Cell Growth, Morphology & Adhesion

Quantitative cell growth, in the form of cell counts, was measured for all the coated samples types and the original uncoated types for comparison. DNA quantification was not possible due to the lack of availability of the larger 49mm sample types and the cost and time required for coating the samples, therefore 11mm sample discs were utilised. Qualitative cell proliferation and morphology studies (similar to those carried out on the uncoated materials in Chapter 3: Experiment 5) were conducted on all 8 of the coated samples: ThG, ThT, SG, ST, TG, TT, NG and NT and were compared with the original samples investigated in a similar manner in 'Qualitative Cell Growth' section of Chapter 3: Results. As the main focus of the investigation was cell reactivity towards NS and its coated counterparts, cell areas on NS, NG and NT were also quantified. While cell numbers and morphology were generally focused on the coated areas, consideration was also given to cell interaction at the mask border. To save upon space and repetition, the majority of the images for quantitative growth, morphology and intracellular labelling for the coated samples are located on the accompanying CD-ROM.

Cell Growth**Qualitative Cell Growth – SEM**

At low magnifications, similar trends of cell coverage and growth were observed in comparison to those observed previously on uncoated versions of the sample types. Cells on coated Th, SS, TS and NS all behaved similarly, reaching confluency on all sample types except NS at 10 days. The images of gold and titanium coated Th, SS, TS are included on the CD-ROM, while NG and NT are demonstrated below. Cells were unspread or elongated at all timepoints and their numbers did not increase (Fig 6.6).

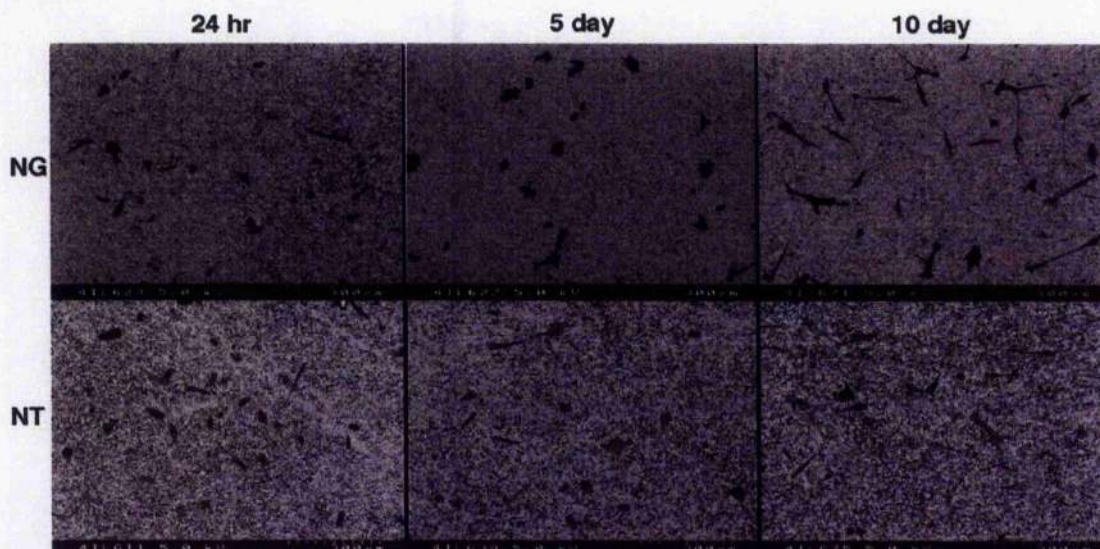
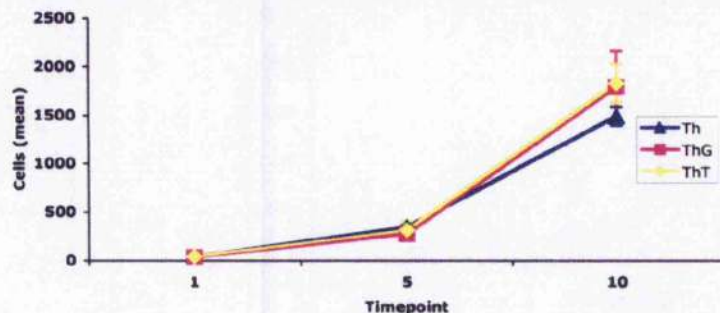


Fig 6.6 - SEM micrographs (BSE mode) of hTERT fibroblasts cultured gold (NG) and titanium (NT) coated NS. Cell morphology was generally unspread or elongated and cell numbers did not increase at the later timepoints.

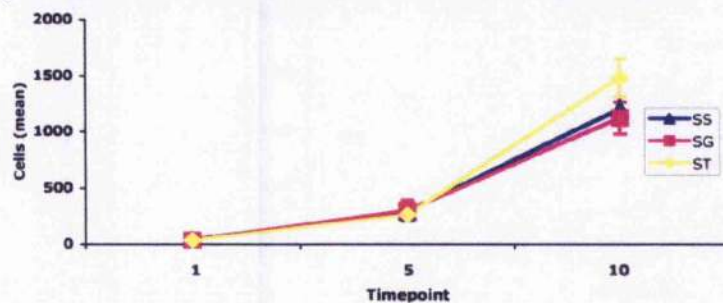
Quantitative Cell Growth – Cell Counts

With the exception of NS, NG and NT, all other materials supported a confluent monolayer of cells by 10 days. At a x10 objective, covering $1418\mu\text{m} \times 1128\mu\text{m}$ of the sample surface, this amounted to an average of 1500 cells per field of view at 10 days (Graph 6.1). 45 fields of view were counted, spread over three replicates, for each timepoint and for each sample type. The cell counts confirmed that for each surface, cell growth behaved similarly with or without masking of the surface chemistry. This was also demonstrated statistically, where the only significance found between a set of coated and uncoated sample types e.g SS, SG and ST, was between the timepoints ($p < 0.01$). Quantitatively, NS also elicited a low cell number when its chemistry was masked, with a significant difference only observed at the timepoints ($p < 0.01$). As was previously observed using DNA quantification (see Chapter 3; Results, 'Quantitative Cell Growth'), the initial number of cells on NS decreases between 24hr and 5 days, however, in this instance cell numbers continued to decrease further at 10 days.

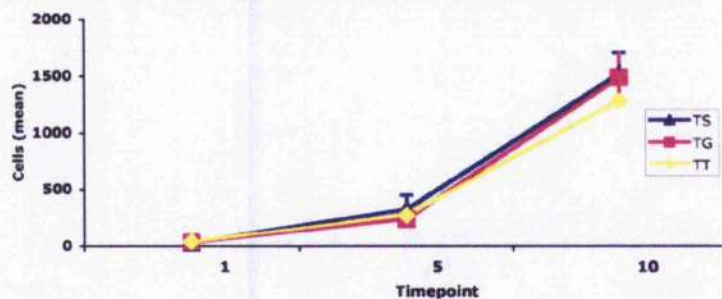
a) Mean Cell numbers on Th,ThG and ThT at various timepoints



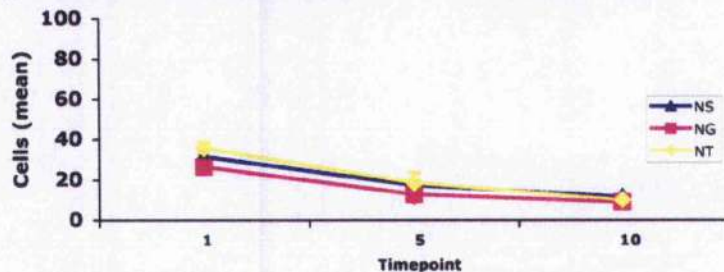
b) Mean Cell numbers on SS,SG and ST at various timepoints



c) Mean Cell numbers on TS,TG and TT at various timepoints



d) Mean Cell numbers on NS,NG and NT at various timepoints



Graph 6.1 – Plot of mean cell counts ($n=45$), for a $1418\mu\text{m} \times 1128\mu\text{m}$ field of view, at the three timepoints, for each standard surface type and modified surfaces coated with either gold or titanium. Plot (a) is for Thermanox, (b) SS, (c) TS and (d) NS. Note that the scale for NS is lower than the other plots to allow the smaller differences in numbers to be displayed.

Cell Morphology and Intracellular Labelling

High magnification SEM, and fluorescence imaging (48hr, vinculin, tubulin, actin and DNA) of cells on the coated samples was conducted to ensure that qualitatively there were no outstanding discrepancies in the features noted of cells on the coated surfaces in comparison to the uncoated samples. No differences were observed, which confirmed the cell growth observations for each set of surfaces. These qualitative features are summarised in Table 6.2 and high magnification SEM and fluorescent images are included on the accompanying CD-ROM.

As stated previously, the main focus of the investigation was cell reactivity towards NS and its coated counterparts. Cell counts were not statistically different, and at higher magnifications the cell morphology on both NG and NT was unspread or elongated with a ruffled membrane, similar to those cultured on uncoated NS at 24 hr (Fig 6.7). For the majority of cells observed, filopodia projected from points originating from further within the cell boundary and attached primarily to the protruding β -phase particles (Fig 6.7a,c,e,g). For NG, it was apparent in both SE and more clearly in BSE that small patches of the coating had come away from the surface exposing the original underlying surface (Fig 6.7b,d). The shape of the patches indicates that these were sites of loose β -phase particles that had been removed, however, the scattered nature of the areas would suggest that involvement of cells in the removal process was unlikely. It was more plausible that the particles had been removed during the culturing or SEM preparation phases. The cells appeared disinterested in these patches, indicated by an absence of filopodia interaction, and could suggest that the cells primarily interacted with the topography. Another possibility to explain the reaction would be that these patches had become exposed post-fixation (Fig 6.7d). Due to the lower atomic number contrast between the surface coat and the original surface on NT, it was difficult to observe any traces of β -phase particle removal in this instance (Fig 6.7f,g).

Fluorescence labelling on coated NS demonstrated familiar features such as small punctuate focal adhesion sites, restricted spreading and intermittent breaches in the microtubule network. Examples of cells on NG are included in Fig 6.8.

Sample Type	Cell Growth	Cell Morphology		Intracellular Staining		
		Spreading	Filopodia	Cytoskel.	Microntubules	Focal Adhesions
Th	+/+	Spread cells	Minimal interaction	√	√	Elongated 'dash' adhesions
ThG	+/+	Spread cells	Minimal	√	√	'Dash' adhesions
ThT	+/+	Spread cells	Minimal	√	√	'Dash' adhesions
SS	+/+	Spread cells	Minimal	√	√	'Dash' adhesions
SG	+/+	Spread cells	Minimal	√	√	'Dash' adhesions
ST	+/+	Spread cells	Minimal	√	√	'Dash' adhesions
TS	+/+	Visible spreading alignment to the topography	Highly prominent on cells at 24 hr and 5 days and utilised to sense the topography	√	√	Smaller adhesions
TG	+/+	Visible spreading alignment to the topography	Visible at 24 hr and 5 days	√	√	Smaller adhesions
TT	+/+	Visible spreading alignment to the topography	Visible at 24 hr and 5 days	√	√	Smaller adhesions
NS	-/-	Elongated or unspread morphology	Interacting with the particulate topography at all timepoints	√	Network punctuated with holes at the sites of protruding particulates	Smaller adhesions, visibly influenced by the topography
NG	-/-	Elongated or unspread morphology	Interacting with the particulate topography	√	Holes at sites of protruding particles	Smaller, influenced by topography
NT	-/-	Elongated or unspread morphology	Interacting with the particulate topography	√	Holes at sites of protruding particles	Smaller, influenced by topography

Table 6.2 – Summary table of the qualitative and quantitative observations for hTERT cells cultured of Th, SS, TS and NS and their counterparts coated with either 50nm gold or titanium. All qualitative observations are described apart from '√' which denotes that the surface did not affect the labelled structure. For quantitative measures; '+/+' indicates a high value and '-/-' a low value.

Fig 6.7 – (opposite page) Cells cultured for 24 hr on NG (a-d) and NT (e-h). Left column of images are SE and right are BSE of the same cell, (a) SE mode image the cell morphology was generally unspread with a ruffled membrane and protruding filopodia (b) BSE demonstrated that small patches of the coating covering the surface area had come away from the surface. (c) Numerous filopodia extended from the cell body and attached to the protruding β -phase particles. (d) The shape of the coating gaps would suggest that these were in fact site of loose β -phase particles that have been removed. (e) On NT the cell remains unspread and demonstrates numerous filopodia extending from the cell body. (f) The lower atomic number contrast between the surface coat and the original surface made it difficult to see any traces of β -phase particle removal. (g) Filopodia attacking and bridging the titanium coated β -phase particles. (h) High magnification BSE further demonstrates the elemental homogeneity of the surface.

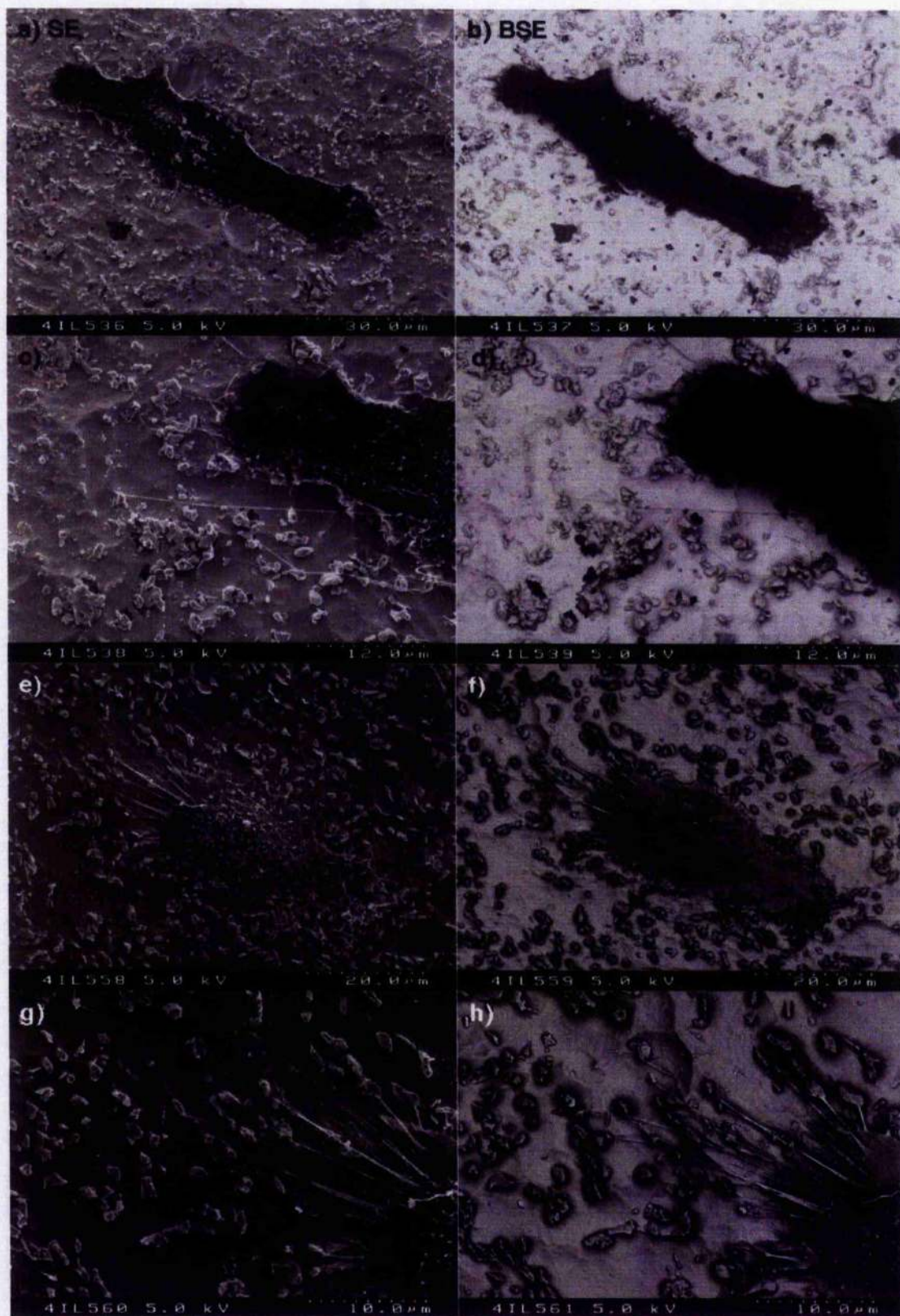


Fig 6.7 – (legend on opposite page)

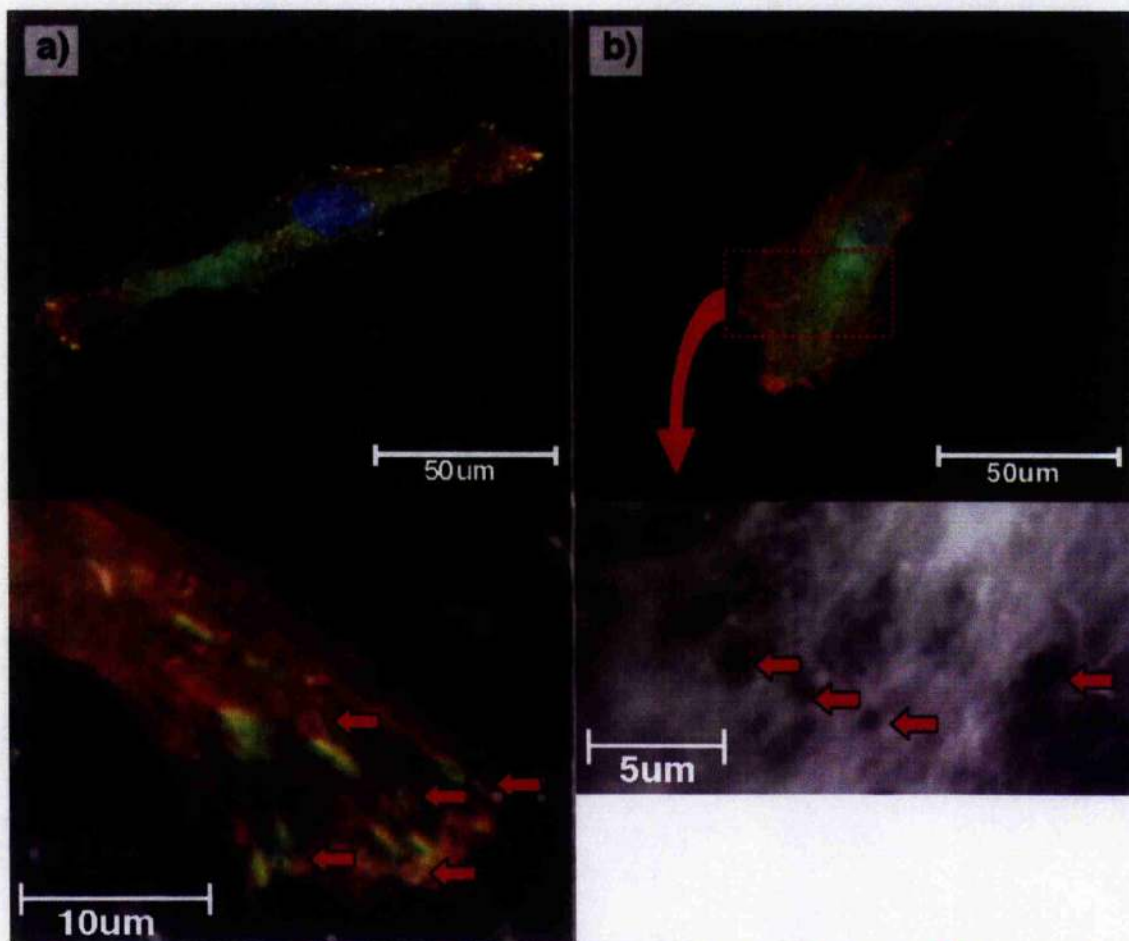
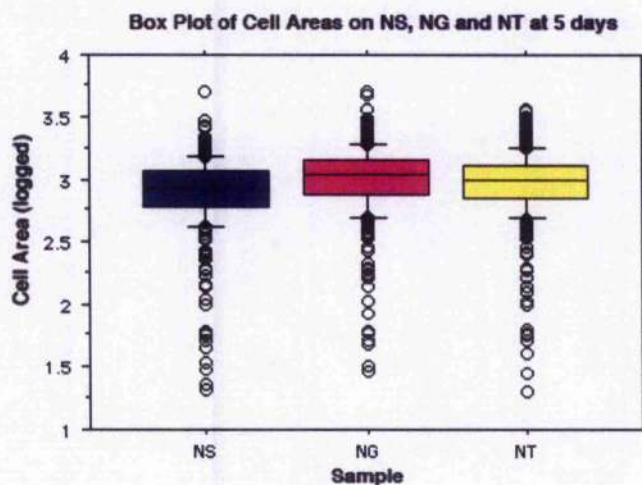


Fig 6.8 – Cell cultured on NG for 48 hr and (a) Triple labelled for ● Vinculin, ▼ Actin and ◆ DNA. Cells were not very well spread with small ‘dot’ like focal adhesion sites. These sites could be observed avoiding particles present on the surface (red arrows). (b) ● Tubulin, ▼ Actin and ◆ DNA. The microtubule network was present throughout the cell body, however it was punctuated with gaps corresponding to particles protruding from the surface (red arrows).

At 5 days all other sample types, with the exception of NS, cells were already present at high numbers and had established close cell-cell contacts. However, on NS cells were solitary and unspread or elongated. Therefore the 5 day timepoint was considered a good representative that would best reveal any variation in reactivity towards the coated versions of the surface. The cell quantification was confined to cell spreading area, due to the fact that the very elongated nature of some cells would make them undetectable to the image analysis protocol, and therefore allowing for the possible calculation of erroneous aspect ratios. An average of 450 cell areas per surface type, NS, NG and NT, were quantified and found to be significantly different, with both NG and NT different from NS ($p < 0.01$). From the box plot it was apparent that cell areas on NG, and to some extent NT, were larger with the median corresponding to the highest quartile found on NS (Graph 6.2). While an interesting observation, the low cell counts found on all surfaces indicated that this did not correspond to a change in cell growth.



Graph 6.2 – Box plot of variation in cell areas measured on NS, NG and NT. Note that the values have been logged. The median for cell areas on NS was lower than that found on the two coated surfaces.

Cell Alignment to the Mask Border

While the focus of this study was to investigate the involvement of chemistry in cell behaviour on NS, an interesting observation on all surfaces (with the exception of TT) was that at the earlier timepoints of 24hr and 5 days cell alignment could occasionally be observed at the mask border between the surfaces (Fig 6.9).

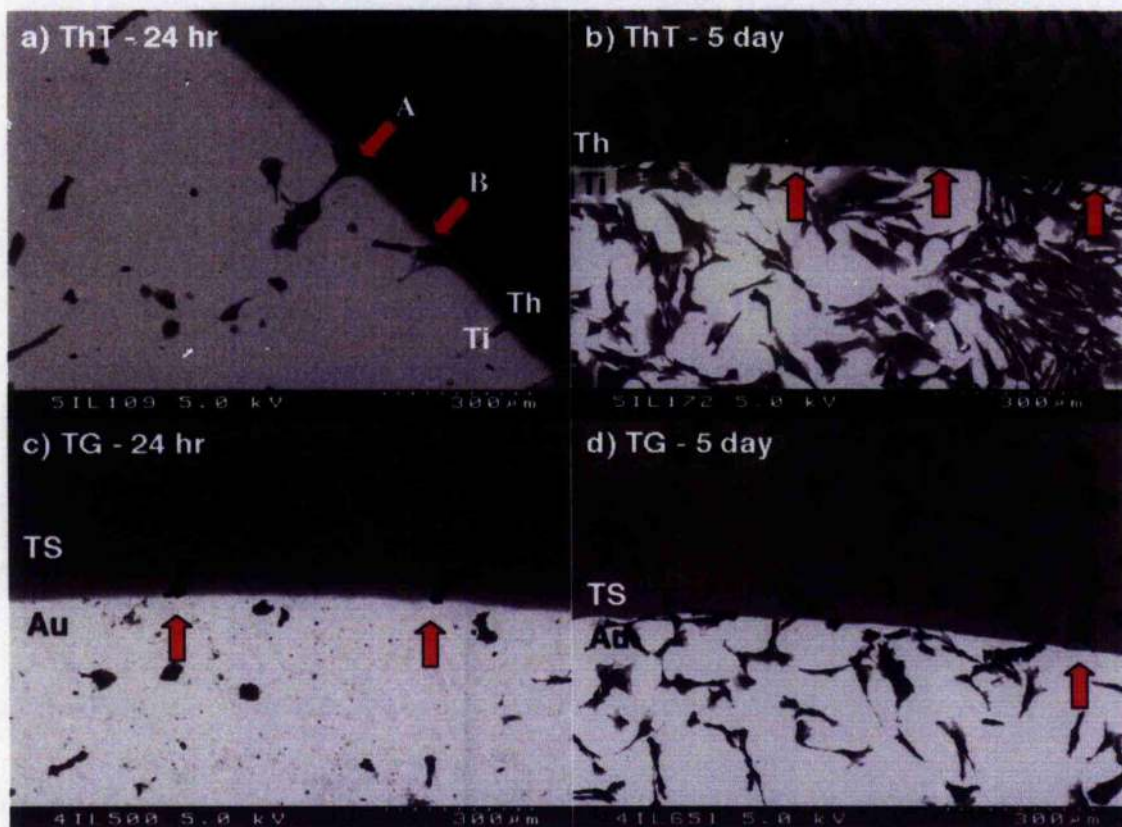


Fig 6.9 – Cell growth at the mask border at 24hr and 5 days. (a & b) Cells on titanium coated Thermanox (ThG). (a) Some cells could be observed aligning to the mask border (red arrow 'A'), while others could be observed crossing it (red arrow 'B'). (b) By 5 days this alignment still occurred with some cells found adhering on the original Th surface and aligning with the titanium border (red arrows). (c & d) Cells on gold coated TS (TG). (c) At 24hr, cells were observed aligning to the mask border (red arrows). (d) At day 5 some cells display alignment or at least detect the mask border while other are observed crossing it (red arrow).

Cell counts at the 24hr and 5 days were conducted at the border of 5 sample images of each type to examine the instance of cell alignment and crossing of the border. To compare if these observations were artefact, theoretical borders (tb) were drawn at random on 5 other images of cells on the materials, away from the mask border, and the instances of alignment and crossing to the tb were recorded. Note that TT was omitted, as the border could not be

resolved when cells were present. The low cell numbers present at 24hr made it impossible to conduct statistical analysis, however, some observations could be made. At 24hr consistently more cells aligned at the mask border than the tb, while lower crossing was observed (with the exception of NT). At 5 days, more alignment was again observed for the mask border, however crossing was high on both. The crossing cells demonstrate that this was not an impervious border and the increased number at 5 days makes it difficult to resolve single cells, however at 24hr alignment was visible at the border mask.

(i) Mask Border

	Aligning		Crossing	
	24hr	5 days	24hr	5 days
<i>ThT</i>	2	3	0	10
<i>ThG</i>	1	3	0	8
<i>SG</i>	1	4	1	6
<i>ST</i>	2	2	1	4
<i>TG</i>	1	3	1	2
<i>NG</i>	2	2	0	0
<i>NT</i>	1	1	1	2

(ii) Theoretical Border

	Aligning		Crossing	
	24hr	5 days	24hr	5 days
<i>ThT</i>	0	1	2	19
<i>ThG</i>	0	2	1	12
<i>SG</i>	0	1	2	10
<i>ST</i>	0	0	2	6
<i>TG</i>	0	1	1	5
<i>NG</i>	0	0	1	1
<i>NT</i>	1	0	1	2

Table 6.3 – Cell counts at the mask and theoretical border examining the number of cells aligning and crossing the border on the samples as 24hr and 5 days.

On titanium coated SS (ST), SEM at a higher magnification allowed for the sensitivity to the mask border to be examined in detail. While BSE displayed the material border clearly (Fig 6.10a), surface detail could be resolved with better clarity from the SE images. The material border observed in BSE mode was marked as a yellow line on the SE images (Fig 6.10b). At a further higher magnification it was possible to observe that the cell was spreading out and its filopodia were reacting to the mask border by alignment and not by crossing. It was interesting to note that the attachment of filopodia appeared inhibited by an 'invisible border' 1-2 μm adjacent to the actual material border (Fig 6.10c,d).

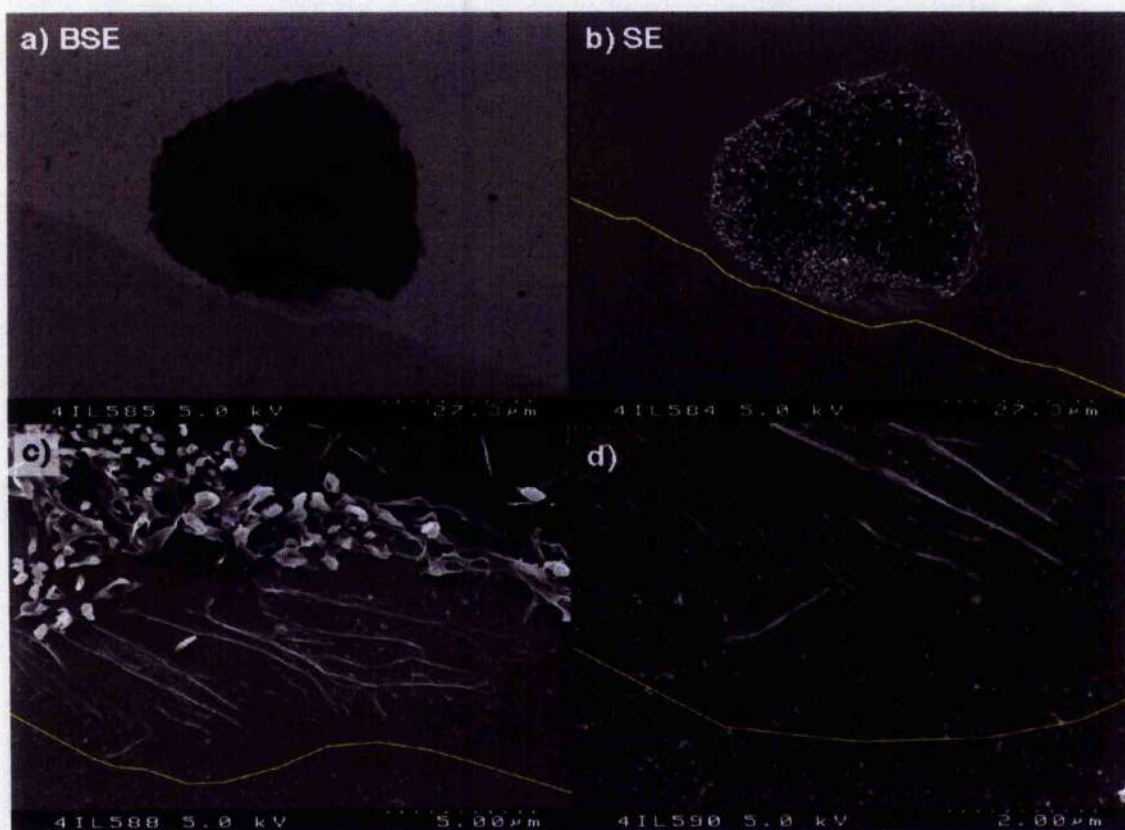


Fig 6.10 - Cell cultured at the ST border for 24hr. (a) Low magnification BSE image of a cell adhering at the border. The BSE detector allows for resolving the titanium coating and the original SS elements on the surface. (b) SE image of the same cell with a superimposed material border drawn as yellow line resolving more cell surface detail. (c & d) Higher magnifications of the cell demonstrates its filopodia are sensitive to the material border although its investigation did seem inhibited by an 'invisible border' adjacent to the actual material border.

Fluorescent staining of intracellular features demonstrates some interesting features at the mask border. On SG the focal adhesion sites could be observed to form a mature dash morphology, however, they did not cross the mask border (Fig 6.11a). On NG, the cell periphery aligned with the border, however the microtubule network had yet to form a network to the edge of the aligned cell body (Fig 6.11b).

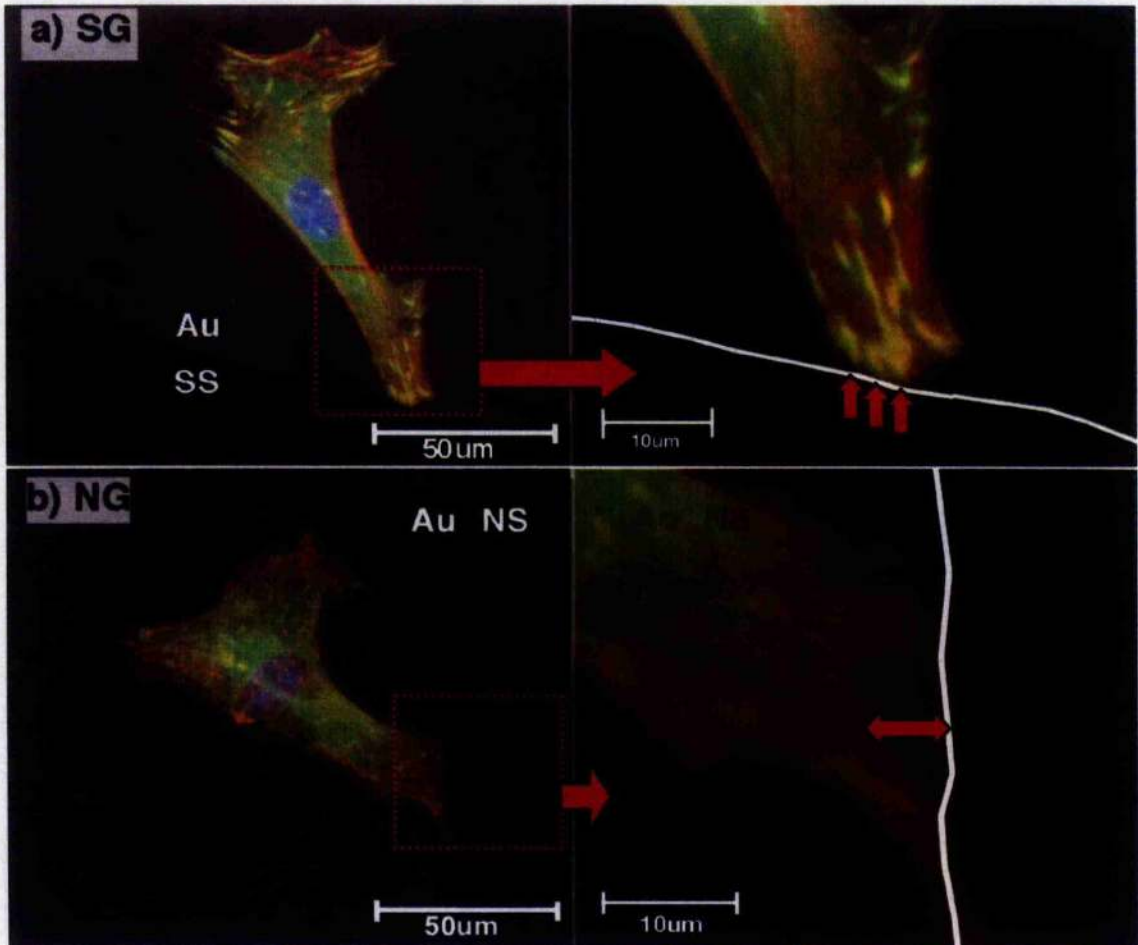


Fig 6.11 – (a) Cell cultured on SG for 48 hr triple labelled for ● Vinculin, ▼ Actin and ◆ DNA. Focal adhesion sites (red arrows) were mature dash sites that did not cross the mask border (white line). (b) Cell cultured on NG for 48hr and labelled for ● Tubulin, ▼ Actin and ◆ DNA. While the cell periphery lined up adjacent with the border, the microtubule network had not formed to the edge of this area (red arrow).

Discussion

Coated Metal Characterisation

Using profilometry and SEM, surface characterisation of the modified surfaces demonstrated that the coating technique and thickness had effectively masked the samples including NS. SEM in BSE mode demonstrated this clearly; in most instances the atomic number contrast of the coating was sufficiently different from the underlying sample surface to reveal a homogenous mask of the surfaces and their features, with the exception of TT. Profilometry Ra revealed no differences between coated and uncoated samples, thus the large-scale sample topography remained unchanged. SEM also demonstrated that at the smaller scale, the evaporating process generally did not introduce any new roughness. It is apparent that the evaporating methods have successfully reproduced two different sets of standard topographies with homogenous surface chemistries. This enabled cellular reactions to the topography to be concluded minimising the involvement of the chemistry.

Cell Reactivity to the Coated Metals

The coating of Th, SS and TS with either gold or titanium elicited identical reactions to their uncoated counterparts both qualitatively and quantitatively. Cells on coated Th, SS and TS were well spread, their intracellular structure was unaffected with mature focal adhesion sites, actin cytoskeleton, microtubule structure and cell growth to confluency at later timepoints observed on all surfaces. Cell behaviour on Th, SS and TS indicated that the surface chemistry on these materials did not play a role in cell reactions.

Cell behaviour on NS concurred with that observed on the other coated materials, in that there were no significant variations in cell growth that were dependent on the surface coating. It was interesting to note that quantified cell areas differed slightly on the surfaces, however, this did not have any downstream effect on cell behaviour. A possible reason for this slight cell area increase for both coated surfaces might be that the coating deposition may have 'smoothed' out the sharper topographical changes. This could be tested using the Atomic Force Microscope. Generally cells at all timepoints demonstrated an unspread or elongated morphology, the cell filopodia attached and probed the coated surface and the particles, and both the focal adhesion sites and the microtubule network were again

disrupted by the presence of the particles. For NS, the standardised surface chemistry in two separate instances demonstrated that its unique surface topography was the primary cause of the low cell growth observed.

The atomic number contrast of the gold-coated NS (NG) surface yielded an additional observation helping to clarify the cause of particle removal on NS. In Chapter 3, this particle removal was hypothesised to be due to cell removal and endocytosis of loosened particles, however, as demonstrated in Chapter 4 this could not be confirmed. Examining higher magnification images of cells cultured on NG, holes in the coating could be observed surface-wide, and these holes were of similar dimensions to the β -phase particles. This surface-wide removal of particles could not be due only to cell interaction as previously suspected, it was more plausible that the immersion in culture media or cell fixation protocol could cause the loosened particle removal. The observation of the particles in cells cultured in the presence of NS, observed in Chapter 4, would correspond to their removal during the culture period. If the removal occurs at this point, this reinforces the observation that NS topography was the primary factor for cell behaviour as no reactivity to the exposed underlying surface chemistry was observed, but rather filopodia probed the coated particles. This phenomenon could not be seen on NT due to similarity that the coatings' atomic number contrast to that of the underlying surface. While the endocytosis of particles was ruled out as a contributory factor in suppressing cell growth on NS, it would be interesting to compare cell reactivity on pre-washed NS in comparison to normal NS to see if immersion in culture media alone would remove loosened particles, and what effect that might have on cells behaviour.

Topography vs. Chemistry

Cells on all the materials, with the exception of TT, demonstrated an interesting contradiction in that if a cell reacted identically to the surface coating as it did to the original surface, then why was cell alignment and sensitivity observed in relation to the border between the masked and original surface? One possible reason was that the cells were able to differentiate and sense the approximate 50nm step produced by the coating thickness and align to this. This might be plausible for the smoother samples such

Thermanox and SS as cells have been shown to be sensitive to features of 50nm down to 10nm (Dalby *et al.*, 2004b; Wojciak-Stothart *et al.*, 1996; Wood *et al.*, 2002), and are found aligning to increments of 70-30nm (Feixeira *et al.*, 2003; Zhu *et al.*, 2004). However, features of these dimensions would be lost on rougher surfaces such as TS and NS as cells would have a wealth of topographical cues of much larger and more imposing dimensions with which to align (Brunette, 1986; Brunette, 2001). This is supported by a lack of cells aligning on TT (titanium evaporated TS). Theoretically TT has the same surface chemistry on both its coated and uncoated areas with only a topographical border, and cells could not be seen aligning anywhere on this surface. All other sample/mask combinations contained primarily different elements from the underlying substrate and cells could be seen aligning to these borders in all instances at early timepoints. From this we can conclude that the heterogeneity of the surface coating chemistry from the underlying surface is a possible reason for the cells' reactivity.

Limited studies were found in the literature examining a possible hierarchy of surface chemistry over surface topography. Utilising a grooved microtopography with orthogonally superimposed adhesive strips; Britland noted that a majority of cells aligned preferentially to chemically patterned adhesive tracks with fibroblasts (Britland *et al.*, 1996a) and to some extent with nerve cells (Britland *et al.*, 1996b), although this decreased with increasing groove depth. Tan (2002) concluded that strong chemical properties were more compelling for neutrophils than surface microgeometry. This would be in keeping with observations of cell reactivity to coated TS and NS. The mechanism of this cell response is speculated to be associated with changes in surface protein absorption termed the 'shining through' phenomenon (von Recum and van Kooten, 1995). This refers to underlying changes in surface free energy and surface charge, reflected in its protein absorption (Davies, 1988; von Recum and van Kooten, 1995). Surface free energy determines the hydrophobicity of the surface (Schakenraad *et al.*, 1989; Schakenraad *et al.*, 1986) while surface charge can attract or repel protein and cells (Davies, 1988; Shelton and Davies, 2001). Changes in protein absorption have been demonstrated for homogenous metal oxides layers; protein adsorption onto aluminium differed from that of titanium, niobium and vanadium due to aluminium's positive charge at a physiological pH (pH 7.3) (Scotchford *et al.*, 2003; Voros

et al., 2001). However, these cell interactions are only seen at earlier timepoints of 24hr (SEM) and 48hr (fluorescence). Scotchford noted that the majority of oxide based differential adhesion had diminished during the first 90 mins post-seeding (Scotchford *et al.*, 2003). An account for this is the 'Vroman effect' of a turnover of adsorbed proteins diminishing any initial differential protein absorption, especially when the majority of the materials are deemed cytocompatible (von Recum and van Kooten, 1995; Vroman and Adam, 1986). The downstream effects of this, with the exception of NS, were that cells still produced a confluent monolayer and disregarded the material border at later timepoints. It also seems unlikely that the influence of the border has anything to do with cell reactions to the whole surface.

Numerous cellular and intracellular reactions were observed in relation to the masking border, however none could be conclusively attributed to be exclusively surface chemistry or topography. Filopodia, found exploring near the topography boundary, have been observed in fibroblasts sensing topographical features down to a height of 10nm (Dalby *et al.*, 2004b) and also surface chemistry in a neuronal growth cone (Koleske, 2003). Cell alignment has been observed to features within the region of 100nm in height (Clark *et al.*, 1991; Wojciak-Stothart *et al.*, 1996) but has also been observed aligning to chemically adhesive surface strips (Britland *et al.*, 1996a; Britland *et al.*, 1996b). For the alignment of focal adhesion (FA) sites, it has been demonstrated that FA are sensitive to topography features of 160nm high nano columns (Dalby *et al.*, 2004a) and align to feature sizes down to 44nm (Wojciak-Stothart *et al.*, 1996). However, focal adhesions have also been demonstrated to be sensitive to chemistry (Britland *et al.*, 1996a; Britland *et al.*, 1996b; Ireland *et al.*, 1989; O'Neill *et al.*, 1990). The microtubule gap observed aligning to the border on NG (gold coated NS) was more indicative of the mechanics of cell spreading as observed by Britland and Wojciak-Stothard, with the actin condensing prior to the involvement of the microtubules (Britland *et al.*, 1996a; Wojciak-Stothart *et al.*, 1995). It must also be noted that the NG surface impaired the production of the microtubule network therefore this might contribute to the observed effect.

Conclusion

To extend this study, it is obvious that the timepoints need to be reduced to the first 24 to 48hr of cell interaction. The timescale employed in this instance was due to the primary requirement of the experiments, which was to compare with previous investigations into the original uncoated materials. Also at these early timepoints it would be useful to examine protein adsorption; as mentioned previously, fibronectin absorption has been reported to vary on different metal oxides (Brunette *et al.*, 2001; Scotchford *et al.*, 2003). A similar study in this instance might clarify the conflict of topography and chemistry at the masking border.

The process of photolithography to produce patterns of different chemical topography areas provides interesting possibilities and could be utilised on metals to produce different surface chemistry patches on an array of industrially produced metal substrates (Winkelmann *et al.*, 2003). It is also interesting that while chemistry versus topography has been the subject of study, the hierarchal effect of micro and nanotopographies has not been investigated in depth (Wieland *et al.*, 2005). Britland noted that the adhesive stripes utilised in their studies possessed a nanotopography, however, the topography's fabrication was incidental and could not be proven to contribute to the results observed in a study using baby hamster kidney cells (Britland *et al.*, 1996a), and were dismissed in another study using neurites (Britland *et al.*, 1996b). Tan attempted to mimic bone matrix by depositing hydroxyapatite onto microgrooves, however cells reacted synergistically to both the nano- and micro topographical cues (Tan and Saltzman, 2004). Brunette noted some hierarchy as cells only aligned to smaller grooves in the absence of larger grooves, though all the features were at the micrometer scale (Brunette, 1986). The author believes that with the today's modern standards of fabrication (Wilkinson, 2004), micron dimension features possessing varying organised nanopatterns could be produced to assist in further understanding cell reactivity to topography, and could possibly have implications in tissue engineering constructs.

A cell/material paradox has been touched upon here; the study has demonstrated that the cause of the observed cellular reactivity to the standard materials was the surface

topography, however in the process of investigating this we have demonstrated cellular sensitivity primarily caused by surface chemistry changes on these same materials.

Chapter 7 – Surface Topography

Abstract

It was hypothesised that the microspikes found on the NS topography identified in Chapter 2, 3 and 6, were the underlying cause for the poor cell growth and survival on these surfaces. To test this hypothesis, the dimensions and spatial frequency of the microspikes were created based on an artificial, representative microtopography. Cell behaviour on this microtopography compared with that found on NS. This suggests that the microspike surface feature of NS, represented in the form of a fabricated topography, contributed significantly if not completely to the observed cell growth suppression.

Chapter 7 – Surface Topography

Introduction

The study of metallic topographies is split into two main categories; metals with standard or modified surfaces, and metal-coated topographies fabricated from non-metallic materials. The use of unmodified and modified metal substrates provides a realistic representation of an implant material, as generally the methods utilised are similar to those employed for industrial processes for mass production of implants (Brunette *et al.*, 2001; Meredith *et al.*, 2005). Essentially, these modifications produce either smooth surfaces or surfaces with varying degrees of roughness. More recent methods such as glow discharge plasma treatment (Aronsson *et al.*, 1997) add to the established industrial methods for roughening such as etching, ceramic tumbling, sand and ball blasting, however, all methods result in random surface discontinuities of varying dimensions. There are novel exceptions to this rule: laser patterning and photolithography combined with wet etching have recently been utilised to produce novel topographies such as pits and grooves directly in titanium (Brunette *et al.*, 2001; Hallgren *et al.*, 2001; Kasemo and Gold, 1999; Madore and Landolt, 1997), although designed patterns of organised features are generally confined to conventional microfabrication techniques. Utilising methods developed in the electronics industry, novel features can be designed, fabricated and finally coated with a metal to mimic a metallic topography. The features are generally biomimetic structures inspired, for example, by the nanoscale shape of the basement or descelements-membrane (Flemming *et al.*, 1999; Teixeira *et al.*, 2003), extracellular matrix (Clark *et al.*, 1991), or connective tissue collagen networks (Tan *et al.*, 2000). These topographies are used for research purposes and are advantageous in elucidating cellular response towards specific features rather than the hierarchy of various topographies usually associated with metal surfaces modified using the industrial methods.

In Chapter 6, surface topography, and not surface or bulk chemistry, emerged as the most probable cause for the cell reactions observed on NS. Based on these observations I developed the hypothesis that specifically the microspiked surface topography of the NS β -phase particles could be the agent causing low cell adhesion, survival, and proliferation on

NS. In this chapter, I will test this hypothesis by designing a surface mimicking the NS surface topography. This mimicry surface consists of evenly spaced micrometric pyramids, whose form, dimensions, and spacing were inspired by the NS topography. The design and fabrication of the master die used to produce the topography is included within the 'Materials & Methods' section. To my knowledge, this is the first time a metallic topography existing on implant surfaces has been used as an inspiration for the design of a fabricated surface. Due to the limitations of the fabrication process available a polymeric replica substrate was used, which was either gold or titanium coated in order to not only investigate the effects of the topography but also surface chemistry.

Materials and Methods

Experiment 17 – AFM Cross-sectioning

The AFM data file was analysed using the Nanoscope software noted in Chapter 2: Experiment 2.

Experiment 18 - Fabricated Topography

A pyramid design was chosen as a compromise of required design features and fabrication limitations. As the final surface was a protruding pyramid design, the initial fabricated die was an inverted version of this design.

Microstructure Master Die Fabrication

The inverted pyramid design utilised to emboss polycaprolactone (PCL) was produced using a series of fabrication methods. In brief, a mask was written using electron beam (e-beam) lithography. Photolithography was then utilised to produce a master die by transferring the pattern from the mask into a silicon substrate. A series of etching techniques were subsequently employed to produce the inverted pyramid design on the master die.

Electron-Beam Lithography

The initial e-beam lithography writing step was used to produce a stencil of a pattern known as the primary lithographic master, often referred to as a mask. In the e-beam writer a focused beam of electrons is directed onto a sensitive polymer substrate to write a pre-programmed design. In this instance the pattern was a series of circles 5 μm in diameter and spaced regularly with 10 μm pitch in x and y – this forms the ‘feature map’ indicating where the inverted pyramids will be formed on the die substrate at a later stage. The substrate used for writing was a quartz wafer (Hoya, Japan) evaporated with chromium followed by a spun on layer of beam-resist. The pattern was written in the resist by the electron beam, sectioning the polymer and resulting in an alteration in its solubility. This sectioned polymer resist is removed using a developer and results in the transfer of the design imprint or latent image (Fig 7.1a,b). The chromium layer, used to make the quartz opaque and thus block light used during subsequent photolithography steps, relative to the original pattern,

was then wet etched removing the chromium exposed by the resist and the remaining undeveloped resist (Fig 7.1c). It is through these exposed areas that the light can pass to transfer the pattern to the master die being fabricated utilising photolithography.

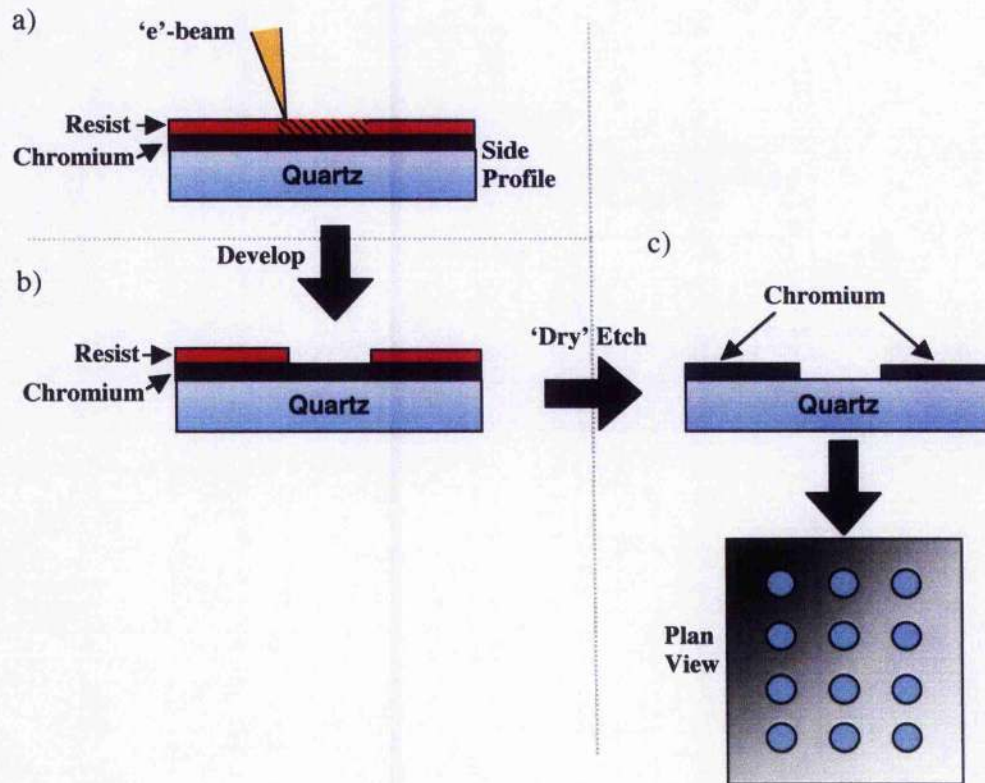


Fig 7.1 – Production of the mask. (a) The e-beam writer exposes the resist, writing the programmed pattern. The exposed resist is then removed during development. (b) The developed resist exposes the underlying chromium layer. (c) By 'wet' etching the surface, the untreated resist and exposed chromium are etched. In the plan view, this results in an opaque surface with transparent holes where the chromium is etched away.

Photolithography

The mask was now used to produce a set of master dies, consequently used to emboss the polymer. The master die was fabricated as follows: a silicon wafer (100) was evaporated with 260nm of silicon nitride (Si_3N_4) followed by a coating of ultraviolet (UV) sensitive resist (S1818 photoresist, Shipley Chemicals, UK). By exposing the resist-coated master die with UV light through the mask, the pattern was transferred into the substrate surface (Fig 7.2a). The exposed resist was developed with an alkaline developer, producing a duplicate of the mask pattern and uncovering the underlying Si_3N_4 (Fig 7.2b).

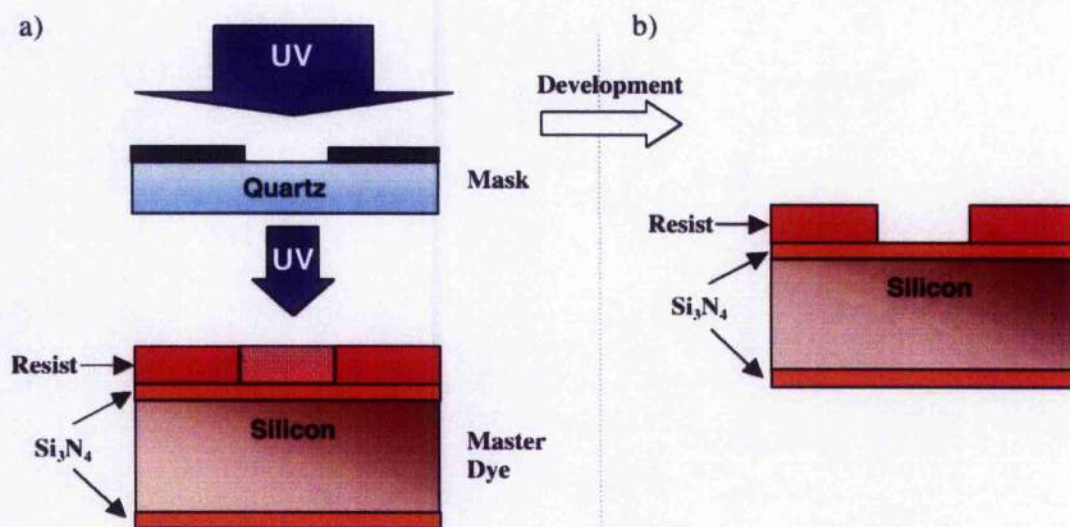


Fig 7.2 – Pattern writing on the master die. (a) UV light is illuminated through the mask projecting the pattern onto the master die surface. The UV sensitive resist coating on the master die surface was exposed, duplicating the pattern. (b) Upon development the exposed resist was removed uncovering the underlying Si_3N_4 .

Dry and Wet Etching

The patterned resist does not produce the significant surface features required, in this instance the inverted pyramid microtopography - it serves more as a guide for subsequent etching processes. Dry etching was used to remove the exposed Si_3N_4 , uncovering the underlying silicon wafer surface (Fig 7.3a). The sample was then wet etched with potassium hydroxide (KOH) (25% for 1 hour at 80°C) to degrade the exposed material (Fig 7.3b), etching the silicon along the 111-crystallographic plane. This step changes the round resist pattern into self-aligned inverted pyramids. By undercutting the unexposed resist, which remains supported by the non-etched Si_3N_4 , the inverted pyramid topography is produced. Samples were subsequently wet etched in hydrofluoric acid (HF) (40% in H_2O (1:5)) to remove the Si_3N_4 coating (Fig 7.3c). The samples with the inverted pyramid microstructure were finally cleaned with Piranha (concentrated sulphuric acid 3:1 hydrogen peroxide) to remove any contaminants (Fig 7.4).

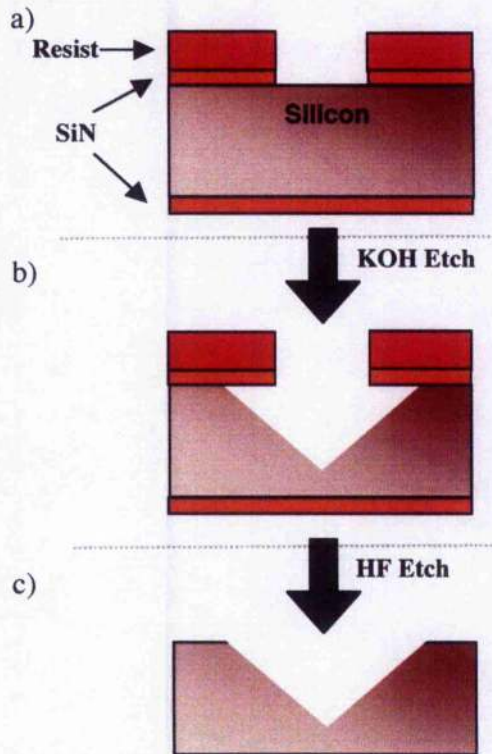


Fig 7.3 – The etching steps required for fabricating the master die. (a) The sample is dry etched to remove the exposed Si_3N_4 . (b) The sample is then wet etched using potassium hydroxide (KOH) to produce the inverted pyramid topography. This etching also undercuts the unexposed resin and Si_3N_4 . (c) Hydrofluoric Acid (HF) is then used to wet etch the resist and Si_3N_4 .

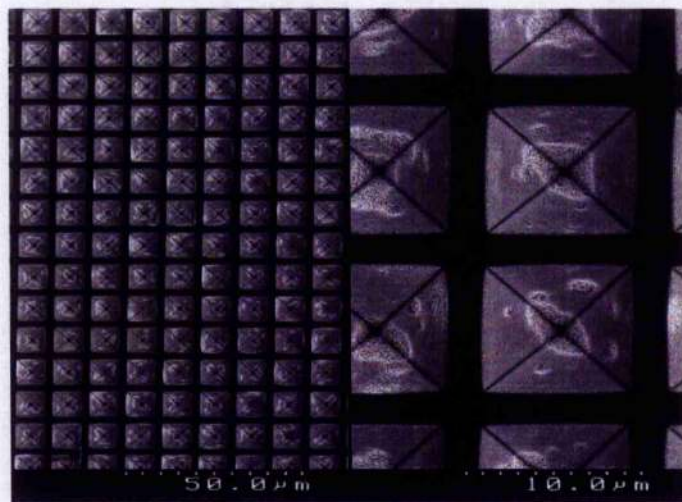


Fig 7.4 – SEM micrograph (SE) of the inverted pyramid master die etched into silicon.

Embossing into Polycaprolactone

The pyramid microtopography was replicated by embossing in Polycaprolactone (PCL) as follows.

Clean powder free latex gloves were used at all times, and all handling of the silicon die and of PCL was done using Teflon coated tweezers. The hotplate was wiped clean of any debris prior to use as this could have damaged the silicon wafer.

- The silicon die was placed in the centre of a preheated hotplate set to 80–85°C and left for 1 minute.
- Once the silicon wafer had reached the desired temperature a 1cm² sheet of PCL was placed on the die, directly over the area of etched microtopography. The sheet melted almost immediately, indicated by a change from a translucent to a transparent material.
- A clean microscope slide was placed on top of the molten PCL and, using one thumb, pressed down, with firm pressure maintained for 30 seconds. Both the silicon die and glass slide firmly adhered to the PCL.
- The silicon die/PCL/glass slides were then immersed in ddH₂O and left to cool for 5 minutes. The PCL solidified indicated by a change from clear to translucent polymer.
- After 5 minutes the glass slide had separated from the polymer to reveal the PCL adhered to the silicon die. Using tweezers the silicon die/PCL sandwich was removed from the ddH₂O and dried with a filtered nitrogen gun. Once dry, the PCL was separated from the silicon die using a combination of gentle pulling and the nitrogen air stream. The PCL was completely dried with the nitrogen air stream and placed in a Petri dish for storage. The silicon die was also dried and reused or stored.

Embossing Control Surface

In order to create a flat PCL for controls, the silicon die was substituted by a microscope slide and the PCL sheet embossed as described above.

Sample Coating

Both the pyramid topography PCL and the planar control PCL were evaporated with either 50nm gold or titanium using the same method described in Chapter 6: Experiment 14.

Scanning Electron Microscopy

Samples were assessed using the same operating conditions optimised in Chapter 2: Experiment 3 utilising both SE and BSE imaging.

White Light Profilometry

Samples were assessed with an analysis area of 200 μ m x 200 μ m and 1mm x 1mm.

Atomic Force Microscopy

An exemplary PCL pyramid replicate was scanned with the AFM, as described in Chapter 2: Experiment 2.

Experiment 19 - Cell Growth and Morphology

Cells were seeded and fixed following the protocol described in Chapter 3: Experiment 5.

Experiment 20 – Cell Counts

Quantitative cell counts were conducted following the protocol included in Chapter 6: Experiment 16.

Experiment 21 - Vinculin, Tubulin and Actin Immunostaining

Cells were seeded and cultured for 48hr and processed as noted in Chapter 3: Experiment 7. Focal adhesion sites were measured also following the protocol listed in that section.

Results

Experiment 17- AFM Cross-sectioning

Data files from AFM measurements of NS (Chapter 2: Experiment 2) were further analysed using cross sectional analysis. Cross sectional analysis revealed that the peaks typical of NS surface topography all had a strikingly similar shape, height and slope (Fig 7.5a,b). The data presented in Fig 7.5 is representative of such measurements. The analysis software allowed these dimensions to be measured and revealed that the peaks had uniform heights and a uniform gradient from peak to trough (Fig 7.5c).

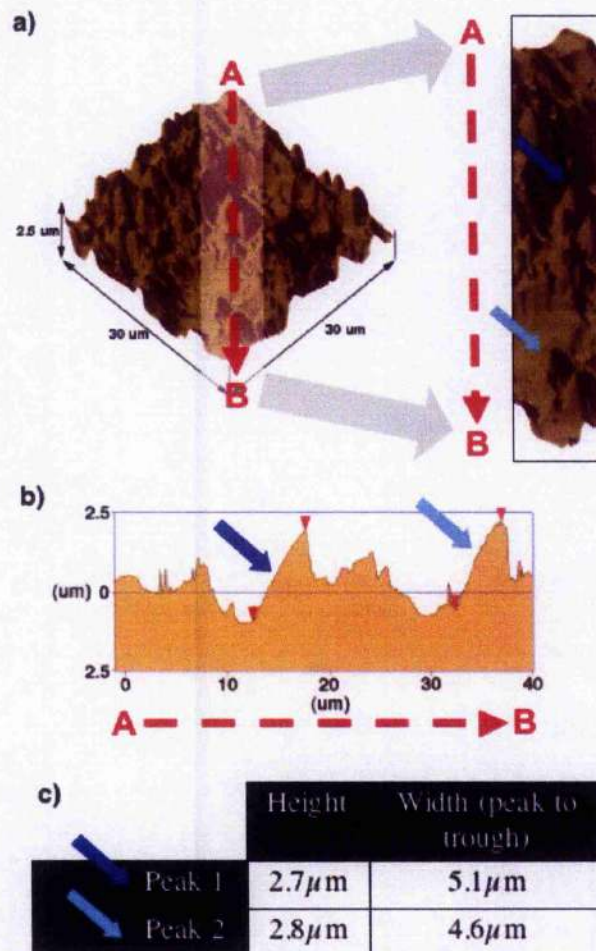


Fig 7.5 – (a) NS AFM data was further analysed using cross sectional analysis. (a & b) A cross section demonstrated that the prominent surface feature, the microspikes, have similar shape and dimension. (c) The microspikes dimensions were measured and found to have similar heights and a similar gradient from peak to trough.

Experiment 18 - Fabricated Topography

I developed the hypothesis that the topography of the microspikes identified in Experiment 17 was one of the causes for the observed cellular reaction towards NS. To explore this hypothesis, a pyramid microtopography based on these dimensions was first designed then fabricated. PCL was used to mass-produce numerous faithful copies of the pyramid design. As the previous experiments using metal coatings to mask the surface chemistry had demonstrated, the cell effect was due to topography, thus it was important that these coatings were also employed on the polymer pyramid microtopography. The following experiments seek to validate the embossing procedure and to demonstrate that PCL could be coated with a metal without any major impairment of topography.

Pyr – Pyramid topography embossed into PCL

The embossing of PCL with the pyramid microtopography proved successful with each type and size of pyramid reproduced. At a higher magnification the pyramids were not smooth but slightly rippled, this is possibly due to the spheruloids of the polymer, or alternatively due to uneven pressure during embossing or the PCL adhering to the die upon removal (Fig 7.6).

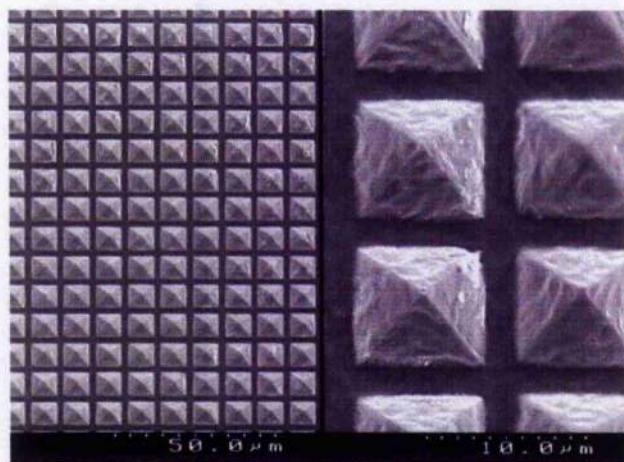


Fig 7.6 – PCL embossing of the pyramid microtopography proved successful with each pyramid reproduced. At a higher magnification the pyramids are not smooth but slightly rippled.

In a comparison with the NS topography, the dimensions specified were not quite accurate, as the particles seemed considerably smaller (Fig 7.7a,b). However, the AFM did not differentiate between the particles and the base material, therefore it can be assumed that

the particles are protruding from a crest in the material which would make them considerably larger in comparison to their appearance with SEM. AFM analysis of the pyramids' demonstrated that the emulated microspiked topography did mimic that of NS, however, the spacing made the features less frequent and it must be noted that the z-axis scales were different (Fig 7.7c,d). The pyramid's gradient, and thus their spacing, was governed by the etching gradient possible in the fabrication of the initial silicon die.

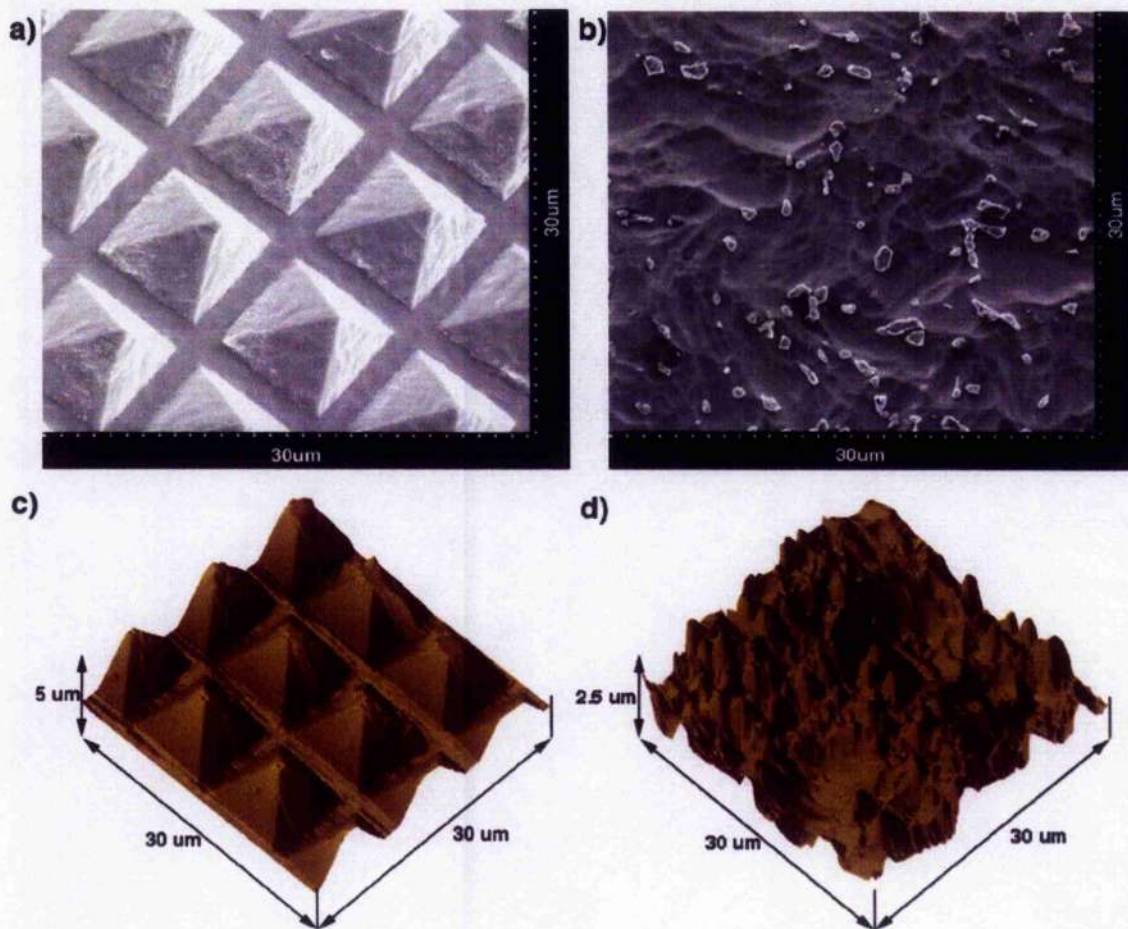


Fig 7.7 – Dimensions of (a) the pyramids embossed into PCL and (b) NS. The pyramids dimensions are not quite of the same dimensions as the NS particles which seem considerably smaller. The AFM does not differentiate between the particles and the base material, however generally the particles are protruding from a crest in the material, which would make them considerably larger than their appearance here. (c&d) AFM of the pyramid surfaces demonstrates that while the feature spacing is different, microspikes have been produced that mimic the surface of NS (d).

Profilometry demonstrated some interesting features of the pyramid microtopography. At a large area scan, the surface looked similar to the standard metals (Fig 7.8a). The more punctuated design of the microtopography became apparent at a smaller scan range (Fig

7.8b). It is also possible to see that the features are not entirely uniform with some pyramids missing. The Ra original measurement for the microtopography was $1.22 \pm 0.008\mu\text{m}$, considerably rougher than the surface it was intended to imitate.

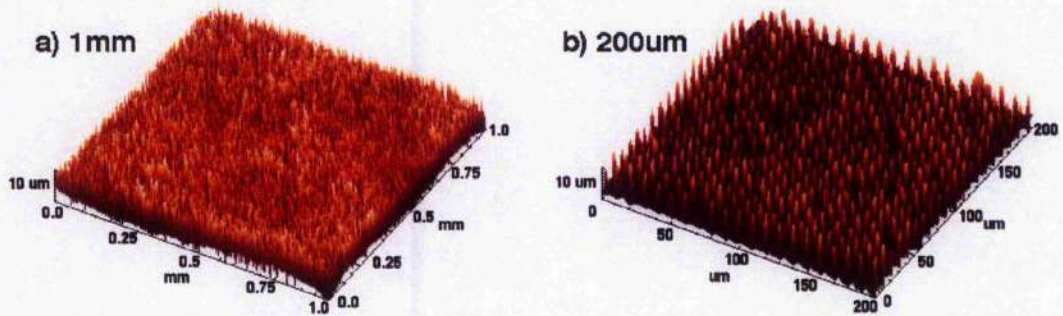


Fig 7.8 - Examples of three-dimensional reconstruction of the microtopography as captured by profilometry at (a) 1mm x 1mm - the surface looks similar to the standard metals. (b) 200 μm x 200 μm - the punctuated design of the microtopography becomes apparent and it is possible to see that the features are not entirely uniform with some pyramids missing.

Plan - Planar PCL topography

A PCL planar control topography was fabricated as, for experimental purposes, the effect of PCL chemistry on the cellular reaction to the pyramids ought to also be investigated. The topography was generally smooth, however, at a higher magnification the rippled topography present indicated that this was perhaps an inherent property of PCL observed also in the pyramid microtopography (Fig 7.9).

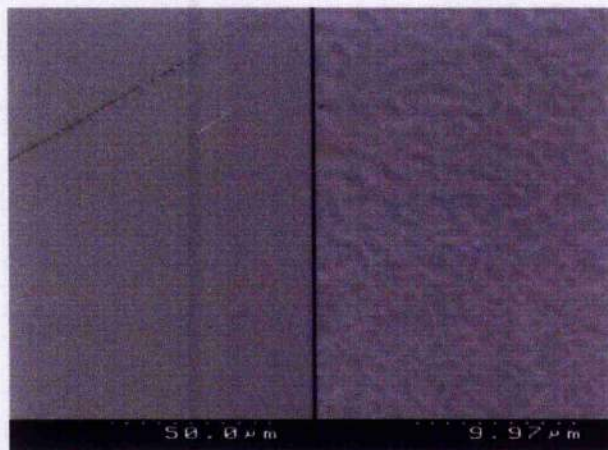


Fig 7.9 - The planar control of PCL was a flat surface, which if viewed at a higher magnification becomes slightly rippled.

AuPyr and AuPlan - Gold Coated PCL in Pyramid and Planar Topographies

The gold coating of the pyramids did not destroy the microtopography nor did it modify it significantly. The small surface deformities on the pyramids appeared to be most likely related to difficulties in their removal from the die (Fig 7.10a). Excessive cracking of the surface gold coating was in fact islets of gold, an artefact from the sputtering method. These cracks could inadvertently expose the cultured cells to a mix of gold and PCL surface chemistry, however, BSE of the surface demonstrated that while cracked, the underlying material was not accessible to the cells (Fig 7.10b). The gold coating on the planar surface also showed a similarly cracked surface (Fig 7.10c).

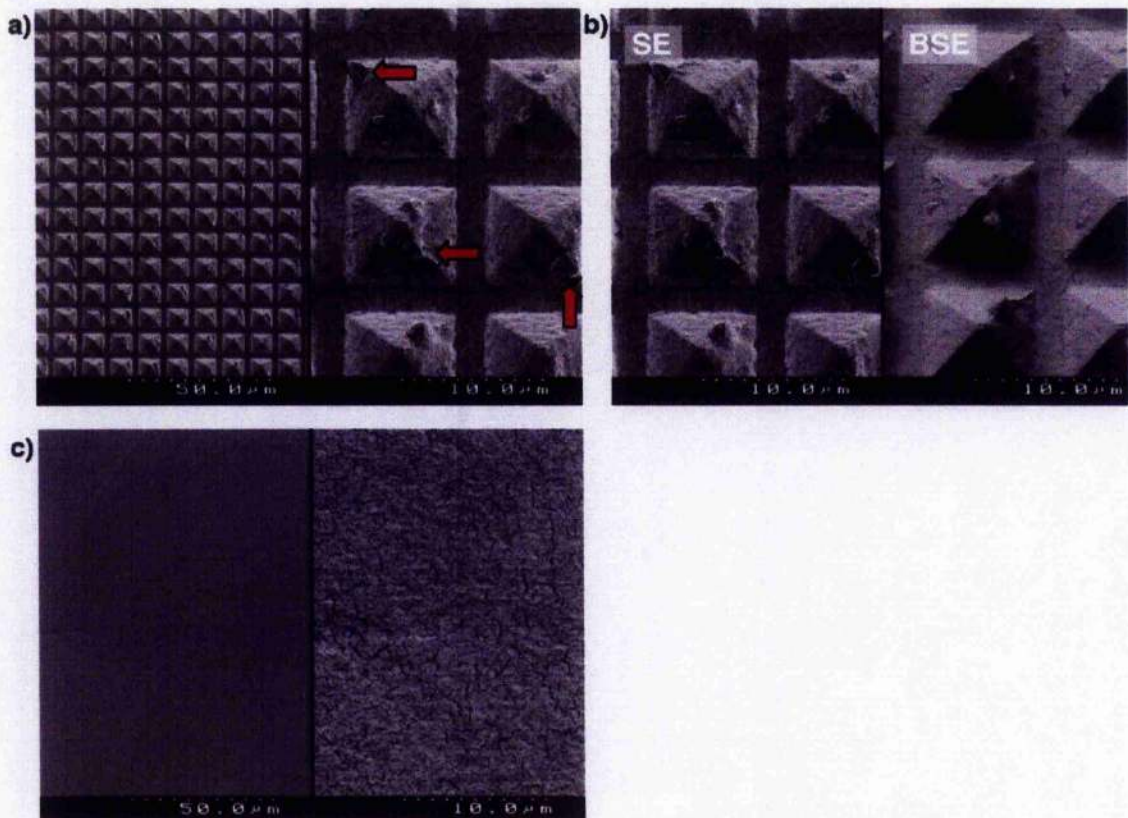


Fig 7.10 – (a) The gold coating did not modify the microtopography, as the small surface deformities on the pyramids (indicated by the red arrows) appeared to be most likely related to difficulties in their removal from the die. Excessive cracking of the surface gold coating was in fact islets of gold, an artefact from the sputtering method (b), BSE on the surface demonstrates that while the surface was excessively cracked, the surface does not demonstrate the presence of the underlying material (c) The planar surface also demonstrated this cracking.

TiPyr and TiPlan - Titanium Coated PCL in Pyramid and Planar Topographies

Coating the PCL surface with titanium did not modify the topography, and the coating on the pyramids was much more homogenous than gold with only minimal cracking (Fig 7.11a). Similarly, the coating of the planar PCL was also homogenous, however, there was considerably more cracking on the surface (Fig 7.11b). The cracking is thought to occur immediately after the metal evaporation, as the process produces considerable heat that could dissipate at different rates from the underlying polymer and the metal coating.

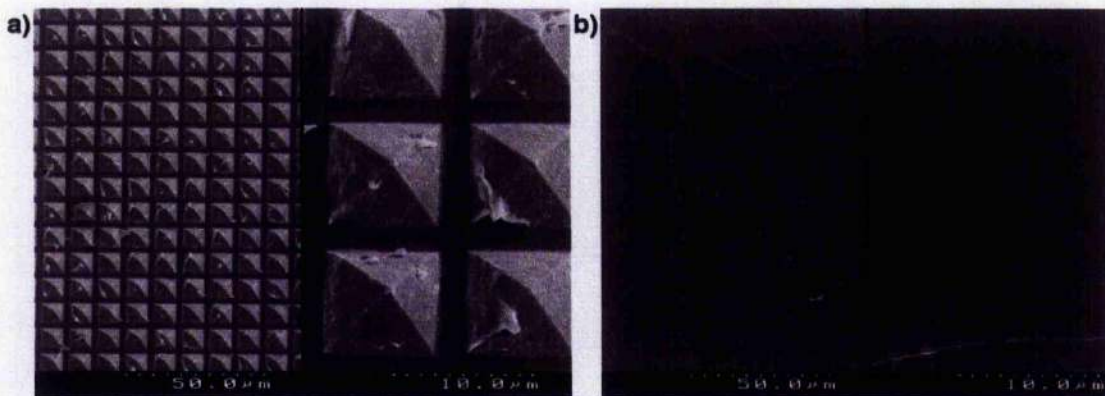


Fig 7.11 – (a) The titanium coating did not modify the topography and was homogenous with minimal cracking. (b) The planar topography coating was also homogenous but with increased cracking.

Experiment 19, 20, 21 - Cell Growth, Morphology and Adhesion

The results have been organised into 'Cell Growth' and 'Cell Morphology and Adhesion', with the relevant results documented within each section.

Cell Growth

Qualitative cell growth and morphology studies (similar to Chapter 3: Experiment 5 and Chapter 6: Experiment 15), and quantitative cell counts (similar to Chapter 6: Experiment 16), were conducted on uncoated, titanium coated PCL microtopography and planar topography. Culturing difficulties, expanded upon in Experiment 21, on both gold coated planar and pyramid microtopography necessitated their omission from the study. Regarding growth and morphology, there were no notable variations between the uncoated PCL and titanium coated surfaces, therefore, in the interest of saving space only images of the titanium coated surfaces are included, while SEM images of cells on the uncoated topographies are included on the accompanying CD-ROM.

Qualitative Cell Growth on Pyr and TiPyr- PCL Pyramid Topography and Titanium Coated Pyramid Topography

At 24 hr the cells displayed unspread or elongated bipolar morphologies. The bipolar cells were arranged at 45° increments of horizontal, diagonal or vertical orientation. By the proximity of numerous pairs of unspread cells it was possible to speculate that these were cells exiting the mitotic cell cycle phase (Fig 7.12a). By day 5, the cell number had increased, as had the number of cells adopting the bipolar morphology (Fig 7.12b). At day 10 the cell numbers remain unchanged from day 5, while cells of a tri-polar morphology could be observed along with the bipolar and rounded morphologies (Fig 7.12c).

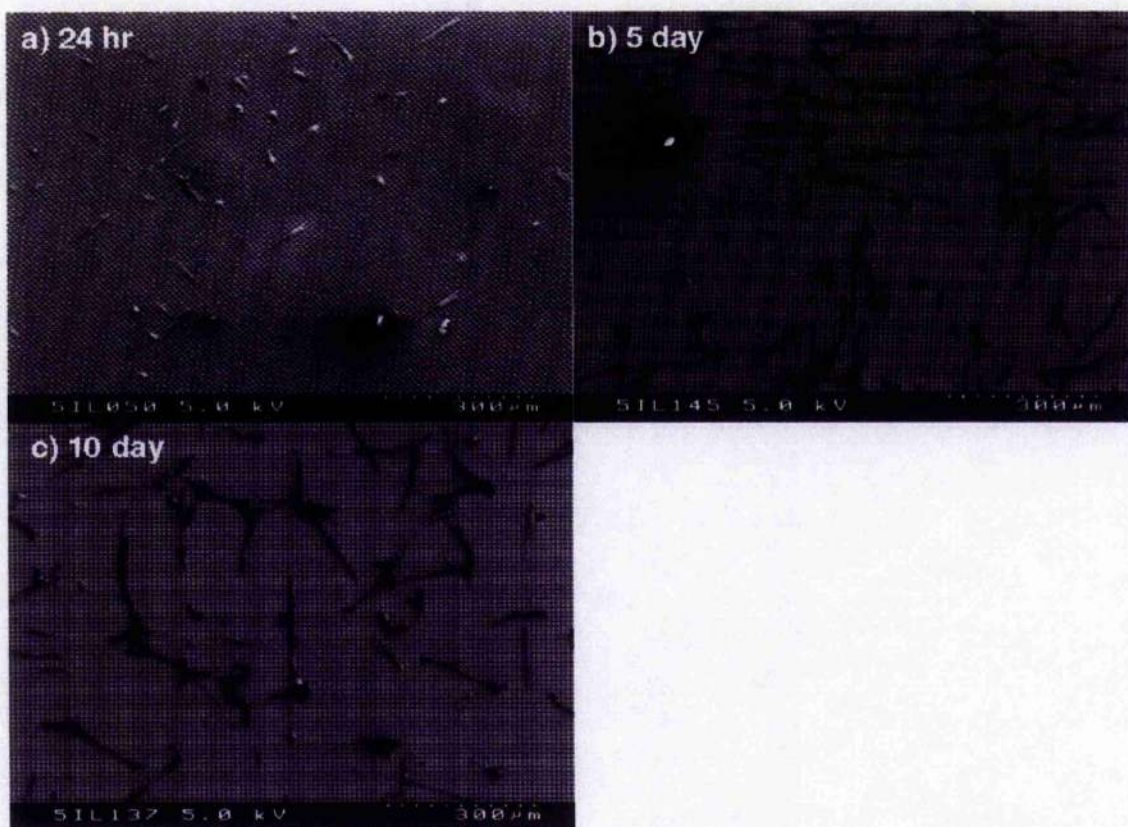


Fig 7.12 – Cells cultured on TiPyr for (a) 24hr, cells were unspread with a bipolar or rounded morphology. The bipolar cells were arranged at 45° increments of horizontal, diagonal or vertical orientation with respect to the two symmetry axis of the pattern. (b) 5 days, the cell number had increased, as had the number of cells adopting the bipolar morphology. (c) At day 10 the cell numbers remained unchanged from day 5, while cells of a tri-polar morphology could be observed along with the bipolar and rounded morphologies.

The area patterned with microtopography was smaller than the size of the PCL samples thus a planar edge was present on the microtopography samples. Examining this border at 24hr the cells were in relatively equal numbers on the topography and on the planar sample edge. On the planar part of the sample more cells demonstrated a “typical” spread morphology, also seen on the other planar surfaces, rather than the rounded or bipolar morphology found on the topography (Fig 7.13a). At 5 days the number of cells had increased on both the planar and microtopography surface although the spread cells on the planar surface covered a larger area (Fig 7.13b). By 10 days cells were confluent on the planar side of the surface while on the microtopography side cell numbers were considerably lower (Fig 7.13c).

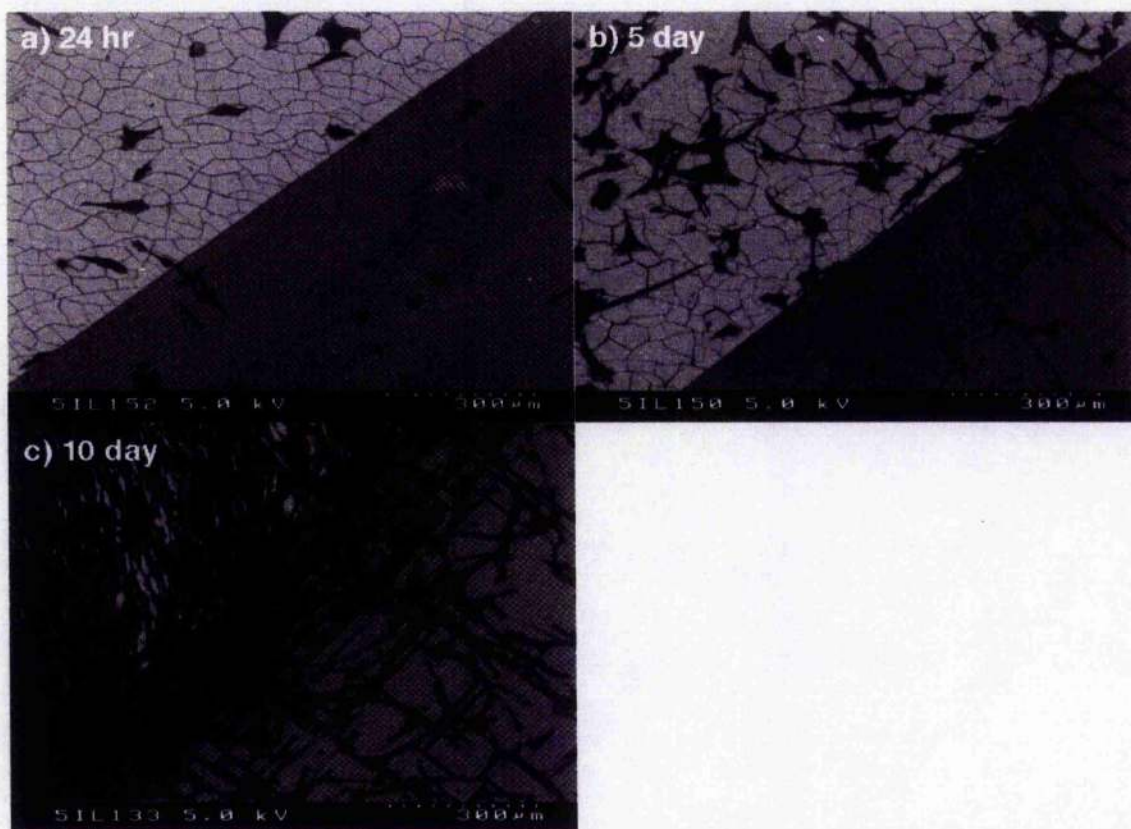


Fig 7.13 – Cells cultured on TiPyr for (a) 24hr, cell numbers were similar on the planar and microtopography surface areas, however, cells were more spread on the planar surface while the cells adopted the characteristic rounded or bipolar morphology on the microtopography. The cracking of the metallic coating was also visible in the planar region (b) 5 days, cell numbers had increased on both the planar and microtopography areas although the spread cells on the planar side covered more of the surface. (c) 10 days, cells were confluent on the planar side of the surface while the cell numbers were considerably lower on the microtopography.

Plan and TiPlan – Uncoated and Titanium Coated Planar PCL Topography

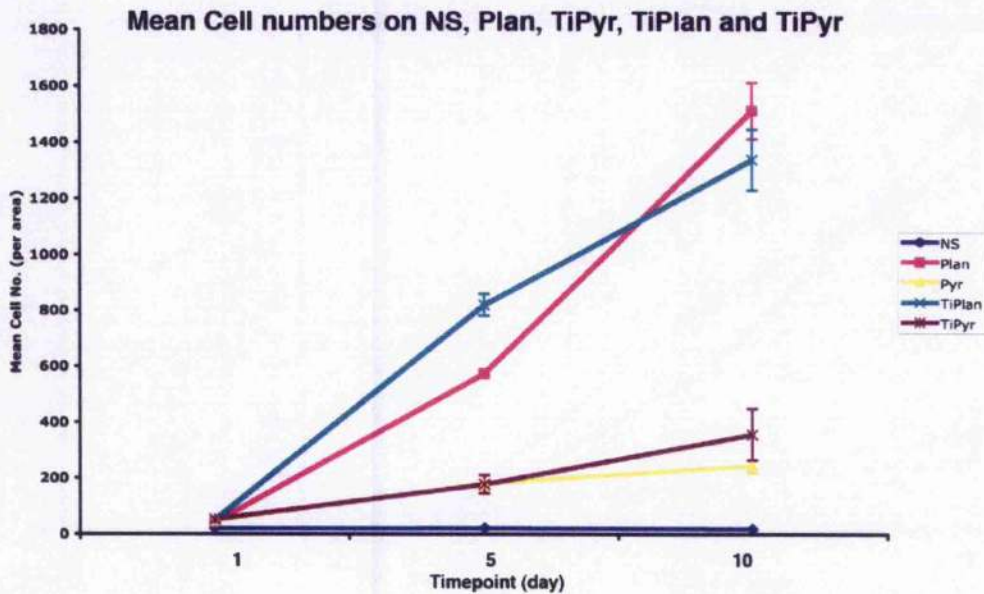
At 24hr cells were well spread and scattered about both surface types (Fig 7.14a). At day 5 neither the number nor the spreading appeared to have increased (Fig 7.14b), and by day 10 there was considerable change as the cells produced a confluent monolayer on the surface (Fig 7.14c) (Plan images on CD-ROM).



Fig 7.14 – Cells cultured on TiPlan for (a) 24hr, there was a scattering of cells and they appeared to be well spread. (b) 5 days, cell number not increased. (c) 10 days, cell numbers had increased considerably and formed a confluent monolayer on the surface.

Quantitative Cell Growth – Cell Counts on both Planar, Pyramids and NS

To confirm the SEM observations, quantitative cell counts were performed at the three timepoints on all sample types, Pyr, Plan, TiPyr and TiPlan. As this topography was designed to mimic the microspike features present on NS, this sample type was also included in the growth experiment for comparison.



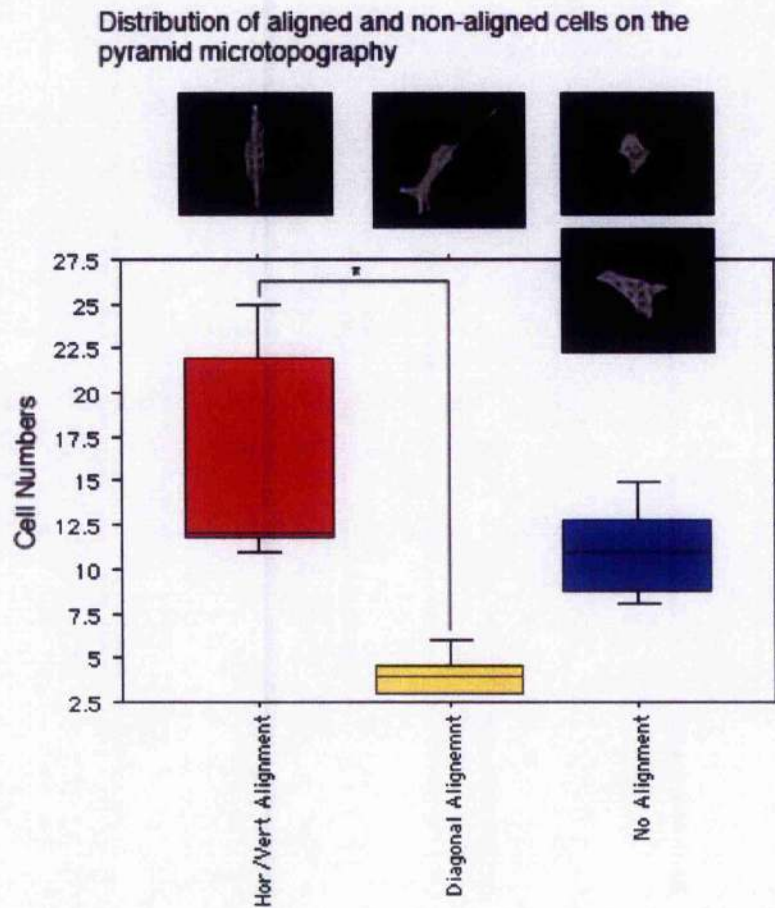
Graph 7.1 – A plot of the means of cell numbers quantified on the samples at the three timepoints. Both planar sample types follow a similar trend of increasing cell numbers. Both pyramid sample types allow for some cell growth although the numbers are severely reduced. NS again inhibited cell growth on the surface.

The means of the cell numbers quantified on the samples at the three timepoints were plotted in Graph 7.1. Cell counts at day 1 on all the planar and pyramids samples (coated and uncoated) demonstrated similar cell numbers, however, NS was already lower in cell numbers. At day 5 and 10 differences were observed, with numbers on both planar surfaces considerably higher than both pyramid surfaces, however cell numbers on both pyramid surfaces were noticeably higher than on NS. Statistically, a two-way ANOVA demonstrated that significant differences were due to sample type and time ($p < 0.01$) ('n' numbers varied from 50 per field of view for 24hr to 1500 for 10 days, with 45 observations per sample type per timepoint). Comparisons demonstrated that Plan, Pyr, TiPlan and TiPyr were all significantly different from NS ($p < 0.01$). Significant differences

were also found separating both the planar topographies (Plan and TiPlan) and the pyramid topography (Pyr and TiPyr) ($p < 0.01$).

Cell Alignment to the Pyramid Topography

From the low magnification SEM images it appeared that cells on the pyramid surface were generally aligned horizontally or vertically utilising the 'between pyramid' run off space. To further assess this, cells seeded for 24hr on TiPyr ($n=156$) were investigated and classed as either horizontally/vertically aligned, diagonally (45°) aligned, on non-aligned– this last classification included unspread cells as the cells longest axis was taken as indication of its alignment. A box plot demonstrated that the majority of cells were grouped to the horizontal/vertical alignment, with only a few demonstrating diagonal alignment (Graph 7.2). The instance of cell non-alignment was greater than the diagonal alignment, but less than that of the horizontal/vertical alignment. Utilising a one-way ANOVA test, the only significant difference was identified between horizontal/vertical alignment and diagonal alignment ($p < 0.01$, $n=156$). This suggested that horizontal/vertical topography pattern favours cell elongation and alignment in comparison to the diagonal topography. Referring again to the low magnification SEM images, it appeared that the majority of cells classed as non-aligned were unspread, suggesting their reduced interaction with the topography. This may account for their apparent lack of alignment to the features.



*Graph 7.2 – A box plot demonstrated the distribution of cells displaying the three categories of alignment on the pyramid topography. The majority of cells were grouped to the horizontal/vertical alignment, with only a few demonstrating diagonal alignment. The instance of cell non-alignment was greater than the diagonal alignment, but less than that of the horizontal/vertical alignments. *There were statistically significant differences between the numbers of cells aligning horizontally/vertically compared to those demonstrating diagonal alignment ($p < 0.01$).*

*Cell Morphology***Qualitative Cell Morphology on Pyr and TiPyr**

When cell morphology at 24hr was visualised using a higher magnification, cells generally were either bipolar or rounded with some membrane protrusions (Fig 7.15a,b). Filopodia were seen to be extending from the cell periphery and attaching to and bridging the pyramid structures, while rarely were they observed attaching to the base of the topography between the features (Fig 7.15a,d,e). It was unclear if the cross-linked web-like structure observed underneath the cell body suspended on the pyramid tips was derived from filopodia or was in fact a form of extracellular matrix protein (Fig 7.15c). Evidence would suggest a possible filopodial network, as these webs could also be observed further away from the cell body confined in attachment to the pyramid features (Fig 7.15d,e). An additional feature observed with cells on TiPyr was that they were more prone to envelope the pyramid tips and stretch themselves onto the surface topography while still exploring their surroundings (Fig 7.16a,b,d). The cells were observed to be suspended on the pyramid tips, however, at closer inspection the 'filopodia' and cell body appeared to have dropped to explore and fill the 'between pyramid' spaces that the cells were previously thought to be stretching over (Fig 7.16b). At 5 days, cells could be observed with multi-polar elongations or lamellapodia, and the main cell body stretched over a considerable pyramid area (Fig 7.17a,c). Occasionally, the cell body was stretched so thin that the pyramid tips protruded through the top of the cell body, however, this could also be a fixation artefact (Fig 7.17c). Filopodia numbers appeared reduced but could be observed exploring and bridging from pyramid to pyramid (Fig 7.17b). At 10 days, the general morphology remained unchanged although the cell periphery now was drawn out in typical tension dictated "chain curves" by filopodia adhering to the tips of the surrounding pyramids (Fig 7.18a,c). The cells demonstrated some surface ruffling and occasionally appeared to utilise whole pyramids as purchases for spreading while their filopodia were still exploring and attaching to the pyramid tips (Fig 7.18a,b,c,d).

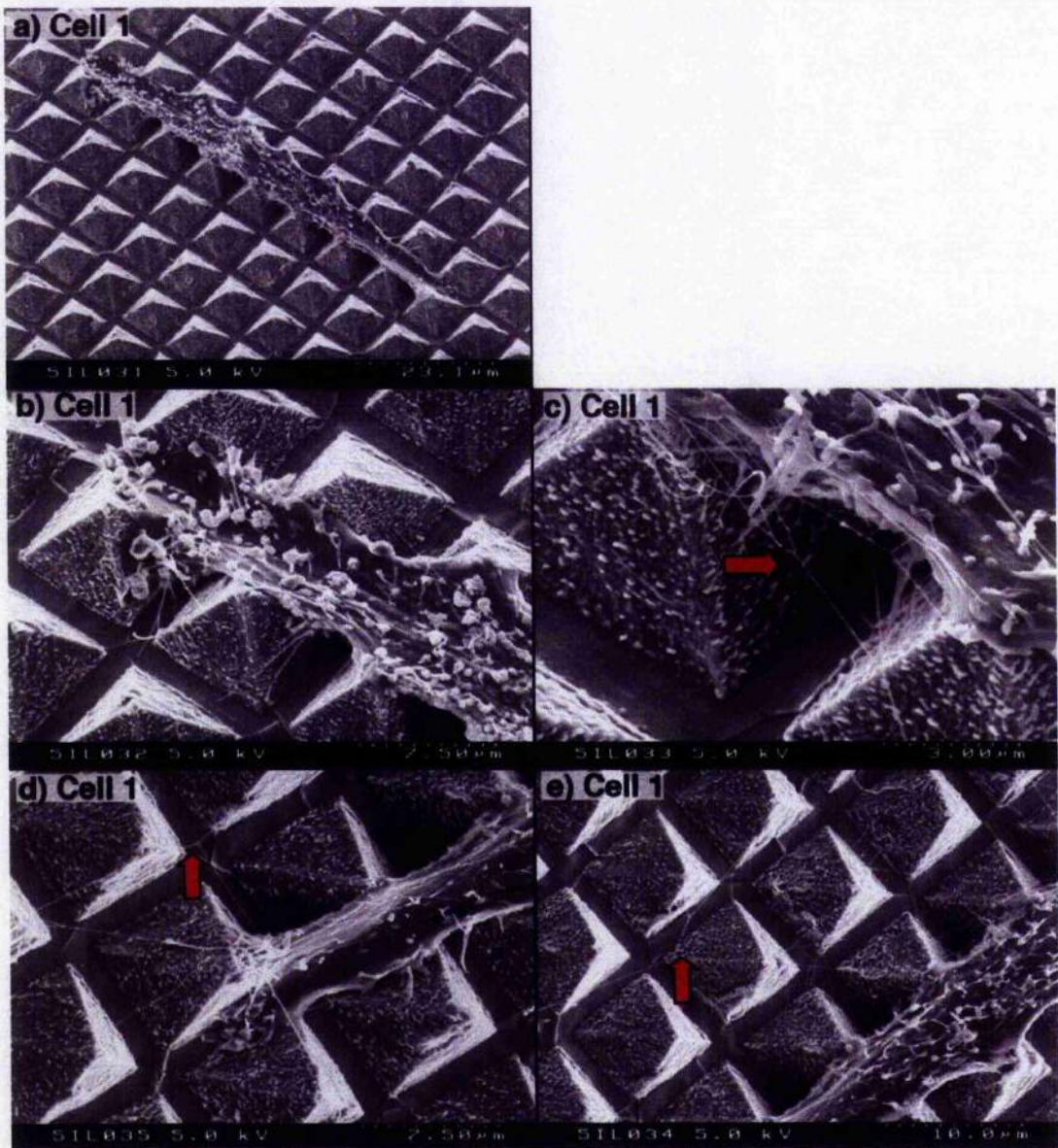


Fig 7.15 – Cells cultured for 24 hr on TiPyr. (a) A characteristic cell morphology on this topography was the bipolar shape. (b) Considerable surface ruffling was seen on the cell body surface and filopodia were seen extending from the cell periphery and attaching the pyramid structures. (c) A cross-linked web-like structure observed underneath the cell body suspended on the pyramid tips and was possibly derived from filopodia (red arrow) (d & e) These cross-linked filopodia webs could also be observed further away from the cell attachment on the pyramid features (red arrows).

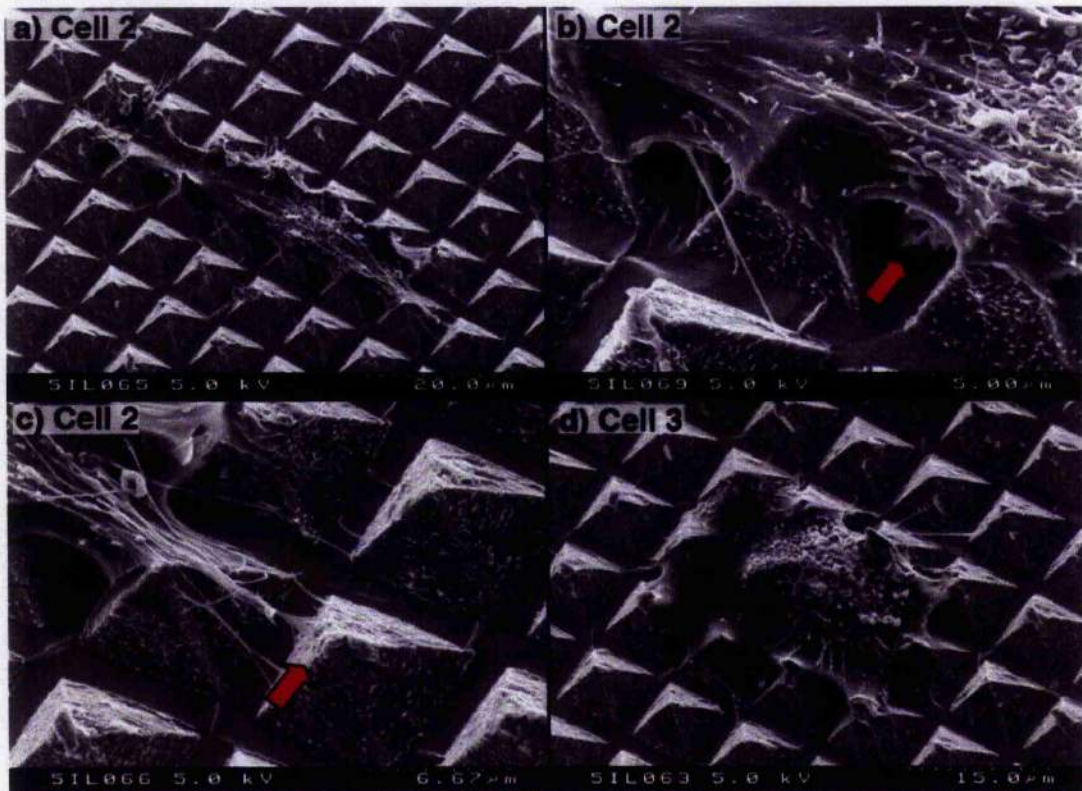


Fig 7.16 – Cells cultured for 24 hr on TiPyr. (a) Cell 2 - In addition to the bipolar morphology and surface ruffling, it was observed that cells on TiPyr were more prone to envelope the pyramid tips and stretch onto the surface topography while still exploring their surroundings (b) A higher magnification of Cell 2 – the pyramid stretching demonstrates more clearly. Also, the cells were previously observed to be suspended on the pyramid tips, however it was apparent here that the filopodia and cell body drop to explore and fill the 'between pyramid' spaces (red arrow) (c). A higher magnification of Cell 2 – demonstrates that the filopodia are also still confined to generally attaching to the pyramid tips (red arrow). (d) Cell 3 – a more rounded cell that has spread equally in all directions spreading itself over numerous pyramids. The cell body was thin enough that the pyramids can be seen through the cell body.

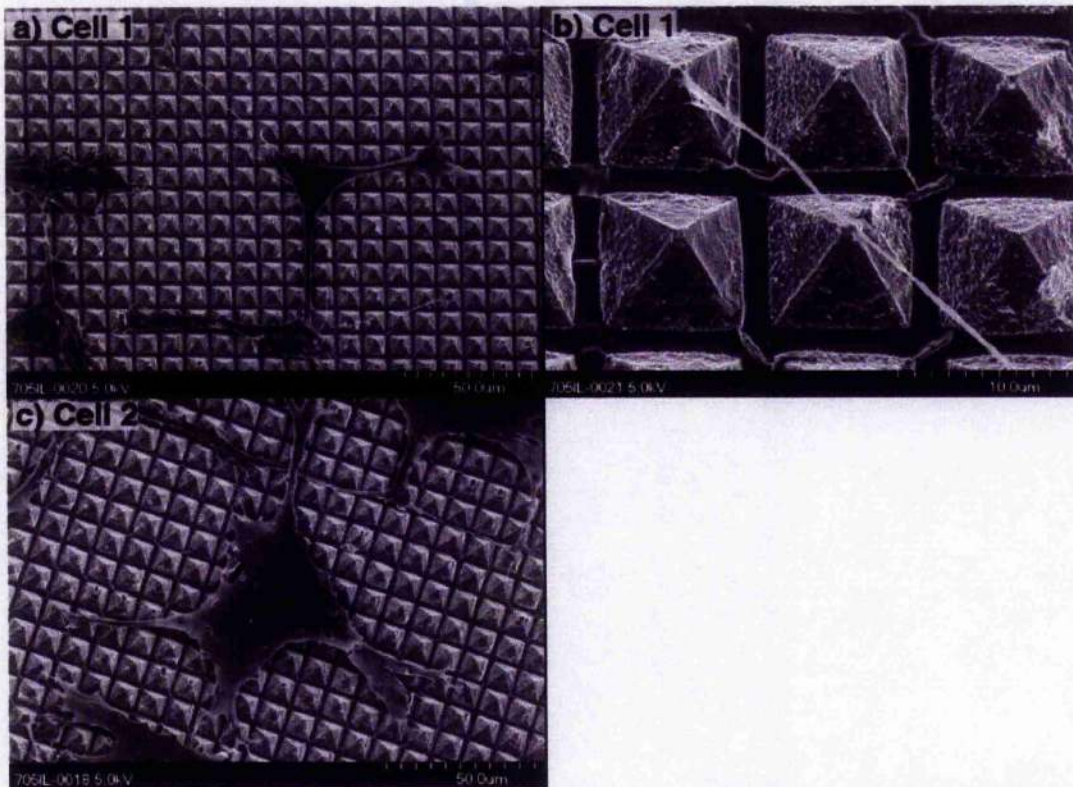


Fig 7.17 – Cells cultured for 5 days on TiPyr – (a) Cell 1 - cells could be observed with multi-polar elongations and the main cell body stretched over a considerable pyramid area (b) A higher magnification of Cell 1 - Filopodia numbers appeared reduced but could be observed exploring and bridging from pyramids to pyramid. (c) Cell 2 - Occasionally the cell body was stretched so thin that the pyramid tips protrude through the top of the cell body, however this could also be a fixation artefact.

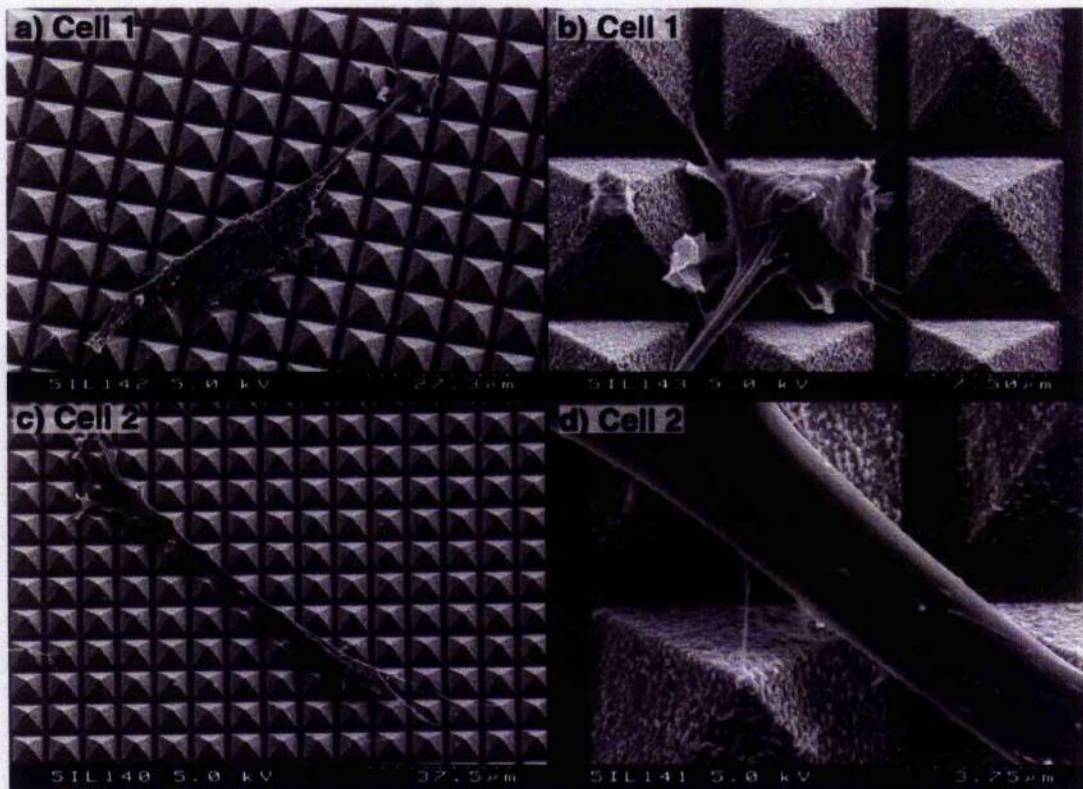


Fig 7.18 – Cells cultured on TiPyr for 10 days. (a) Cell 1 – General cell morphology remained unchanged although the cell periphery now undulated, dictated by the location of the pyramid tips. (b) A higher magnification of Cell 1 – It was interesting to note that cells could utilise whole pyramids as purchases for attachment and spreading. (c) Cell 2 – A bipolar cell with a clear undulating periphery (d) A high magnification of Cell 2 – Filopodia were still exploring and attaching to the pyramid tips.

Plan and TiPlan – Uncoated and Titanium Coated Planar PCL Topography

Examples of cell morphology on the smooth surfaces of Plan and TiPlan are included on the accompanying CD-ROM. At a higher magnification some artefacts from the fixation and drying become apparent with TiPlan as the surface coating appeared cracked and sometimes peeled away from the polymer substrate. The morphology at 24hr and 5 days on both uncoated and titanium coated appeared similar exhibiting well spread cells with minimal surface ruffling and a few filopodia probing of the surface. On titanium, the cells did not appear to react to the cracked titanium layer. It was impossible to locate isolated cells for imaging at 10 days due to the high cell number found on both uncoated and coated versions of the surface.

Vinculin, Tubulin and Actin Immunostaining

Intracellular immunostaining was conducted to observe cell reactions towards the pyramid topography. Cells cultured on the uncoated pyramid microtopography, and titanium and gold coated, were stained for actin, DNA and vinculin or tubulin. Results from both TiPyr and Pyr are included while TiPlan and Plan are found on the CD-ROM.

Pyr – Pyramid embossed into PCL

Due to the non-reflective nature of uncoated PCL, it was not possible to superimpose the topography onto the immunostaining composites. The stained focal adhesion sites were generally yellow coloured patches found at the cell extremities (co-localisation of both the vinculin and actin staining); smaller sites were difficult to differentiate due to the high staining background caused by the thicker unspread cell cytoplasm (Fig 7.19a). Focal adhesions were observed to avoid the pyramids and were generally located in the 'between pyramid' areas. The vinculin inset of Fig 7.19b demonstrated the relation of the topography to the dense (white) focal adhesion sites, and also shows that the orientation of the focal adhesions was influenced by the direction of the 'between pyramid' features (Fig 7.19b). Similarly the f-actin filaments were also confined to these trenches and were aligned in the same manner (Fig 7.19b actin inset). The cell nuclei were generally central in the cell (Fig 7.19a, 7.20a,b) with some exceptions (Fig 7.19b), and their shape could be distorted by the presence of pyramids (Fig 7.19a DNA inset). The microtubule network was impaired by the topography with clear gaps in the network at the site of protruding of pyramid tips (Fig 7.20a main picture and tubulin inset) and the remaining microtubules were orientated in the direction the 'between pyramid' feature was running (Fig 7.20a tubulin inset). It was also interesting, with the actin and tubulin staining, to observe possible dynamics of cell exploration and spreading on the pyramid microtopography. Fig 7.20a,b demonstrated parallel cell elongations or lamellapodia similar to a forked cell body, only one pyramid apart, that were linked only by actin at 'between pyramid' intervals. Further up these forks microtubules could also be observed crossing the 'between pyramid' intervals.

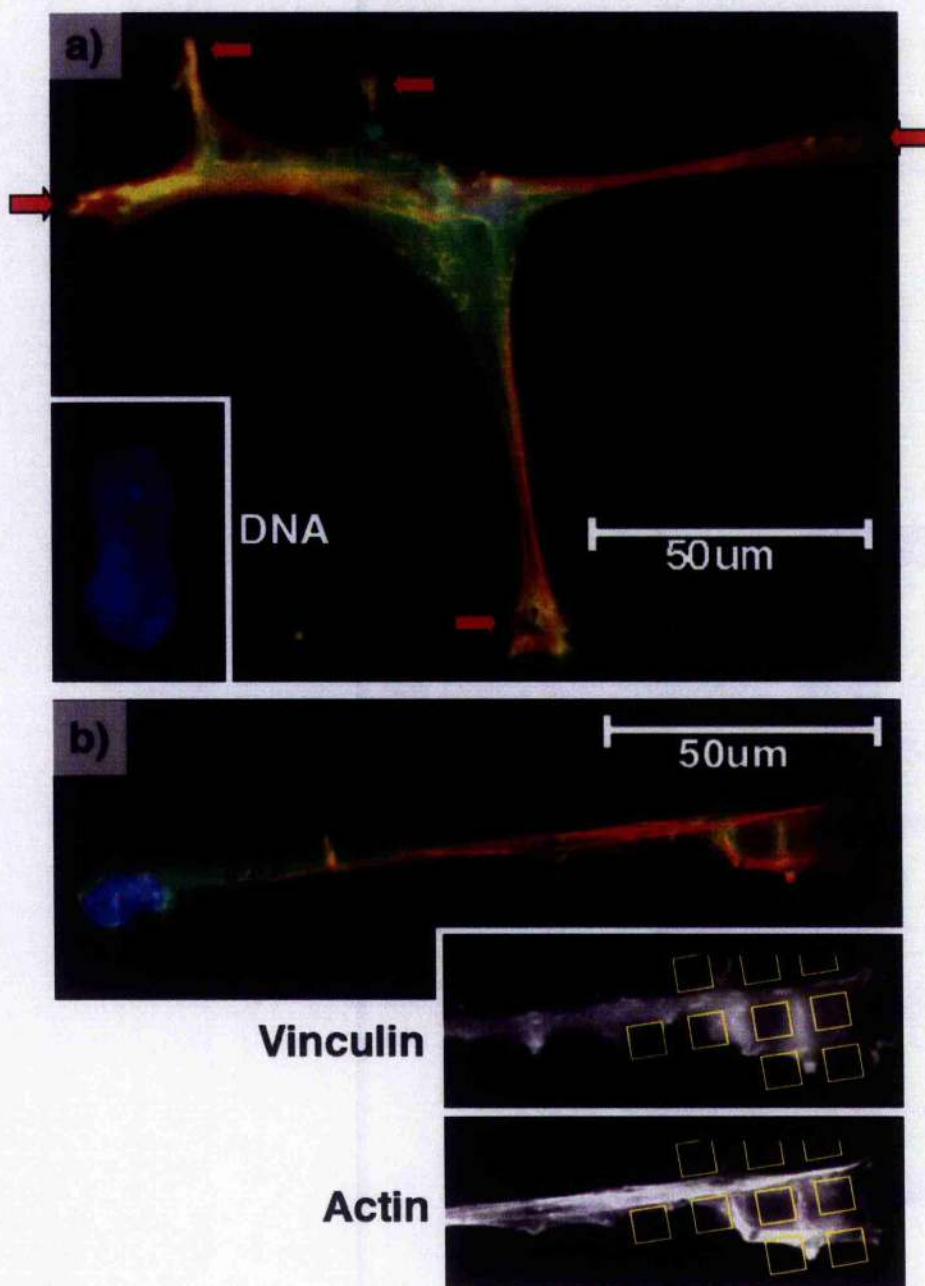


Fig 7.19 – Cells cultured on Pyr for 48 hr and triple labelled for ● Vinculin, ▼ Actin and ◆ DNA. (a). The stained focal adhesion sites were generally yellow coloured patches found at the cell extremities (indicated by the red arrows); smaller sites were difficult to differentiate due to the high staining background caused by the thicker unspread cell cytoplasm. The cell nuclei were generally central in the cell and their shape could be distorted by the presence of pyramids (see DNA inset). (b) The focal adhesions were observed to avoid the pyramids and generally located in the 'between pyramid' areas. The vinculin inset demonstrates the relation of the topography to the dense white focal adhesion sites, and also shows that the orientation of the focal adhesions was influenced by the direction of the 'between pyramid' features. Similarly, the actin filaments were also confined to these trenches and were aligned in the same manner.

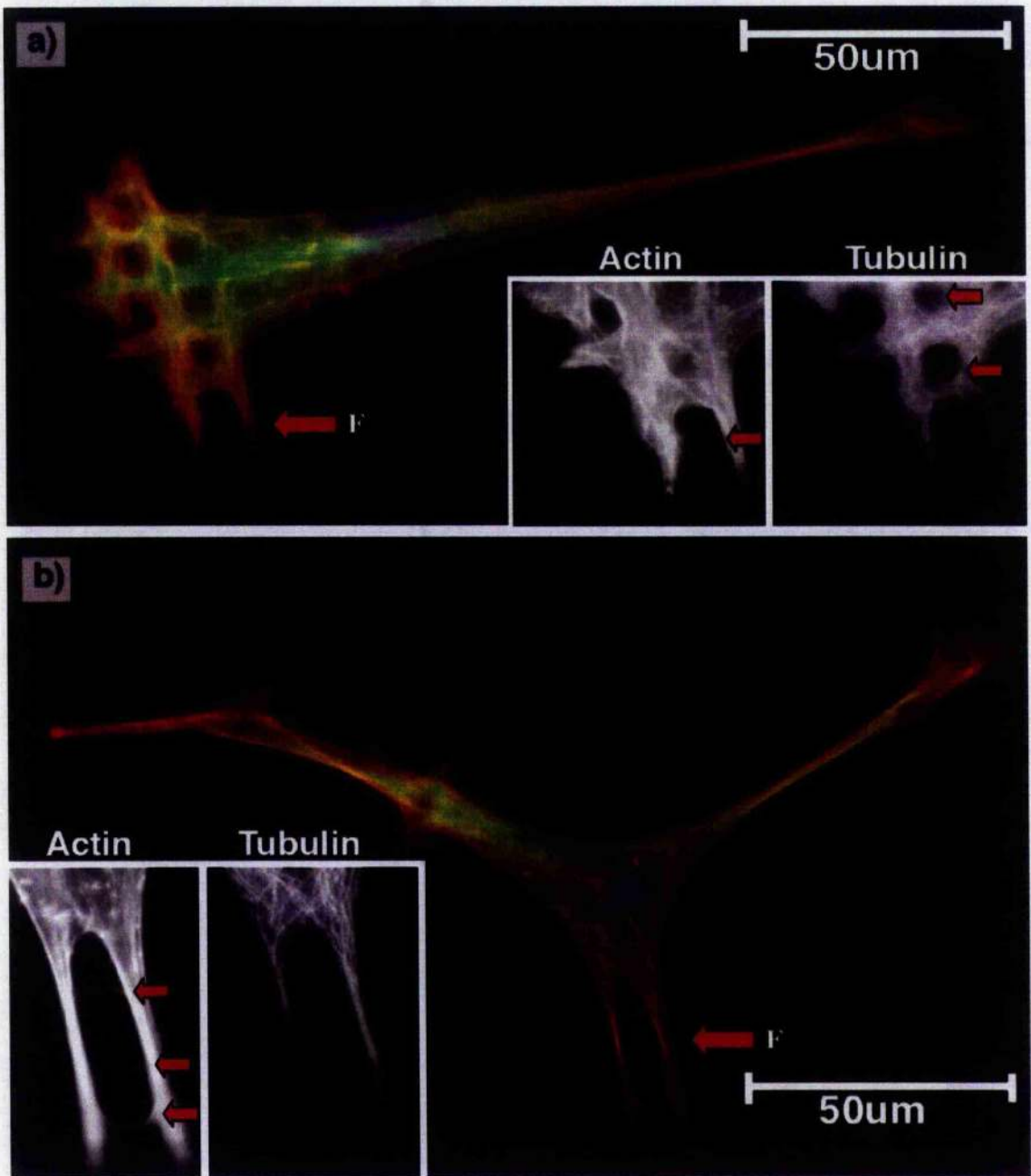


Fig 7.20 - Cells cultured on Pyr for 48 hr and triple labelled for ●Tubulin, ▼Actin and ◆DNA. (a) The microtubule network was clearly impaired by the topography with gaps in the network at the sites of protruding pyramid tips, and the remaining microtubules were orientated to the direction of the 'between pyramid' feature (tubulin inset). (b) An example of a tripolar cell still aligning to the surface orientation. The actin and tubulin staining suggests possible dynamics of cell exploration and spreading on the pyramid microtopography. Both cells 'a' & 'b' demonstrated parallel cell elongations similar to a forked cell body, only one pyramid apart (red arrow 'F'), that were linked only by actin at 'between pyramid' intervals (actin insets, red arrows). Further up these forks microtubules could also be observed crossing the 'between pyramid' intervals (tubulin inset, red arrows).

TiPyr – Titanium coated PCL Pyramid Topography

With the high optical reflectivity of the titanium layer, it was possible to superimpose the topography over the pseudo-coloured image to give a direct indication of reactivity to the topography. The reactions noted for the Pyr samples could again be observed here. For the vinculin immunostaining, there was again problems with background caused by the thicker cell body of the bipolar cells (Fig 7.21a). With cells elongated over larger areas (note that they were not more spread), it was clear that the focal adhesions played an important part in the cells' investigation of the surface. The adhesions were again limited to the 'between pyramid' areas and orientated to the direction of that area (Fig 7.21b). Parallel cell elongations were observed again here, however, at a distance of two pyramids there was no communication or actin connection (Fig 7.21b). The better spread cells demonstrated that far from being elevated on the pyramid tips, the cell body was present and adhering 'between pyramids' throughout the spread cell body (Fig 7.21c). In addition, some adhesion formation could be observed to occur on the lower side areas of the pyramids, and also some faint vinculin condensation could be seen at the sharp edges of the protruding pyramid (Fig 7.21d). While the majority of actin filaments aligned to the topography, in better spread cells a proportion did not follow this alignment suggesting that there could be intracellular tension maintained at different height levels of cells (Fig 7.21c). The microtubule staining also demonstrated similar features such as interruptions in the network for protruding pyramids and orientation to the 'between pyramid' features (Fig 7.22a,b). It was also possible to see parallel cell elongations at a distance of one pyramid joined with actin at the extremity and also by microtubules further in the cell body (Fig 7.22c actin and tubulin insets).

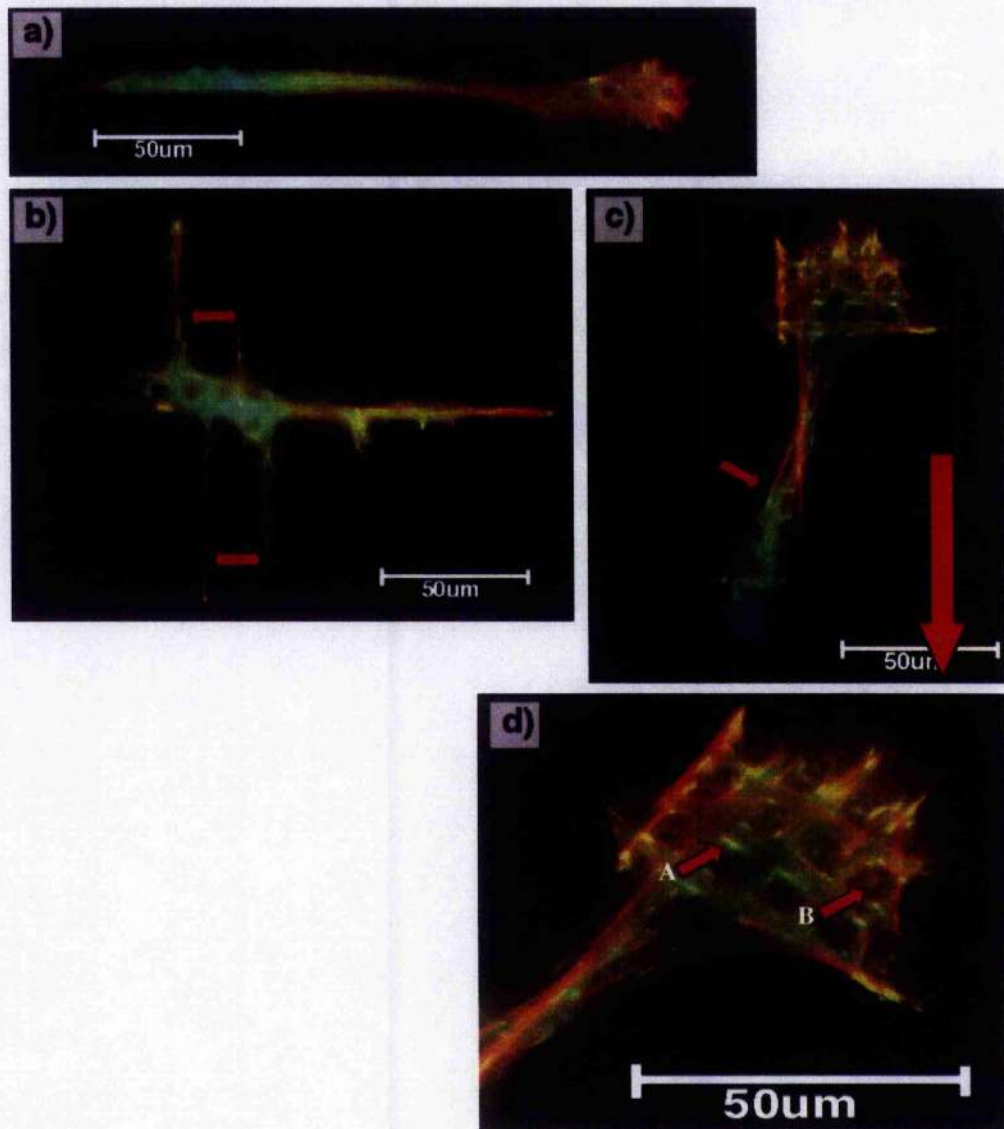


Fig 7.21 – Cells cultured on TiPyr for 48 hr and triple labelled for ● Vinculin, ▼ Actin and ◆ DNA. (a) The vinculin immunostaining was hindered by the thicker cell body of the bipolar cells. (b) With cells elongated over larger areas the adhesions were again limited to the ‘between pyramid’ areas and they were again orientated to the direction of that feature. Parallel cell elongations were observed again here, however, at a distance of two pyramids there was no communication or actin connection (double-ended red arrows). (c) Better spread cells demonstrated that far from being elevated on the pyramid tips, the cell body was present and adhering ‘between pyramids’ throughout the spread cell body. While the majority of actin filaments aligned to the topography, in better spread cells a proportion did not follow this alignment, suggesting that there could be intracellular tension maintained at different height levels of cells (red arrow). (d) At closer examination of image (c), focal adhesion sites could be observed to have formed at the lower sides of the pyramids (red arrow ‘A’) and some vinculin condensation was also observed aligning to the sharp edges higher up the pyramid protrusion (red arrow ‘B’).

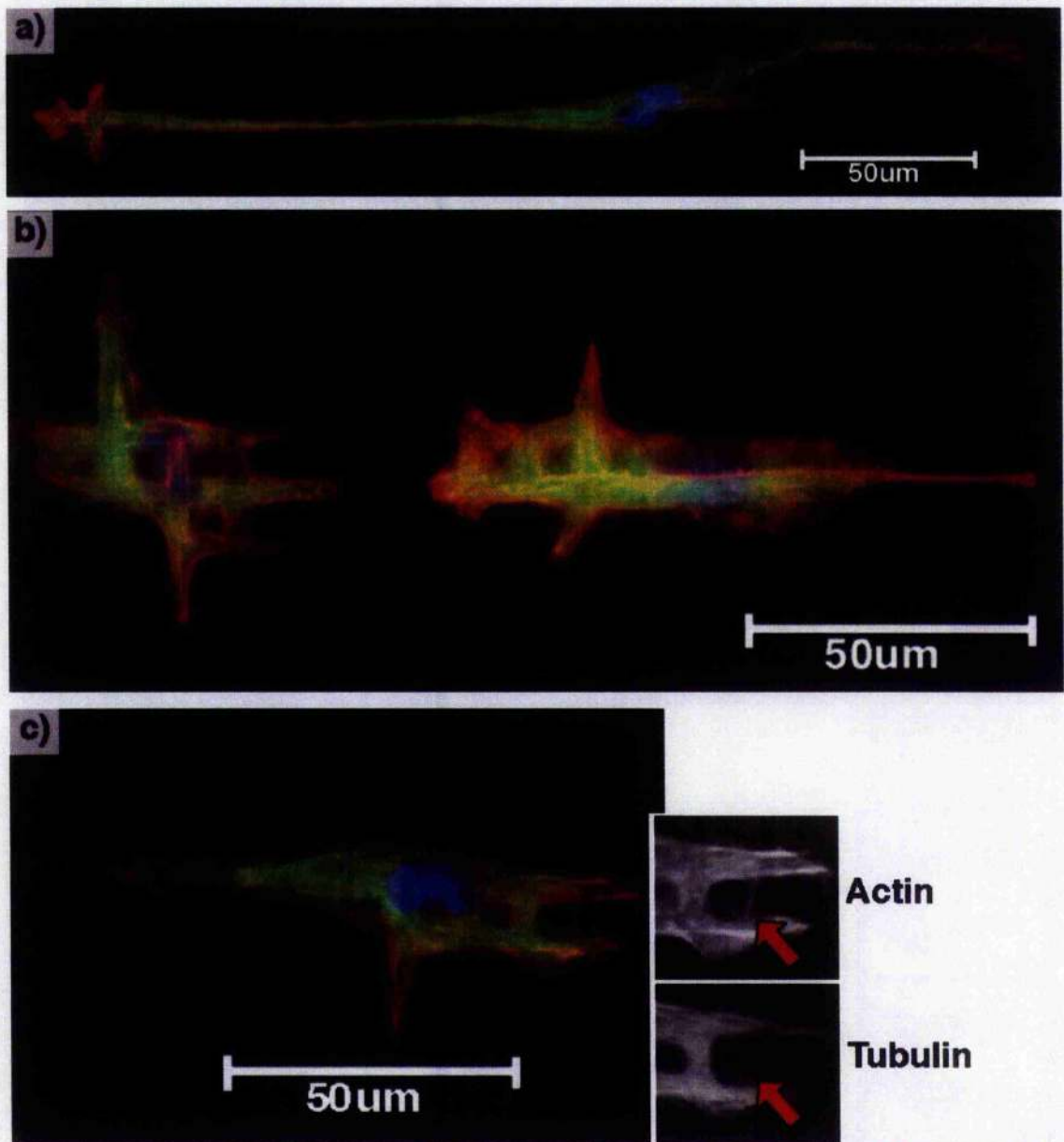


Fig 7.22 – Cells cultured on TiPyr for 48 hr and triple labelled for ●Tubulin, ▼Actin and ◆DNA. (a & b) The microtubule staining demonstrated similar features such as interruptions in the network for protruding pyramids and orientation to the ‘between pyramid’ features. (c) It was also possible to see parallel cell elongations at a distance of one pyramid joined with actin at the extremity and also by microtubules further in the cell body (red arrows on both actin and tubulin insets).

Plan and TiPlan

Images of vinculin and microtubule staining are included on the CD-ROM. On both Plan and TiPlan cells were well spread with mature focal adhesion sites and associated actin cytoskeleton. The microtubule network radiated to all areas of the cell body. No intracellular reactivity or alignment could be observed related to the cracking of the TiPlan surface.

AuPyr and AuPlan – Gold Coated PCL Pyramid and Planar Topographies

An interesting reaction was observed for cells cultured on gold-coated PCL of both pyramid microtopography and planar types. Cells did not survive on either surface and all that remained were fluorescently stained vacuoles possibly indicative of apoptosis (Fig 7.23).

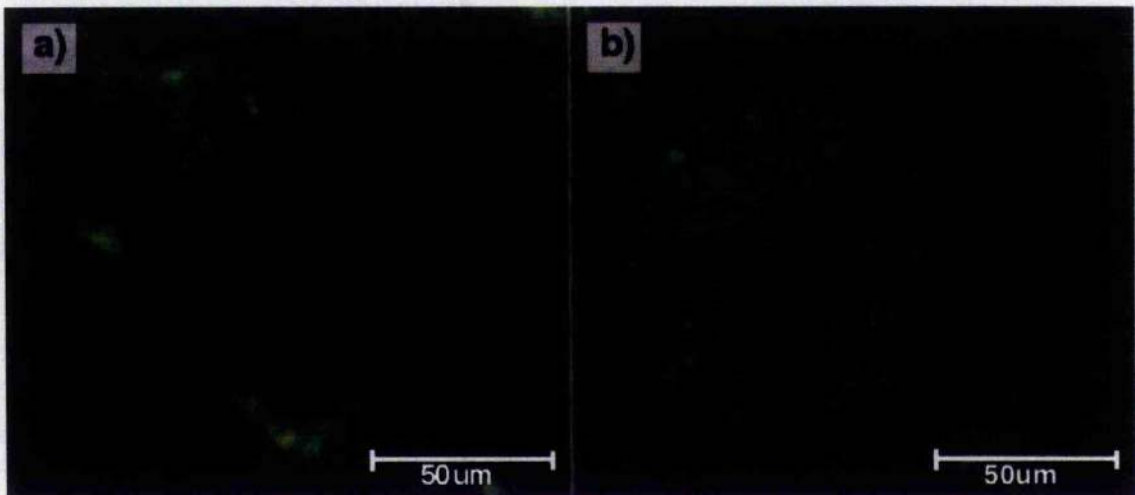
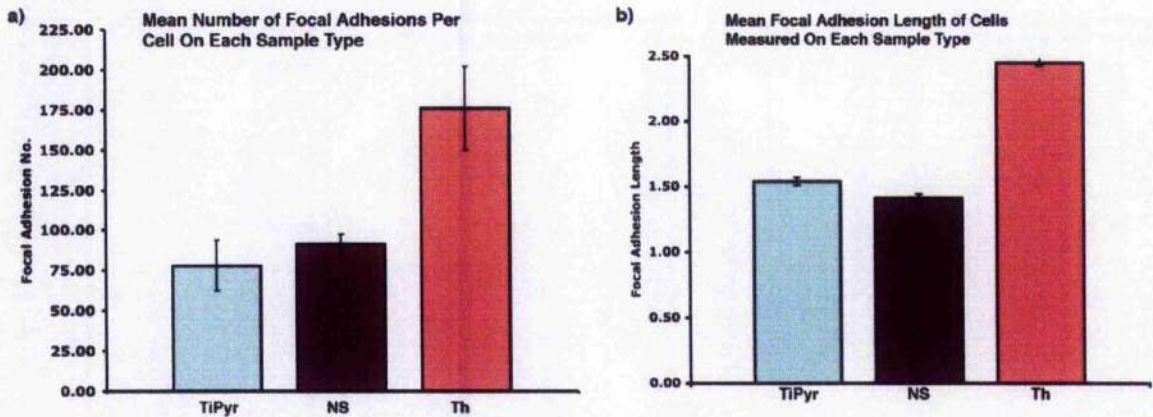


Fig 7.23 - Cell cultured for 48 hr on (a) AuPyr and (b) AuPlan. Cells did not survive on either surface and all that remained were fluorescently stained vacuoles possibly indicative of apoptosis.

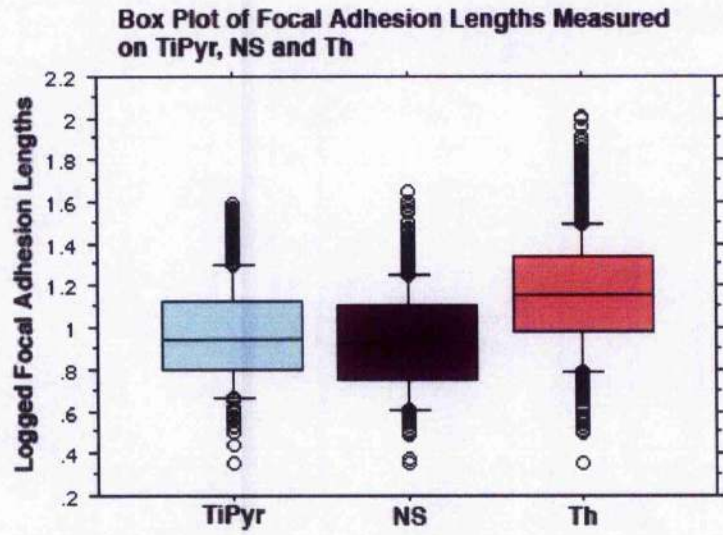
Focal Adhesion (FA) Measurement

Due to the unspread morphology of cells on the pyramids it was generally difficult to obtain images with clear focal adhesion sites for measurement. Twelve usable examples were imaged on TiPyr and measured. When the numbers and length were compared with NS they were found to be surprisingly similar in both number and lengths, and both were much lower than the planar control of Thermanox (Graph 7.3).



Graph 7.3 – (a) Mean number of focal adhesions counted on cells cultured on TiPyr, NS and Th. (b) Mean length of focal adhesion sites measured on TiPyr, NS and Th (μm).

Utilising One-way ANOVA, the sample types were all found to have statistically significant effects on focal adhesion length ($p < 0.01$, 'n' between 77 and 176). When compared, measured focal adhesion lengths on TiPyr were significantly different to both Th and more surprisingly NS ($p < 0.01$). However, a box plot demonstrates that the distribution of the focal adhesion lengths on both TiPyr and NS were quite similar and were much lower than on Th (Graph 7.4).



Graph 7.4 - Box plot of cell area variation on the samples. Note that the values have been logged. The distribution of focal adhesion length was similar on both TiPyr and NS, while both varied considerably from Th.

Discussion

Characterisation of the Pyramid Topography

The cell behaviour observed on various substrates suggested the involvement of the β -phase particle topography in its coated or uncoated form; however, the particles' dimensions present somewhat of a problem. AFM demonstrated that the NS surface was a collection of rough microspikes (note that this was emphasised by the $2.5\mu\text{m}$ height scale bar used in the 3D representation). What the method did not differentiate was the material boundary where the β -phase particle ends and the underlying α -phase of the topography begins. SEM, though at a less emphasised height scale, demonstrated that the β -phase particles were generally present on the crest of the underlying undulating α -phase topography. Thus, the general height dimensions taken from the AFM cross-section for the design of the pyramid topography do not solely represent the β -phase particles, but a peak of an α plus β crest.

The design of the topography was a compromise of required design features and fabrication limitations. From the SEM characterisation (Chapter 2, Experiment 3), the β -phase particle shapes were non-uniform and could vary $2\text{-}4\mu\text{m}^2$ in area. The AFM imaging demonstrated a more uniform inverted cone shape, therefore this was utilised as the microspike design feature. A cone shaped feature was desirable but difficult to produce, therefore a pyramid shape was chosen due to ease of fabrication. The etching method used in the pyramid fabrication also determined the gradient, and ultimately the pitching of the features. Closer pitching would have been optimal, however, the design also incorporated a planar run-off space between the microspikes similar to the underlying α -phase of NS. The finished topography was therefore not an accurate depiction of NS, however, it did include some essential features. It would be an interesting study to attempt to fabricate the unrealised elements of the topography design both from the viewpoint of microfabrication and cell biology.

Cell Reactivity to the Pyramid Topography

Some key reactions were observed concerning cell reactivity towards the pyramid surface. At the intracellular level, the focal adhesions generally avoided adhering to the pyramid tips favouring instead the planar spacing between the pyramids. The topography also influenced focal adhesion size and numbers, with similar number and length to that measured on NS. Higher portions of the pyramids disrupted the microtubule network and these tips could occasionally be observed protruding through the cell cytoplasm. Cell filopodia were located primarily attaching to the pyramid tips and rarely to the 'between pyramid' planar space. Overall, cell morphology was generally limited to unspread or elongated shapes and cell growth was suppressed at the later timepoints. It could be argued that the cells had simply migrated away from the surface utilising the 'between pyramid' spaces as channels. However, if this were the case, the conclusion that the topography does not support the cells reaching confluency would still be valid. Time-lapse video microscopy could prove useful in establishing the fate of the cells, and possibly a proliferative stain such as bromodeoxyuridine (BrdU) could be employed to confirm any presence of cell proliferation.

To the author's knowledge, pyramid structures of micrometer dimensions have only been fabricated previously by Liao for studying osteoblast response (Liao *et al.*, 2003). The pyramids in Liao's study were considerably larger in dimension (33 μm base length) with no planar run-off region between the pyramid features, and were found to elevate alkaline phosphatase expression in osteoblasts. In this study, the pyramids had a diameter of 8 μm , spaced by a run-off of 2 μm and a tip height of 4.5 μm .

Due to the lack of cell studies into a pyramid topography, it was more logical to compare cell reactivity to certain features found on this microtopography. Micro-pillars or columns have been studied extensively, with pillars of 2 or 5 μm^2 plan area, a height of 0.5 μm and 2 or 5 μm spacing allowing cells to become well spread. In addition, cells on these pillars had a faster growth rate than cells cultured on an inverted topography of the same dimensions (Green *et al.*, 1994; von Recum and van Kooten, 1995). Craighead demonstrated that the height of the column was not as influential as cells preferred both 1 μm and 2.7 μm high

columns in comparison to a planar surface (Craighead *et al.*, 1998). Two important differences of these documented features to the pyramid topography were that the tips of the columns had a flat area, and that the feature spacing was tightly packed. Flat column tips of $2\mu\text{m}^2$ area have been hypothesised as being large enough to accommodate the minimal focal adhesion size (Izzard and Lochner, 1976), and therefore enable cells to maintain an elevated status on the topography. However, the larger the tip size, the less influence its shape has as Rovinsky demonstrated whole unspread fibroblasts adhering to a hemispherical shaped tip of between 4-10 μm in diameter (Rovinsky *et al.*, 1991). The elevated cells at the tips of columns brings with it the advantage that there is no physical impairment to cell spreading such as protruding topographical features. Cell elevation and spreading was apparent on the pyramid topography at later timepoints, however, it was not a common occurrence and only some vinculin condensation was observed around the pyramid tips. The second difference was the feature spacing. It has been demonstrated that a spacing of 10 μm between pillars impaired neutrophil motility and, due to a lack of elevation on the pillar tips, also influenced their spreading (Tan *et al.*, 2000). Similar spacing of the pyramid features (tip-to-tip) saw the majority of cells align in the planar space bridging the features. It would be interesting to culture cells on the original surface die of inverted pyramids as I would predict that cells would spread well on the surfaces due to a reasonable surface area and no impediment protruding through cell membranes.

The pyramid topography could be considered as a bidirectional hybrid of square and V-shaped grooves producing a trapezoid form. Studies using square, V and trapezoid grooves have found cells aligning at groove depths of 1-10 μm (Chehroudi *et al.*, 1989; Clark *et al.*, 1991; Oakley and Brunette, 1993; Wojcik-Stodart *et al.*, 1995). The general alignment of cells to the 'between-pyramid' grooves was in keeping with these observations, however, the bi-directional topographical cues available to the cells produce curious multi-polar morphologies indicating that while the grooves are generally preferred there is no directional hierarchy in the cell elongation. This was similarly seen intracellularly with the cytoskeleton, microtubule network and focal adhesions changing orientation 'within a cell' dependent on the between pyramid orientation.

An interesting feature of parallel cell elongations in multi-polar cells indicated a possible novel mechanism of cell spreading. It was observed that these parallel cell bodies were sometimes joined between features by means of actin bundles presumed to be lamellapodia. Further up these parallel bodies, cell cytoplasm and microtubules could be seen oriented to 'between pyramid' features. I suggest that the investigatory lamellapodia extend filopodia that fuse upon sensing each other and trigger a cascade that culminates in the cell cytoplasm fusing over the surface or at least enabling the cell body to spread downwards from the main cell body, similar to closing a zip. The topography also indicates that this is dependent on distance as a spacing of one pyramid allowed filopodial communication while it was not observed with a distance of two or more. An additional piece of evidence supporting this theory was that while cells, spread over multiple pyramids, appeared elevated in the SEM, fluorescence labelling demonstrated the presence of focal adhesions orientated to the concealed 'between pyramid' areas and even formed on the sides of the pyramids. This suggests that the cells are always in close contact with the substrate and the presence of these adhesion sites might indicate the topographical route the cells have taken in their spreading.

Surface Chemistry

Surface chemistry proved to be a more influential factor in studying cell reactivity using polycaprolactone (PCL) than anticipated. PCL is a commonly utilised biodegradable polymer with FDA approval (Gadegaard *et al.*, 2003) and has been demonstrated to elicit favourable cell reactivity (Curtis *et al.*, 2004; Dalby *et al.*, 2004b). While the coating of titanium on PCL did not prove problematic, a rather more curious anomaly was the non-cytocompatibility of the gold coating on PCL. Throughout the course of this study gold had proven itself to be compatible coating on all other surfaces including other polymers such as Thermanox. A possible theory was that when evaporated on PCL, the natural islet formation of gold rendered the surface highly hydrophobic (this was observed practically) and this hydrophobicity was beyond the limits of protein adsorption or critical cell adhesion. Another possibility would be the contamination of the surface during the coating process with vacuum oil.

Summary

The association of numerous cellular reactions, culminating in a lack of cell growth, ties the cellular reactivity on the pyramid topography to that observed on NS topography. It is therefore acceptable to conclude that the microspike surface feature of NS represented in the form of a fabricated topography contributes significantly if not completely to the observed cell growth suppression. Additionally, it is possible to conclude that some or all of the fibroblast responses observed in relation to both the NS and the pyramid topographies are contributory to the non-cytocompatible outcome of cell growth upon NS.

The pyramid topography itself offers a wealth of possibilities not only into cell reactivity towards metallic inspired defined topographies, but also investigating the cellular mechanics to such features. As previously stated concluding the coated metal topographies, the timescale of investigating cellular reaction to the topography should be reduced to examine cells reactivity from contact onwards. In addition to time-lapse video microscopy, the use of GFP labelled intracellular components such as actin and vinculin would be optimal here to elucidate the probing and spreading mechanisms of cells on the topography.

References

- Chehroudi, B., Gould, T. R. and Brunette, D. M.** (1989). Effects of a grooved titanium-coated implant surface on epithelial cell behavior in vitro and in vivo. *J Biomed Mater Res* **23**, 9, 1067-85.
- Clark, P., Connolly, P., Curtis, A., Dow, J. A. and Wilkinson, C.** (1991). Cell guidance by ultrafine topography in vitro. *J Cell Sci*, **1**, 73-7.
- Craighead, H. G., Turner, S. W., Davies, R. C., James, C., Perez, A. M., St John, P. M., Isaacson, M., Kam, L., Shain, W., Turner, J. N. and Banker, G.** (1998). Chemical and topographical surface modification for control of central nervous system cell adhesion. *Journal of Biomedical Microdevices* **1**, 1, 49-64.
- Curtis, A. S., Gadegaard, N., Dalby, M. J., Riehle, M. O., Wilkinson, C. D. and Aitchison, G.** (2004). Cells react to nanoscale order and symmetry in their surroundings. *IEEE Trans Nanobioscience* **3**, 1, 61-5.
- Dalby, M. J., Gadegaard, N., Riehle, M. O., Wilkinson, C. D. and Curtis, A. S.** (2004). Investigating filopodia sensing using arrays of defined nano-pits down to 35 nm diameter in size. *Int J Biochem Cell Biol* **36**, 10, 2015-2025.
- Gadegaard, N., Thoms, S., Macintyre, D. S., McGee, K., Gallager, J., Casey, B. and Wilkinson, C.** (2003). Array of nano-dots for cellular engineering. *Microelectronic Engineering* **67-68**, 162-168.
- Green, A. M., Jansen, J. A., van der Waerden, J. P. C. M. and von Recum, A.** (1994). Fibroblast response to microtextured silicone surface: Texture orientation into or out of the surface. *J Biomed Mater Res* **28**, 647-653.
- Izzard, C. S. and Lochner, L. R.** (1976). Cell-to-substrate contacts in living fibroblasts: an interference reflexion study with an evaluation of the technique. *J Cell Sci* **21**, 1, 129-59.
- Liao, H., Andersson, A. S., Sutherland, D. S., Petronis, S., Kasemo, B. and Thomsen, P.** (2003). Response of rat osteoblast-like cells to microstructured model surfaces in vitro. *Biomaterials* **24**, 4, 649-654.
- Oakley, C. and Brunette, D. M.** (1993). The sequence of alignment of microtubules, focal contacts and actin filaments in fibroblasts spreading on smooth and grooved titanium substrata. *J Cell Sci* **106** (Pt 1), 343-54.
- Rovensky, Y. A., Bershinsky, A., Gavargizov, E. I., Obolenskaya, L. N. and Vasiliev, J. M.** (1991). Spreading of mouse fibroblasts on the substrate with multiple spikes. *Exp Cell Res* **197**, 107-112.
- Tan, J., Shen, H., Carter, K. L. and Saltzman, W. M.** (2000). Controlling human polymorphonuclear leukocytes motility using microfabrication technology. *J Biomed Mater Res* **51**, 4, 694-702.
- von Recum, A. and van Kooten, T. G.** (1995). The influence of micro-topography on cellular response and the implications for silicone implants. *J. Biomater. Sci. Polymer Edn* **7**, 2, 181-198.
- Wojciak-Stodart, B., Curtis, A., Monaghan, W., McGrath, M., Sommer, I. and Wilkinson, C.** (1995). Role of the cytoskeleton in the reaction of fibroblasts to multiple grooved substrate. *Cell Mot Cytoskel.* **31**, 147-158.

Discussion

Characterisation of the Pyramid Topography

The cell behaviour observed on various substrates suggested the involvement of the β -phase particle topography in its coated or uncoated form; however, the particles' dimensions present somewhat of a problem. AFM demonstrated that the NS surface was a collection of rough microspikes (note that this was emphasised by the $2.5\mu\text{m}$ height scale bar used in the 3D representation). What the method did not differentiate was the material boundary where the β -phase particle ends and the underlying α -phase of the topography begins. SEM, though at a less emphasised height scale, demonstrated that the β -phase particles were generally present on the crest of the underlying undulating α -phase topography. Thus, the general height dimensions taken from the AFM cross-section for the design of the pyramid topography do not solely represent the β -phase particles, but a peak of an α plus β crest.

The design of the topography was a compromise of required design features and fabrication limitations. From the SEM characterisation (Chapter 2, Experiment 3), the β -phase particle shapes were non-uniform and could vary $2\text{-}4\mu\text{m}^2$ in area. The AFM imaging demonstrated a more uniform inverted cone shape, therefore this was utilised as the microspike design feature. A cone shaped feature was desirable but difficult to produce, therefore a pyramid shape was chosen due to ease of fabrication. The etching method used in the pyramid fabrication also determined the gradient, and ultimately the pitching of the features. Closer pitching would have been optimal, however, the design also incorporated a planar run-off space between the microspikes similar to the underlying α -phase of NS. The finished topography was therefore not an accurate depiction of NS, however, it did include some essential features. It would be an interesting study to attempt to fabricate the unrealised elements of the topography design both from the viewpoint of microfabrication and cell biology.

Cell Reactivity to the Pyramid Topography

Some key reactions were observed concerning cell reactivity towards the pyramid surface. At the intracellular level, the focal adhesions generally avoided adhering to the pyramid tips favouring instead the planar spacing between the pyramids. The topography also influenced focal adhesion size and numbers, with similar number and length to that measured on NS. Higher portions of the pyramids disrupted the microtubule network and these tips could occasionally be observed protruding through the cell cytoplasm. Cell filopodia were located primarily attaching to the pyramid tips and rarely to the 'between pyramid' planar space. Overall, cell morphology was generally limited to unspread or elongated shapes and cell growth was suppressed at the later timepoints. It could be argued that the cells had simply migrated away from the surface utilising the 'between pyramid' spaces as channels. However, if this were the case, the conclusion that the topography does not support the cells reaching confluency would still be valid. Time-lapse video microscopy could prove useful in establishing the fate of the cells, and possibly a proliferative stain such as bromodeoxyuridine (BrdU) could be employed to confirm any presence of cell proliferation.

To the author's knowledge, pyramid structures of micrometer dimensions have only been fabricated previously by Liao for studying osteoblast response (Liao *et al.*, 2003). The pyramids in Liao's study were considerably larger in dimension (33 μm base length) with no planar run-off region between the pyramid features, and were found to elevate alkaline phosphatase expression in osteoblasts. In this study, the pyramids had a diameter of 8 μm , spaced by a run-off of 2 μm and a tip height of 4.5 μm .

Due to the lack of cell studies into a pyramid topography, it was more logical to compare cell reactivity to certain features found on this microtopography. Micro-pillars or columns have been studied extensively, with pillars of 2 or 5 μm^2 plan area, a height of 0.5 μm and 2 or 5 μm spacing allowing cells to become well spread. In addition, cells on these pillars had a faster growth rate than cells cultured on an inverted topography of the same dimensions (Green *et al.*, 1994; von Recum and van Kooten, 1995). Craighead demonstrated that the height of the column was not as influential as cells preferred both 1 μm and 2.7 μm high

columns in comparison to a planar surface (Craighead *et al.*, 1998). Two important differences of these documented features to the pyramid topography were that the tips of the columns had a flat area, and that the feature spacing was tightly packed. Flat column tips of $2\mu\text{m}^2$ area have been hypothesised as being large enough to accommodate the minimal focal adhesion size (Izzard and Lochner, 1976), and therefore enable cells to maintain an elevated status on the topography. However, the larger the tip size, the less influence its shape has as Rovinsky demonstrated whole unspread fibroblasts adhering to a hemispherical shaped tip of between 4-10 μm in diameter (Rovinsky *et al.*, 1991). The elevated cells at the tips of columns brings with it the advantage that there is no physical impairment to cell spreading such as protruding topographical features. Cell elevation and spreading was apparent on the pyramid topography at later timepoints, however, it was not a common occurrence and only some vinculin condensation was observed around the pyramid tips. The second difference was the feature spacing. It has been demonstrated that a spacing of 10 μm between pillars impaired neutrophil motility and, due to a lack of elevation on the pillar tips, also influenced their spreading (Tan *et al.*, 2000). Similar spacing of the pyramid features (tip-to-tip) saw the majority of cells align in the planar space bridging the features. It would be interesting to culture cells on the original surface die of inverted pyramids as I would predict that cells would spread well on the surfaces due to a reasonable surface area and no impediment protruding through cell membranes.

The pyramid topography could be considered as a bidirectional hybrid of square and V-shaped grooves producing a trapezoid form. Studies using square, V and trapezoid grooves have found cells aligning at groove depths of 1-10 μm (Chehroudi *et al.*, 1989; Clark *et al.*, 1991; Oakley and Brunette, 1993; Wojciak-Stodart *et al.*, 1995). The general alignment of cells to the 'between-pyramid' grooves was in keeping with these observations, however, the bi-directional topographical cues available to the cells produce curious multi-polar morphologies indicating that while the grooves are generally preferred there is no directional hierarchy in the cell elongation. This was similarly seen intracellularly with the cytoskeleton, microtubule network and focal adhesions changing orientation 'within a cell' dependent on the between pyramid orientation.

An interesting feature of parallel cell elongations in multi-polar cells indicated a possible novel mechanism of cell spreading. It was observed that these parallel cell bodies were sometimes joined between features by means of actin bundles presumed to be lamellapodia. Further up these parallel bodies, cell cytoplasm and microtubules could be seen oriented to 'between pyramid' features. I suggest that the investigatory lamellapodia extend filopodia that fuse upon sensing each other and trigger a cascade that culminates in the cell cytoplasm fusing over the surface or at least enabling the cell body to spread downwards from the main cell body, similar to closing a zip. The topography also indicates that this is dependent on distance as a spacing of one pyramid allowed filopodial communication while it was not observed with a distance of two or more. An additional piece of evidence supporting this theory was that while cells, spread over multiple pyramids, appeared elevated in the SEM, fluorescence labelling demonstrated the presence of focal adhesions orientated to the concealed 'between pyramid' areas and even formed on the sides of the pyramids. This suggests that the cells are always in close contact with the substrate and the presence of these adhesion sites might indicate the topographical route the cells have taken in their spreading.

Surface Chemistry

Surface chemistry proved to be a more influential factor in studying cell reactivity using polycaprolactone (PCL) than anticipated. PCL is a commonly utilised biodegradable polymer with FDA approval (Gadegaard *et al.*, 2003) and has been demonstrated to elicit favourable cell reactivity (Curtis *et al.*, 2004; Dalby *et al.*, 2004b). While the coating of titanium on PCL did not prove problematic, a rather more curious anomaly was the non-cytocompatibility of the gold coating on PCL. Throughout the course of this study gold had proven itself to be compatible coating on all other surfaces including other polymers such as Thermanox. A possible theory was that when evaporated on PCL, the natural islet formation of gold rendered the surface highly hydrophobic (this was observed practically) and this hydrophobicity was beyond the limits of protein adsorption or critical cell adhesion. Another possibility would be the contamination of the surface during the coating process with vacuum oil.

Summary

The association of numerous cellular reactions, culminating in a lack of cell growth, ties the cellular reactivity on the pyramid topography to that observed on NS topography. It is therefore acceptable to conclude that the microspike surface feature of NS represented in the form of a fabricated topography contributes significantly if not completely to the observed cell growth suppression. Additionally, it is possible to conclude that some or all of the fibroblast responses observed in relation to both the NS and the pyramid topographies are contributory to the non-cytocompatible outcome of cell growth upon NS.

The pyramid topography itself offers a wealth of possibilities not only into cell reactivity towards metallic inspired defined topographies, but also investigating the cellular mechanics to such features. As previously stated concluding the coated metal topographies, the timescale of investigating cellular reaction to the topography should be reduced to examine cells reactivity from contact onwards. In addition to time-lapse video microscopy, the use of GFP labelled intracellular components such as actin and vinculin would be optimal here to elucidate the probing and spreading mechanisms of cells on the topography.

Chapter 8 – General Discussion

The initial aim of this work was to investigate the *in vitro* fibroblastic response to the orthopaedic grade materials stainless steel, titanium and Ti-6Al-7Nb (TAN), with the primary aim of assessing and comparing the soft tissue response towards TAN. Initially, the study involved a comprehensive characterisation of the sample surfaces and assessment of cell behaviour in relation to these surfaces. The observation of lower adhesion, spreading and growth on the surface of NS necessitated the design of a series of experiments to help distinguish between the effects of material and those of topography. These experiments eventually drew to the conclusion that behavioural cues for fibroblasts on implant metal surfaces were generally confined to the influence of surface topography over that of surface chemistry.

1. Materials and Surfaces

1.1- Material Characterisation

It has been stated previously, in Chapters 1 and 2, that the industrial surface finish of orthopaedic material varies, however, this comment originally related to the more obvious difference between electropolished SS and the roughened standard titanium and its alloys. Over the course of characterising the sample types and subsequent cellular work, the validity of this comment pertaining to all the materials became apparent, particularly for TS and NS. While TS and NS had numerically similar roughness and indistinguishable 3D profiles (profilometry), higher resolution methods demonstrated NS and TS to have very different surface morphologies. TS demonstrated a series of parallel cuts oriented similar to a 'basket weave' pattern while NS had an undulating topography punctuated by protruding particles. These topographies were produced by the combination of their microstructure and surface etching treatments. Only by using several high-resolution characterisation techniques could these differences be discovered and documented. For this type of surface characterisation, utilising more methods equates to a clearer quantification of surface morphology.

The considerable detail that was obtained for surface morphology could not be matched by an equivalent degree of assessment of surface chemistry due to the limited methods

available. While SEM in backscattered electron mode (BSE) demonstrated the heterogeneous chemistries of SS, NE and NS, this was limited to the spatial characteristics of the different elements present on the surfaces; in practice greyscale contrast demonstrates the location of denser areas of the surface (equating to higher atomic numbers). This method proved useful for demonstrating that the protruding particles of NS were elementally different from the base material (in practice a higher contrast). As noted previously, EDX could not be conducted on the surfaces as the $1\mu\text{m}$ depth of generated X-rays utilised would comprise both the bulk and surface information, found within such a reaction volume, and compromise any elemental findings (Kasemo and Lausmaa, 1988). The utilisation of X-ray photon electron spectroscopy (XPS) would prove a constructive extension to the characterisation, as the first few surface nanometres could be analysed without relation to the underlying bulk material (LaBerge, 1999). In the instance of TAN, the resolution of this method would confirm that there was a differing surface oxide chemistry overlying β -phase particles of the electropolished and standard TAN finishes, as observed in other studies (Sittig *et al.*, 1999; Textor *et al.*, 2001). The surface coating experiments of Chapter 6 and 7 also would have benefited as XPS could have confirmed that the coating did mask all areas of the surfaces, especially in the instance of the protruding β -phase particles of NS, and the cracked gold coat on PCL.

Contact angle studies demonstrated that increase in surface roughness (defined by Ra) went hand in hand with an observed increase in hydrophobicity. However, as discussed in Chapter 2, the relationship could not conclusively be attributed to topography as aspects of surface chemistry could be involved. Specifically, the heterogeneous oxide layer of TAN provides a mix of different oxides with different isoelectric points that could prove to be influencing surface free energy (Sittig *et al.*, 1999). A possible way to disentangle the respective influence of topography and that of chemistry on contact angles would be to coat the surface uniformly, thus, producing the necessary homogenous surface chemistry whilst preserving the unique surface topography of NS.

A pertinent follow-up study related to the contact angle measurement would be to look at the influence of topo-chemistry on biomolecules, specifically protein adsorption as a

prelude to cell adhesion. As mentioned briefly in the discussion section of Chapter 6, this could be expanded upon with the inclusion of the coated metals, with NS of particular interest because of the possible influence its microstructure has upon its surface chemistry. While investigating quantitative protein absorption characteristics, similar to tests utilised by Webster (Webster *et al.*, 2000; Webster *et al.*, 2001), would be of use, it would be more interesting to examine protein adsorption spatially, especially to TAN's β -phase particles with regard to the native and synthetic (coated) chemistries. Scotchford *et al.* examined fibronectin adsorption to different surface oxides and found differences with Al_2O_3 (Scotchford *et al.*, 2003), which is also present in the β -phase of TAN, however, this was not competitive adsorption as no other proteins were involved and might not reflect the *in vitro* or *in vivo* situation. It would be more accurate would be to produce a 'pseudo-serum', a mix of various "prominent" proteins and immunolabel their locations on the surfaces (Rediske *et al.*, 2002). This would reduce the 200+ proteins present in serum to a manageable amount, but also be more complex than a single protein solution. From this fibroblast interaction viewpoint, such studies might assist in concluding that the interaction with the β -phase structures was due to its prominent morphology, as suspected, or if a level of surface chemistry might still be involved.

1.2 - Coated Materials

Coating the standard materials with a uniform chemistry provided a practical model to investigate how surface chemistry and the various topographies interact in their effect on cells. There are other methodologies for the production of surface replicas, generally involving the production of a negative die or mould that can consequently be utilised to reproduce positive replicas (Wieland *et al.*, 2002; Wieland *et al.*, 2005). These have been used with great success in the study of the effect of different roughness of titanium, and would be beneficial for the study of both SS and titanium - however, initial attempts with TAN in its standard form have proven to be difficult as during the removal of the negative replica the resin also removed some of the looser β -phase particles from the surface. With regard to fibroblast surface interaction, the β -phase particles were identified in this study to be NS's most significant characteristic, and the absence of a portion of these particles, as

would be the case with replica production, could influence any results obtained from the replica use.

Surface characterisation on the coated materials demonstrated that the topography remained relatively unchanged after coating and that a homogenous coating covered the whole surface. While the methods utilised observed no obvious topographical differences, some more subtle differences were possibly overlooked. While fibroblast growth on coated NS was still inhibited, cell spreading was observed to be statistically greater on both coated surfaces. A hypothesis formed on the basis of these observations is that applying the coating 'smoothed out' some of the pointed topography present on NS. AFM analysis of these surfaces would have been able to confirm or disprove this assumption, however, due to time and sample limitation this was not conducted. SEM in BSE mode demonstrated conclusively that the coating covered all aspects of the surface topographies, however, as with all methods confirmation by other means such as XPS would have been an useful addition. Mentioned earlier (Section 1.1), contact angle measurements on the different surface chemistries, produced by coating, might prove an interesting study to further elucidate the extent of standard NS topography's influence on wettability.

In retrospect, the utilisation of the surface coating technique might have assisted in the initial study by providing a form of roughened SS with similar characteristics to TS or even NS. SS in a roughened form is industrially and clinically non-viable due to the removal of the corrosion resistant surface layer of Cr_2O_3 . A TS replica, or TS itself, could theoretically be coated with Cr_2O_3 to provide the roughened SS for experimental *in vitro* study. An SS version of the NS surface could also be included to further elucidate the influence of its unique topography over that of chemistry.

1.3 - Topography vs. Chemistry

The alignment of cells to the mask border brought about numerous questions as to the hierarchy of cues on the rough and smooth materials. As previously discussed (Chapter 6, Discussion), I believe that the alignment at the mask border was due to a difference between the chemistry of the coating and original surface, supported by the observation that

no alignment could be observed on TS sputtered with titanium. However, it must be acknowledged that the mask border line did present itself as a continuous 50nm step, to which cells could align to, in the midst of other relatively random albeit larger features. Cell alignment of this kind has been demonstrated by Andersson *et al* with 40nm continuous groove edges (Andersson *et al.*, 2003). A possible method of addressing this would be to fabricate micron dimension grooves orthogonally arranged with nanometric grooves or interspersed with other features. This has been investigated indirectly by Britland using chemically adhesive tracks with 5nm nanometre steps, although cell alignment could not be directly attributed to the nanometric dimension of the strip (Britland *et al.*, 1996a), and in another study he completely dismisses this topographical influence (Britland *et al.*, 1996b). Britland also demonstrated that sensitivity to the chemistry/nanotopography diminished when laid orthogonally to grooves of 5 μ m or larger in depth, however, most features encountered on both TS and NS are far below these dimensions, therefore this phenomenon could possibly apply.

Another possible method of confirming the influence of surface chemistry might also be to reduce the thickness of the evaporation coat. Kasemo and Lausmaa noted that the cell interaction is limited to the first 1nm (Kasemo and Lausmaa, 1988), therefore thinner coatings of 10 or 5nm could be utilised provided they present themselves as a homogenous surface, and therefore decreasing the material step down below the known limits of cell alignment sensitivity (Wojciak-Stothard *et al.*, 1996). A possible argument against doing this is that greater fibroblast density was observed by Jain and Von Recum when increasing the thickness of sputtered titanium on PET from 20nm gradually up to 350nm (Jain and von Recum, 2003). While this would indicate that the masking effect might be decreased with a lower thickness, further observations have noted that the thicker coating of titanium modified the surface roughness, thus introducing new factors that might account for the differences (Jain and von Recum, 2004).

If the difference between the surface chemistry of the original and the coated metal were confirmed as the cause of the cell alignment, then photolithographic techniques could be utilised to produce a number of surface chemistry patterns on different metal implant

surfaces (Winkelmann et al., 2003). For instance, cells have been demonstrated to be initially sensitive to Al_2O_3 (Scotchford et al., 2003). A pattern could be produced on roughened TS, allowing for small 'cell-size' circular patches of the underlying TS to be exposed through a mask of Al_2O_3 thus controlling initial cell adhesion and morphology. For osteoblasts, this inability to spread due to the surrounding Al_2O_3 and the presence of an underlying rough topography might encourage early differentiation into a bone forming phenotype. Apart from these examples, numerous other cytocompatible and even possibly cytotoxic metals could be experimented with to help organise and direct cellular interaction perhaps as a viable option of modifying commercially produced metal surfaces. The advantage of these patterned metal layers would be their stability and robustness compared to other wet chemical methods of surface modification.

2. Cell Growth, Morphology and Adhesion

As a model for general biological tissue interactions, the hTERT fibroblast cell line provided a reliable and reproducible model with which to gauge the reactions of the surfaces.

2.1 – Cell Growth, Morphology and Adhesion on Metal Surfaces

In summary, cell reactivity to the original sample types demonstrated that none of the three metals utilised, SS, titanium or TAN, proved problematic for fibroblasts. The electropolished topographies of the metals demonstrated some nanotopographical features, and cells were observed to detect these features - however, this did not affect cell adhesion, spreading or growth. The surface morphology of TS and NS differed considerably, therefore the reaction to both were summarised separately. Fibroblasts on TS appeared less spread (although this could not be confirmed quantitatively) with numerous filopodia probing the surface. Cells on TS also displayed a lower average number and length of focal adhesion sites in comparison with the electropolished surfaces, SS, TE, NE and Th. These differences did not equate to any notable differences for cell growth either qualitatively or quantitatively on TS compared with its electropolished counterpart, TE. For NS, the differences were more pronounced, specifically due to the influence of the protruding β -phase microspikes. In comparison to the other surfaces and materials, cells were less spread

on NS and generally adopted a more elongated morphology with filopodia extending and attaching to the protruding β -phase microspikes. The microspikes were also observed intracellularly disrupting the cells microtubule network, and influenced the location of focal adhesion sites. On average, the number and length of focal adhesion sites on NS were lower than any other material or surface tested. The observed cell behaviour culminated in protracted or inhibited cell growth on the surface of NS.

The introduction of coated materials provided a model whereby the general morphological intricacies of the standard surface topographies, especially NS, could be retained while the original surface chemistry was masked. The results conclusively demonstrated that for NS, its unique surface topography was the primary factor in the observed inhibition of cell growth on the surface. This result inspired me to mimic this topography by initiating the microfabrication of pyramid arrays discussed in Section 3. The coating model was extended to TS and demonstrated, in this instance, that the roughened surface morphology of this material was equally conducive to cell growth with different surface chemistries. Studies into coated SS could be interpreted as further evidence for the fibroblastic compatibility of its relatively featureless surface, or that electropolished titanium and gold are also compatible materials.

2.2 – The Cell Cycle and Focal Adhesions

It was proposed that cell cycle progress on NS was protracted or inhibited because focal adhesion maturation and cell spreading were impaired to below a sufficiency threshold, due to the involvement of topographical features found on NS. While the growth rates, demonstrated by cell counts, conclusively established low growth on NS, these findings would be further supported by direct evidence of proliferation. Due to time constraints, this was not investigated further, however, cell cycle studies would be the next step in the expansion of the theory. The S-phase is the most straightforward cell cycle phase for labelling, as it is the only phase where the incorporation of extracellular nucleosides occurs (Alberts et al., 1994). This mechanism can be exploited by pulse labelling cultures with tritiated thymidine ($6\text{-}^3\text{H}$) or bromodeoxyuridine (BrdU), and visualising the stained nuclei cells in S-phase either by autoradiography or fluorescence labelling. If the incorporation of

this label ($6\text{-}^3\text{H}$ or BrdU) was delayed for at least 24 to 48hr after seeding on NS, then incorporation as a result of S-phase initiation could be relatively certain to have occurred, or not, due to the influence of the substrate. The involvement of cell shape and adhesion is paramount for the transition of G1 to the S-phase, and demonstrated to be modified on NS; therefore evidence of low or no proliferation would further strengthen this 'sufficiency threshold' hypothesis.

It was interesting to note that the number and length of focal adhesion sites on the flatter surfaces (Th, SS, TE and NE) were all similar. This indicates that although there was high variability due to a random sampling of cells, the lack of visible topographical restriction allowed for an equilibrium of adhesion lengths and numbers to develop. I have previously shown that regardless of the cell cycle phase, the actual area of cell adhesion remains surprisingly consistent, further evidence of a possible finite area/amount of adhesion (Meredith *et al.*, 2004). In one respect, these observations actually increase the significance of the lower number and length of measurements observed on both TS and NS. As hypothesised in the Chapter 3, the lower lengths and numbers observed on NS might fall below a certain sufficiency threshold.

The use of microfabrication techniques might help prove this 'sufficiency threshold' hypothesis. The fabrication of surface chemistries to regulate cell shapes is well established (Chen *et al.*, 1997; Ingber *et al.*, 1995; Ireland *et al.*, 1989), however, a means to confine focal adhesion lengths or morphology is not common. Chen utilised the micro-contact printing of circular fibronectin patches of $3\mu\text{m}$ or more in diameter and observed them to be able to elicit or prevent cell growth dependent on their sizes (Chen *et al.*, 2003; Chen *et al.*, 1997). While micro-contact printing could be promising, another possibility might be to combine today's micro and nanofabrication techniques (Wilkinson, 2004) with the Ireland and O'Neill system of vanadium (adhesive) patterning on a polyHEMA (non-adhesive) background (Ireland *et al.*, 1989; O'Neill *et al.*, 1990). In this instance, a variety of patterns could be created such as squares, circles or strips of different dimensions and spacing that could be experimented with to modulate cell adhesion similar to that found on NS. Not only could experimentation with this system prove the 'sufficiency threshold' hypothesis,

but also provide a tool for investigating the importance of focal adhesion morphology, size and spacing for cells.

2.4 - Microtubules

As discussed in Chapter 3, the protruding β -phase microspikes on NS disrupted the formulation and maintenance of a "normal" microtubule cytoskeleton, but this effect was not conclusively found to contribute to the inhibition of cell growth on NS. The main effect of a disrupted microtubule network may be a generally compromised ability to transport components such as organelles and mRNA within the cell. The attempt to stain mitochondria, which failed due to the metallic substrates, was undertaken because the distribution and movement of mitochondria could have allowed an adequate demonstration of any impaired microtubule function. In a future experiment one could attempt to circumvent the incompatibility of this membrane staining technique by immunostaining mitochondrial membrane-bound proteins involved in oxidative phosphorylation.

2.5 - Gene expression

The gene expression results of Chapter 5 demonstrated that for implant metals, the primary cause of regulation changes was the surface topography. The lower instance of significant changes on the electropolished SS, TE and NE in comparison with Thermanox concurred with the cell growth data in demonstrating that the surface chemistries of the metals utilised, SS, titanium or TAN, were not problematic for fibroblasts. The regulation of numerous genes was affected by the presence of the standard titanium topography (TS), and while some were investigated further, time did not permit the investigation of others. The most notable gene changes indicated variance in the ECM, which was investigated by means of the endogenous fibronectin (Fn) production. While early differences were observed between the rough and smooth topographies (TE and TE), at the later timepoints there were no differences in the Fn network supported by the confluent cell layers. In the production of the fibrous tissue observed in the *in vivo* foreign body reaction, collagen is also a very important component and therefore its formation on the surfaces might also be of interest in demonstrating possible differences related to chemistry and/or topography (Shannon *et al.*, 1997).

The necessity of the amplification method for mRNA extracted from cells on NS was unfortunate in possibly masking many of the significant upregulations due to the cell interaction with the surface topography. As previously mentioned, it might have been possible to circumvent mRNA amplification by utilising higher cell numbers and then incubating for a shorter time. These shorter times would also be interesting for TS to compare if the reaction changed over the experimental time-period set. While longer time-periods would be more in keeping with the *in vivo* situation, the observation of apoptosis at 10 days on the generally compatible TS suggests that new factors such as media depletion might interfere with any results obtained with regard to static fibroblast cultures.

One limiting factor in further microarray studies is the production of a sufficient number of 49mm diameter discs, as these are expensive with respect to both materials and processing. With the exception of NS, this might possibly be avoided in future with the use of large resin surface replicas taken from various metallic surfaces. Numerous topographies from different metals could be introduced with identical or varying surface chemistries. The use of replicates might also aid in improving the consistency of the results, as it would allow identical replicates (the exact same topography) to be utilised for each experimental repeat of a study.

It was interesting that the most significant changes in gene regulation were observed for TS, generally noted as being the most compatible material *in vivo* in relation to soft tissue adhesion (Ungersbock *et al.*, 1994; Ungersbock *et al.*, 1996). The gene regulation results for this *in vitro* study could therefore possibly demonstrate cues to help elucidate the mechanism whereby soft tissue adheres under motion to the plate. However, one drawback of the current culture system is a lack of motion or shear. As a logical next step the introduction of motion, possibly through flow, that might emulate or at least attempt to mimic a situation found *in vivo*, would be of benefit. In this instance, staining techniques, cell growth and gene expression might uncover a considerable amount of information concerning fibroblastic changes that allow it to adhere to the surface under motion.

2.6 – Standard TAN ‘In Vivo’

Regarding the initial aim, introduced in Chapter 1, of assessing the *in vitro* soft tissue compatibility of TAN, the results prove to be promising for the material, however, more negative for the ‘standard topography’. Electropolished TAN (NE) demonstrates that the material promotes cell adhesion and growth, however, in the form of its standard topography it does not. In speculating how this standard topography of TAN might perform *in vivo*, it actually possesses characteristics of an undesirable material, summarised in the following points.

- The lower adhesion and growth suggests inhibition or difficulties during the initial granulation phase of wound healing, where rapid colonisation of the area is essential. This poor cell adhesion and lack of cell coverage might result, in areas of motion, in the formation of a liquid filled void around the implant and possibly further related complications. While it might be argued that the numerically similar roughness of standard roughened titanium (TS) performs well under motion *in vivo*, this study has also demonstrated that TS also performs equally well *in vitro*.
- The jagged sharp edged surface of NS might prove a source of irritation for soft tissue and could help sustain inflammation at the surface. Misiek *et al.* demonstrated considerable difference of *in vivo* soft tissue reactions to implanted hydroxyapatite based on their form, and concluded that irregular sharp edged surfaces produced sustained soft tissue irritation and inflammation (Misiek *et al.*, 1984).
- Macrophage reaction could also prove problematic, as the surface demonstrates two separate sources for its activation: roughness and particles. *In vitro*, titanium surface roughness has been demonstrated to influence macrophage activity, assayed by their production of the pro-inflammatory cytokines TNF- α , IL-1 β and IL-6 (Refai *et al.*, 2005; Takabe *et al.*, 2003), therefore it would be reasonable to assume that the rough surface on NS might elicit a similar reaction. In addition, the presence of metallic particles that can be removed with relative ease might also trigger phagocytosis; in the instance of titanium alloy particles (Ti-6V-7Al) this also initiated TNF- α , IL-1 β and IL-6 cytokine production (Haynes *et al.*, 1997; Rogers *et al.*, 1997). Both TNF- α and IL-6 are also associated with the downregulation of

fibroblast proliferation and could therefore prove problematic for fibroblast colonisation and consequently soft tissue integration.

2.7 - Further Studies

Whilst *in vitro*, the interaction between inflammation and fibrous tissue formation is downplayed due to the simplicity of focusing on a single biological model, it would appear that a study into the interplay between the two systems would be the next logical step in studying soft tissue reaction to the materials. Co-cultures of fibroblasts and macrophages *in vitro* would be difficult to establish and such systems are not commonly found in the literature (Bacakova *et al.*, 1999). A more practical method would be through indirect co-culturing means where media from macrophages adherent on a material surface (in the first instance, NS) would be used on fibroblasts cultured separately on NS. Thus, the media from the macrophages could be assayed for cytokines, and also the downstream effect of cytokine production could be assessed directly on the fibroblasts, possibly through gene regulation studies.

3. Microfabrication

The utilisation of AFM surface characterisation demonstrated that the profile of NS consisted of microspikes with surprisingly uniform dimensions. These microspikes were observed to interfere with numerous cellular functions and hypothesised to cause the inhibition of cell growth observed on NS. Utilising the surface morphology information, a microtopography was designed inspired by the microspikes observed on NS.

3.1 – Pyramid Topography

The pyramid topography was a compromise of required design features and fabrication limitations, and could possibly be more accurately described as a depiction of the essential topographical features of NS. As an initial attempt, this design was successful in incorporating some key features such as an underlying smooth surface with protruding features. Cell reactivity on these features also mimicked those found on NS, with elongated cell morphology, lower mean lengths and numbers of focal adhesions, and disruptions to the microtubule network. While qualitative and quantitative studies demonstrated lower cell

growth on the topography, the presence of a confluent monolayer of cells surrounding the topography area might indicate the possible migration of cells from the topography. Time-lapse video microscopy could prove useful in establishing the movement of the cells, and possibly a proliferative assay such as $6\text{-}^3\text{H}$ or BrdU could be employed to confirm any cell proliferation directly on the topography. However, the fact remains that this attempt at mimicking the surface of NS has produced similar cell behaviour, indicating that this aspect contributes significantly if not completely to the cell behaviour observed on NS.

3.2 – Further Studies

As a design concept, this topography offers a number of adjustable features such as pyramid size, width of the planar run-off spacing and feature pitching. Changes in the arrangement of the pattern could be made with irregular patterning of the features over the surface and possibly even different sized pyramids on the same sample. Initially, the pyramid design was to be an inverted cone-shape, although this proved difficult to fabricate. Given more time this might be an interesting addition, as it would further complicate the surface by reducing the amount of planar surfaces and straight edges available for cell interaction.

While the assessment of fibroblast interaction on these surfaces is important, the reactions of other cell types that thrive on rougher topographies might also prove interesting. Osteoblast reactivity on the larger dimension pyramids (33 μm width) produced by Liao proved promising in demonstrating the production of bone matrix markers (Liao et al., 2003), however, the smaller pyramids and surface run-off between the features should further enhance the cuboidal morphology required by osteoblasts to differentiate into a bone-forming phenotype. Perhaps, even the omission of the surface run-off would be beneficial in this instance to mimic a more three-dimensional substrate of bone. Similarly, the documented preference of macrophages for surface roughness (Rich and Harris, 1981; Wojciak-Stothard *et al.*, 1995) might demonstrate increased production of inflammatory cytokines. While not necessarily beneficial, investigations into different permutations of the topography might help elucidate cues for macrophage activation when adherent on implanted surfaces.

It should not be overlooked that the initial topography design originated from a non-cytocompatible metallic surface topography, created through conventional industrial methods. With the development of numerous new metallic implant materials there is considerable scope for investigating these materials in the search for features that might enhance or decrease the compatibility of surfaces to soft and hard tissue. While it might be argued that the fabrication of microtopographies for metal implants would be difficult, this avenue of research could provide recommendations on general improvement of the surfaces utilised. Taking NS as an example, the protrusion of the β -phase microspikes originate from the acid-etching step that dissolves the harder β -phase particles at a slower rate than the α -phase. My studies using coatings and microfabricated mimicry surfaces demonstrated it was this form of topography that was unfavourable *in vitro* for fibroblasts. The results obtained with these and all the other materials further suggest that another form of roughening should be introduced for TAN to modify the existing type of roughness morphology, possibly to resemble that of standard titanium (TS). A reciprocal trend could be developed, as metal topographies could provide inspiration for fabricated microtopographies that in turn could be utilised to produce optimal metallic implant topographies.

4. Summary

- The initial aim of this project, to assess the *in vitro* soft tissue compatibility of TAN, demonstrated that while the material was suitable, its standard topography in its current form was not. For implanting TAN in sites near soft tissues, a different surface topography or roughening treatment would be recommended.
- With reference to the Williams definition for material biocompatibility; that a material should elicit an “*appropriate host response in a specific application*” (Williams, 1999), the TAN material would still be classed as biocompatible for soft tissue. Result for NS, however, indicate that its topography might preclude its use as a biocompatible material; whereas its electropolished counterpart (NE) is biocompatible.
- The assessment of surface topography, especially for rough surfaces, cannot be reduced into numerical parameters such as roughness height. The roughness

morphology of a surface is far more important and comprehensive assessment utilising numerous methods is essential to allow an accurate representation of the surface roughness.

- The behavioural cues for fibroblasts on implant metal surfaces were generally confined to the influence of surface topography over that of surface chemistry.
- Cell behaviour on an artificial, representative NS topography compared with that found on NS, suggesting that the microspike surface feature of NS contributed significantly if not completely to the observed cell growth suppression.
- The microfabrication of specific surface characteristics identified from implant metals is a novel approach into elucidating important factors of implant surface topographies. As an initial design, the pyramid surface proved promising for further studies utilising design variations and investigating other cell types.
- It is hoped that the experimental approach applied and the general concepts discussed in this study might aid in future developments of metal implants for optimisation of both soft and hard tissue integration to the metal implant.

Chapter 9 – References

- Abiko, Y. and Brunette, D. M.** (1993). Immunohistochemical investigation of tracks left by the migration of fibroblasts on titanium surfaces. *Cells and Materials* **3**, 2, 161-170.
- Abrahamsson, I., Zitzmann, N. U., Berglundh, T., Linder, E., Wennerberg, A. and Lindhe, J.** (2002). The mucosal attachment to titanium implants with different surface characteristics: an experimental study in dogs. *Journal of Clinical Periodontology* **29**, 5, 448-455.
- Adbelsalam, M. E., Bartlett, P. N., Kelf, T. and Baumberg, J.** (2005). Wetting of regularly structured gold surfaces. *Langmuir* **21**, 1753-1757.
- Albrektsson, T.** (1990). Tissue reactions to metallic biomaterials. In *Implant bone interface*, (ed. J. Older). London: Springer-Verlag Ltd.
- Alberts, B., Bray, D., Lewis, J., Raff, M., Roberts, K. and Watson, J. D.** (1994). *Molecular Biology of the Cell*. New York & London: Garland Publishing.
- Anderson, J. M., Cook, G., Costerton, B., Hanson, S. R., Hensten-Pettersen, A., Jacobsen, N., Johnson, R. J., Mitchell, R. N., Pasmore, M., Schoen, F. J., Shirliff, M. and Stoodley, P.** (2004). 4. Host reactions to biomaterials and their evaluation. In *Biomaterials Science: an introduction to materials in medicine*, (eds B. D. Ratner A. S. Hoffman F. J. Schoen and J. E. Lemons). Amsterdam: Elsevier Academic Press.
- Anderson, J. M.** (1999). The cellular cascades of wound healing. In *Bone Engineering*, (ed. J. E. Davies). Toronto: em squared.
- Andersson, A. S., Olsson, P., Lidberg, U. and Sutherland, D. S.** (2003). The effects of continuous and discontinuous groove edges on cell shape and alignment. *Exp Cell Res.* **288**, 1, 177-188.
- Andrade, J. D.** (1985a). Chapter 1: Introduction to Surface Chemistry and Physics of Polymers. In *Surface and Interfacial Aspects of Biomedical Polymers: Surface Chemistry and Physics*, vol. 1 (ed. J. D. Andrade). New York and London: Plenum Press.
- Andrade, J. D.** (1985b). Chapter 7: The Contact Angle and Interface Energetics. In *Surface and Interfacial Aspects of Biomedical Polymers: Surface Chemistry and Physics*, vol. 1 (ed. J. D. Andrade). New York and London: Plenum Press.
- Anselme, K., Bigarelle, M., Noel, B. and Hardouin, P.** (2002). Effect of grooved titanium substratum on human osteoblastic cell growth. *J Biomed Mater Res A* **60**, 529-540.
- Anselme, K., Bigarelle, M., Noel, B., Dufresne, E., Judas, D., Iost, A. and Hardouin, P.** (2000a). Qualitative and quantitative study of human osteoblast adhesion on materials with various surface roughness. *J Biomed Mater Res* **49**, 155-166.
- Anselme, K., Linez, P., Bigarelle, M., Le Maguer, D., Le Maguer, A., Hardouin, P., Hildebrand, H., Iost, A. and Leroy, J. M.** (2000b). The relative influence of the topography and chemistry of TiAl6V4 surfaces on osteoblastic cell behaviour. *Biomaterials* **21**, 1567-1577.
- Anselme, K., Noel, B. and Hardouin, P.** (1999). Human osteoblast adhesion on titanium alloy, stainless steel, glass and plastic substrates with same surface topography. *J Mater Sci Mater Med* **10**, 815-819.
- Aronsson, B. O., Lausmaa, J. and Kasemo, B.** (1997). Glow discharge plasma treatment for surface cleaning and modification of metallic biomaterials. *J Biomed Mater Res* **35**, 1, 49-73.

- Bacakova, L., Herget, J. and Wilhelm, J. (1999). Influence of Macrophages and Macrophage-Modified Collagen I on the Adhesion and Proliferation of Vascular Smooth Muscle Cells in Culture. *Physiological Research* **48**, 341-351.
- Baharloo, B., Textor, M. and Brunette, D. M. (2005). Substratum roughness alters the growth, area, and focal adhesions of epithelial cell, and their proximity to titanium surfaces. *J Biomed Mater Res A* **74**, 12-22.
- Ballock, R. T., Heydemann, A., Wakefield, L. M., Flanders, K. C., Roberts, A. B. and Sporn, M. B. (1993). TGF-Beta1 prevents hypertrophy of epiphyseal chondrocytes: regulation of gene expression for cartilage matrix proteins and metalloproteases. *Dev Biol.* **158**, 414-429.
- Barrett, J. C. and Kawasaki, E. S. (2003). Microarray: the use of oligonucleotides and cDNA for the analysis of gene expression. *Drug Discovery Today* **8**, 3, 134-141.
- Bataille, L., Judas, D., Rocher, P., Laffargue, P., Lecomte-Houcke, M., Iost, A., Lefevre, A. and Hildebrand, H. (1997). In vitro and in vivo biocompatibility of stainless steel as a function of surface treatments: roughness and surficing with hydroxyapatite. *Rev Stomatol Chir Maxillofac* **98**, Suppl. 1, 58-60.
- Berry, C. C., Charles, S., Wells, S., Dalby, M. J. and Curtis, A. (2003). The influence of transferrin stabilised magnetic nanoparticles on human dermal fibroblasts in culture. *Int J Pharm* **2004**, 269, 1.
- Bershadsky, A., Balaban, N. Q. and Geiger, B. (2003). Adhesion-dependent cell mechanosensitivity. *Annu. Rev. Cell Dev. Biol.* **19**, 677-95.
- Bershadsky, A. and Geiger, B. (1999). Cytoskeleton-associated anchor and signal transduction proteins: Introduction. In *Guidebook to the extracellular matrix, anchor, and adhesion proteins*, (eds T. Kreis and R. Vale). Oxford: Oxford University Press.
- Bershadsky, A. D., Tint, I. S., Neyfakh, A. A., Jr. and Vasiliev, J. M. (1985). Focal contacts of normal and RSV-transformed quail cells. Hypothesis of the transformation-induced deficient maturation of focal contacts. *Exp Cell Res* **158**, 2, 433-44.
- Bigarelle, M. and Anselme, K. (2005). Statistical correlation between cell adhesion and proliferation on biocompatible metallic materials. *J Biomed Mater Res A* **71**, 1, 36-46.
- Bigarelle, M., Anselme, K., Noel, B., Ruderman, I., Hardouin, P. and Iost, A. (2002). Improvement in the morphology of Ti-base surfaces: a new process to increase in vitro osteoblast response. *Biomaterials* **23**, 1563-1577.
- Black, J. (1988). Does corrosion matter? *J Bone Joint Surg Br* **70**, 4, 517-20.
- Bordji, K., Jouzau, J. Y., Mainard, D., Payan, E., Delagoutte, J. P. and Netter, P. (1996). Evaluation of the effect of three surface treatments on the biocompatibility of 316L stainless steel using human differentiated cells. *Biomaterials* **17**, 5, 491-500.
- Boudreau, N. J. and Jones, P. L. (1999). Extracellular matrix and integrins signalling: the shape of things to come. *Biochem J.* **339**, 481-488.
- Boyan, B. D., Lossdorfer, S., Wang, L., Zhao, G., Lohmann, C. H., Cochran, D. L. and Schwartz, Z. (2003). Osteoblasts generate an osteogenic microenvironment when grown on surfaces with rough microtopographies. *Eur Cell Mater* **6**, 22-27.
- Bozzola, J. J. and Russell, L. D. (1992). *Electron Microscopy; Principles and Techniques for Biologists*. Boston: Jones and Bartlett Publishers, Inc.
- Brett, P. M., Harle, J., Salih, V., Mihoc, R., Olsen, I., Jones, F. and Tonetti, M. (2004). Roughness response genes in osteoblasts. *Bone* **35**, 124-133.

- Brett, P. M., Harle, J., Salih, V., Olsen, I., Jones, F. and Tonetti, M.** (2003). Expression profiling on bone cells grown on titanium surfaces. In *18th European Conference on Biomaterials*, pp. T005. Stuttgart, Germany.
- Britland, S., Morgan, H., Wojciak-Stothard, B., Riehle, M., Curtis, A. and Wilkinson, C.** (1996a). Synergistic and hierarchical adhesive and topographic guidance of BHK cells. *Exp Cell Res* **228**, 2, 313-25.
- Britland, S., Perridge, C., Denyer, M., Morgan, H., Curtis, A. and Wilkinson, C.** (1996b). Morphogenetic guidance cues can interact synergistically and hierarchically in steering nerve cell growth. *Exp. Biol. Online* **1**, 2.
- Brodbeck, W. G., Nakayama, Y., Matsuda, T., Colton, E., Ziats, N. P. and Anderson, J. M.** (2002a). Biomaterial surface chemistry dictates adherent monocyte/macrophage cytokine expression in vitro. *Cytokine* **18**, 6, 311-319.
- Brodbeck, W. G., Shive, M. S., Colton, E., Ziats, N. P. and Anderson, J. M.** (2002b). Interleukin-4 inhibits tumor necrosis factor-alpha-induced and spontaneous apoptosis of biomaterial-adherent macrophages. *J. Lab Clin. Med.* **139**, 2, 90-100.
- Brogi, E., Wu, T., Namiki, A. and Isner, J. M.** (1994). Indirect angiogenic cytokines upregulate VEGF and bFGF gene expression in vascular smooth muscle cells, whereas hypoxia upregulates VEGF expression only. *Circulation* **90**, 2, 649-652.
- Brunc, D., Hellborg, R., Whitlow, H. J. and Hunderi, O.** (1997). Surface characterization. A user's sourcebook. Weinheim: Scandinavian Science Publisher, Wiley-VCH.
- Brunette, D. M.** (2001). 15. Principles of cell behavior on titanium surfaces and their application to implanted devices. In *Titanium in medicine*, (eds D. M. Brunette P. Tengvall M. Textor and P. Thomsen). Berlin, Heidelberg, New York: Springer.
- Brunette, D. M. and Chehroudi, B.** (1999). The effects of the surface topography of micromachined titanium substrata on cell behaviour in vitro and in vivo. *J Biomech Eng.* **121**, 1, 49-57.
- Brunette, D. M.** (1988). The effect of implant surface topography on behaviour of cells. *Int J Oral Maxillofac Implants.* **3**, 4, 231-246.
- Brunette, D. M.** (1986). Fibroblast on micromachined substrate orient hierachically to grooves of different dimensions. *Exp Cell Res* **164**, 11-26.
- Brunski, J. B.** (2004). 2.9 Metals. In *Biomaterials Science: an introduction to materials in medicine*, (eds B. D. Ratner A. S. Hoffman F. J. Schoen and J. E. Lemons). Amsterdam: Elsevier Academic Press.
- Bundy, K. J., Harris, L., G., Rahn, B. A. and Richards, R. G.** (2001). Measurement of fibroblast and bacterial detachment from biomaterials using jet impingement. *Cell Biol Int* **25**, 4, 289-307.
- Burridge, K. and Chrzanowska-Wodnicka, M.** (1996). Focal adhesions, contractility, and signaling. *Annu. Rev. Cell Dev. Biol.* **12**, 463-519.
- Buser, D., Weber, H. P., Donath, K., Fiorelli, J. P., Paquette, D. W. and Williams, R. C.** (1992). Soft tissue reactions to non-submerged unloaded titanium implants in beagle dogs. *Journal of Peridontology* **63**, 3.
- Campbell, N. A.** (1996). *Biology*. New York: The Benjamin/Cummings Publishing Company, Inc.
- Campisi, J.** (1997). The biology of replicative senescence. *Eur J Cancer* **33**, 5, 703-9.

- Carinci, F., Pezzetti, F., Volinia, S., Francioso, F., Arcelli, D., Marchesini, J., Caramelli, E. and Piattelli, A. (2004). Analysis of MG63 osteoblastic-cell response to a new nanoporous implant surface by means of a microarray technology. *Clin. Oral Impl. Res.* **15**, 180-186.
- Carinci, F., Pezzetti, F., Volinia, S., Francioso, F., Arcelli, D., Marchesini, J., Scapoli, L. and Piattelli, A. (2003a). Analysis of osteoblast-like MG63 cells' response to a rough implant surface by means of DNA microarray. *J Oral Implantol* **29**, 5, 215-20.
- Carinci, F., Volinia, S., Pezzetti, F., Francioso, F., Tosi, L. and Piattelli, A. (2003b). Titanium-cell interaction: analysis of gene expression profiling. *J.Biomed.Mater.Res.* **66B**, 1, 341-346.
- Cawston, T. E. (1995). Proteinases and connective tissue breakdown. In *Mechanisms and models in rheumatoid arthritis*, (eds B. Henderson J. C. W. Edwards and E. R. Pettipher). London, San Diego, New York, Boston, Sydney, Tokyo, Toronto: Academic Press.
- Chapman, S. K. (1986). Working with a Scanning Electron Microscope. Chislehurst, England: Lodgemark Press Ltd.
- Chchroudi, B., Gould, T. R. and Brunette, D. M. (1989). Effects of a grooved titanium-coated implant surface on epithelial cell behavior in vitro and in vivo. *J Biomed Mater Res* **23**, 9, 1067-85.
- Chen, C. S., Tan, J. and Tien, J. (2004). Mechanotransduction at cell-matrix and cell-cell contacts. *Annu. Rev. Biomed. Eng* **6**, 275-302.
- Chen, C. S., Alonso, J. E., Ostuno, E., Whitesides, G. M. and Ingber, D. E. (2003). Cell shape provides control of focal adhesion assembly. *Biochem Biophys Res Commun* **307**, 2, 355-361.
- Chen, C. S., Mrksich, M., Huang, S., Whitesides, G. M. and Ingber, D. E. (1997). Geometric control of cell life and death. *Science* **276**, 5317, 1425-8.
- Chen, W. T. and Singer, S. J. (1982). Immunoelectron microscopic studies of the sites of cell-substratum and cell-cell contacts in cultured fibroblasts. *J Cell Biol* **95**, 1, 205-22.
- Chou, L., Firth, J. D., Nathanson, D., Uitto, V. J. and Brunette, D. M. (1996). Effects of titanium on transcriptional and post-transcriptional regulation of fibronectin in human fibroblasts. *J Biomed Mater Res* **31**, 2, 209-17.
- Chou, L., Firth, J. D., Uitto, V. J. and Brunette, D. M. (1995). Substratum surface topography alters cell shape and regulates fibronectin mRNA level, mRNA stability, secretion and assembly in human fibroblasts. *J.Cell Sci.* **108** (Pt 4), 1563-1573.
- Clarke, P. G. H. (1990). Developmental cell death: morphological diversity and multiple mechanisms. *Anat Embryol* **181**, 195-213.
- Clark, P., Connolly, P., Curtis, A., Dow, J. A. and Wilkinson, C. (1991). Cell guidance by ultrafine topography in vitro. *J Cell Sci*, 1, 73-7.
- Clark, P., Connolly, P., Curtis, A. S., Dow, J. A. and Wilkinson, C. D. (1990). Topographical control of cell behaviour: II. Multiple grooved substrata. *Development* **108**, 4, 635-644.
- Cleveland, D. W. (1999). Tubulin and associated proteins. In *Guidebook to the cytoskeletal and motor proteins*, (eds T. Kreis and R. Vale), pp. 189-193. Oxford: Oxford University Press.
- Clivaz, X., Emch, R., Descouts, P., Vaudaux, P., Lew, D., Delmi, M. and Vasey, H. (1990). A multidisciplinary approach to the problem of tissue and microbial adhesion to metallic implant material. *Clin Materials* **5**, 2-4, 191-200.

- Cole, P. A., Zlowodzki, M. and Kregor, P. J.** (2003). Less Invasive Stabilization System (LISS) for fractures of the proximal tibia: indications, surgical technique and preliminary results of the UMC Clinical Trial. *Injury* **34 Suppl 1**, 16-29.
- Conner, S. D. and Schmid, S. L.** (2003). Regulated portals of entry into the cell. *Nature* **422**, 37-44.
- Cooper, G. M. and Hausman, R. E.** (2003). *The Cell: A Molecular Approach*: Sinauer Associates, Inc.
- Craighead, H. G., Turner, S. W., Davies, R. C., James, C., Perez, A. M., St John, P. M., Isaacson, M., Kam, L., Shain, W., Turner, J. N. and Banker, G.** (1998). Chemical and topographical surface modification for control of central nervous system cell adhesion. *Journal of Biomedical Microdevices* **1**, 1, 49-64.
- Curtis, A. S., Gadegaard, N., Dalby, M. J., Riehle, M. O., Wilkinson, C. D. and Aitchison, G.** (2004). Cells react to nanoscale order and symmetry in their surroundings. *IEEE Trans Nanobioscience* **3**, 1, 61-5.
- Curtis, A. S. and Varde, M.** (1964). Control of cell behavior: topological factors. *J Natl Cancer Inst* **33**, 15-26.
- Dalby, M. J., Riehle, M., Sutherland, D. S., Agheli, H. and Curtis, A.** (2005). Morphological and micrarray analysis of human fibroblasts cultured on nanocolumns produced by colloidal lithography. *Eur Cell Mater* **9**, 1-8.
- Dalby, M. J., Gadegaard, N., Riehle, M. O., Wilkinson, C. D. and Curtis, A. S.** (2004a). Investigating filopodia sensing using arrays of defined nano-pits down to 35 nm diameter in size. *Int J Biochem Cell Biol* **36**, 10, 2015-2025.
- Dalby, M. J., Riehle, M. O., Johnstone, H., Affrossman, S. and Curtis, A. S.** (2004b). Investigating the limits of filopodial sensing: a brief report using SEM to image the interaction between 10 nm high nano-topography and fibroblast filopodia. *Cell Biol Int* **28**, 3, 229-236.
- Dalby, M. J., Berry, C. C., Riehle, M., Sutherland, D. S., Agheli, H. and Curtis, A.** (2004c). Attempted endocytosis of nano-environment produced by colloidal lithography by human fibroblasts. *Exp Cell Res* **395**, 387-394.
- Dalby, M. J., Riehle, M., Yarwood, S. J., Wilkinson, C. and Curtis, A.** (2003). Nucleus alignment and cell signaling in fibroblasts: response to a micro-grooved topography. *Exp Cell Res* **284**, 2, 274-82.
- Dalby, M. J., Yarwood, S. J., Riehle, M., Johnstone, H., Affrossman, S. and Curtis, A.** (2002). Increasing fibroblast response to materials using nanotopography: morphological and genetic measurements of cell response to 13-nm-high polymer demixed islands. *Exp Cell Res* **276**, 1-9.
- Dartsch, D. C., Schaefer, A., Boldt, S., Kolch, W. and Marquardt, H.** (2002). Comparison of anthracycline-induced death of human leukemia cells: programmed cell death versus necrosis. *Apoptosis* **7**, 6, 537-548.
- Davies, P. F., Robotewskyj, A. and Griem, M. I.** (1993). Endothelial cell adhesion in real time. Measurements in vitro by tandem scanning confocal image analysis. *J Clin Invest* **91**, 6, 2640-52.
- Davies, J. E.** (1996). In vitro modeling of the bone/implant interface. *Anat Rec.* **1996** **245**, 2, 426-445.

- Davies, J. E.** (1988). The importance and measurement of surface charge species in cell behaviour at the biomaterial interface. In *Surface Characterization of Biomaterials*, (ed. B. D. Ratner). Amsterdam: Elsevier Science Publishers.
- Dee, K. P., Puelo, D. A. and Bizios, R.** (2002a). Biomaterials. In *An Introduction To Tissue-Biomaterials Interactions*, (eds K. P. Dee D. A. Puelo and R. Bizios): John Wiley & Sons Inc.
- Dee, K. P., Puelo, D. A. and Bizios, R.** (2002b). Wound Healing. In *An Introduction To Tissue-Biomaterials Interactions*, (eds K. P. Dee D. A. Puelo and R. Bizios): John Wiley & Sons Inc.
- Diehn, M., Sherlock, G., Binkley, G., Jin, H., Matese, J. C., Hernandez-Boussard, T., Rees, C. A., Cherry, J. M., Botstein, D., Brown, P. O. and Alizadeh, A. A.** (2003). SOURCE: a unified genomic resource of functional annotations, ontologies, and gene expression data. *Nucleic Acids Res* **31**, 1, 219-23.
- Diener, A., Nebe, B., Luthen, F., Becker, P., Beck, U., Neumann, H. G. and Rychly, J.** (2005). Control of focal adhesion dynamics by material surface characteristics. *Biomaterials* **26**, 4, 383-92.
- Disegi, J. A.** (2000). Titanium alloys for fracture fixation implants. *Injury* **31 Suppl 4**, 14-17.
- Disegi, J. A. and Eschbach, L.** (2000). Stainless steel in bone surgery. *Injury* **31 Suppl 4**, 2-6.
- Disegi, J. A.** (1998a). AO ASIF: Unalloyed Titanium Implant Material: AO Technical Commission (AOTK).
- Disegi, J. A.** (1998b). AO ASIF: Wrought 18% Chromium- 14% Nickel - 2.5% Molybdenum Stainless Steel Implant Material: AOTK.
- Disegi, J. A.** (1997). Anodizing Treatments for Titanium Implants. In *Sixteenth Southern Biomedical Engineering Conference*, pp. 129-132. Biloxi, MS, USA: IEEE.
- Disegi, J. A.** (1993). AO ASIF: Titanium - 6% Aluminium - 7% Niobium Implant Material: AO Technical Commission (AOTK).
- Disegi, J. and Wyss, H.** (1989). Implant materials for fracture fixation: a clinical perspective. *Orthopedics* **12** 1, 75-79.
- Dohle, J., Becker, W. and Braun, M.** (2002). Bone remodelling along a titanium hip arthroplasty stem after resection of a chondrosarcoma. *Arch Orthop Trauma Surg* **122**, 5, 291-294.
- Drake, B., Prater, C. B., Weisenhorn, A. L., Gould, S. A., Albrecht, T. R., Quate, C. F., Cannell, D. S., Hansma, H. G. and Hansma, P. K.** (1989). Imaging crystals, polymers, and processes in water with the atomic force microscope. *Science* **243**, 4898, 1586-9.
- Duggan, D. J., Bittner, M., Chen, Y., Meltzer, P. and Trent, J. M.** (1999). Expression profiling using cDNA microarrays. *Nt. Genet.* **21**, 1 Suppl, 10-14.
- Edelson, P. J. and Cohn, Z. A.** (1976). Purification and cultivation of monocyted and macrophages. In *In vitro methods in cell-mediated and tumor immunity*, (eds B. R. Bloom and J. R. David). New York: Academic Press.
- Eisenbarth, E., Velten, D., Muller, M., Thull, R. and Breme, J.** (2004). Biocompatibility of beta-stabilizing elements of titanium alloys. *Biomaterials* **25**, 26, 5705-13.
- Ellis, S. and Mellor, H.** (2000). Regulation of endocytic traffic by Rho family GTPases. *Trends in Cell Biology* **10**, 85-88.

- Etienne-Manneville, S.** (2004). Actin and microtubules in cell motility: which one is in control? *Traffic* **5**, 470-477.
- Everhart, L. P., Jr. and Rubin, R. W.** (1974). Cyclic changes in the cell surface. I. Change in thymidine transport and its inhibition by cytochalasin B in Chinese hamster ovary cells. *J Cell Biol* **60**, 2, 434-41.
- Everhart, T. E., Wells, O. C. and Oatley, C. W.** (1959). Factors affecting contrast and resolution in the scanning electron microscope. *J Electron Control* **7**, 97-111.
- Ezratty, E. J., Partridge, M. A. and Gundersen, G. G.** (2005). Microtubule-induced focal adhesion disassembly is mediated by dynamin and focal adhesion kinase. *Nat Cell Biol* **7**, 6, 581-90.
- Fadok, V. A. and Henson, P. M.** (1998). Apoptosis: getting rid of the bodies. *Curr Biol* **8**, 19, R693-5.
- Fedorko, M. E. and Hirsch, J. G.** (1970). Structure of monocytes and macrophages. *Seminars in Hematology* **7**, 2, 109-124.
- Fini, M., Nicoli, A. N., Torricelli, P., Giavaresi, G., Borsari, V., Lenger, H., Bernauer, J., Giardino, R., Chiesa, R. and Cigada, A.** (2003). A new austenitic stainless steel with negligible nickel content: an in vitro and in vivo comparative investigation. *Biomaterials* **24**, 27, 4929-4939.
- Flemming, R. G., Murphy, C. J., Abrams, G. A., Goodman, S. L. and Nealey, P. F.** (1999). Effects of synthetic micro- and nano-structured surfaces on cell behavior. *Biomaterials* **20**, 6, 573-88.
- Folkman, J. and Moscona, A.** (1978). Role of cell shape in growth control. *Nature* **273**, 5661, 345-9.
- Freese, H. L., Volas, M. G. and Wood, J. R.** (2001). 3. Metallurgy and technological properties of titanium and titanium alloys. In *Titanium in medicine*, (eds D. M. Brunette P. Tengvall M. Textor and P. Thomsen). Berlin: Springer.
- Frigg, R., Appenzeller, A., Christensen, R., Frenk, A., Gilbert, S. and Schavan, R.** (2001). The development of the distal femur Less Invasive Stabilization System (LISS). *Injury* **32 Suppl 3**, 24-31.
- Gadegaard, N.** (2005). Atomic force microscopy in Biology: technology and techniques. *Biotechnic submitted*.
- Gadegaard, N., Thoms, S., Macintyre, D. S., McGee, K., Gallager, J., Casey, B. and Wilkinson, C.** (2003). Array of nano-dots for cellular engineering. *Microelectronic Engineering* **67-68**, 162-168.
- Garratt-Reed, A. J. and Bell, D. C.** (2003). Energy-Dispersive X-Ray Analysis in the Electron Microscope: BIOS Scientific Publishers Ltd.
- Gasser, B.** (2001). 20. Design and engineering criteria for titanium devices. In *Titanium in medicine*, (eds D. M. Brunette P. Tengvall M. Textor and P. Thomsen). Berlin: Springer.
- Geiger, B. and Bershadsky, A.** (2002). Exploring the neighborhood: adhesion-coupled cell mechanosensors. *Cell* **110**, 139-142.
- Geiger, B. and Bershadsky, A.** (2001). Assembly and mechanosensory function of focal contacts. *Curr Opin Cell Biol.* **13**, 584-592.
- Geiger, B., Bershadsky, A., Pankov, R. and Yamada, K. M.** (2001). Transmembrane extracellular matrix-cytoskeleton crosstalk. *Nat Rev Mol Cell Biol* **2**, 793-805.

- Gerber, H. and Perren, S. M. (1980). Evaluation of tissue compatibility of in-vitro cultures of embryonic bone. In *Evaluation of Biomaterials*, (eds G. D. Winter J. L. Leray and K. deGroot). Chichester: John Wiley & Sons Ltd.
- Giordano, G., Sandrini, E., Del Curto, B., Signorelli, E., Rondelli, G. and Di Silvio, L. (2004). Titanium for osteointegration: Comparison between a novel biomimetic treatment and commercially exploited surfaces. *J App Biomat & Biomech*, 2, 35-44.
- Gjertsen, B. T., Cressey, L. I., Ruchaud, S., Houge, G., Lanotte, M. and Doskeland, S. O. (1994). Multiple apoptotic death types triggered through activation of separate pathways by cAMP and inhibitors of protein phosphatases in one (IPC leukemia) cell line. *J Cell Sci* 107 (Pt 12), 3363-3377.
- Goldstein, J., Newbury, D., Joy, D., Lyman, C., Echlin, P., Lifshin, E., Sawyer, L. and Michael, J. (2003). Scanning Electron Microscopy and X-Ray Microanalysis. New York: Kluwer Academic/Plenum Publishers.
- Grainger, D. W. and Healy, K. E. (1999). Biomaterial Surface Analysis. In *Handbook of Biomaterial Evaluation - Scientific, Technical, and Clinical Testing of Implant Materials*, (ed. A. von Recum): Taylor & Francis.
- Granjeaud, S., Bertucci, F. and Jordan, B. R. (1999). Expression profiling: DNA arrays in many guises. *BioEssays* 21, 9, 781-790.
- Green, A. M., Jansen, J. A., van der Waerden, J. P. C. M. and von Recum, A. (1994). Fibroblast response to microtextured silicone surface: Texture orientation into or out of the surface. *J Biomed Mater Res* 28, 647-653.
- Gristina, A. G. (1994). Implant failure and the immuno-incompetent fibro-inflammatory zone. *Clin Orthop*, 298, 106-118.
- Groessner-Schreiber, B., Neubert, A., Muller, W.-D., Hopp, M., Gricpentrog, M. and Lange, K.-P. (2002). Fibroblast growth on surface-modified dental implants: An in vitro study. *J Biomed Mater Res A* 15, 64, 591-599.
- Hallab, N. J., Anderson, S., Caicedo, M., Brasher, A., Mikecz, K. and Jacobs, J. J. (2005). Effect of soluble metals on human peri-implant cells. *J Biomed Mater Res A* 74, 124-140.
- Hallgren, C., Reimers, H., Gold, J. and Wennerberg, A. (2001). The importance of surface texture for bone integration of screw shaped implants: an in vivo study of implants by photolithography. *J Biomed Mater Res* 57, 4, 485-496.
- Harle, J., Salih, V., Olsen, I., Brett, P. M., Jones, F. and Tonetti, M. (2004). Gene expression profiling of bone cells on smooth and rough titanium surfaces. *J Mater Sci Mater Med* 15, 11, 1255-8.
- Harris, L., G., Patterson, L. M., Bacon, C., ap Gwynn, I. and Richards, R. G. (2005). Assessment of the compatibility of different coated titanium surfaces to fibroblasts and osteoblasts. *J Biomed Mater Res A* 73A, 1, 12-20.
- Haynes, D. R., Hay, S. J., Rogers, S. D., Ohta, S., Howie, D. W. and Graves, S. E. (1997). Regulation of bone cells by particle-activated mononuclear phagocytes. *J. Bone Joint Surg.Br.* 79, 6, 988-994.
- Heroux, P., Kyrychenko, I. and Bourdages, M. (2004). Proliferation and apoptosis rates of living human erythroleukemia Cells. *Micriscopy and Analysis* 18, 3, 19-21.
- Hinshaw, J. E. (2000). Dynamin and its role in membrane fission. *Annu. Rev. Cell Dev. Biol.* 16, 432-519.

- Holgers, K.-M., Esposito, M., Kalltorp, M. and Thomsen, P. (2001). 16. Titanium in soft tissues. In *Titanium in medicine*, (eds D. M. Brunette P. Tengvall M. Textor and P. Thomsen). Berlin, Heidelberg, New York: Springer.
- Huang, S. and Ingber, D. E. (1999). The structural and mechanical complexity of cell-growth control. *Nat Cell Biol* 1, 5, E131-8.
- Huhtala, P., Humphries, M. J., McCarthy, J. B., Tremble, P. M., Werb, Z. and Damsky, C. H. (1995). Cooperative signaling by alpha5 beta1 and alpha4 beta1 integrins regulated metalloproteinase gene expression in fibroblasts adhering to fibronectin. *J Cell Biol* 129, 3, 867-879.
- Hunter, A., Archer, C. W., Walker, P. S. and Blunn, G. (1995). Attachment and proliferation of osteoblasts and fibroblasts on biomaterials for orthopaedic use. *Biomaterials* 16, 4.
- Hynes, R. (1999). Fibronectins. In *Guidebook to the Extracellular Matrix, Anchor, and Adhesion Proteins*, (eds T. Kreis and R. Vale). Oxford: Oxford University Press.
- Hynes, R. O. and Bader, B. L. (1997). Target mutations in integrin and their ligands: their implications for vascular biology. *Thromb Haemost* 78, 83-7.
- Hynes, R. and Yamada, K. M. (1982). Fibronectins: multifunctional modular glycoproteins. *J Cell Biol*. 95, 369-377.
- Ingber, D. E., Prusty, D., Sun, Z., Betensky, H. and Wang, N. (1995). Cell shape, cytoskeletal mechanics, and cell cycle control in angiogenesis. *J Biomech* 28, 12, 1471-84.
- Ireland, G., Dopping-Hepenstal, P. J. C., Jordan, P. and O'Neill, C. (1989). Limitation of substratum size alters cytoskeletal organization and behaviour of swiss 3T3 fibroblasts. *Cell Biol Int Rep*. 13, 9, 781-790.
- Irizarry, R. A., Warren, D., Spencer, F., Kim, I. F., Biswal, S., Frank, B. C., Gabrielson, E., Garcia, J. G. N., Geoghegan, J., Germino, G., Griffin, C., Hilmer, S. C., Hoffman, E., Jedlicka, A. E., Kawasaki, E. et al. (2005). Multiple-laboratory comparison of microarray platforms. *Nat Meth* 2, 5, 345-349.
- Iwig, M., Czeslick, E., Muller, A., Gruner, M., Spindler, M. and Glaesser, D. (1995). Growth regulation by cell shape alteration and organization of the cytoskeleton. *Eur J Cell Biol* 67, 2, 145-57.
- Iwig, M. and Glaesser, D. (1991). Cell-substratum interactions and the cytoskeleton in cell shape-mediated growth regulation of lens epithelial cells. *Lens Eye Toxic Res* 8, 2-3, 281-309.
- Izzard, C. S. and Lochner, L. R. (1976). Cell-to-substrate contacts in living fibroblasts: an interference reflexion study with an evaluation of the technique. *J Cell Sci* 21, 1, 129-59.
- Jain, R. and von Recum, A. (2004). Fibroblast attachment to smooth and microtextured PER and thin cp-Ti films. *J Biomed Mater Res A*. 68, 2, 294-304.
- Jain, R. and von Recum, A. (2003). Effect of titanium surface texture on the cell-biomaterial interface. *J Invest Surg*. 16, 5, 263-273.
- Johansson, C., Lausmaa, J., Ask, M., Hansson, H. A. and Abbrektsson, T. (1989). Ultrastructural differenced of the interface zone between bona and Ti 6Al 4V or commercially pure titanium. *J Biomed Eng*. 11, 1, 3-8.
- Jupiter, J. B. and Ring, D. C. (2005). AO fracture managment: Hand and wrist. Stuttgart: Thieme.

- Kale, S., Biermann, S., Edwards, C., Tarnowski, C., Morris, M. and Long, M. W.** (2000). Three-dimensional cellular development is essential for ex vivo formation of human bone. *Nature Biotechnology* **18**, 954-958.
- Kasemo, B. and Gold, J.** (1999). Implant surfaces and interface processes. *Adv Dent Res* **13**, 8-20.
- Kasemo, B. and Lausmaa, J.** (1988). Biomaterial and implant surfaces: a surface science approach. *Int J Oral Maxillofac Implants* **3**, 4, 247-259.
- Kasemo, B.** (1983). Biocompatibility of titanium implants: Surface Science aspects. *The Journal of Prosthetic Dentistry* **49**, 6, 832-837.
- Kessel, R. G. and Kardon, R. H.** (1979). Connective tissue. In *Tissue and organ: a text-atlas of scanning electron microscopy*, (eds R. G. Kessel and R. H. Kardon).
- Khan, M. A., Williams, R. L. and Williams, D. F.** (1999). The corrosion behaviour of Ti-6Al-4V, Ti-6Al-7Nb and Ti-13Nb-13Zr in protein solutions. *Biomaterials* **20**, 7, 631-637.
- Kim, Y., Jang, J.-H., Ku, Y., Koak, J.-Y., Chang, I.-T., Kim, H.-E., Lee, J.-B. and Heo, S.-J.** (2004). Microarray-based expression analysis of human osteoblast-like cell response to anodized titanium surface. *Biotechnology Letters* **26**, 399-402.
- Koleske, A. J.** (2003). Do filopodia enable the growth cone to find its way? *Sci STKE* **183**, 20.
- Kononen, M., Hormia, M., Kivilahti, J., Hautaniemi, J. and Thesleff, I.** (1992). Effect of surface processing on the attachment, orientation, and proliferation of human gingival fibroblasts on titanium. *J Biomed Mater Res* **26**, 10, 1325-41.
- Koopmann, C. F., Jr.** (1995). Cutaneous wound healing. An overview. *Otolaryngol Clin North Am* **28**, 5, 835-845.
- Kramer, K.-H.** (2000). Implants for Surgery - A Survey on Metallic Materials. In *Materials for Medical Engineering: EUROMAT- Volume 2*, (eds H. Stallforth and P. Revell), pp. 9-29. Weinheim, New York, Chichester, Brisbane, Singapore, Toronto: Wiley-VHC.
- Kreis, T. and Vale, R.** (1999). Guidebook to the extracellular matrix, anchor, and adhesion proteins: Oxford.
- Krettek, C.** (2000). 3.3.1 Intramedullary nailing. In *AO Principles of fracture management*, (eds T. P. Ruedi and W. M. Murphy). Stuttgart: Thieme.
- Ku, Y., Chung, C.-P. and Jang, J.-H.** (2005). The effect of the surface modification of titanium using recombinant fragment of fibronectin and vitronectin on cell behavior. *Biomaterials* **26**, 5153-5157.
- Kyriakides, T. R., Leach, K. J., Hoffman, A. S., Ratner, B. D. and Bornstein, P.** (1999). Mice that lack the angiogenesis inhibitor, thrombospondin 2, mount an altered foreign body reaction characterized by increased vascularity. *Proc Natl Acad Sci USA* **96**, 8, 4449-54.
- LaBerge, M.** (1999). Surface Characterisation. In *Handbook of biomaterials evaluation - Scientific, technical, and clinical testing of implant materials*, (ed. A. von Recum). New York: Macmillan Publishing Company.
- Laing, P. G.** (1979). Clinical experience with prosthetic materials: historical perspectives, current problems, and future directions. In *Corrosion and degradation of implant materials*, vol. ASTM Special Technical Publication 684 (eds B. C. Syrett and A. Acharya). Philadelphia: American Society for Testing and Materials.
- Langford, R. J. and Frame, J. W.** (2002). Tissue changes adjacent to titanium plates in patients. *J Craniomaxillofac Surg* **30**, 2, 103-107.

- Laurencin, C. T., Ambrosio, A. M. A., Borden, M. D. and Cooper, J. A. (1999). Tissue engineering: orthopedic applications. *Annu. Rev. Biomed. Eng* **1**, 19, 19-46.
- Lavos-Valereto, I. C., Konig, B., Jr., Rossa, C. J., Marcantonio, E. J. and Zavaglia, A. C. (2001a). A study of histological responses from Ti-6Al-7Nb alloy dental implants with and without plasma-sprayed hydroxyapatite coatings in dogs. *J Mater Sci Mater Med* **12**, 273-276.
- Lavos-Valereto, I. C., Wolynecc, S., Deboni, M. C. and Konig, B., Jr. (2001b). In vitro and in vivo biocompatibility testing of Ti-6Al-7Nb alloy with and without plasma-sprayed hydroxyapatite coating. *J Biomed Mater Res* **58**, 6, 727-733.
- Layens, C. and Peters, M. (2003). Titanium and Titanium Alloys: Fundamentals and Applications. Weinheim, New York, Chichester, Brisbane, Singapore, Toronto: Wiley-VCH.
- Leask, A. and Abraham, D. J. (2004). TGF-beta and the fibrotic response. *FASEB* **18**, 816-827.
- Leven, R. M., Viridi, A. S. and Sumner, D. R. (2004). Patterns of gene expression in rat bone marrow stromal cells cultured on titanium alloy discs of different roughness. *J Biomed Mater Res A* **70**, 3, 391-401.
- Li, J. M., Lu, L., Lai, M. O. and Ralph, B. (2003). Fractal measurements of projection microstructures. In *Image-based fractal description of microstructures*: Kluwer Academic Publisher.
- Liao, H., Andersson, A. S., Sutherland, D. S., Petronis, S., Kasemo, B. and Thomsen, P. (2003). Response of rat osteoblast-like cells to microstructured model surfaces in vitro. *Biomaterials* **24**, 4, 649-654.
- Lincks, J., Boyan, B. D., Blanchard, C. R., Lohmann, C. H., Liu, Y., Cochran, D. L., Dean, D. D. and Schwartz, Z. (1998). Response of MG63 osteoblast-like cells to titanium and titanium alloy is dependent on surface roughness and composition. *Biomaterials* **19**, 23, 2219-2232.
- Lipschutz, R. J., Fodor, S. P. A., Gingeras, T. R. and Lockhart, D. J. (1999). High density synthetic oligonucleotide arrays. *Nat. Gen* **21**, Suppl., 20-24.
- Lodish, H., Berk, A., Zipursky, L., Matsudaira, P., Baltimore, D. and Darnell, J. (1999). *Molecular Cell Biology*.
- Lotz, M. M., Burdsal, C. A., Erickson, H. P. and McClay, D. R. (1989). Cell adhesion to fibronectin and tenascin: quantitative measurements of initial binding and subsequent strengthening response. *J Cell Biol* **109**, 4 Pt 1, 1795-805.
- Luthen, F., Lange, R., Becker, P., Rychly, J., Beck, U. and Nebe, J. G. (2005). The influence of surface roughness of titanium on beta1- and beta3-integrin adhesion and the organization of fibronectin in human osteoblastic cells. *Biomaterials* **26**, 15, 2423-40.
- MacDonald, D. E., Markovic, B., Allen, M., Somasundaran, P. and Boskey, A. L. (1998). Surface analysis of human plasma fibronectin adsorbed to commercially pure titanium materials. *J Biomed Mater. Res.* **41**, 1, 120-130.
- Maddox, A. S. and Burridge, K. (2003). RhoA is required for cortical retraction and rigidity during mitotic cell rounding. *The Journal of Cell Biology* **160**, 2, 255-265.
- Madore, C. and Landolt, D. (1997). Electrochemical micromachining of controlled topographies in titanium for biological applications. *J. Micromech. Microeng* **7**, 270-275.

- Martin, J. Y., Schwartz, Z., Hummert, T. W., Schraub, D. M., Simpson, J., Lankford, J., Jr., Dean, D. D., Cochran, D. L. and Boyan, B. D. (1995). Effect of titanium surface roughness on proliferation, differentiation, and protein synthesis of human osteoblast-like cells (MG63). *J Biomed Mater Res* **29**, 3, 389-401.
- Martines, E., Seunarine, K., Morgan, H., Gadegaard, N., Wilkinson, C. and Riehle, M. O. (2005). Superhydrophobicity and superhydrophilicity of regular nanopatterns. *Nano Lett* **5**, 10, 2097-2103.
- May, R. C. and Machesky, L. M. (2001). Phagocytosis and the actin cytoskeleton. *J Cell Sci* **114**, 6, 1061-1077.
- Meredith, D. O., Eschbach, L., Wood, M. A., Riehle, M., Curtis, A. and Richards, R. G. (2005). Human Fibroblast Reactions to Standard and Electropolished Titanium and Ti-6Al-7Nb, and Electropolished Stainless Steel. *J Biomed Mater Res A* **75**, 3, 541-555.
- Meredith, D. O., Owen, G. R., ap Gwynn, I. and Richards, R. G. (2004). Variation in cell-substratum adhesion in relation to cell cycle phases. *Exp Cell Res* **293**, 1, 58-67.
- Miller, T. and Boettiger, D. (2003). Control of intracellular signaling by modulation of fibronectin conformation at the cell-materials interface. *Langmuir* **19**, 1723-1729.
- Misiak, D. J., Kent, J. N. and Carr, R. F. (1984). Soft tissue responses to hydroxyapatite particles of different shapes. *J Oral Maxillofac Surg* **43**, 150-160.
- Miyazaki, K., Hattori, Y., Umenishi, F., Yasumitsu, H. and Umeda, M. (1999). Purification and characterization of extracellular matrix-degrading metalloproteinase, matrin (pump-1), secreted from human rectal carcinoma cell line. *Cancer Res* **50**, 24, 7758-64.
- Morehead, J. M. and Holt, G. R. (1994). Soft-tissue response to synthetic biomaterials. *Otolaryngol Clin North Am* **27**, 1, 195-201.
- Morgan, A. J. (1985). X-Ray Microanalysis in Electron Microscopy for Biologists. Oxford: Oxford University Press.
- Mostardi, R. A., Meerbaum, S. O., Kovacic, M. W. and Gradisar, I. A., Jr. (1999). In vitro response of human fibroblasts to commercially pure titanium. *J Biomed Mater Res* **47**, 1, 60-64.
- Mostardi, R. A., Pentello, A., Kovacic, M. W. and Askew, M. J. (2002). Prosthetic metals have a variable necrotic threshold in human fibroblasts: an in vitro study. *J Biomed Mater Res* **59**, 4, 605-610.
- Mott, J. D. and Werb, Z. (2004). Regulation of matrix biology by matrix metalloproteinases. *Curr Opin Cell Biol* **16**, 5, 558-64.
- Murphy, G., Crockett, M. I., Ward, R. V. and Decherty, A. J. (1991). Matrix metalloproteinase degradation of elastin, type IV collagen and proteoglycan. A quantitative comparison of the activities of 95 kDa and 72 kDa gelatinases, stromelysins-1 and -2 and punctuated metalloproteinase (PUMP). *Biochem J* **277**, Pt 1, 277-9.
- Murray, A. and Hunt, T. (1993). The Cell Cycle an Introduction: Oxford University Press.
- Mustafa, K., Silva Lopez, B., Hultenby, K., Wennerberg, A. and Arvidson, K. (1998). Attachment and proliferation of human oral fibroblasts to titanium surfaces blasted with TiO₂ particles. A scanning electron microscopic and histomorphometric analysis. *Clin Oral Implants Res* **9**, 3, 195-207.
- Nobes, C. D. and Hall, A. (1995). Rho, Rac, and Cdc42 GTPases regulate the assembly of multimolecular focal complexes associated with actin stress fibres, lamellipodia, and filopodia. *Cell* **81**, 53-62.

- O'Neill, C., Jordan, P., Riddle, P. and Ireland, G. (1990). Narrow linear strips of adhesive substratum are powerful inducers of both growth and total focal contact area. *J Cell Sci* **95**, 577-586.
- O'Neill, C., Jordan, P. and Ireland, G. (1986). Evidence for two distinct mechanisms of anchorage stimulation in freshly explanted and 3T3 Swiss mouse fibroblasts. *Cell* **44**, 3, 489-96.
- Oakley, C. and Brunette, D. M. (1993). The sequence of alignment of microtubules, focal contacts and actin filaments in fibroblasts spreading on smooth and grooved titanium substrata. *J Cell Sci* **106** (Pt 1), 343-54.
- Ohashi, T., Keihart, D. P. and Erickson, H. P. (2002). Dual labeling of the fibronectin matrix and actin cytoskeleton with green fluorescent protein variants. *J Cell Sci.* **115**, 6, 1221-1229.
- Ohnishi, R. (1981). Dynamics of cultured L cells as studied by cinemicroscopy and scanning electron microscopy. *Biomed.Res.Suppl.* **2**, 1-12.
- Okazaki, Y. and Gotoh, E. (2005). Comparison of metal release from various metallic biomaterials in vitro. *Biomaterials* **26**, 11-21.
- Okazaki, Y., Rao, S., Ito, Y. and Tateishi, T. (1998). Corrosion resistance, mechanical properties, corrosion fatigue strength and cytocompatibility of new Ti alloys without Al and V. *Biomaterials* **19**, 13, 1197-1215.
- Oliveira, V., Chaves, R. R., Bertazzoli, R. and Caram, R. (1998). Preparation and characterization of Ti-Al-Nb alloys for orthopaedic implants. *Braz. J. Chem. Eng* **15**, 4, 326-333.
- Osano, E., Kishi, J. and Takahashi, Y. (2003). Phagocytosis of titanium particles and necrosis in TNF-alpha-resistant mouse sarcoma L929 cells. *Toxicol In Vitro* **17**, 1, 41-47.
- Qualmann, B. and Kessels, M. M. (2002). Endocytosis and the cytoskeleton. *Int Rev Cyt* **220**, 93-144.
- Qualmann, B., Kessels, M. M. and Kelly, R. B. (2000). Molecular links between endocytosis and the actin cytoskeleton. *J Cell Biol* **150**, 5, 111-6.
- Owen, G. R., Meredith, D. O., ap Gwynn, I. and Richards, R. G. (2005). Focal adhesion quantification - A new aecay of material biocompatibility?:Review. *Eur Cell Mater* **9**, 85-96.
- Owen, G. R., Meredith, D. O., ap Gwynn, I. and Richards, R. G. (2002). Simultaneously identifying S-phase labelled cells and immunogold-labelling of vinculin in focal adhesions. *J Microsc* **207**, Pt 1, 27-36.
- Owen, G. R., Meredith, D. O., Ap Gwynn, I. and Richards, R. G. (2001). Enhancement of immunogold-labelled focal adhesion sites in fibroblasts cultured on metal substrates: problems and solutions. *Cell Biol Int* **25**, 12, 1251-9.
- Owen, T. A., Aronow, M., Shalhoub, V., Barone, L. M., Wilming, L., Tassinari, M. S., Kennedy, M. B., Pockwinse, S., Lian, J. B. and Stein, G. S. (1990). Progressive development of the rat osteoblast phenotype in vitro: reciprocal relationships in expression of genes associated with osteoblast proliferation and differentiation during formation of the bone extracellular matrix. *J Cell Physiol* **143**, 3, 420-430.
- Palluel, P. (1947). Diffusion composition of secondary electron rays in metals. *C.R. Acad. Sci. Paris* **224**, 1492-4.
- Pardee, A. B. (1989). G1 events and regulation of cell proliferation. *Science* **246**, 4930, 603-8.

- Perren, S. M.** (1991). The concept of biological plating using the limited contact-dynamic compression plate (LC-DCP). *Injury* **22**, Suppl. 1, 1-41.
- Perren, S. M. and Pohler, O.** (1987). News from the Lab: Titanium as Implant Material. *AO/ASIF Dialogue*, 1, 11-12.
- Pohler, O. E.** (2000). Unalloyed titanium for implants in bone surgery. *Injury* **31** Suppl 4, 7-13.
- Porter, K., Prescott, D. and Frye, J.** (1973). Changes in surface morphology of Chinese hamster ovary cells during the cell cycle. *J Cell Biol* **57**, 3, 815-36.
- Ratner, B. D.** (2004). A history of biomaterials. In *Biomaterials Science: an introduction to materials in medicine*, (eds B. D. Ratner A. S. Hoffman F. J. Schoen and J. E. Lemons). Amsterdam: Elsevier Academic Press.
- Ratner, B. D.** (2001). 1. A perspective on titanium biocompatibility. In *Titanium in medicine*, (eds D. M. Brunette P. Tengvall M. Textor and P. Thomsen). Berlin, Heidelberg, New York: Springer.
- Rediske, A. M., Koenig, A. L., Barezzi, N., Ameen, L. C., Slunt, J. B. and Grainger, D. W.** (2002). Polyclonal human antibodies reduce bacterial attachment to soft contact lens and corneal cell surfaces. *Biomaterials* **23**, 23, 4565-4572.
- Refai, A. K., Textor, M., Brunette, D. M. and Waterfield, J. D.** (2005). Effect of titanium surface topography on macrophage activation and secretion on proinflammatory cytokines and chemokines. *J Biomed Mater Res A* **70**, 2, 194-205.
- Rich, A. and Harris, A. K.** (1981). Anomalous preferences of cultured macrophages for hydrophobic and roughened substrata. *J Cell Sci* **50**, 1-7.
- Richards, R. G., Gasser, B. and Weiling, R.** (1999a). Influence of surface microtopography of stainless steel implants in fracture fixation on the formation of capsules: an in vivo study. In *European Society of Biomaterials*. Arcachon, France.
- Richards, R. G., Owen, G. R. and ap Gwynn, I.** (1999b). Low voltage backscattered electron imagin (<5kV) using field emission scanning electron microscopy. *Scanning Microsc.* **13**, 55-60.
- Richards, R. G.** (1996). The effect of surface roughness on fibroblast adhesion in vitro. *Injury* **27**, Suppl. 3, 38-43.
- Richards, R. G. and ap Gwynn, I.** (1995a). Backscattered electron imaging of the undersurface of resin-embedded cells by field emission scanning electron microscopy. *J. Microscopy* **177**, 43-52.
- Richards, R. G., Rahn, B. A. and ap Gwynn, I.** (1995b). Scanning electron microscopy of the undersurface of cell monolayers grown on metallic implants. *J. Mar. Sci. - Mat. Med.* **6**, 120-124.
- Rogers, S. D., Howie, D. W., Graves, S. E., Pearcy, M. J. and Haynes, D. R.** (1997). In vitro human monocyte response to wear particles of titanium alloy containing vanadium or niobium. *J Bone Joint Surg Br* **79**, 2, 311-5.
- Rosengren, A., Johansson, B. R., Danielsen, N., Thomsen, P. and Ericson, L. E.** (1996). Immunohistochemical studies on the distribution of albumin, fibrinogen, fibronectin, IgG and collagen around PTFE and titanium implants. *Biomaterials* **17**, 18, 1779-1786.
- Rottner, K., Hall, A. and Small, J. V.** (1999). Interplay between Rac and Rho in the control of substrate contact dynamics. *Curr. Biol* **9**, 640-648.

- Rovensky, Y. A., Bershadsky, A., Gavargizov, E. I., Obolenskaya, L. N. and Vasiliev, J. M. (1991). Spreading of mouse fibroblasts on the substrate with multiple spikes. *Exp Cell Res* **197**, 107-112.
- Rubin, R. W. and Everhart, L. P. (1973). The effect of cell-to-cell contact on the surface morphology of Chinese hamster ovary cells. *J Cell Biol* **57**, 3, 837-44.
- Schakenraad, J. M., Arends, J., Busscher, H. J., Dijk, F., van Wachem, P. B. and Wildevuur, C. R. H. (1989). Kinetics of cell spreading on protein precoated substrata: a study of interfacial aspects. *Biomaterials* **10**, 43-49.
- Schakenraad, J. M., Busscher, H. J., Wildevuur, C. R. H. and Arends, J. (1986). The influence of substratum surface free energy on growth and spreading of human fibroblasts in the presence and absence of serum proteins. *J Biomed Mater Res* **20**, 773-784.
- Schatzker, J. (2000). 1.1 AO philosophy and principles. In *AO Principles of fracture management*, (eds T. P. Ruedi and W. M. Murphy). Stuttgart: Thieme.
- Schen, Y. and Schaller, M. D. (1999). Focal Adhesion Kinase (FAK). In *Guidebook to the extracellular matrix, anchor, and adhesion proteins*, (eds T. Kreis and R. Vale). Oxford: Oxford University Press.
- Schlich, T. (2002). Dealing with broken bones. In *Surgery, Science and Industry: A revolution in fracture care, 1950s-1990s*, (ed. T. Schlich). Basingstoke: Palgrave Macmillan.
- Schmidt, C., Kaspar, D., Sarkar, M. R., Claes, L. E. and Ignatius, A. A. (2002). A scanning electron microscopy study of human osteoblast morphology on five orthopedic metals. *J Biomed Mater Res* **63**, 3, 252-261.
- Schmidt, C., Ignatius, A. A. and Claes, L. E. (2001). Proliferation and differentiation parameters of human osteoblasts on titanium and steel surfaces. *J Biomed Mater Res* **54**, 2, 209-215.
- Schmit, J., Novak, E. and Olszak, A. G. (2005). White-light interferometer with internal length standard, vol. 2005: Veeco Metrology.
- Schoenwaelder, S. M. and Burridge, K. (1999). Bidirectional signaling between the cytoskeleton and integrins. *Curr Opin Cell Biol* **11**, 2, 274-86.
- Schwartzman, R. A. and Cidlowski, J. A. (1993). Apoptosis: The biochemistry and molecular biology of programmed cell death. *Endocrine Rev.* **14**, 2, 133-150.
- Schwarzbauer, J. E. and Schler, J. L. (1999). Fibronectin fibrillogenesis: a paradigm for extracellular matrix assembly. *Curr Opin Cell Biol.* **11**, 5, 622-627.
- Scotchford, C. A., Ball, M., Winkelmann, M., Voros, J., Csucs, C., Brunette, D. M., Danuser, G. and Textor, M. (2003). Chemically patterned, metal-oxide-based surfaces produced by photolithographic techniques for studying protein- and cell-interactions. II: Protein adsorption and early cell interactions. *Biomaterials* **24**, 7, 1147-58.
- Semlitsch, M. (1987). Titanium alloys for hip joint replacements. *Clin Materials* **2**, 1-13.
- Semlitsch, M., Staub, F. and Weber, H. (1985). Titanium-aluminum-niobium alloy, development for biocompatible, high strength surgical implants. *Biomed Tech (Berl)* **30**, 12, 334-9.
- Sen, B. H., Kazemi, R. B. and Spangberg, L. S. W. (1998). Morphologic effects on L929 fibroblasts of titanium tetrafluoride application. *Oral Surg Oral Med Oral Pathol Oral Radiol Endod* **86**, 3, 341-346.
- Shannon, C., Thull, R. and von Recum, A. (1997). Types I and III collagen in the tissue capsules of titanium and stainless-steel implants. *J Biomed Mater Res* **34**, 3, 401-408.

- Shelton, R. M. and Davies, J. E. (2001). Osteoblast reactions to charged polymers. In *The bone-biomaterial interface*, (ed. J. E. Davies). Toronto: University of Toronto Press.
- Sires, U. I., Schmid, T. M., Filszar, C. J., Wang, Z. Q., Gluck, S. L. and Welgus, H. G. (1995). Complete degradation of type X collagen requires the combined action of interstitial collagenase and osteoclast-derived cathepsin-B. *J Clin Invest.* **95**, 5, 2089-95.
- Sittig, C., Hahner, G., Marti, A., Textor, M. and Spencer, N. D. (1999a). The implant material, Ti6Al7Nb: surface microstructure, composition and properties. *Journal of Materials Science: Materials in Medicine* **10**, 191-198.
- Sittig, C., Textor, M., Spencer, N. D., Weiland, M. and Vallotton, P.-H. (1999b). Surface characterization of implant materials c.p.Ti, Ti-6Al-7Nb and Ti-6Al-4V with different pretreatments. *Journal of Materials Science: Materials in Medicine*, **10**, 35-46.
- Small, J. V., Geiger, B., Kaverina, I. and Bershadsky, A. (2002). How do microtubules guide migrating cells? *Nat Rev Mol Cell Biol* **3**, 957-964.
- Stannard, J. P., Wilson, T. C., Volgas, D. A. and Alonso, J. E. (2003). Fracture stabilization of proximal tibial fractures with the proximal tibial LISS: early experience in Birmingham, Alabama (USA). *Injury* **34**, Supp. 1, 36-43.
- Steinemann, S. G. (1998). Titanium - the material of choice? *Peridontol 2000* **17**, 7-21.
- Steinemann, S. G. (1996). Metal implants and surface reactions. *Injury* **27**, Suppl 3, 16-22.
- Syed, A. A., Agarwal, M., Giannoudis, P. V., Matthews, S. J. and Smith, R. M. (2004). Distal femoral fractures: long-term outcome following stabilisation with the LISS. *Injury* **35**, 6, 599-607.
- Taborelli, M., Jobin, M., Francois, P., Vaudaux, P., Tonetti, M., Szmukler-moncler, S., Simpson, J. P. and Descouts, P. (1997). Influence of surface treatments developed for oral implants on the physical and biological properties of titanium. (I) Surface characterization. *Clin Oral Implants Res.* **8**, 3, 208-216.
- Takebe, J., Champagne, C. M., Offenbacher, S., Ishibashi, K. and Cooper, L. (2002). Titanium surface topography alters cell shape and modulates bone morphogenic protein 2 expression in the J774A.1 macrophage cell line. *J Biomed Mater Res.* **64A**, 2, 207-216.
- Tan, J. and Saltzman, W. M. (2004). Biomaterials with hierarchically defined micro- and nanoscale structure. *Biomaterials* **25**, 17, 3593-601.
- Tan, J., Shen, H., Carter, K. L. and Saltzman, W. M. (2000). Controlling human polymorphonuclear leukocytes motility using microfabrication technology. *J Biomed Mater Res* **51**, 4, 694-702.
- Tanaka, Y., Kanai, Y., Okada, Y., Nonaka, S., Takeda, S., Harada, A. and Hirokawa, N. (1998). Targeted disruption of mouse conventional kinesin heavy chain, kif5B, results in abnormal perinuclear clustering of mitochondria. *Cell* **93**, 1147-1158.
- Teixeira, A. I., Abrams, G. A., Bertics, P. J., Murphy, C. J. and Nealey, P. F. (2003). Epithelial contact guidance on well-defined micro- and nanostructured substrates. *J.Cell Sci.* **116**, Pt 10, 1881-1892.
- Textor, M., Sittig, C., Frauchiger, V., Tosatti, S. and Brunette, D. M. (2001). 7. Properties and biological significance of natural oxide films on titanium and its alloys. In *Titanium in medicine*, (eds D. M. Brunette P. Tengvall M. Textor and P. Thomsen). Berlin: Springer.
- Tomlinson, A. and Ferguson, M. W. J. (2003). Wound healing: a model of dermal wound repair. *Methods Mol Biol.* **225**, 249-60.

- Turner, C. E. and Burrige, K. (1991). Transmembrane molecular assemblies in cell-extracellular matrix interactions. *Curr Opin Cell Biol* **3**, 5, 849-53.
- Ungersbock, A., Pohler, O. E. and Perren, S. M. (1996). Evaluation of soft tissue reactions at the interface of titanium limited contact dynamic compression plate implants with different surface treatments: an experimental sheep study. *Biomaterials* **17**, 8, 797-806.
- Ungersbock, A., Hunt, J., Krahenbuhl, U. and Perren, S. M. (1995). Soft tissue reactions to stainless steel/titanium LC-DCPs. A multicenter prospective clinical study. In *Transactions of the 41st annual meeting of orthopaedic research society*, pp. 577. Orlando.
- Ungersbock, A., Pohler, O. and Perren, S. M. (1994). Evaluation of the soft tissue interface at titanium implants with different surface treatments: experimental study on rabbits. *Biomed Mater Eng* **4**, 4, 317-325.
- Velten, D., Eisenbarth, E., Schanne, N. and Breme, J. (2004). Biocompatible Nb2O5 thin films prepared by means of the sol-gel process. *J Mater Sci Mater Med* **15**, 4, 457-61.
- Verhoven, B., Schlegel, R. A. and Williamson, P. (1995). Mechanisms of phosphatidylserine exposure, a phagocyte recognition signal, on apoptotic T lymphocytes. *J. Exp. Med.* **182**, 1597-1601.
- Vermes, I., Haanen, C., Steffens-Nakken, H. and Reutelingsperger, C. (1995). A novel assay for apoptosis. Flow cytometric detection of phosphatidylserine expression on early apoptotic cells using fluorescein labelled Annexin V. *J Immunol Methods*. **184**, 1, 39-51.
- Voggenreiter, G., Leiting, S., Brauer, H., Leiting, P., Majetschak, M., Bardenheuer, M. and Obertacke, U. (2003). Immuno-inflammatory tissue reaction to stainless-steel and titanium plates used for internal fixation of long bones. *Biomaterials* **24**, 2, 247-254.
- Vogler, E. A. (1998). Structure and reactivity of water at biomaterial surfaces. *Adv. Colloid Interface Sci.* **74**, 69-117.
- von Bredow, D. C., Nagle, R. B., Bowden, G. T. and Cress, A. E. (1995). Degradation of fibronectin fibrils by matrilysin and characterization of the degradation products. *Exp Cell Res* **221**, 83-91.
- von Recum, A. (1999). Handbook of biomaterials evaluation - Scientific, technical, and clinical testing of implant materials. New York: Macmillan Publishing Company.
- von Recum, A. and van Kooten, T. G. (1995). The influence of micro-topography on cellular response and the implications for silicone implants. *J. Biomater. Sci. Polymer Edn* **7**, 2, 181-198.
- von Recum, A., Opitz, H. and Wu, E. (1993). Collagen types I and III at the implant/tissue interface. *J Biomed Mater Res* **27**, 6, 757-61.
- von Recum, A. (1986). Handbook of biomaterials evaluation - Scientific, technical, and clinical testing of implant materials. New York: Macmillan Publishing Company.
- Voros, J., Wieland, M., Ruiz-Taylor, L., Textor, M. and Brunette, D. M. (2001). 5. Characterization of titanium surfaces. In *Titanium in medicine*, (eds D. M. Brunette P. Tengvall M. Textor and P. Thomsen). Berlin: Springer.
- Vroman, L. and Adam, A. L. (1986). Adsorption of proteins out of plasma and solutions in narrow spaces. *J Coll Int Sci.* **111**, 2, 391-402.
- Waldorf, H. and Fawkes, J. (1995). Wound Healing. *Adv Dermatol.* **10**, 77-96.
- Walivaara, B., Aronsson, B. O., Rodahl, M., Lausmaa, J. and Tengvall, P. (1994). Titanium with different oxides: in vitro studies of protein adsorption and contact activation. *Biomaterials* **15**, 10, 827-834.

- Wallin, R. F.** (1999). In vitro assesment of safety. In *Handbook of biomaterials evaluation - Scientific, technical, and clinical testing of implant materials*, (ed. A. von Recum). New York: Macmillan Publishing Company.
- Wang, N. and Ingber, D. E.** (1994). Control of cytoskeleton mechanics by extracellular matrix, cell shape, and mechanical tension. *Biophys J* **66**, 2181-9.
- Wapner, K. L.** (1991). Implications of metallic corrosion in total knee arthroplasty. *Clin Orthop Relat Res.* **271**, 12-20.
- Webster, T. J., Ergun, C., Doremus, R. H., Siegel, R. W. and Bizios, R.** (2000). Specific proteins mediate enhanced osteoblast adhesion on nanophase ceramics. *Biomaterials* **51**, 3, 475-483.
- Webster, T. J., Ergun, C., Doremus, R. H., Siegel, R. W. and Bizios, R.** (2001). Enhanced osteoclast-like cell functions on nanophase ceramics 1. *Biomaterials* **22**, 11, 1327-1333.
- Wieland, M., Chehroudi, B., Textor, M. and Brunette, D. M.** (2002). Use of Ti-coated replicas to investigate the effects on fibroblast shape of surfaces with varying roughness and constant chemical composition. *J.Biomed.Mater.Res.* **60**, 3, 434-444.
- Wieland, M., Textor, M., Chehroudi, B. and Brunette, D. M.** (2005). Synergistic interaction of topographic features in the production of bone-like nodules on Ti surfaces by rat osteoblasts. *Biomaterials* **26**, 10, 1119-30.
- Wilkinson, C. D.** (2004). Making structures for cell engineering. *Eur Cell Mater* **8**, 21-6; discussion 21-6.
- Williams, D. F.** (1999). *The Williams Dictionary of Biomaterials*. Liverpool: Liverpool University Press.
- Winkelmann, M., Gold, J., Hauert, R., Kasemo, B., Spencer, N. D., Brunette, D. M. and Textor, M.** (2003). Chemically patterned, metal oxide based surfaces produced by photolithographic techniques for studying protein- and cell-surface interactions I: Microfabrication and surface characterization. *Biomaterials* **24**, 7, 1133-45.
- Wojciak-Stothart, B., Curtis, A., Monaghan, W., MacDonald, K. and Wilkinson, C.** (1996). Guidance and activation of murine macrophages by nanometric scale topography. *Exp Cell Res* **223**, 426-435.
- Wojciak-Stodart, B., Madeja, Z., Korohoda, W., Curtis, A. and Wilkinson, C.** (1995a). Activation of macrophage-like cells by multiple grooved substrata. Topographical control of cell behaviour. *Cell Biol Int* **19**, 6, 485-490.
- Wojciak-Stodart, B., Curtis, A., Monaghan, W., McGrath, M., Sommer, I. and Wilkinson, C.** (1995b). Role of the cytoskeleton in the reaction of fibroblasts to multiple grooved substrate. *Cell Mot Cytoskel.* **31**, 147-158.
- Wood, M. A., Mercedith, D. O. and Owen, G. R.** (2002). Steps Towards a Model Nanotopography. *IEEE Transaction on Nanobioscience* **1**, 4, 133-140.
- Wood, W. and Martin, P.** (2002). Structures in focus-filopodia. *Int J Biochem Cell Biol* **34**, 7, 726-730.
- Wrana, J. L., Maeno, M., Hawrylyshyn, B., Yao, K.-L. and Domenicucci, C.** (1988). Diifferential effects of transformin growth factor-beta on the synthesis of extracellular matrix proteins by normal retal rat celvarial bone cell populations. *J Cell Biol.* **106**, 3, 915-24.

- Yamakita, Y., Totsukawa, G., Yamashiro, S., Fry, D., Zhang, X., Hanks, S. K. and Matsumura, F.** (1999). Dissociation of FAK/p130(CAS)/c-Src complex during mitosis: role of mitosis-specific serine phosphorylation of FAK. *J Cell Biol* **144**, 2, 315-24.
- Zamir, E. and Geiger, B.** (2001a). Components of cell-matrix adhesions. *J Cell Sci* **114**, 20, 3577-3579.
- Zamir, E. and Geiger, B.** (2001b). Molecular complexity and dynamics of cell-matrix adhesions. *J Cell Sci* **114**, 20, 3583-90.
- Zamir, E., Katz, M., Posen, Y., Erez, N., Yamada, K. M., Katz, B.-Z., Lin, S., Lin, D. C., Bershadsky, A., Kam, Z. and Geiger, B.** (2000). Dynamics and segregation of cell-matrix adhesions in cultured fibroblasts. *Nat Cell Biol* **2**, 4, 191-6.
- Zana, M. S. and Albrecht-Buehler, G.** (1989). What structures, beside adhesions, prevent spread cells from rounding up? *Cell Motil Cytoskeleton* **13**, 195-211.
- Zhao, Q. H., Anderson, J. M., Hiltner, A., Loden, G. A. and Payet, C. R.** (1992). Theroetical analysis on cell size distribution and kinetics of foreign-body giant cell formation in viv on polyurethane elastomers. *J Biomed Mater Res* **26**, 8, 1019-1038.
- Zhu, B., Zhang, Q., Lu, Q., Xu, Y., Yin, J., Hu, J. and Wang, Z.** (2004). Nanotopographical guidance of C6 glioma cell alignment and oriented growth. *Biomaterials* **25**, 4215-4223.
- Zimerman, B., Volberg, T. and Geiger, B.** (2004). Early molecular events in the assembly of focal adhesion-stress fiber complex during fibroblast spreading. *Cell Mot Cytoskel.* **58**, 143-159.
- Zislis, T., Martin, S. A., Cerbas, E., Heath, J. R., III, Mansfield, J. L. and Hollinger, J. O.** (1989). A scanning electron microscopic study of in vitro toxicity of ethylene-oxide-sterilized bone repair materials. *J Oral Implantol* **15**, 1, 41-46.